ECN › TNO innovation for life

TNO report

TNO 2019 R11212
CO$_2$ storage feasibility in the P18-6 depleted gas field

Date	March 2020
Author(s)	Filip Neele
	Ton Wildenborg
	Kees Geel
	Daniel Loeve
	Lies Peters
	Siavash Kahrobaei
	Thibault Candela
	Mariëlle Koenen
	Paul Hopmans
	Kaj van der Valk
	Bogdan Orlic
	Vincent Vandeweijer
Number of pages	192 (incl. appendices)
Number of appendices	
Sponsor	
Project name	P18-6 feasibility study
Project number	060.40697

Summary

Objective
This study presents the results from a CO_2 storage feasibility study on the P18-depleted gas field that is located in the Netherlands offshore. The aim of the study was to understand the risks associated with injecting CO_2 into the field, to outline injection strategies that lead to safe and secure storage and, finally, to propose an approach to risk management and monitoring during injection. The results from this study are to form the geoscientific basis for a CO_2 storage permit application.

Background
The study was carried out for the Porthos consortium that plans to transport CO_2 from several industrial sources in the Port of Rotterdam to three P18 fields operated by Taqa: P18-2, P18-4 and P18-6. TAQA already obtained a storage permit for the P18-4 field in 2013, with the aim to store CO_2 for the ROAD project, with a mass of about 5 Mt. However, the ROAD project was cancelled in 2017.

The Porthos consortium builds onto the work done by the ROAD project. The consortium plans to transport and store more CO_2 than the 5 Mt target of the ROAD project and, hence, will need storage capacity in addition to that offered by the already permitted P18-4 field. Operated from the same P18-A platform and also close to the end of production, the P18-2 and P18-6 fields represent a maximum storage capacity 32.3 Mt and 1.5 Mt (in both cases for a final reservoir pressure of just under original gas pressure). The current study is directed to the P18-6 field only.

In 2011 a CO_2 storage feasibility study of the P18 fields was performed. The present study provides an update for the P18-6 field based on new data and improved methods and workflows to investigate the response of the depleted field to injection of CO_2.

Study approach
The requirements for a CO_2 storage permit application are set out in the Dutch Mining Act, which was amended in 2011 to include a transposition of the EU Storage Directive (EU Directive 2009/31/EC). The results presented in this report cover the requirements described in the EU Storage Directive. The present study follows a workflow that was developed in a consortium of several EU Member States, building on combined experience in CO_2 storage feasibility assessments.

The workflow is risk-based, with the aim to understand the site-specific risks associated with CO_2 storage, to reduce them to a level that is as low as reasonably possible through site-specific design of injection scenarios and to develop a monitoring program and mitigation plan aimed at the most relevant, remaining risks.

Overall conclusion regarding storage of CO_2 in the P18-6 field
The overall conclusion of the study is that CO_2 can be stored safely and securely in the P18-6 field. The CO_2 can be injected into the field in a way that is safe; during and after the end of injection, the P18-6 field will retain the CO_2 securely. There is no reason to assume that CO_2 could migrate out of the field after proper decommissioning of the injection well after the end of injection.

Managing relevant risks

The identified risks that are related to the potential leakage of CO_2 out of the P18-6 storage complex during or after CO_2 injection have been studied in detail and classified in a risk register. Most of the risks have been classified as 'very low', with 'very low likelihood' that a small ('nil to negligible') amount of CO_2 could migrate out of the reservoir; this corresponds with the lowest possible risk class. The risks associated with the injection well have been classified as 'low', with a 'low likelihood' and a small ('nil to negligible') amount of CO_2 could migrate out of the reservoir.

The risks assessed are related to (1) lateral CO_2 migration out of the storage reservoir, (2) the integrity of the well in the field, (3) the stability of the faults in the storage system and integrity of the caprock.

(1) Simulation of the flow of CO_2 during injection into the storage formations shows that the injected CO_2 will be retained within the confines of the original gas field. There is no risk of CO_2 spilling, even when the pressure in the reservoir is brought back to the initial pressure.

(2) Analysis of available data on the integrity of the well in the P18-6 field shows that a workover is required for the existing well, P18-A-07-S1. Once this is performed, the risk of CO_2 leaking along the well, based on pre-injection status, is considered low.

   The initial low reservoir pressure leads to low temperature of the CO_2 at the bottom of the well, causing significant temperature gradients in the well. These might lead to de-bonding of well liner (casing) and cement, potentially allowing leakage pathways to form (micro-annuli) for CO_2. However, only when the pressure in the reservoir is above hydrostatic pressure could CO_2 enter these micro-annuli and potentially migrate into overlying aquifers. Therefore, the pressure in the reservoir is to be maximized at hydrostatic pressure, to reduce the likelihood of CO_2 flowing through these micro-annuli to 'low', with an amount of CO_2 that is 'small to negligible'.

(3) The cold CO_2 is injected into the reservoir formations, where it will create a low-temperature zone around the injection well. In case injection into the P18-6 reservoir on a continuous basis, this zone could reach faults that are present in the reservoir, affecting fault stability; however, at the same time, faults become more stable during the injection process due to increasing reservoir pressure. If the P18-6 reservoir is only used to store the cold contents of the surface transport pipeline after a shut-in period, the mass of injected (colder) CO_2 is small and the low-temperature front does not reach faults near the well. In both modes of operation, monitoring of injection rate and temperature is recommended to measure the pressure and collect the information to track the temperature development in the reservoir through modelling and ensure that faults remain stable. However, all analysis points to small to negligible impact of fault reactivation; none of the faults in the P18-6 reservoir extend to above the caprock of 450 m to 750 m thick. This ensures that, fault destabilization, if any, will not lead to CO_2 movement through the caprock.

The likelihood that CO_2 injection in the P18-6 reservoir affects caprock integrity is very low.

Recommendations

(1) In the study presented here the modelling of the injection process was performed with an isothermal reservoir simulator that could not simultaneously handle pressure and temperature variations in the reservoir. The impact of the low temperature of the injected CO_2 was estimated through the use of an additional simulator and analytical approaches. While the results obtained thus far are considered sufficient for the assessment of the risks associated with CO_2 storage, detailed coupled modelling of pressure and temperature in the storage formations is required prior to the start of injection. This is needed for pressure and temperature predictions that are sufficiently reliable for the management of the injection process and for the interpretation of monitoring data.

(2) The aim of the present study was to provide the basis for a storage permit application, by understanding the current status of the storage formations, the caprock, the faults and the wells, and their response to the injection of CO_2. The study established that conditions can be established under which CO_2 can be injected and stored safely and securely in the P18-6 field. The study did not aim to arrive at a complete and detailed description of these conditions. Such an 'operational plan' for CO_2 injection into the P18-6 field will be required prior to the start of injection, as a basis for the detailed monitoring plan and for the operational management of the injection process. The present study is the first step towards the P18-6 operational plan.

Contents

1 Introduction

This report presents the results of a study into the technical feasibility of storing CO_2 in the depleted offshore gas field P18-6. This field is one of several fields in the P18 cluster. The Porthos consortium[1] is developing plans for a multi-user CO_2 transport and storage network that connects industrial emitters of CO_2 in the Rotterdam harbour area with geological storage capacity in the Dutch sector of the North Sea. The consortium is targeting the P18 cluster as the first candidate for CO_2 storage. Operation of the network is planned for 2022 / 2023 [2].

The Porthos network is still in its planning stage and no certainty exists at this point in time regarding the supply of CO_2. A recent study of the P18 gas field cluster suggested that the fields P18-2, P18-4 and P18-6 together can accommodate a supply rate of the order of 2-3 Mt/yr (million tonnes per year) and possibly up to 5 Mt/yr (Vandeweijer et al., 2011). With a combined storage capacity of approximately 37 Mt, storage at a rate of 2-3 Mt/yr could continue for about 15 years.

The P18-4 gas field has a CO_2 storage permit in place. This permit was awarded irrevocably in 2013. The P18-4 field was planned to be part of the "Rotterdam afvang en opslag demonstratieproject" (ROAD), which aimed to capture CO_2 at a coal-fired power plant at the Maasvlakte, compress the CO_2 and transport it by offshore pipeline to the P18-A platform, located at a distance of about 20 km from the Maasvlakte. The ROAD project was cancelled in 2017; all close-out reports are available online (ROAD, 2018).

The Porthos consortium now builds onto the ROAD legacy. The Porthos network is planned to be a multi-user transport and storage network, building up to much higher CO_2 supply rates than those considered in the ROAD project. In addition, the Porthos network has a longer operational phase planned. This means that more depleted gas fields are required for storage, in addition to P18-4. The first candidates are the P18-2 and, potentially, the P18-6 gas fields.

The starting point of the present study was the storage feasibility study of the P18 cluster that was performed under the CATO-2 R&D programme (Vandeweijer et al., 2011). While the scope of that study was the entire P18 complex – including the P18-2, P18-4 and P18-6 compartments – the focus of the analyses was on the P18-4 structure. The P18-4 storage feasibility study was used in a storage permit application that resulted in the permit granted in 2013. The analyses of the P18-2 and P18-6 compartments presented by Vandeweijer et al. (2011) were not sufficient for a subsequent storage permit application for these compartments.

The storage feasibility analysis of the P18-2 field was recently completed, building onto the work presented by Vandeweijer et al., (2011) and using up-to-date tools and workflows, to support a storage permit application (Neele et al, 2019).

---

[1] See https://rotterdamccus.nl/.
[2] See Notitie Reikwijdte en Detailniveau – Rotterdam CCUS Project (Porthos), available at https://www.rvo.nl/sites/default/files/2019/02/Porthos%20concept%20NRD%20-%20versie%20finaal.pdf

This report presents the results of a technical CO_2 storage feasibility study of the P18-6 structure. The aim of the feasibility study is to identify risks for the containment of CO_2 in the storage complex, how to minimize those risks and the best way to monitor remaining risks. The study, which extends the analyses and results of the CATO-2 study by using the latest production data and deploying state-of-the-art workflows and tools, provides the necessary input for a CO_2 storage permit application under the Dutch Mining Act and a 'Milieu Effect Rapportage'(MER) (which is a required element for the permit application). In 2011, the Dutch Mining Act transposed the EU Storage Directive (EU, 2009), thus ensuring that a storage permit application submitted under the Dutch Mining Act will comply with European legislation concerning CO_2 storage.

The work presented in this report follows the workflow that was used for the P18-2 feasibility study (Neele et al., 2019).

2 Reading guide

This report presents the results of a technical CO_2 storage feasibility study for the P18-6 depleted gas field. The structure of the report is as follows.

Sections 3 through 5 set the scene for the storage feasibility study. Section 3 introduces the risk-based approach taken in assessing the feasibility of storing CO_2 in the P18-6 field. The geological setting of the P18-6 field is described in Section 4. Section 5 describes some of the key boundary conditions and assumptions used in the study: the CO_2 supply profile until 2035, as well as the preliminary approach to the injection process. Section 5 also provides a brief summary of relevant results from a flow assurance study that was performed previously; this includes the conditions of the CO_2 at the bottom of the injection well, which follow from the modelling of CO_2 flow from the compression station, through a subsea pipeline and down the injection well. These conditions are used in the present study as the starting point for the modelling of the behaviour of the CO_2 inside the reservoir.

Sections 6 through 11 present the results from the storage feasibility analysis. The behaviour of CO_2 in the reservoir and its effect on the temperature and pressure distribution is presented in Section 6. Sections 7 and 8 discuss the impact of injecting CO_2 on reservoir and caprock integrity and stability of the faults within and bounding the reservoir. Well integrity is covered in Section 9, evaluating the current status of the well and discussing simulation results on the effect of CO_2 injection on the long-term structural integrity. Section 10 defines the storage site and storage complex and contains a description of the barriers in the storage site to CO_2 migration. Section 11 presents an analysis of potential migration of CO_2, if it leaves the storage complex. All results are pulled together in Section 12 to assess the risks associated with injecting CO_2 into the P18-6 field.

Section 13, finally, outlines the system that will be designed to monitor the injection process and the behaviour of the CO_2 in the subsurface.

2.1 Definitions

The following definitions are used throughout this document.

Block	An area on a map (e.g., block P18)
License areas	Part or all of a block (e.g., P18a)
Field	A bounded structure where the hydrocarbons were discovered and produced from and includes the sealing faults, rocks, gas-water contact (GWC) and other structural elements (e.g., P18-6)
Reservoir	Part of the field where the reservoir fluids are contained and where the CO_2 will be stored, i.e. the porous rock
Compartment	Part of a field and includes the bounding elements, (e.g. three compartments in P18-2 field)
Storage Site	Defined under the CO_2 Storage Directive and under the Dutch Mining Act and includes the storage reservoir and the wellbores penetrating the storage reservoir

Storage Complex	Includes the storage reservoir, the wellbores penetrating the reservoir and the surrounding and bounding formations and faults which make up the storage field.
Migration of CO_2	Movement out of the storage reservoir but remaining in the storage complex
Leakage of CO_2	Under the CO_2 Storage Directive means movement of CO_2 out of the storage complex
Emission of CO_2	Under the ETS Directive means escape of CO_2 from the storage site to the atmosphere or the water column
Injection facilities	Include well completions and wellheads; *not* included are other facilities on the platform, nor the platform itself.

3 Methodology

3.1 Legal background

This technical CO_2 storage feasibility study aims to provide the basis for a permit application for CO_2 storage in the P18-6 field. The Dutch Mining Act sets out the requirements for a storage permit application. A transposition of the EU Storage Directive (EU, 2009) was included in the Mining Act in 2011[3]. Previous work on the P18-4 field (Vandeweijer et al., 2011) resulted in a successful application for a CO_2 storage permit, proving that the workflow used provided a basis that was both sufficiently detailed and complete.

The present study follows the workflow that was used by Vandeweijer et al. (2011), and that was described in detail by Nepveu et al. (2015), who combined experience from several EU Member States in CO_2 storage feasibility assessments. The workflow covers the full list of requirements set out in Annex II of the EU Storage Directive (EU, 2009). Section 16 shows the link between the elements of site characterisation mentioned in Annex I of the EU Storage Directive and the present report.

3.2 Feasibility study

The workflow is risk-based and site specific, with the aims to understand the storage risks involved, to reduce them to a level that is as low as reasonably possible through site-specific design of injection scenarios and to develop a monitoring program aimed at the most relevant, remaining risks.

This study uses the workflow described by Nepveu et al. (2015) as illustrated in Figure 3-1 and outlined below:
- Phase 1 of the workflow represents a screening study, to find one or multiple sites that meet selection criteria, such as location, storage capacity or expected cost of storage.
- Phase 2 of the workflow represents the detailed CO_2 storage feasibility study, which is presented in this report for the P18-6 depleted gas field. The first part of phase 2 is a 'quick scan' of available data. The purpose of the quick scan is to identify the key risks to storage and 'showstoppers', if any, before entering the detailed assessment, which represents the second part of phase 2. This detailed assessment is shown in the diagram in the figure as the central, large rectangle labelled 'RA' (risk assessment), with several disciplines revolving around the RA. This is the key element of a storage feasibility assessment, with several disciplines analysing the response of the storage system on the injection of CO_2.

For this study, screening was already completed and outside the scope of this report. In addition, a 'quick scan' of available data was already performed in a previous study of the P18 gas fields (Vandeweijer et al., 2011). No showstoppers were identified for the P18-6 field. However, as that study was focused on the P18-4 depleted gas field, the detailed assessment of the P18-6 was incomplete; the

---

[3] See https://www.nlog.nl/en/licences-and-legislation for links to relevant government internet sites.

present report repeats the previous assessment with improved tools and experience where possible and fills the gaps where needed.

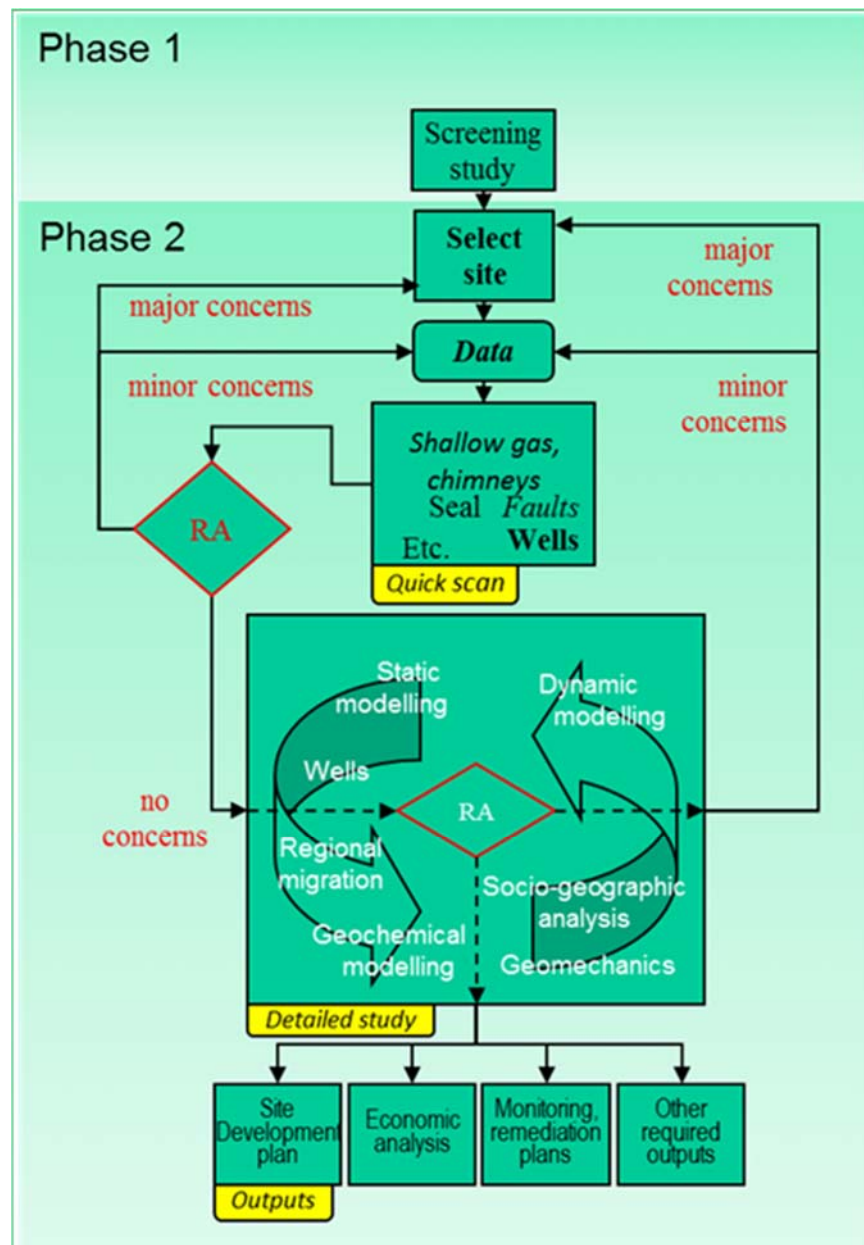Figure 3-1 Workflow for site screening and characterization (Nepveu et al., 2015). RA is Risk Assessment

3.3 Risk assessment

The approach pursued in the risk assessment, (i.e.. the assignment of risk classes) is qualitive in nature and expert-based, although the underlying information used is often of a quantitative nature, e.g. output from model simulations or measurements of physical parameters like pressure.

The risk assessment consists of the following steps:
1. Identification of (a combination of) factors, which directly influence the containment of CO_2
2. Detailed assessment of these (combined) factors and definition of potential risk reduction measures
3. Risk classification

Step 1 was performed in a workshop prior to the project in order to define the required assessment. Step 2, the detailed assessment of the risk factors and definition of potential risk reduction measures, is reported in Sections 6 to 9; step 3 is described in Section 12.

Typically, the results of the risk characterisation and classification are listed in a risk register (see Section 18) and summarized in accompanying risk matrices. For the classification of the risks, a risk matrix with classes of likelihood and consequences has been designed (see Figure 3-2), which is inspired by the work done by Van Eijs et al. (2011) and the risk assessment matrix included in the toolkit of the Energy Institute (website, version 15 Oct 2019). The definition of the classes of consequences has been linked to the concept and definition of the storage complex as described in the EU Storage Directive (EU, 2009).
As shown in Figure 3-2 the following definitions are used for this study:

Five classes of likelihood have been defined with the following definitions:

Very low	Positive evidence for containment and large safety factor
Low	No positive evidence and large safety factor
Medium	Positive evidence and no large safety factor
High	No positive evidence and no large safety factor
Very high	No positive evidence and small or nil safety factor

The classes of consequence have been defined as follows:

Negligible	Within natural variation and cannot be monitored
Very small	Can be monitored and no impact on biosphere
Small	Can be monitored and possible minor impact on biosphere
Large	Can be monitored and possible impact on biosphere
Very large	Can be monitored and possible adverse impact on biosphere

The resulting risk classes have been split in three categories):

Low risk	Strive for continuous improvement; monitoring and risk reduction are optional;
Medium risk	Apply monitoring and risk reduction measures according to ALARP (As Low As Reasonably Practicable) principle;
High risk	Risk reduction to acceptable levels and monitoring are obligatory.

Consequence ->	Likelihood ->	A	B	C	D	E
	Containment function	Very low	Low	Medium	High	Very high
1	Nill or negligible amount of CO2 migrates out of the reservoir.	A-1	B-1	C-1	D-1	E-1
2	Very small amount of CO2 migrates out of the reservoir but stays in the storage complex.	A-2	B-2	C-2	D-2	E-2
3	Small amount of CO2 migrates out of the reservoir and partly ends up outside the storage complex.	A-3	B-3	C-3	D-3	E-3
4	Large amount of CO2 migrates out of the reservoir and partly ends up outside the storage complex.	A-4	B-4	C-4	D-4	E-4
5	Very large amount of CO2 migrates out of the reservoir and out of the storage complex.	A-5	B-5	C-5	D-5	E-5

Risk level		Monitoring necessity	Risk reduction
	Low	Optional	Optional
	Medium	ALARP	ALARP
	High	YES	YES

Figure 3-2   Proposed risk matrix nomenclature (modified after Van Eijs et al., 2011; Energy Institute, 2016)

4 P18-6 field overview

4.1 Introduction

The gas fields P18-2, P18-4, and P18-6, drilled from platform P18-A, are situated at approximately 3500 m depth below sea level and are located some 20 km NW from the port of Rotterdam (Figure 4-1). The reservoir rocks consist of sandstones which belong to the Triassic Main Buntsandstein Subgroup. The primary seal for the gas fields consists of unconformably overlying siltstones, claystones, evaporites and dolostones. The P18 gas fields are located in a heavily faulted area and consist mainly of fault bounded compartments, which are (at least on production time scales) hydraulically isolated from their surroundings. The bounding faults (which are well defined and clear to see on seismic) are sealing on a geological time scale due to juxtaposition of reservoir rock against impermeable rock.

High-calorific gas has been produced from these reservoirs since 1993. The gas is produced through the P18-A satellite platform and the P15-ACD processing and accommodations facilities in the adjacent P15 block, from where it is then transported to the coast by a 40-km-long gas pipeline.
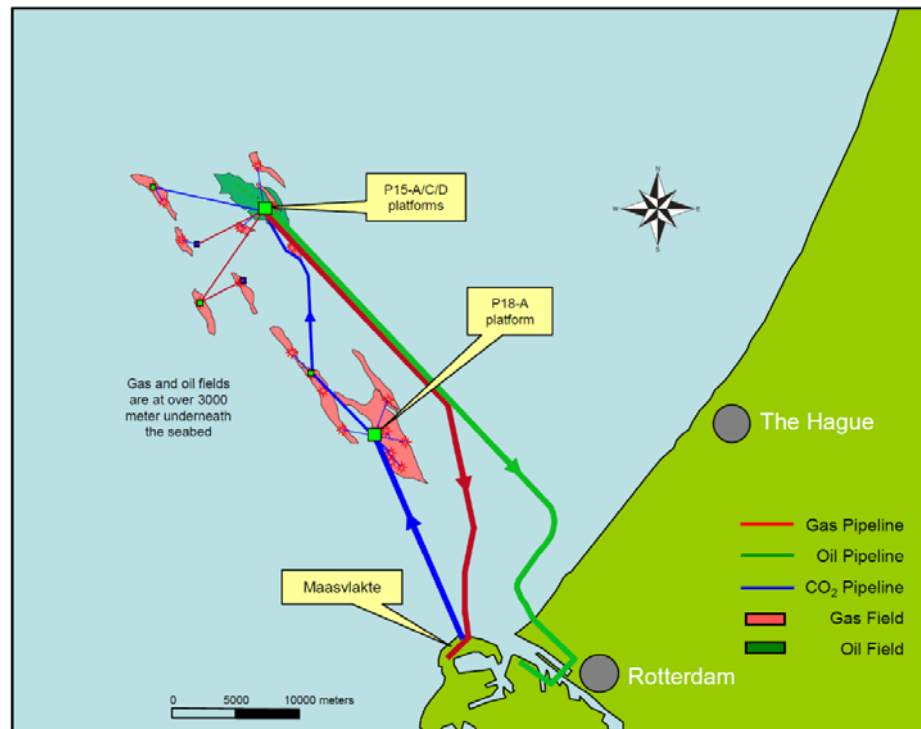
Figure 4-1: Overview of the locations of P15 and P18 fields (After TAQA, 2009)

4.2 Geological description

The P18 cluster consists of three fields, the P18-2, P18-4 and P18-6 fields (Figure 4-2). P18-2 was discovered in 1989 with the exploration well P18-02. It consists of four compartments, 2-I, 2-II, 2-III, and 2-IV. Compartment 2-I came on stream first,

in 1993. It contains three production wells: P18-A-01, P18-A-03-S2, P18-A-05-S1, and the exploration well P18-02. Compartment 2-III contains one production well, P18-02-A6, and came on stream in 1997. Compartment 2-II came on stream in 2003, and also contains one production well, P18-A-06-S1. For a while this side track produced from compartment 2-II only. After the whipstock had been perforated in 2005, well P18-A-06 produced simultaneously from the 2-II and 2-III compartments. The P18-4 Field was discovered in 1991 and production started from well P18-A-02 in 1993. The P18-6 Field was discovered in 2003 and production started from well P18-A-07-S1 in 2003.

The P-18 cluster reached peak production in 1998, with a cumulative annual production of 2.2 bcm. At the end of June 2018, the total cumulative production of all P18 fields was 13.5 bcm. According to the updated Winningsplan from 2016, decommissioning of the different fields is expected in 2024. Recovery factors by that time are expected to be 98% for P18-2 and P18-4, and 90% for P18-6.
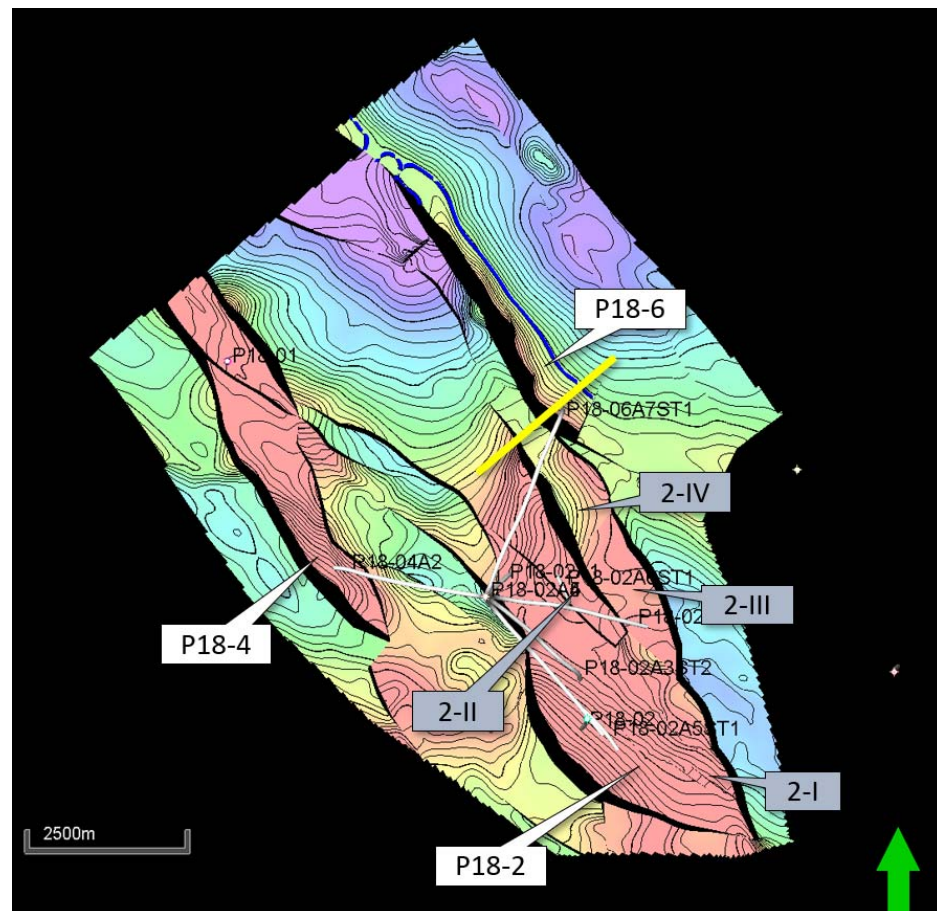
Figure 4-2: Overview of the three P18 fields (P18-2, P18-4, and P18-6), and the compartments of the P18-2 Field (2-I, 2-II, 2-III, and 2-IV). Original gas water contact in P18-6 is indicated by a blue line. Yellow line indicates the position of the cross section shown in Figure 4-3.
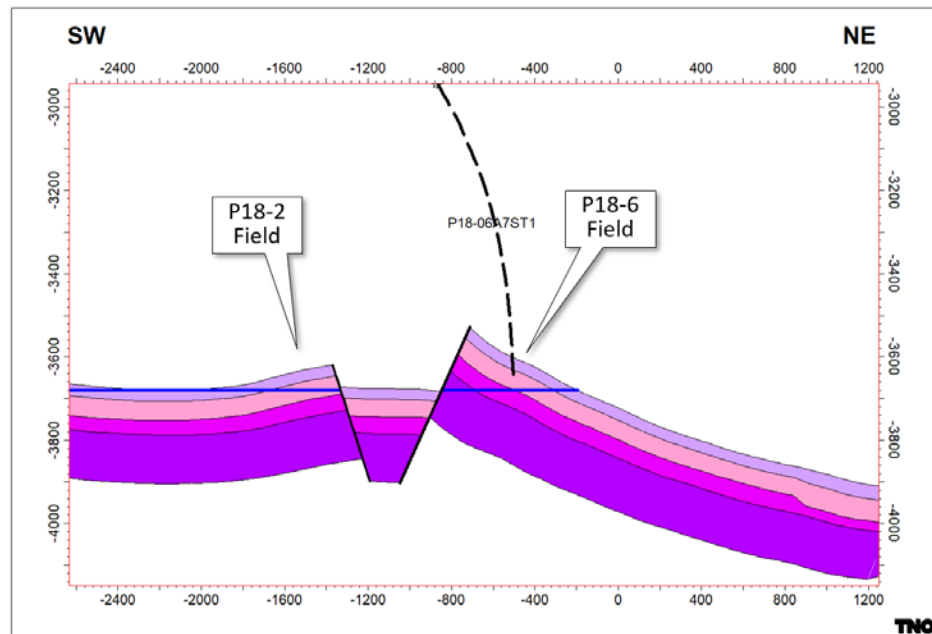
Figure 4-3: Cross section through the P18-6 field with well P18-6-A7 (projected) and a part of the P18-2 field. The various Bunter formations are indicated by different colours, from top to base: Hardegsen, Upper Detfurth, Lower Detfurth, and Volpriehausen Formations. The blue line indicates the original gas water contacts. The location of the cross section is shown in Figure 4-2. Vertical exaggeration is 2x.
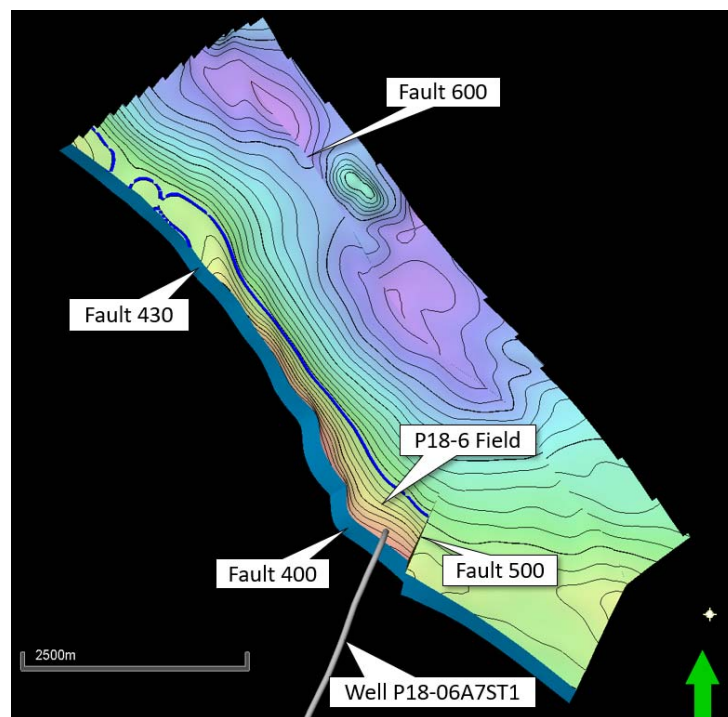
Figure 4-4: Map view of the Top Bunter in the P18-6 area with fault names used in this report.

The structures that contain the reservoirs are bound by a system of NW-SE oriented faults in a horst and graben configuration, with a sinistral strike-slip component. The top of the P18-6 field lies at a depth of 3514 m below sea level and the gas-water contact is at 3680 m below sea level.

The P18-6 Field consists of a NW-SE elongated, tilted fault block. It is bounded to the SW by a large-offset fault and on the SE by a smaller, transverse fault. Both faults are sealing due to juxtaposition of the reservoir zones against impermeable shales of the overlying Upper Triassic and Altena Groups. Figure 4-3 illustrates this for the SW boundary fault.

The reservoir rocks of the P18 fields consist of four sandstone formations that belong to the Lower Germanic Trias Group, informally called Bunter. From top to base these are the Hardegsen, Upper Detfurth, Lower Detfurth and Volpriehausen Formations (Figure 4-5). Each formation has highly variable porosity and permeability values. The Hardegsen Formation has in general the best reservoir properties. Well P18-A-07-S1 has poor reservoir properties, but away from the well reservoir properties must be much better, as testified by the produced gas volume.

4.3   Caprock

The seal to the P18 reservoirs is formed by the Upper Germanic Trias Group and the Jurassic Altena Group. The Upper Germanic Trias Group consists of siltstones, claystones, evaporites and dolostones. In well P18-02 it has a thickness of approx. 155 m. Directly above the Upper Germanic Trias Group lies the approx. 500 m thick Altena Group (Figure 4-5), a thick succession of marine claystones, siltstones and marls of Early Jurassic age with excellent sealing quality.

The total thickness of the P18 reservoir's caprock varies between 450 m and 750 m. The seal is excellent, as proven by the fact that it holds a gas column of nearly 600 m in the P18-2 compartment.

The rest of the overburden is formed by several geological formations, some of which can also be assumed to have good sealing properties. The Vlieland Claystone Formation (Figure 4-5) has proven itself as a good seal, as it forms the seal for the oil-bearing Lower Cretaceous sandstones in the West Netherlands Basin. It is considered here as the secondary caprock. Clayey sequences are also abundant in the North Sea Supergroup, especially in the lower part. These could potentially act as secondary seals.

The nomenclature of the caprock as used in the present study is different from the one used in the CATO study of 2011. In the CATO study, the Upper Germanic Trias Group was designated the primary seal, and the Altena Group the secondary seal. In the present study the Altena Group and the Upper Germanic Trias Group are considered to form one seal, since there are no permeable formations in between the two. Therefore, the Upper Germanic Trias Group plus the Altena Group form the primary seal (Figure 4-6), and the Vlieland Claystone Formation the secondary seal.
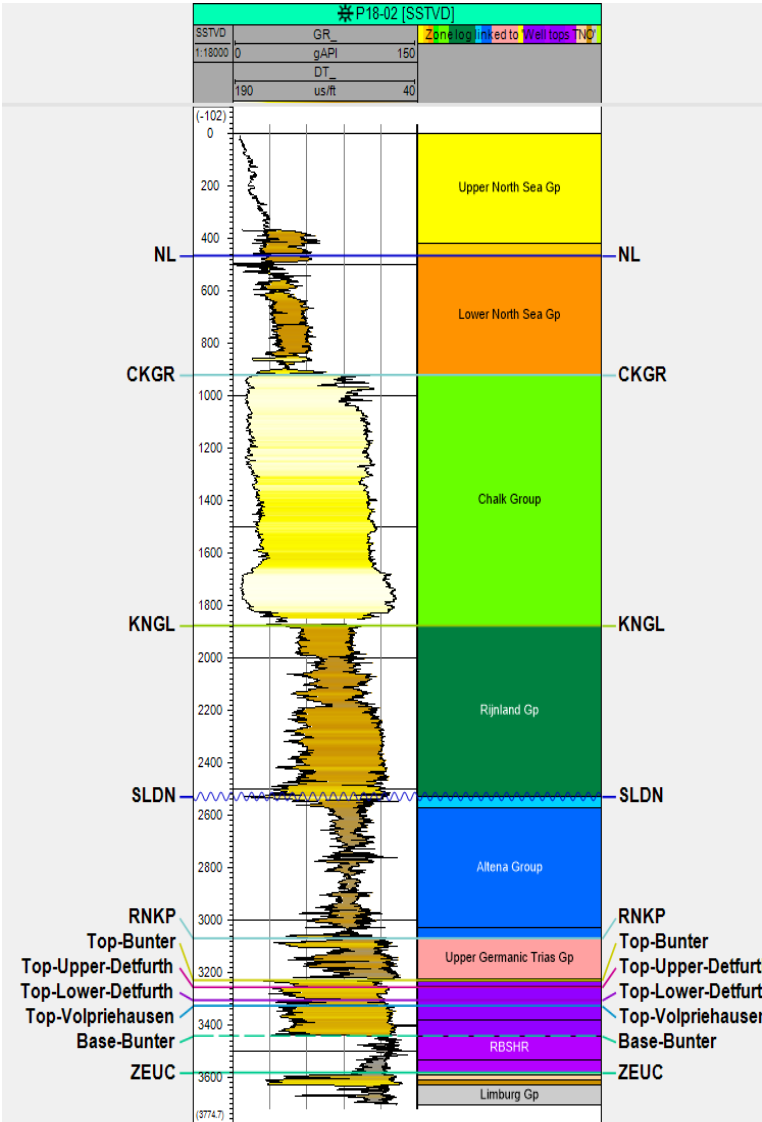
Figure 4-5: Stratigraphy and well logs of the reservoir interval and overburden of the P18 area; well P18-02.
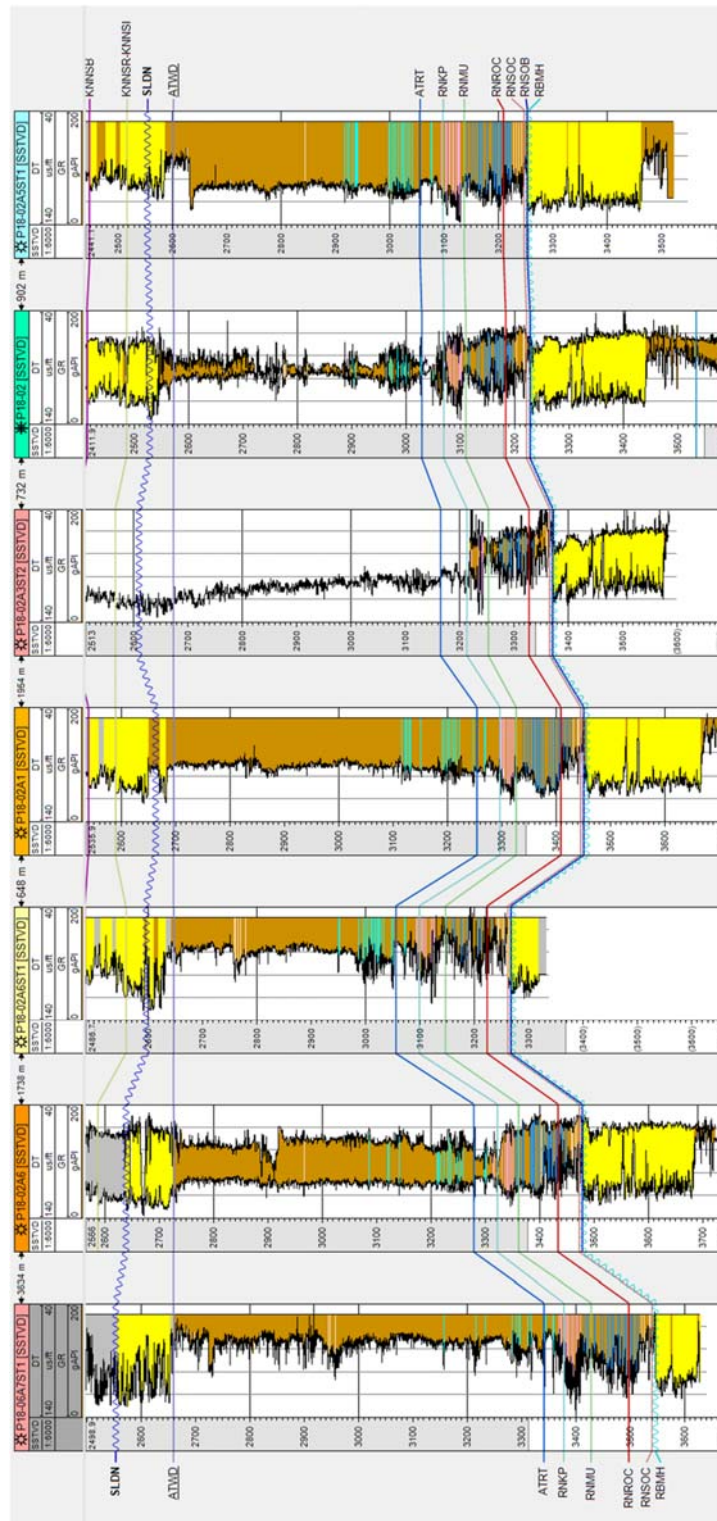
Figure 4-6: Well panel through the P18 wells of the immediate overburden of the Bunter
             formations showing that the Upper Germanic Trias Group plus the Altena Group form
             one continuous, primary seal over the entire storage complex.

4.4   **Naturally sealing formations**

The decommissioning of production platforms and infrastructure in the Southern
North Sea has recently begun. A number of studies were initiated to investigate
whether parts of the decommissioning process could be done more economically.
One of these studies focused on well decommissioning, and specifically on the
question whether naturally occurring ductile formations could be utilised to provide
economic, self-healing and durable long-term sealing of wellbores. The outcome of
the study, essentially based on existing literature, was that in the southern North
Sea some formations are indeed suitable for creating effective annular barriers
(Fischer et al., 2016; Geel, 2016). The idea is that if at the time of well
decommissioning it can be demonstrated that ductile clays or salts are hydraulically
isolating the outer annulus and provide zonal isolation, no additional measures
need to be taken at that point (as already accepted and practice in Norway and
shown by Williams et al. (2009)). Of course, if this sealing behaviour can be
demonstrated before CO_2 injection starts, it also reduces the risk of CO_2 leakage
outside the well.
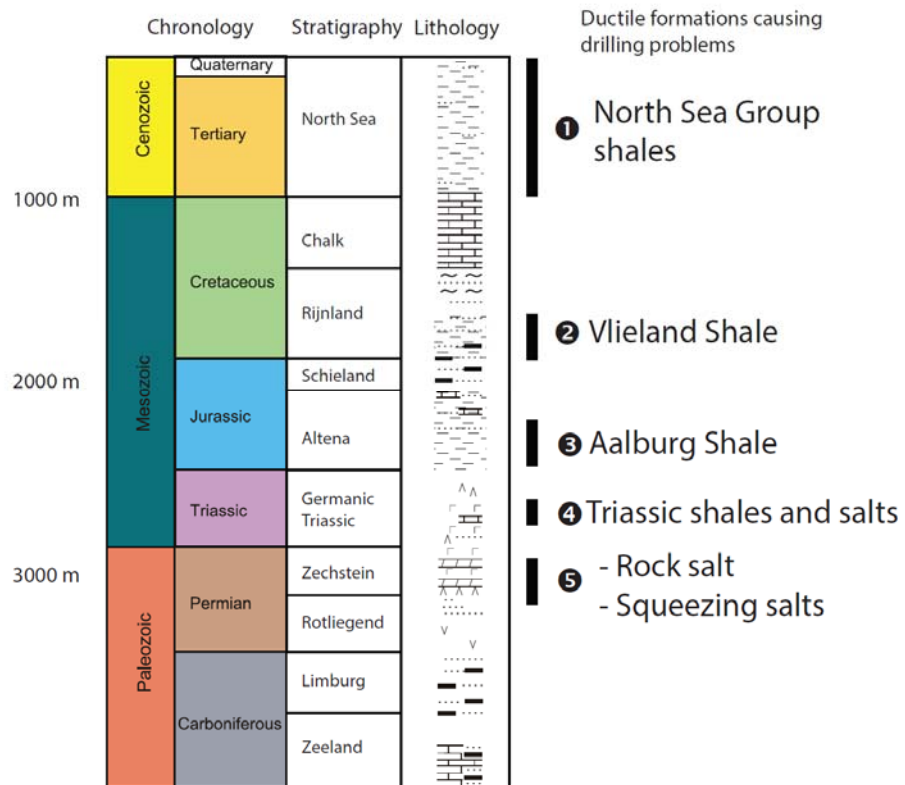
Figure 4-7   Typical stratigraphic column with potential self-sealing formations (Fischer et al, 2016).

The shales from the Lower North Sea Group, The Vlieland Claystone Formation,
and the Aalburg Shale were identified as having sufficiently ductile behaviour and
swelling potential to create a sufficient seal around the casing (Figure 4-7). In
addition, salts and possibly shales from the Upper Germanic Trias Group could
have creeping or swelling behaviour.

The fact that all the above mentioned formations occur in the P18 area, it increases the probability that some or all will contribute to sealing the wells in the long term. This is further dealt with in Section 9.

5 Injection scenario

5.1 Injection wells and well completion

Current plans for CO_2 storage in the P18-2, P18-4 and P18-6 fields are to use up to six injection wells. The P18-4 field has a single well, P18-A-02, which has predicted injection rates in the order of 1 Mt/yr (Vandeweijer et al., 2011). The P18-6 field also has a single well, P18-A-07-S1, but the expected injection rates according to the previous study are significantly lower. This well with a TD of 5066 m is still producing, according to www.nlog.nl web site (P18-A-07-S1, 15 Oct 2019). Up to four injection wells are expected to come online in the P18-2 field (Neele et al., 2019).

The tubing in the existing well (see section 9 for more details) can be replaced prior to injection, and the optimal tubing size needs to be based on dedicated well dynamics simulations (see, for a dynamic simulation of the P18-2 wells Belfroid, 2019). Such simulations for the P18-6 well need to be performed as part of a future study. For the purpose of the current study, the P18-6 well tubing during injection is assumed to be as it currently is, having mainly an external diameter of 4.5" resulting in an internal diameter of 0.1 m.

5.2 CO_2 supply scenarios

The future rate of CO_2 supply, to be delivered by emission sources in the Rotterdam harbour area, was uncertain at the time this study was undertaken. Based on the volumes of the CO_2 currently emitted in the harbour area and the volumes that could be captured at relatively low cost, a 'most likely' CO_2 supply profile was created (Figure 5-1).
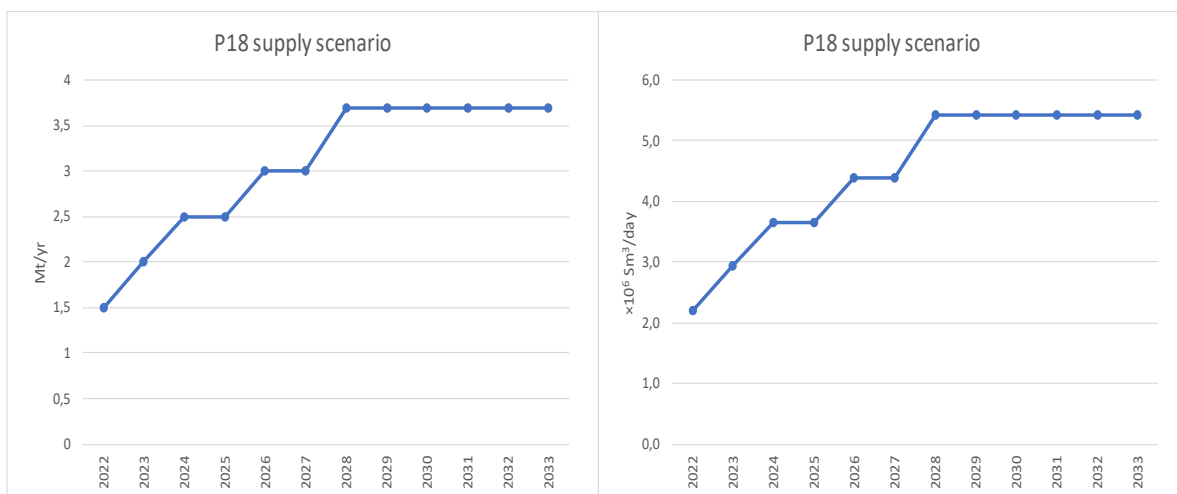
Figure 5-1 Potential future supply scenario for CO_2 from Rotterdam harbour sources. Flow rates increase from 1.5 Mt/yr by 2022 to 3.7 Mt/yr by about 2028 (about $5.5 \cdot 10^6$ Sm^3/day). Left: flow rates in Mt/yr; right: flow rates in Sm^3/day.

5.3 Injection of CO_2 in P18-6

Due to the low productivity of the P18-6 field and the limited amount of connected gas, the well P18-A-07-S1 is not planned to be one of the main injection wells. The productivity of the P18-6 field has been relatively low compared to that of the P18-4 and P18-2 fields. The storage feasibility studies of P18-4 (Vandeweijer et al., 2011) and P18-2 (Neele et al., 2019) suggest that the supply profile shown in Figure 5-1 can be accommodated by these two fields. However, a detailed flow assurance study suggests that during the initial phase of injection, when the reservoir pressure in the P18-2 and P18-4 fields is at its lowest level, injection rates during the start-up of a well may be insufficient to store the supplied CO_2 (Belfroid, 2019). The P18-6 field is considered to be used as back-up storage, to be utilised during starting up if the overall injection capacity of the P18-2 and P18-4 wells becomes insufficient.

An alternative scenario for the P18-6 field is related to a start-up after a shut-in of the pipeline. When the transport pipeline to the P18-A platform is shut in, its contents will equilibrate to sea water temperature. During the period of low reservoir pressure in the P18-2 and P18-4 fields, injection of this cold CO_2 is not possible in the P18-2 and P18-4 wells (see Section 6.4). Due to the relatively low injectivity of the P18-6 well (compared to the injectivity of the P18-2 and P18-4 wells), downhole temperature of injected CO_2 is higher. This presents the opportunity of using the well in the P18-6 field for the injection of the contents of the cooled down shut-in pipeline. Once warm CO_2 arrives at the platform (post shut-in), the P18-2 and P18-4 wells can take over.

In both scenarios, the key property of the P18-6 field is the maximum injection rate it can accommodate. This is the driving factor used in the injection scenarios presented in the sections below.

Therefore, CO_2 injection into P18-6 is investigated using the following two scenarios:
1. The storage scenario.
   This scenario is used to determine the storage capacity, injection capacity (i.e., maximum feasible injection rates) and containment in the P18-6 reservoir.
2. The discharge scenario.
   This scenario is only used to estimate downhole conditions of the CO_2. The aim is to assess the impact on the temperature distribution near the well when injecting CO_2 at a temperature lower than that used in the storage scenario. (Section 6.4.3.2)

5.4 CO_2 quality

At the time of the present study, no information was available about the potential sources of CO_2. Recent work suggests that most available capture technologies can be expected to deliver CO_2 at a purity of 95% or higher (see, e.g., IEAGHG, 2016); sources in the Rotterdam harbour currently deliver CO_2 of more than 99% purity to the OCAP pipeline for use in greenhouses. While impurities alter the behaviour of CO_2 and may affect elements of the CCS chain, the results presented here were derived assuming pure CO_2.

Figure 5-2 illustrates the effect of impurities on the phase behaviour of CO_2. While pure CO_2 has a phase *line* that separates vapour conditions from those in which liquid CO_2 occurs (black curve in the figure), the presence of impurities in the CO_2 changes it into a transition zone of pressure and temperature conditions in which the transition from gas to liquid phase occurs. In this transition zone two phases (gas and liquid) are present. Generally, two-phase flow is to be avoided in the handling of CO_2, e.g. to prevent slugging. Two-phase flow is expected to occur in CO_2 injection wells without causing issues (Belfroid, 2019), but should be avoided in transport pipelines, risers and compressor. The conclusion that can be drawn from Figure 5-2 is that temperature and pressure should be chosen high enough to avoid the two-phase region of the CO_2 mixture being transported.

Impurities have an impact that extends beyond the phase envelope alone – for example, changes in densities will affect the operational window for injection, as well as the storage capacity.

In the current study pure CO_2 was assumed in the simulations.
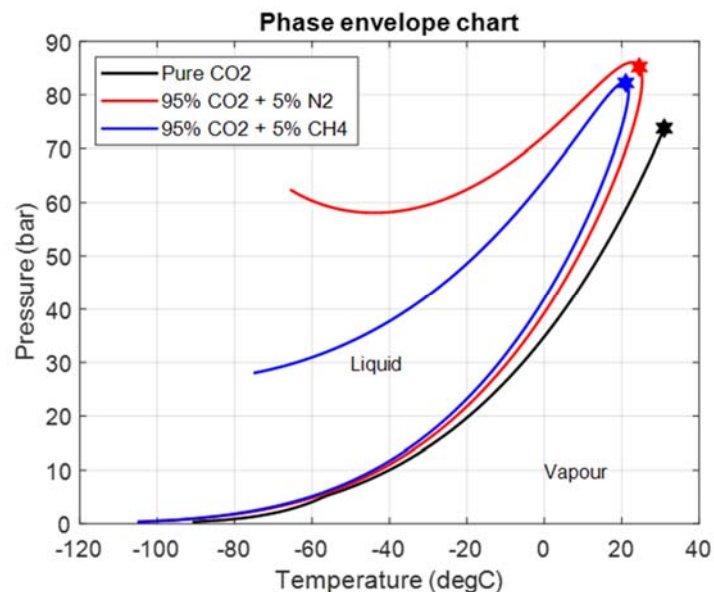
Figure 5-2 Effect of impurities (either 5 wt% N_2 or CH_4, equal to 7.6 and 12.6 mol% respectively) on the location and shape of the CO_2 phase line. The data was generated using NIST REFPROP v10.

5.5   Summary of injection conditions

To summarise, the injection of CO_2 into the P18-6 reservoir is subject to the following conditions.

- The injection simulations are to result in an estimate of the maximum injection rate that the P18-6 reservoir can accommodate at different reservoir pressure levels.
- The tubing in in the injection well will be recompleted (pers. comm. EBN, 2019). The external tubing diameter for the injector well is assumed to be 4.5". The actual well completion will be decided on at a later date, following a more

detailed analysis of the operational window of the wells in the P18-2 and P18-4 fields and the required backup capacity of the P18-6 well.
- The CO_2 is assumed to contain no impurities. At the time of the present study, no quality/specification information was available about potential sources of CO_2.

Additional assumptions apply to the conditions in the reservoir and to the downhole conditions of the CO_2. These are explained in detail in Section 6.
- At the start of injection, the reservoir pressure is 52 bar; see Section 6.3.
- In the injection simulations, the reservoir pressure will have a maximum that is equal to the initial reservoir pressure; see Section 6.3.
- The maximum downhole pressure is assumed to be equal to the initial pressure in the reservoir, 377 bar; see Section 6.3.
- The minimum downhole temperature of the CO_2 was required to always be above 15 °C, to avoid CO_2 hydrate formation in the well and in the near-well area; see Section 6.4.

6   Evaluation of reservoir performance and integrity

6.1   Introduction

This section presents the results of an analysis regarding the process of injecting CO_2 into the P18-6 field. The analysis aims to:
-   estimate of the storage capacity of the field (Section 6.3),
-   establish the flow of CO_2 in the P18-2 field (Section 6.3),
-   estimate the pressure and temperature levels in the injection wells and the fields during and after injection (Sections 6.2 and 6.4),
-   assess the effects of interaction between CO_2 and the reservoir rock (Section 6.5).

Section 6.2 outlines the set-up and assumptions made for the simulation of the injection process.

The conclusions reached in this section are the following:
–   The P18-6 field can store 1.3 Mt of CO_2, assuming a bottomhole pressure during injection that does not exceed initial pressure (i.e., the pressure prior to production of the natural gas).
– CO_2 fills the pore volume that was previously filled with natural gas and does not spill (i.e. flow laterally beyond the storage complex boundaries).
–   The injection process must be managed to ensure that temperature and pressure in the well and in the near-well area remain outside the hydrate formation window.
–   The injection of CO_2 will dry out the reservoir and may lead to salt deposition although the overall effect on permeability is expected to be negligible. Drying out of the reservoir reduces the probability of formation of hydrates.
–   Chemical interaction between the CO_2 and the reservoir formation is insignificant.

The analysis presented in this section reveals no barriers regarding storage performance and integrity to storage of CO_2 in the P18-6 field.

The results are a starting point for the assessment of fault stability (Section 7) and caprock integrity (Section 8).

6.2 CO_2 conditions at bottomhole

The conditions of the CO_2 at bottomhole, inside the wellbore, upon flow into the reservoir, were derived from a flow assurance study performed in parallel to the study presented here. This section gives an overview of how the conditions of the CO_2 at bottomhole (in the wellbore) are determined. These results are used in the analysis of the effect of the low-temperature CO_2 in the reservoir (Section 6.4). The distribution of the cold CO2 is the starting point for the evaluation of fault stability and caprock integrity due to thermal stresses in Sections 7 and 8.

6.2.1　Method

6.2.1.1　The simulator
The simulations of downhole CO_2 conditions have been done using OLGA 2017.1.0 simulator with the single component CO_2 module using the pressure-enthalpy methodology. This method is a tabulation format, properties (viscosity, densities etc.) are tabulates with independent variables pressures and enthalpy
All simulations are done in transient mode, with a long enough simulation to reach steady-state conditions (if achievable).

6.2.1.2　Boundary conditions
The pressure in the transport pipeline is assumed to be 85 bar or 120 bar, depending on the reservoir pressure.

At mid to high reservoir pressures (40 to 300 bar), the pipeline temperature arriving at the platform is set to 30 °C. The setting is an optimization between cooling power and compressor power.

The following boundary conditions/assumptions are set in the project:
−　The pipeline temperature arriving at the platform is set at 30°C.
−　The reservoir pressure at the start of injection is 40 bar (which is slightly below the expected minimum reservoir pressure of 52 bar); the maximum reservoir pressure is 377 bar.
−　Pipeline operation is preferred to be in single liquid phase condition.
−　The downhole temperature (inside the borehole) has a minimum of 15 °C, to avoid hydrate formation, both inside the wellbore (in case of water influx during well shut-in periods), and in the reservoir near the well where expansion of the CO_2 leads to temperature decrease (see Section 6.4).
−　The temperature of the topside piping in the well should remain higher than -10°C. Although the tolerance for low temperatures can be improved by using different materials, this limit was assumed to be representative of current facilities.
−　Parameters not considered at this stage of the simulations are erosion, tubing vibrations and thermal gradients in the well.

6.2.1.3　Model description
The inputs for the model are productivity index, temperature and pressure (PI, T, P), which are based on the Eclipse 300 simulations and shown in Table 6-2.
Productivity index or PI is a measure of the ability of a well to produce fluids and is equal to the rate of fluid production divided by the pressure drawdown, all based on measurements at the well.
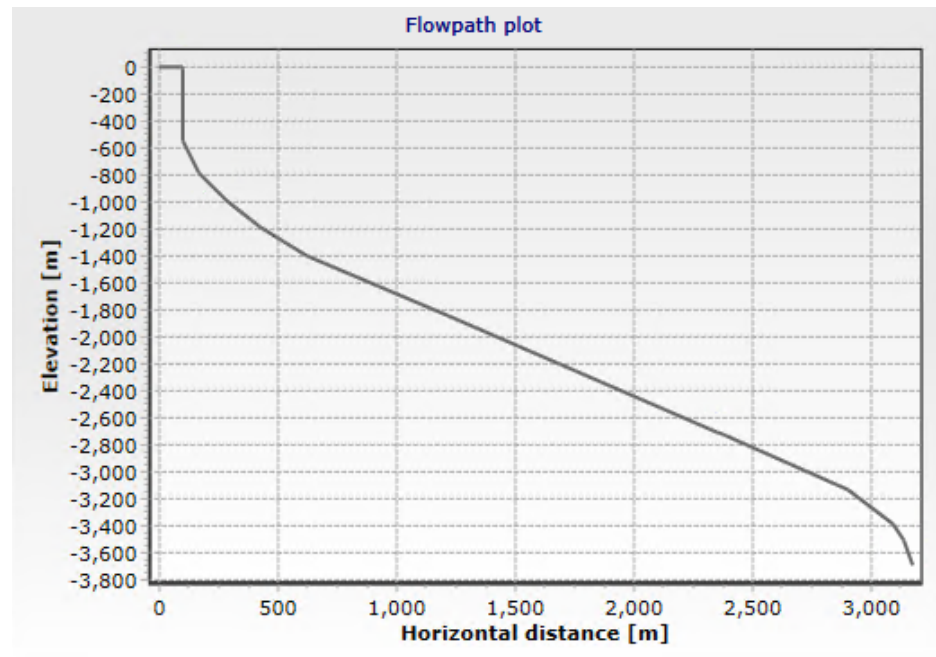
Figure 6-1   Flow path of the well.
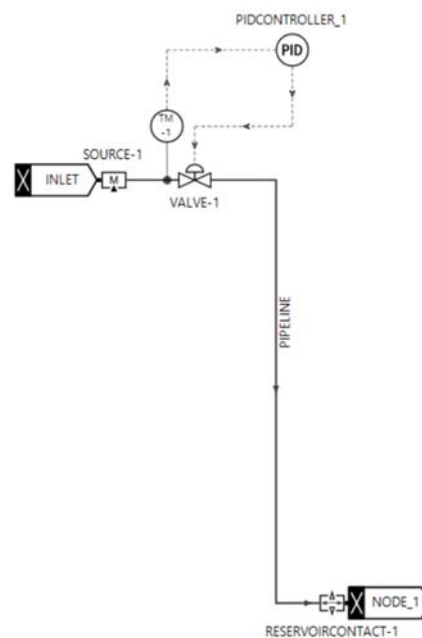
Figure 6-2   Pipeline-well model with control valve.

The model includes 100 m of topside piping (diameter 0.15 m). A mass flow controller is also added to the pipeline. Well inclination is included (Figure 6-2) and as already mentioned a tubing diameter of 0.1 m.

The heat transfer in the well is modelled using a single heat transfer coefficient along the entire well. The heat capacity of the walls is not included, but for steady-state scenarios this produces reliable results. The vertical thermal gradient around the well ranges from 10 °C to 117 °C, with a heat transfer coefficient of 9.5 W/m²/K. The pipeline heat transfer coefficient is taken as 6 W/m²/K with an ambient temperature (sea water) of 4 °C.

6.2.2   Steady-state flow simulations for the storage scenario

The steady-state simulations were conducted for a large range of well characteristics, flow rates, CO_2 temperatures (at the wellhead) and reservoir pressure conditions. The results show that the operational window for the P18-6 reservoir is limited to a maximum injection rate of about 30 kg/s (Table 6-1). At these rates, there is no risk of operational issues or well material degradation.

Pipeline pressure is assumed to be 85 bar and at reservoir pressure above about 200 bar the pipeline pressure is assumed to increase to 120 bar. The temperature of the CO_2 at the wellhead is assumed to be 30 °C.

Table 6-1 shows one feasible injection scenario, in which the mass flow rate is limited to 15 kg/s at the depletion pressure of 40 bar and increases to 20-30 kg/s in the medium to high pressure range (60 to 200 bar). When reservoir pressure approaches initial pressure the injection rate decreases again.

Table 6-1 provides the input for the temperature dependent simulations of injection into the P18-6 reservoir (Section 6.4).

Table 6-1 CO_2 conditions at the platform and downhole for several values of reservoir pressure, for a single well in the storage scenario. Note that the operational pipeline pressure and temperature are 85/120 bar [4] and 30 °C, respectively. PI: productivity index.

Reservoir pressure [bar]	Max mass flow rate [kg/s]	P Pipeline [bar]	P Downhole [bar]	T Pipeline [°C]	T downhole [°C]	PI used [kg/s/Pa]
40	14.5	85	353	30	72.5	$4.6 \cdot 10^{-7}$
60	20	85	338	30	69.7	$7.14 \cdot 10^{-7}$
100	25.7	85	318	30	68.0	$1.17 \cdot 10^{-6}$
200	31.1	120	360	30	62.3	$1.94 \cdot 10^{-6}$
300	21.3	120	395	30	65.0	$2.12 \cdot 10^{-6}$
350	14.2	120	412	30	68.5	$2.26 \cdot 10^{-6}$

6.2.3   Steady-state flow simulations for the discharge scenario

The discharge of a 21 km pipeline filled with CO_2 at 10°C results in downhole temperatures in the range of 43°C to 50°C, for a reservoir pressure of 30 bar up to 300 bar. Table 6-2 lists the conditions of the CO_2 at the wellhead and downhole in the pipeline discharge scenario at different reservoir pressures.

---

[4] 85 bar for reservoir pressure below 200 bar and 120 bar for reservoir pressures above 200 bar.

Table 6-2 CO_2 conditions at platform and downhole for several values of reservoir pressure, for a single well for the discharge scenario. Note that the operational pipeline pressure and temperature are 85 bar and 10 °C, respectively.

Reservoir pressure [bar]	Mass flow rate [kg/s] max	P Pipeline [bar]	T Pipeline [°C]	P Downhole [bar]	T downhole [°C]	PI used [kg/s/Pa]
30	15.5	85	10	396	51.7	$4.20 \cdot 10^{-7}$
40	21.1	85	10	386	47.3	$6.03 \cdot 10^{-7}$
50	24.7	85	10	377	45.3	$7.47 \cdot 10^{-7}$
60	23.2	85	10	383	46.3	$7.14 \cdot 10^{-7}$
100	30.6	85	10	361	43.4	$1.17 \cdot 10^{-6}$
200	31.0	85	10	359	43.2	$1.94 \cdot 10^{-6}$
300	20.3	85	10	391	48.3	$2.12 \cdot 10^{-6}$

6.2.4   Conclusion

- During steady state injection conditions (Table 6-1), the bottomhole conditions of the CO_2 inside the wellbore are typically a temperature of 70 °C at a rate of 20 kg/s. These conditions serve as input for the thermal simulations of injection in the storage scenario.
- During a discharge of the contents of a cooled down pipeline, again a flow rate of 20 kg/s is typical, with a downhole temperature of 43 °C. This applies for reservoir pressures up to about 60 bar.

6.3   Reservoir injection performance and risks

6.3.1   Introduction

This section evaluates the storage capacity and the containment within the reservoir of the injected CO_2. The CO_2 injection into the P18-6 reservoir does not follow the supply scenario shown in Section 5.2, but uses the maximum flow rate that can be injected into the reservoir, as explained in Section 5.3. In these simulations the limitations as evaluated in the flow assurance study (Section 6.2) are not taken into account. In this section, all simulations are done at reservoir temperature (isothermal) and thermal effects are discussed in Section 6.4.

6.3.2   Simulation method

For the simulations in this study a history matched dynamic reservoir model of the P18-6 field is used. (See Section 17.6 for a description of the model and the history match.) The following assumptions were made.

- At the start of injection, the reservoir is depleted to an near-well pressure of 20 bar (shut-in pressure) and 52 bar field average gas pressure of the connected gas (see Section 17.7.7).
- The maximum pressure in the reservoir should not exceed the initial pressure anywhere. Since the reservoir simulation only calculates the grid block average pressure and not the local maximum at the well, this is achieved by setting the maximum bottom hole pressure (BHP) of the well to the initial gas pressure of 377 bar.
- The maximum injection rate is set at 30 kg/s (about 1 Mt/yr), for consistency with the flow assurance results presented in Section 6.2.

− The injection simulation will be conducted isothermally at reservoir temperature (see remarks on the simulator used below).
− It is assumed that the near-well reservoir properties (characterised here by the product of permeability and thickness) as derived from production data and information from logs can be used to simulate the CO_2 injection process.
− No changes occur in the well completion configuration at reservoir level (the relevant factors here are the well diameter and the length of the perforations).
− The saturation curves for gas-water systems are assumed to be the same for CO_2-water systems.

An additional scenario is run in which the maximum BHP is set to 450 bar. This scenario is used to evaluate CO_2 flow paths and containment in case of overfilling the reservoir.

All simulations were performed with the Eclipse 300 reservoir simulator, a state-of-the-art compositional model that can handle the behaviour of CO_2 in the reservoir (including phase transitions) and the interactions between CO_2 and residual gas; see also Section 17.6.1. CO_2 dissolution into the water phase is not taken into account. The reason for ignoring dissolution is that due to the assumption of equilibrium within a grid block, the amount of CO_2 dissolution is considerably overestimated at field scale (Zang, 2013). Evaporation of water into the gas phase is not handled.

Eclipse 300 cannot handle non-isothermal conditions for CO_2 injection. This means that in all results presented in this section the CO_2 is injected at reservoir temperature, even though the temperature of the CO_2 is likely to be significantly lower (see Section 6.2). The TOUGH2 simulator was used to run non-isothermal injection scenarios for the evaluation of fault stability (Section 7.3) and caprock integrity (Section 8.3). See Section 6.4 for the description of the thermal simulations.

6.3.3   Simulation results

The total amount of CO_2 that can be stored in P18-6 for a BHP of 377 bar (initial pressure; field average gas pressure is 379 bar) and injection period of 5.5 years is 1.3 Mt, assuming that before the start of injection the near-well pressure is depleted to 20 bar (shut-in pressure), with field average gas pressure of the connected gas at 52 bar. See Section 17.7.7 for a description of the simulation of the final depletion stage.

Figure 6-3 below shows the injection rate and cumulative mass of CO_2 injected over time. The initial injection rate of 30 kg/s is maintained for approximately three months (for injection at reservoir temperature) and subsequently decreases due to a rapid rise in near well reservoir pressure (Figure 6-4). Figure 6-4 shows the corresponding pressures: BHP, near well pressure and field average gas pressure of the connected gas (i.e. in Hardegsen and Upper-Detfurth) over the injection period. The average field pressure differs from the near-well pressure due to the presence of 'slow' gas, i.e. gas that is available in low permeability deposits and/or behind flow barriers. The near-well pressure shows the typical pressure behaviour also observed during production, namely a fast initial increase and then a slow tail.

The injection is conducted over a period of 5.5 years. Table 6-3 presents the amount stored at yearly intervals. At the end of the simulated injection period the injection rate has dropped to 1.5 kg/s (less than 50 kt/yr). More than half of the injection is completed during the first year.

Table 6-3. Overview of the amount CO_2 stored and the injection rate at the end of each year.

	Amount CO_2 stored [Mt]	CO_2 injection rate [kg/s]	Average connected gas pressure [bar]
After 1 year of injection	0.7	10.7	207
After 2 years of injection	0.9	5.2	256
After 3 years of injection	1.0	3.6	284
Final (after 5.5 years)	1.3	1.5	331
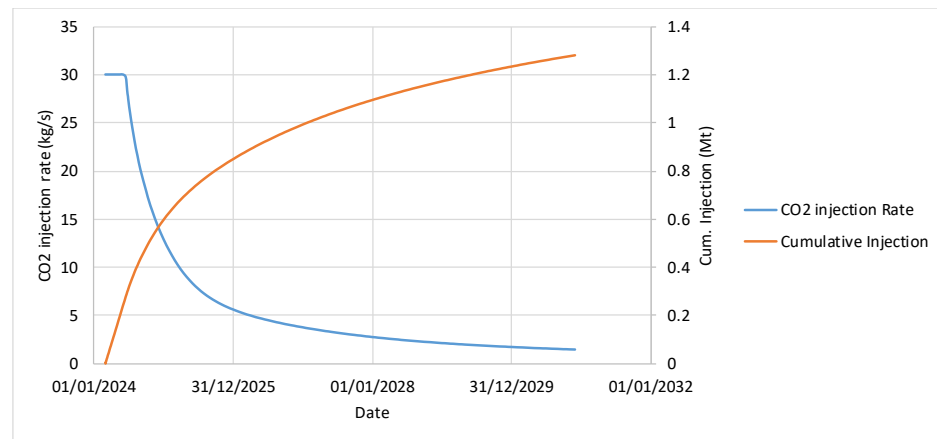
Figure 6-3: Injection rate and cumulative CO_2 mass injected for well P18-06-A7 for a BHP constraint set to 377 bar.
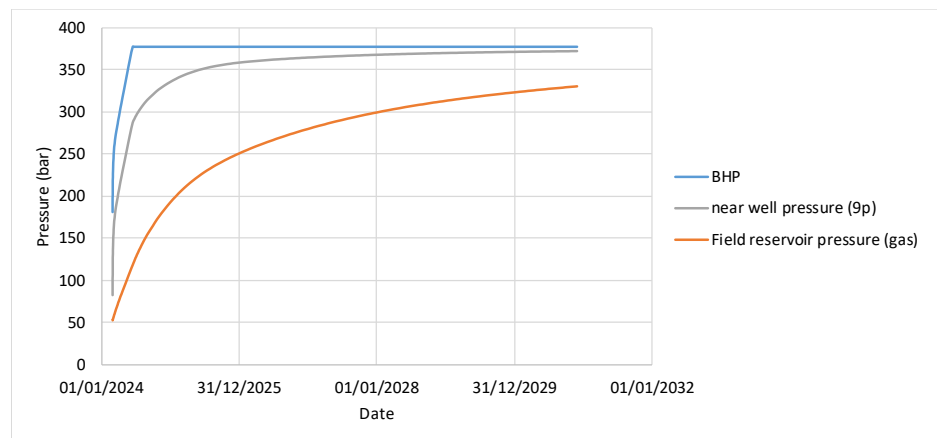
Figure 6-4: BHP, near well reservoir pressure and field average gas pressure during injection.

6.3.4 Pressure, gas and CO_2 behaviour in the reservoir

Figure 6-5, Figure 6-6 and Figure 6-7 show maps of pressure, gas saturation and CO_2 molar density, respectively. Due to the setup of the model, sharp boundaries occur in the model. Section 17.6 gives a detailed description of the model.

2003 (start production)   2024 (start injection)

2025   2026

2030 end of injection   Legend for all plots
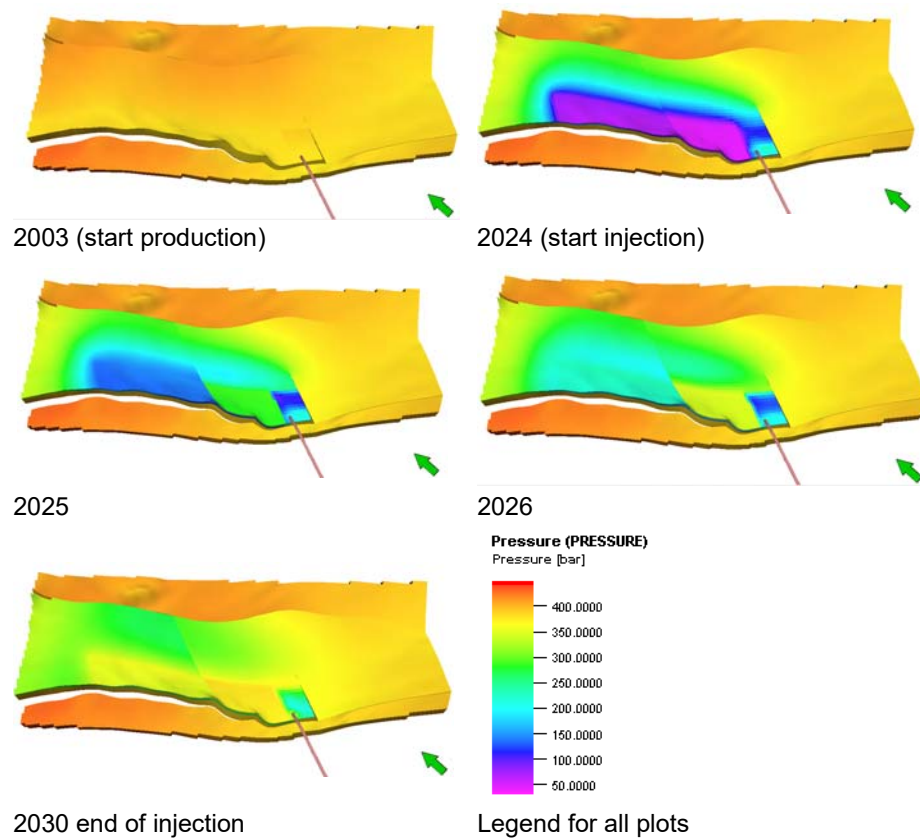
Figure 6-5: Pressure map at different stages of injection into the P18-6 reservoir. The orange line
             at the bottom of each map represents the well trajectory.

From the history match it was clear that mobility in the aquifer must be limited in order to avoid water production in the well (which is not observed). This is reflected in the pressure behaviour (Figure 6-5), which shows a delayed response in the aquifer: the pressure in the aquifer at the end of injection (in 2030) has hardly increased yet as a result of the injection. In the southern part of the aquifer, pressure has not changed much at all. In the pressure in 2025, the impact of a flow barrier in the gas field which was required to achieve a history match is clearly visible. The field average pressure in the gas filled area of Hardegsen and Upper-Detfurth is 52 bar at the start of injection (2024).

In Figure 6-6, it can be seen that the gas saturation in the near well area is lower (i.e. the water saturation is higher) than in the rest of the gas field. This is the result of the poor reservoir flow properties in the near well area. Some water encroachment is visible at the start of injection. The gas distribution at the top of the reservoir at the end of injection is almost the same as the distribution at the start of production.

In Figure 6-7, the CO_2 distribution in the highest permeability layer is shown using the CO_2 molar density. The CO_2 molar density is a measure for the CO_2 gas saturation. Using the molar density gives the opportunity to distinguish between the different fluid components in the P18-6 reservoir. In this high permeable layer, the CO_2 has the widest distribution. A potential spill point in this area is at the end of the small-offset fault near the well that forms the south-eastern limit of the gas-filled

reservoir. Near this fault, the CO_2 migrates to below the original gas-water contact near the well in a downdipping area of the reservoir. However this CO_2 does not move far (even in case of overfilling, see also Figure 6-8) and will migrate back up the slope when injection is stopped. In the north-west corner of the reservoir where there is a spill point, the CO_2 does not move beyond the original gas-water contact.

2003 (start production)   2024 start injection

2025   2026

Water saturation (SWAT)
Water saturation

2030 (end injection)   Legend for all plots
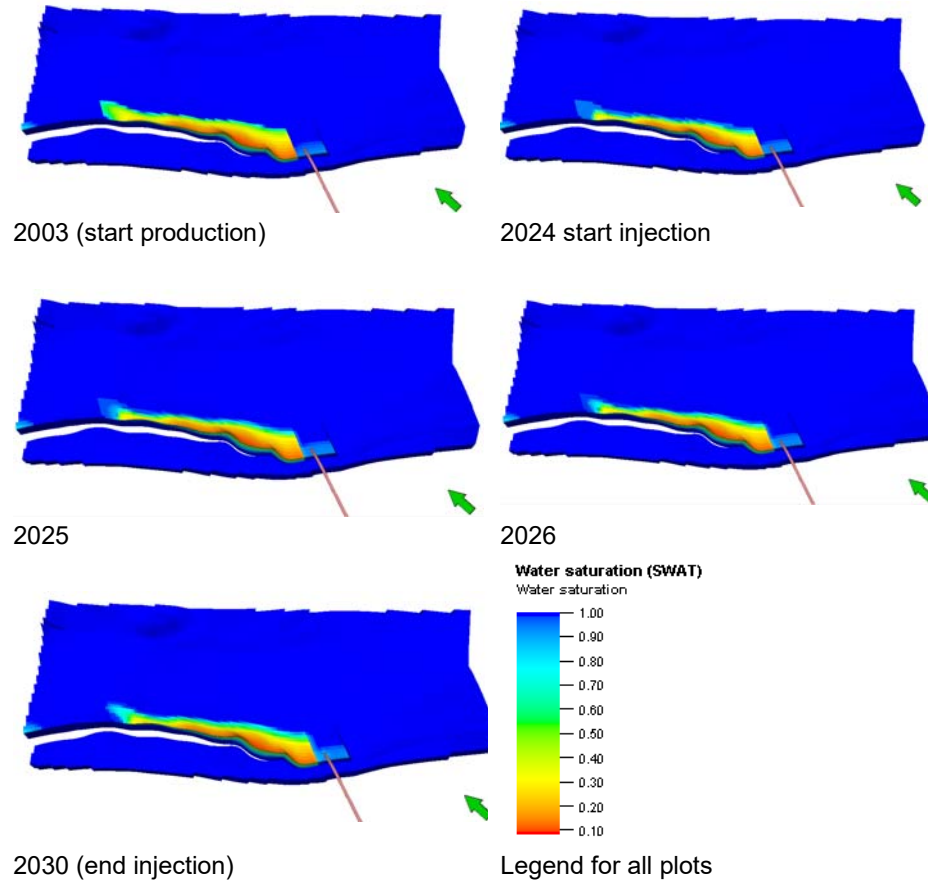
Figure 6-6: Water saturation map at different stages of injection into P18-6. The orange line at the bottom of each map represents the well trajectory.

To investigate the flow paths of the CO_2 further, the CO_2 injection was also done with a maximum BHP of 450 bar to increase the amount of CO_2 injected. Now in total 1.52 Mt CO_2 was injected resulting in a final average reservoir pressure of 389 bar. Figure 6-8 shows the distribution of the CO_2 at the end of injection. The insert shows that even in this case of overfilling the CO_2 does not move beyond the small fault next to the well. Thus once injection is stopped, the CO_2 will move back up the slope into the original gas field. In Figure 6-9, the initial and final gas saturation at the spill point in the north-west is shown. Also here CO_2 does not move beyond the original contact.

2025 (one year into injection)   2026

2030 (end injection)   Legend for all plots
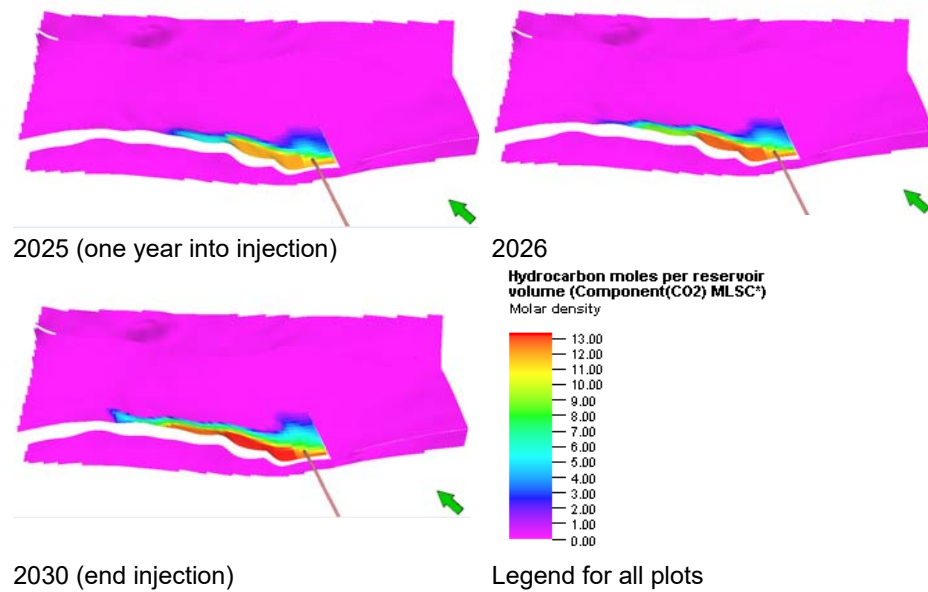
Figure 6-7: CO_2 molar density (kmole/m^3) map at different stages of injection into P18-6 in the highest permeability layer (layer 11). CO_2 migrates beyond the original gas-water contact (compare panels in this figure with the first panel in Figure 6-6).
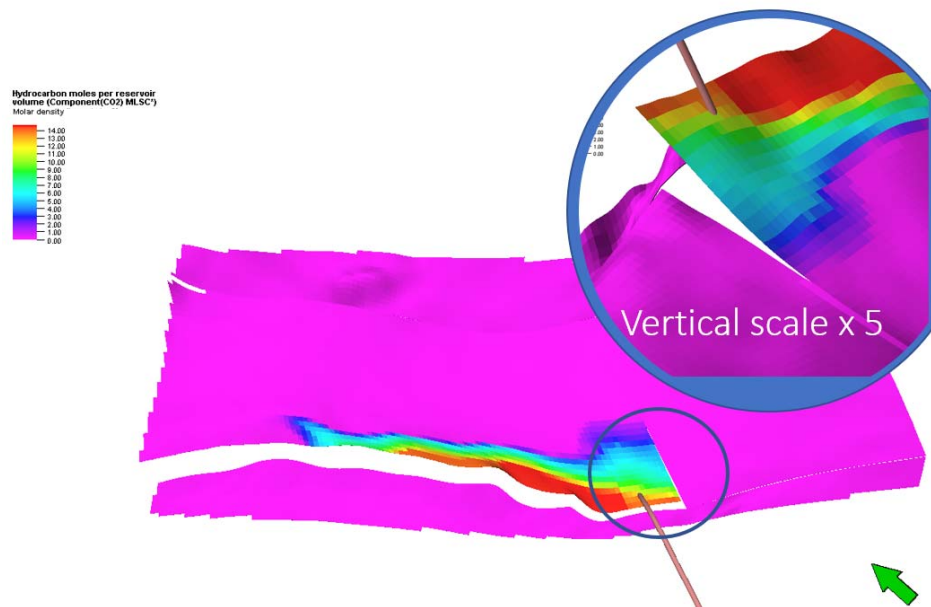
Figure 6-8: CO_2 molar density (kmole/m^3)[5] in the highest permeability layer (layer 11), after overfilling the P18-6 reservoir (1.52 Mton injected and average gas pressure is 389 bar). CO_2 migrates beyond the original gas-water contact (compare panels in this figure with the first panel in Figure 6-6), but does not reach the end of the near-well fault.

---

[5] Molar Density represents the number of moles of a molecule present in a unit of volume, common units are mole/m3 or kmole/m3)
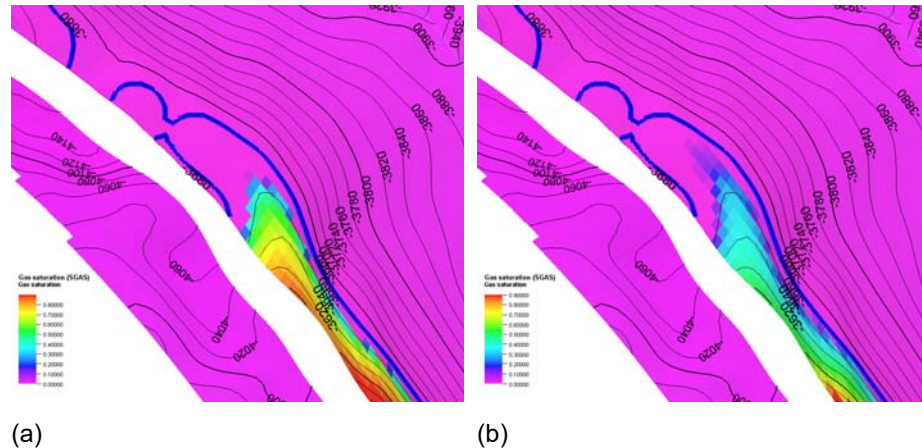
Figure 6-9: (a) Initial gas saturation and (b) gas saturation after overfilling the P18-6 reservoir (1.52 Mton injected and average gas pressure is 389 bar) in the highest-permeability layer (layer 11). The bold blue line indicates the free water level. Contours indicate depth (TVDSS).

6.3.5 Discussion on sources of uncertainty

Both the injection rate and total amount injected are sensitive to choices made in the history match and the final depletion phase. In the history match, a multiplier of two on the well productivity was applied to match the final production phase. No transmissibility or skin estimate are available from well tests, resulting in uncertainty in the productivity of the well. The injectivity is thus also uncertain, even when the impact of the low temperature injection is not taken into account.

For the total amount of CO_2 that can be stored, several factors are important: the uncertain well injectivity, the choices for the final depletion phase and the duration of the injection period. The choices for the final depletion phase determine how far the reservoir is depleted before the start of injection. In general, the more depleted the reservoir, the more CO_2 can be stored. Due to the low permeability of the field, both the depletion phase and the injection can take a long time. Since for neither of these phase stopping criteria are available, final values of the CO_2 storage capacity may differ from the estimates presented here. Also intermittent production or injection has not been included in the current analysis, because the impact on storage capacity is expected to be minor.

Also not included in the current simulation is the impact of a shut-in period at the end of depletion before the start of injection. See Section 17.7.7 for a description of the simulation of the final depletion stage. Due to the nature of the field with slow gas and some aquifer drive, pressure will increase during shut-in. In Table 6-4, the impact of a shut-in period is shown for the final production phase. The history match period runs up to 15 May 2019, when total production was 696 Msm^3. In Table 6-4 the pressure is listed for shut-in periods of 15 days and 1 year for one and two additional years of production and for the end of the simulated production period (five years to 1 April 2024). Figure 6-10 shows the development of the pressure during the last production phase (two more years of production after the end of the history match at 15 May 2019) and during a shut-in. Slow aquifer support causes gradually increasing pressure (curve 'field average p') in the figure.

Table 6-4. Increase in near well gas pressure (9-point average, at well datum) after shut-in of the well for different stages of depletion.

	Total produced volume [M sm^3]	Pressure after 15 days of shut-in [bar]	Pressure after 1 year of shut-in [bar]
After 1 additional year of production	717	32.5	47.7
After 2 additional years of production	732	26.0	39.4
Final (5 years to 1 April 2024)	756	20.4	29.7
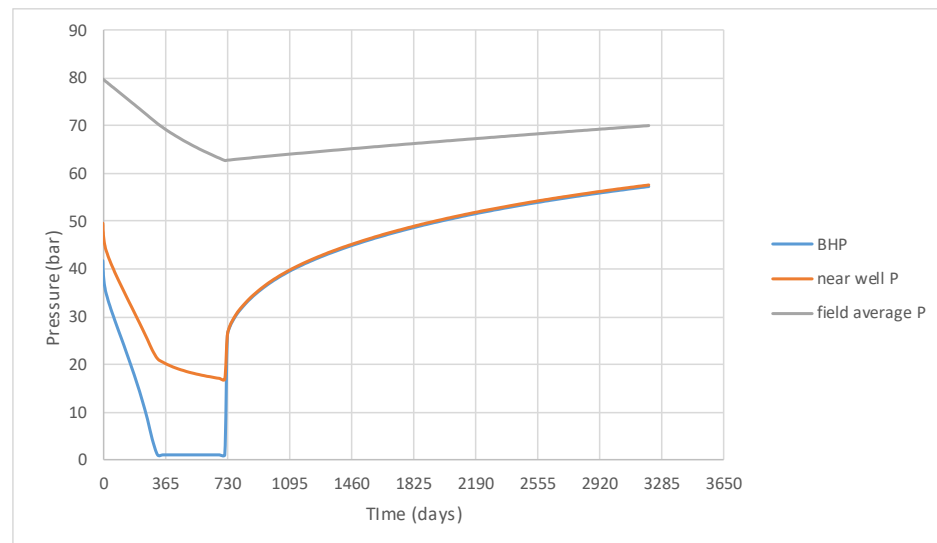
Figure 6-10.   Development of the pressure (BHP, near well pressure and field average gas pressure of the connected gas) in case of shut-in after two additional years of production.

6.3.6   *Pressure communication with P18-2*
Vandeweijer et al. (2011) state, on the potential communication between P18-2 and P18-6: "Reservoir P18-06 is located to the northeast of P18-2 reservoir. It is bounded by faults F13 and F57, of which only F13 has enough offset to be sealing by juxtaposition". This suggests potential communication between P18-6 and Compartment II / Compartment IV of P18-2. An overview is given in Figure 6-11 and Figure 6-12.

A closer look shows that P18-6 is disconnected from P18-2 by two faults, of which P18-6's boundary fault Fault 400 / 430 is the most important one. In between the faults a small graben is filled by overlying shale. The only contact is by Volpriehausen juxtaposition, which has a low permeability (lower than 1 mD).
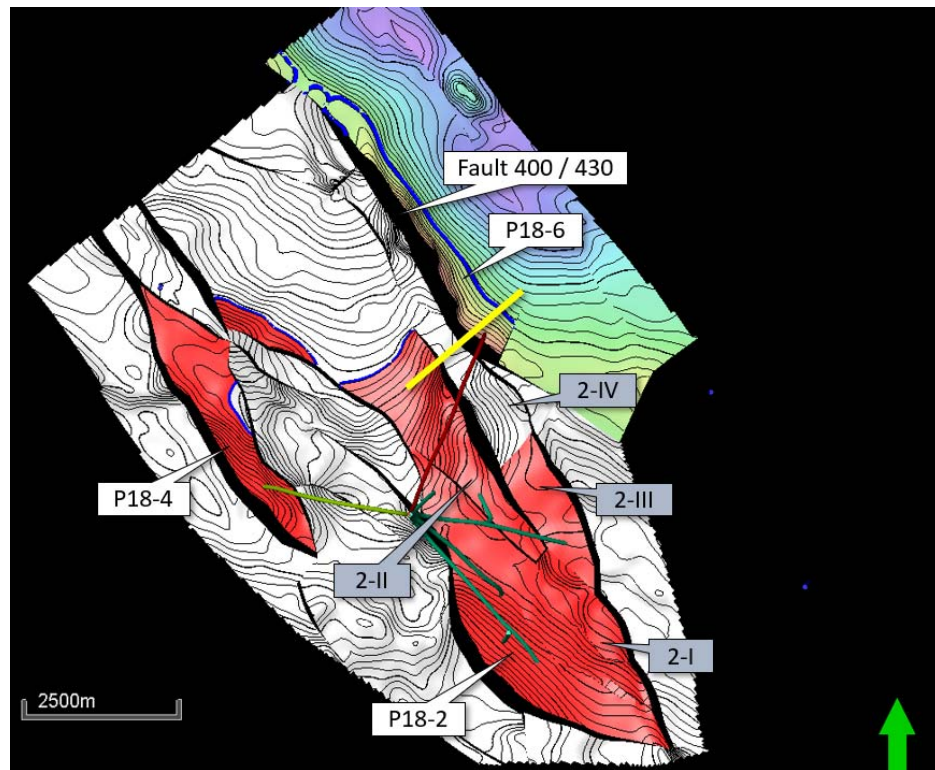
Figure 6-11: Map view of the fault between P18-2 and P18-6.
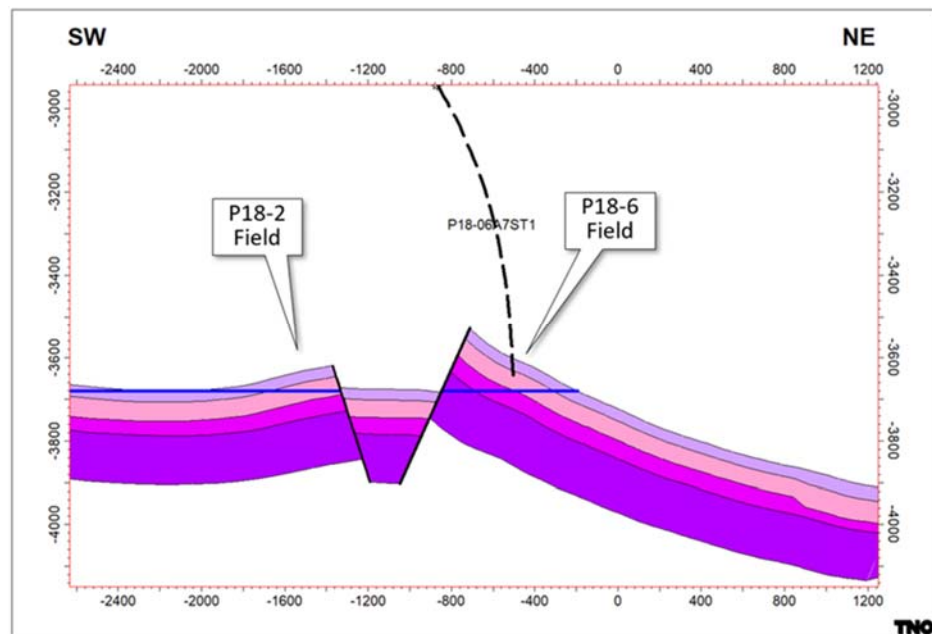
Figure 6-12:   Cross section showing fault between P18-2 and P18-6.

The first pressure value from P18-6 was recorded in the end-of-well report (EOWR), available on nlog.nl; a pressure of 378 bar was inferred, in February 2003.
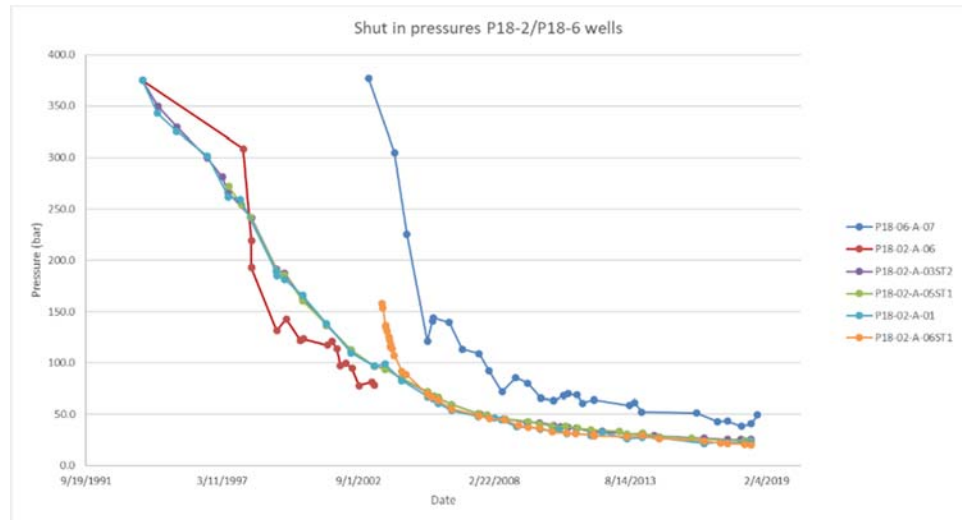
Figure 6-13: Pressure behaviour of P18-2 and P18-6 reservoirs.

The pressure data in Figure 6-13 show that after about 10 years of production from P18-2, the initial pressure found in the P18-6 reservoir was still about 275 bar higher than that in the P18-2 field. This strongly suggests that these two compartments are not in pressure communication.

In addition, during the last years of production the pressure behaviour of the main compartment (Compartment I) of P18-2 is different from that of P18-6 (see Figure 6-13), which suggests that there is no pressure communication between the two reservoirs on production time scale. However, on a geological time scale we cannot exclude pressure communication between both compartments.

6.3.7   *Conclusions*
The injection simulations lead to the following conclusions.

Storage capacity. The storage capacity of the P18-6 field is 1.3 Mt of CO_2, assuming a maximum bottomhole pressure during injection that is equal to the initial pressure (the pressure prior to production of the natural gas).

Containment. CO_2 fills the pore volume that was previously filled with natural gas. Only in a small part of the reservoir, the CO_2 moves down-dip below the original gas-water contact. Even when the reservoir is overfilled, i.e., when the average reservoir pressure increases beyond the initial pressure, the CO_2 does not move far and will move back up the slope when injection is stopped. In the north-west corner of the reservoir where a spill point is, the CO_2 does not move beyond the original gas-water contact. Thus, the conclusion is that the reservoir contains the injected CO_2, without risk of spilling.

6.4 Reservoir behaviour: temperature effect

6.4.1   *Introduction*
The simulations presented in the previous section do not take into account the temperature difference between the injected CO_2 and the reservoir, or the evolution of the CO_2 temperature in the reservoir. Water evaporation and the associated

temperature effect was also not taken into account in the previously presented results. The injection scenarios presented in Section 5.2 show that CO_2 is to be injected at a temperature well below that of the reservoir, due to pipeline transport and well operational constraints. The evolution of the temperature field within the reservoir is a key modelling result and input for the geomechanical analysis of temperature induced stress within the storage reservoir.

One of the issues with depleted gas fields in general is the relatively low pressure at the onset of injection. In combination with the low bottomhole temperature of the CO_2, additional expansion (and, hence, cooling) in the near-well zone could lead to the CO_2 entering into the hydrate formation window, potentially reducing injectivity or even preventing further CO_2 injection completely.

However, hydrate formation is not expected since the injection temperature at the bottomhole (inside the wellbore) is around 70°C (Table 6-1). Furthermore, the quality of the P18-6 field is relatively poor compared to the P18-2 field and the expected abandonment pressure is relatively high (about 40 to 60 bar). As a consequence the Joule Thomson coefficient is relatively small, which results in relatively small cooling effect in the reservoir.

In his chapter two injections scenarios are modelled with a focus on the temperature effects: the storage scenario (Section 6.4.3.1) and the discharge scenario described in Section 6.4.3.2.

The next subsections describe the simulator, the P18-6 model and the results of two injection scenarios.

6.4.2   Method

6.4.2.1   TOUGH2 simulator

The TOUGH2 simulator is used in combination with the ECO2MG module (Pruess, 2011; Loeve et al., 2014). The ECO2MG module is designed to model the behaviour of CO_2 in the presence of brine in both gas reservoirs and aquifers, including estimates of the dry out zone around the injection well where possible salt precipitation may occur. A key feature of the ECO2MG module is that it takes into consideration the transition from low to high pressure across the CO_2 saturation line, which is an important process in the injection of CO_2 into a depleted gas field.

6.4.2.2   P18-6 model

A 26-layer radially symmetric model was created (Figure 6-14) that covers the different geological formations to analyse the temperature and pressure field over time. The radial direction has 47 cells, which increase exponentially in size away from the well into the reservoir from 0.15 m to 137 m. The grid cell distribution is dense close to the well (left side of Figure 6-15) and also more dense on the interface with the Hardegsen and the caprock to allow a detailed modelling around this interface. The average porosity and permeability of the eclipse model is used in the TOUGH2 model (Table 6-5). The values are based on the history matched Eclipse model described in section 17.7.

Other parameters which are important for the temperature distribution and heat flow in the P18-6 reservoir are the heat conductivity of each formation (2.0 W/m/°C for all formations) and the rock grain specific heat (1000 J/kg/°C for all formations).

Table 6-5: P18-6 properties used in the radial symmetric model used for the modelling of the temperature field within the P18-6 reservoir.

Formation	Near Well area		Far well Area	
	Average Porosity	Average Permeability (mD)	Average Porosity	Average Permeability (mD)
Caprock	0.01	0.001	0.01	0.01
Hardegsen	0.023	0.01	0.09	24
Hardegsen-High Perm	0.09	29.6	0.2	550
Upper Detfurth	0.015	0.002	0.075	12.6
Lower Detfurth	0.015	0.002	0.075	0.29
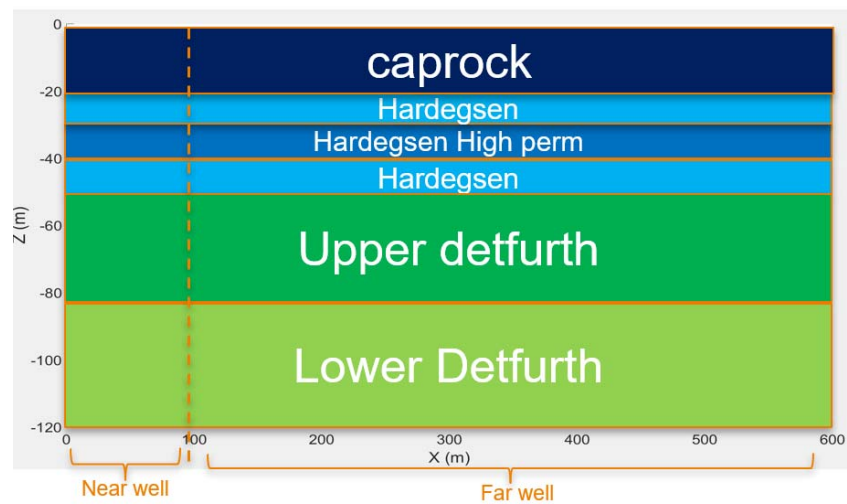
Figure 6-14: Radially symmetric model used for the modelling of the temperature field within the P18-6 reservoir.
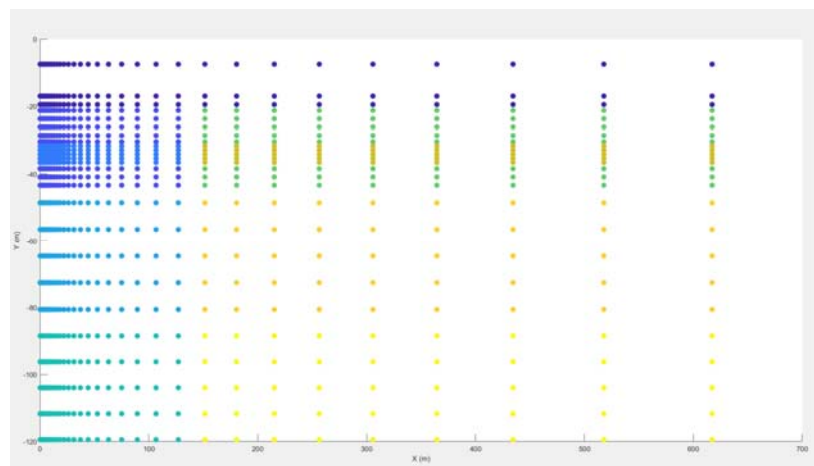
Figure 6-15: Grid cell distribution of P18-6 radially symmetric model; see also Figure 6-14.

The initial reservoir conditions used for the storage scenario are:
‒ Reservoir pressure 50 bar;
‒ Reservoir temperature 100 °C;
‒ Injection temperature 70 °C;
‒ Injection duration 5 years;
‒ Constant injection rate of 20 kg/s;
‒ Initial brine saturation varies according saturation height function shown in (Section 17: equation (17-1)).

The initial reservoir pressure of 50 bar is based on the abandonment pressure of about 52 bar in the Eclipse model (average pressure of the connected gas), see also the discussion in Section 6.3.3.

The reservoir temperature in reality is 117 °C, but the TOUHG2 simulator is limited to a maximum temperature of 103 °C; therefore a reservoir temperature of 100 °C in used in the simulations.

The injection temperature of 70 °C and injection rate is based on the flow assurance simulations (Section 6.2). The injection rate of 0.63 Mt/yr corresponds to constant injection rate of 20 kg/s.

Since the reservoir simulations (see section 6.3.3) showed that most of the CO_2 migrates into the high-permeability part of the Hardegsen Fm upon injection and almost none migrates into the Hardegsen Fm Upper and Lower Detfurth Fm, the injection rates in the thermal simulations were distributed only in the high-permeability layers of the Hardegsen Formation.

6.4.3   Results

6.4.3.1   The storage scenario

The temperature distribution and profiles from the modelling for the storage scenario are presented in Figure 6-16 to Figure 6-19, The CO_2 is injected in the high-permeability Hardegsen Fm. The cold zone is demonstrated to be progressing up to 200-250 m into the reservoir in Figure 6-16. In the vertical direction the temperate front is extending symmetrically around the injection area. After four years of injection a few degrees cooling is observed 20m above the bottom of the caprock (Figure 6-17). Just below the caprock a maximum cooling of 15 °C is observed (Figure 6-18). These effects are caused by thermal conductivity of the rock, since almost all CO_2 is in the high-permeability Hardegsen Formation. The Joule-Thomson effect and cooling due to the evaporation of water is only present in the high-permeability Hardegsen Formation (Figure 6-19); the injected CO_2 of 70°C cools down to just below 55°C. The temperatures in the model shows no risk of hydrate formation.

The distance of the fault in P18-6 to the injection well P18-A-7-S1 is 100m. The temperature change at the fault and associated stress changes (see section 7.3 and 7.5) becomes noticeable about 70 days after the start of injection (Figure 6-20). The temperature contrast at the low-temperature front is 30 °C in the TOUGH2 simulations and taking into account that the reservoir temperature is

17 °C higher than can be represented in the TOUGH2 model, the actual
temperature contrast at the low-temperature front is close to 50 °C.
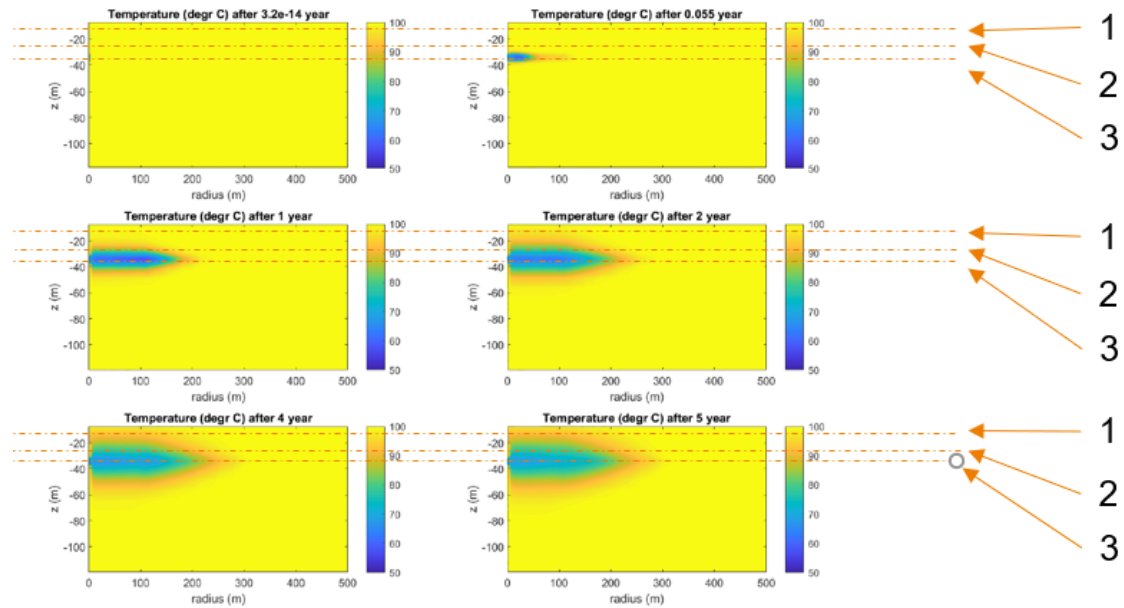
Figure 6-16: Temperature distribution in the P18-6 radially symmetric model for the storage
scenario. The numbers indicate three vertical levels in the model: level 1 is 20 m above
caprock/Hardegsen interface, level 2 is 2.5 m below caprock/Hardegsen interface and level
3 is 60 m below caprock/Hardegsen interface. 0.055 years is 20 days.
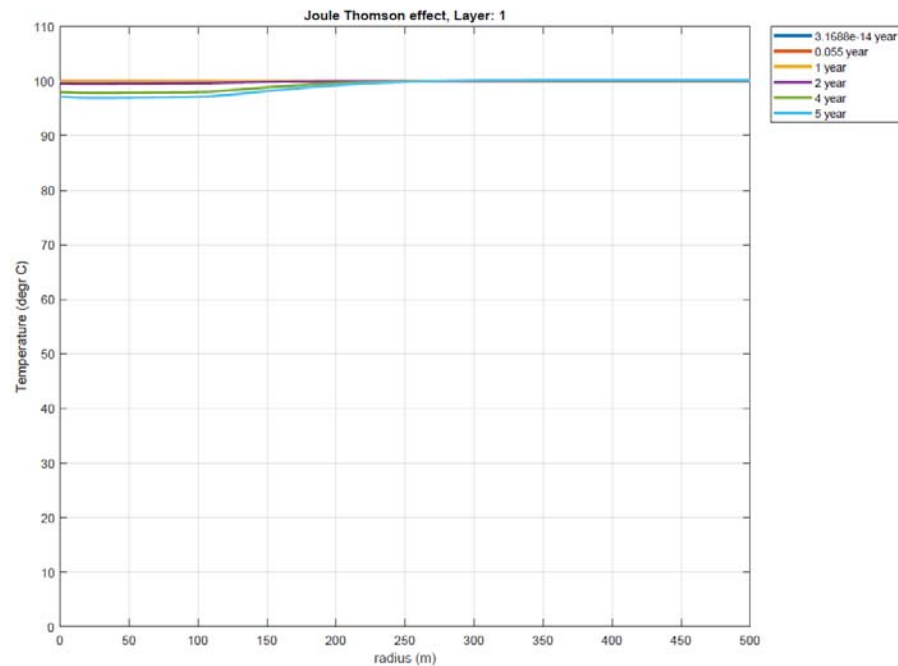
Figure 6-17: Temperature profile in the maximum injection rate scenario for level 1, which is 20 m
above the caprock / Hardegsen interface.
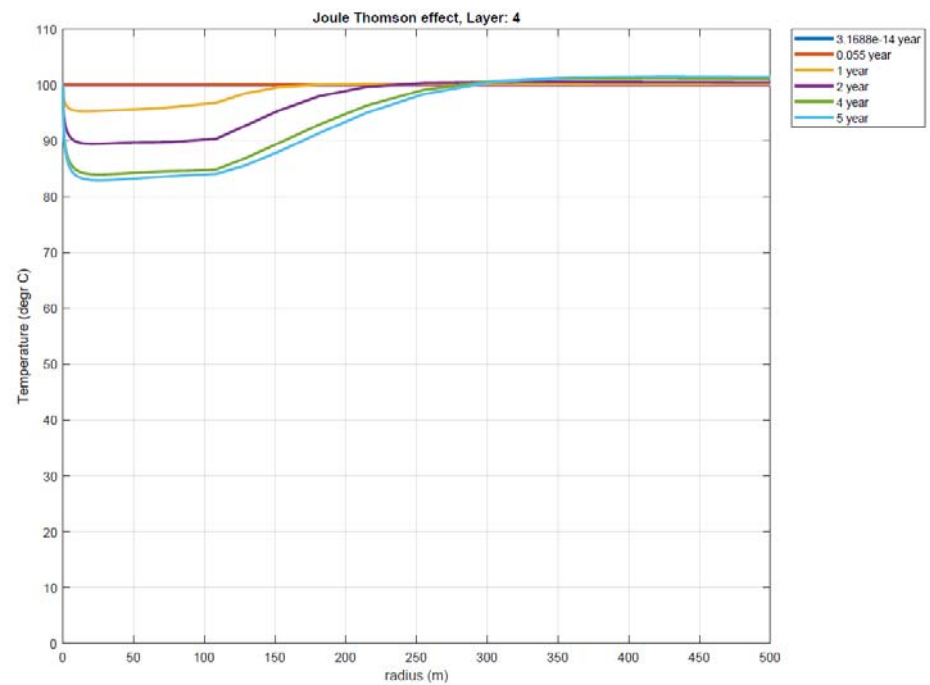
Figure 6-18: Temperature profile in the maximum injection rate scenario for level 2, which is 2.5 m below the caprock / Hardegsen interface.
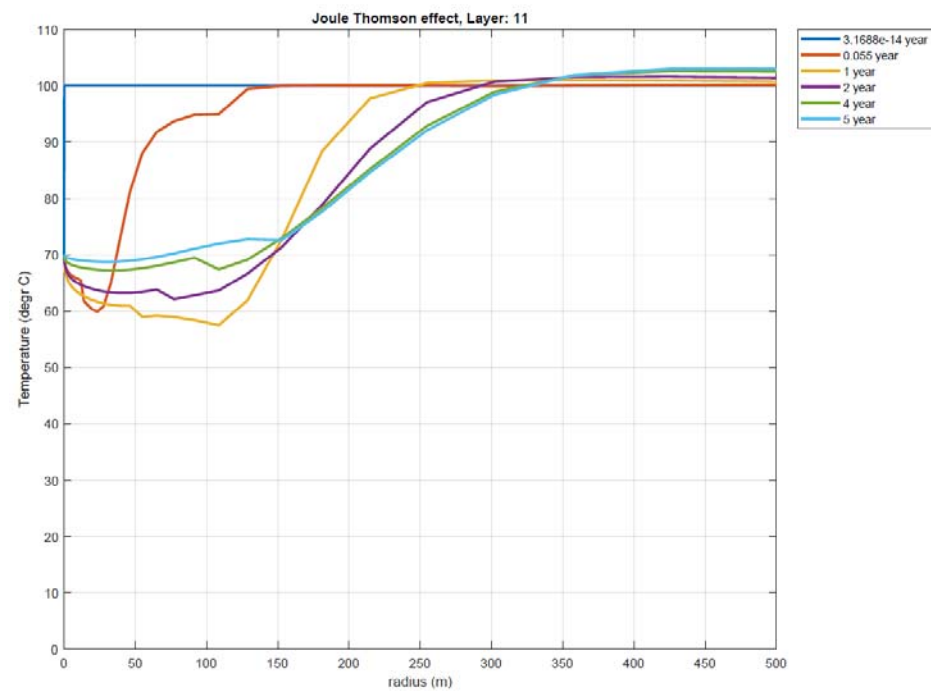
Figure 6-19: Temperature profile in the maximum injection rate scenario for level 3, which is in the middle of the high-permeable Hardegsen Fm.
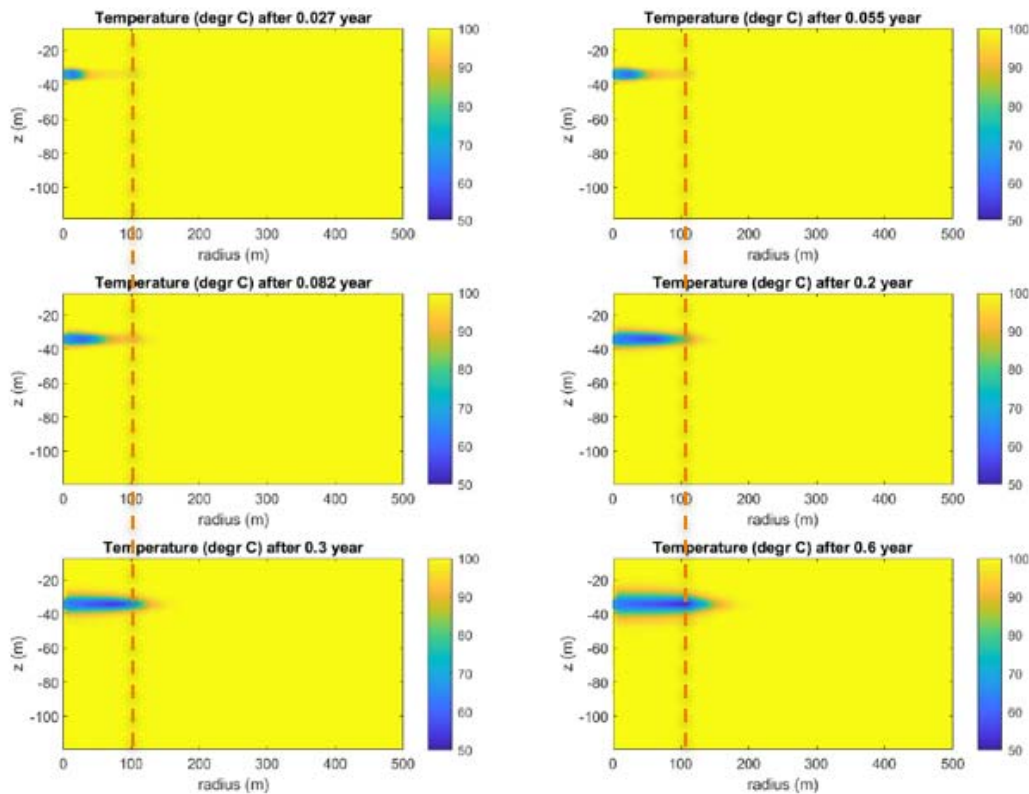
Figure 6-20:   Temperature distribution in the P18-6 radially symmetric model for the storage
scenario. The orange dashed line is the 100m from the injection well, corresponding to the
closest fault to the P18-6-A7 well. After 70 days (0.2 years) the cold CO_2 front arrives at the
this fault.

6.4.3.2   The discharge scenario

The discharge scenario models a start-up after a shut-in of the pipeline. During the
start-up cold CO_2 (10°C) is injected into the P18-6 reservoir. This section estimates
the impact of discharging the CO_2 into the P18-6 reservoir with regards to cooling
and the location of the cold front.

The total mass of CO_2 in the a 21 km pipeline with a diameter of 16 inch is 2.8 kt [6].
This value was derived assuming that injection starts when the pipeline has been
brought back to a pressure of 85 bar; the average temperature in the pipeline will be
close to 10 °C. The 2.8 kt is an overestimation of the total volume of cold CO_2.

The initial reservoir conditions used for the discharge scenario are:
−   Reservoir pressure 60 bar;
−   Reservoir temperature 100 °C;

---

[6] Based on CO_2 density of 907 kg/m^3 at 85 bar and 10°C, which is the assumed pressure and
temperature of the pipeline.

- Injection temperature 46.3 °C; (see section 6.2)
- Constant Injection rate of 23.2 kg/s;
- Injection duration 1.4 days is needed to empty the total pipeline filled with CO_2;
- Initial brine saturation varies according saturation height function (equation (17-1).

The temperature distribution of the discharge scenario is shown in Figure 6-21. The pipeline is fully discharged after 1.4 days at which time the cold front is at about 15 m from the well. The maximum additional cooling is 6°C (i.e. a reservoir temperature of 40°C). After 1.4 days injection stops and it takes about 1.5 years for the cold front to disappear through heat influx from the surrounding formations.
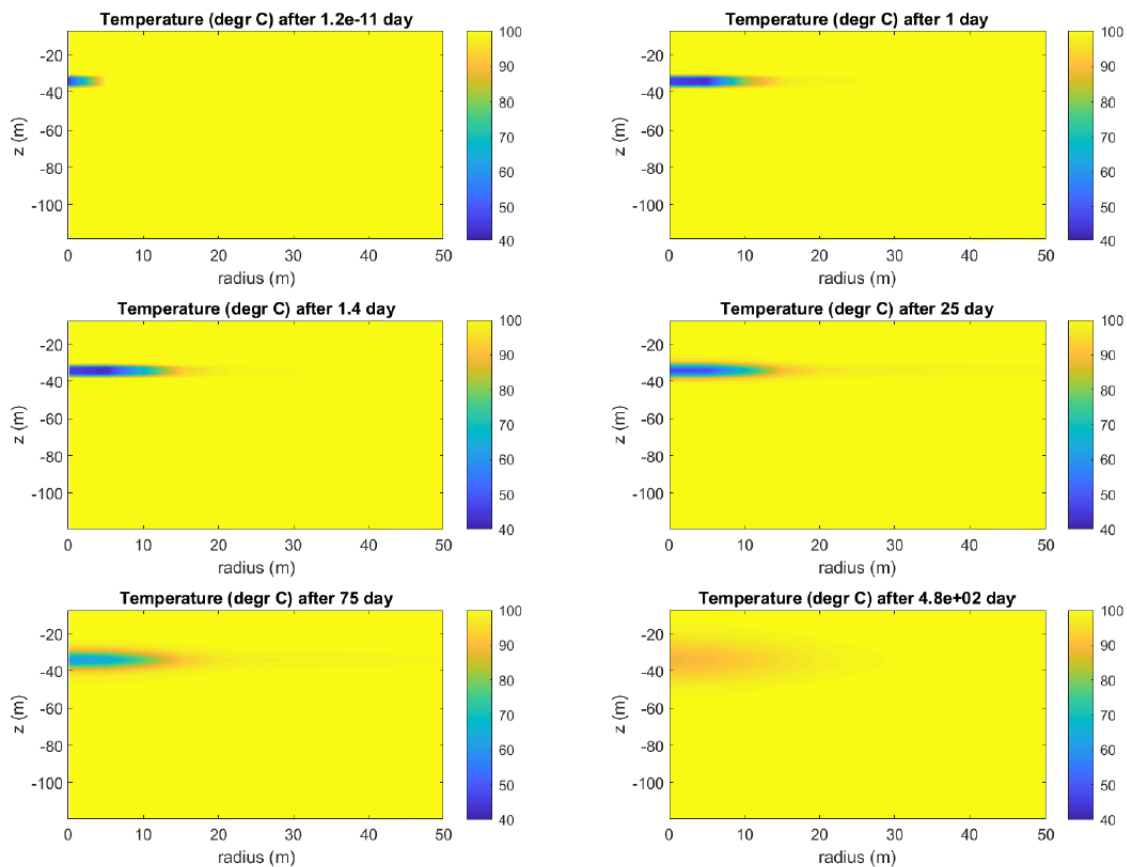
Figure 6-21: Temperature distribution of the discharge scenario. After 1.4 days of injection a cold front of ± 15m develops. The minimum temperature observed is 40°C, which corresponds to a maximum cooling of 6.3°C, since the injection temperature is 46.3. After 1.4 days of injection the reservoir starts to equilibrate and after 1.3 years (480 days) the CO_2 is almost at initial reservoir temperature.

6.4.4   Discussion

The cold front of CO_2 and the fluid itself propagates mainly in the high-permeability Hardegsen Fm. The temperature effect in the vertical direction is mainly due to thermal conductivity. At a continuous injection rate of 20 kg/s, the cold front reaches the fault closest to the well; the temperature contrast at the front is about 50 °C.

On the other hand if the purpose of the P18-6 reservoir is to discharge cold CO_2 in the pipeline, the cold front reaches 20 m from the well after a single discharge and a temperature change close to the P18-6 faults is not expected.

Hydrate formation is also not expected in P18-6 since the downhole pressure and temperature ranges expected are outside the possible hydrate formation window.

6.4.5   *Conclusions*
The TOUGH2 simulations used a simplified, radial symmetric model, which demonstrated that the temperature effects of injecting cold CO_2 result in the following conclusions.

– Near-well temperatures and pressures are outside the hydrate zone. No injectivity impairment due to clogging of the reservoir due to hydrates is expected.
– CO_2 injection at a constant rate of 20 kg/s and a temperature of about 70 °C results in a cold front that progresses to about 200 m into the reservoir. The temperature contrast at the front is about 50 °C.
– At the same injection rate and temperature, the cold front reaches the nearest fault after about 70 days.
– Progression of the cold front in a single discharge of the cold pipeline contents is of the order of 20 m.

More detailed reservoir simulations with a more advanced, non-isothermal reservoir simulator are needed to improve predictions regarding:
– the temperature development near the injection wells;
– the temperature development near existing faults, taking into account the geometry of reservoir and faults;
– the post-injection reservoir pressure related to temperature equilibration on the long term.

6.5 Chemical interactions

6.5.1   *Introduction*
Within the reservoir, physical and chemical interactions between the CO_2, the formation water and rock minerals will occur during and after CO_2 injection. On the short term, during the injection phase, the risk of porosity and permeability decrease and corresponding injection issues needs to be evaluated. In the long term, during the post-decommissioning phase, the CCS Directive (EU, 2009) requires evaluation of the fate of CO_2, for which geochemical reactions play an important role. This section describes the short-term (injection phase) and long-term (post-decommissioning phase) CO_2-water-rock interactions and their impact on the feasibility of CO_2 injection and storage in the P18-6 reservoir, using recent literature.

6.5.2   *Injection phase: Effect of dry-out and salt precipitation on injectivity*
During the injection of dry CO_2, (residual) formation water will evaporate into the CO_2 in the near-well area. A dry-out zone will develop which can extend up to several tens of meters into the reservoir. As the mass of water decreases the concentration of the aqueous species increases and minerals start to precipitate when the remaining water becomes saturated (Miri and Hellevang, 2016). The most

common mineral to precipitate is halite salt (NaCl), since formation waters contain mostly Na^+ and Cl^-, although other minerals such as sulphates or hydroxides can also form. Salt precipitation during CO_2 injection and the corresponding permeability reduction and injectivity issues have been studied in the laboratory and by numerical simulations for the purpose of CO_2 storage in saline aquifers (e.g. Bacci et al., 2011, Kim et al., 2012, Roels et al., 2014). Field evidence of salt precipitation and injectivity impairment was obtained from the Ketzin injection pilot in Germany (Baumann et al., 2014) and the Snøhvit storage site in Norway (Grude et al., 2014). The key parameter that would allow for salt precipitation to result in permeability and injectivity impairment is the availability of saline water for capillary backflow (migration of salt water towards the injection well) and hence a continuous supply of salt. In the absence of capillary backflow of saline water, the maximum amount of salt precipitation is constrained by the volume of residual formation water and the concentration of aqueous species. The available species will then precipitate as thin coatings around the rock grains in the space that was occupied by the residual brine, without significantly affecting the permeability.

In the P18-6 reservoir the water saturation at the beginning of CO_2 injection will be close to residual and hence it will be immobile. This is supported by the lack of (significant) water (brine) production during the production history of the field (see P18-6 production data at www.nlog.nl). As a result, capillary backflow of brine during injection will not occur. Production data did not give any evidence for the presence of a strong aquifer support, implying that brine supply from below is also not expected to occur. Tambach et al. (2015a) report on the modelling of CO_2 injection into a depleted gas reservoir (based on P18 characteristics) and the effect on salt precipitation. The report showed that in the case of immobile brine the maximum amount of salt precipitation was 2.7% of the pore volume, with a corresponding permeability decrease of 23%. It should be noted that the extent of permeability decrease upon a reduction in porosity is highly uncertain, but much higher values than 23% are not to be expected. With permeability values as high as those of the P18-6 reservoir, injectivity impairment by this amount of salt precipitation is not expected to occur. The temperature decrease in the near well area related to the low temperature of injected CO_2 will not have major impact on the extent of salt precipitation.

Another effect resulting from the formation of a dry-out zone is that the relative permeability of CO_2 increases when the water saturation decreases. Hence, the absolute permeability reduction due to salt precipitation could be (partially) counteracted by the increased relative CO_2 permeability (Miri and Hellevang, 2016).

6.5.3   *Injection phase: CO_2-water-rock interactions*
When CO_2 is injected into the reservoir, it will try to form a new physico-chemical balance with the (residual) formation water. The water starts to evaporate into the dry supercritical CO_2 (scCO_2), as described in the previous section, and CO_2 starts to dissolve into the formation water. In the near-well area, the dry-out zone will progress quickly, leaving no formation water for CO_2 to dissolve in. Beyond the progressing dry-out zone, CO_2 dissolves into the formation water and further dissociates by the following reactions:

$$CO_2(g) + H_2O_{(l)} \leftrightarrow H_2CO_{3(aq)} \leftrightarrow H^+ + HCO_3^- \leftrightarrow 2H^+ + CO_3^{2-}$$
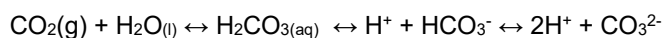
These reactions result in an increased acidity of the formation water and a disequilibrium with the rock mineralogy. Both experimental and modelling studies show that on the short term the main result is the partial dissolution of carbonates, and potentially sulfides and sulphates, to buffer the pH. Of the carbonates, calcite dissolution is fastest, while the dissolution of other carbonates such as dolomite and ankerite is much slower. The mineralogy of the P18-6 reservoir will be very similar to the mineralogy of the P18-2 reservoir, the latter being reported in the core analysis report for P18-A-01 (P/18-3 well), and consists of mainly quartz, with lower amounts of K-feldspar, albite, plagioclase, dolomite, and clay minerals. Only occasionally anhydrite or calcite have been found, and only in small amounts.

Equilibrium batch reaction modelling with PHREEQC software, performed for the feasibility study of P18 in the CATO-2 project, predicted the dissolution of very small amounts of dolomite and pyrite, with negligible amounts of anhydrite and dawsonite precipitation (Vandeweijer et al., 2011). These reactions present a worst case scenario as the simulation was based on equilibrium modelling and did not consider kinetics. Also, these reactions would not occur in the near well zone where dry-out would occur.

Given that the worst case conditions predict negligible impacts on porosity (and hence on permeability), in the reservoir beyond the dry-out zone from CO_2-water-rock interactions it can be concluded that geochemical interactions will not negatively impact on injectivity.

6.5.4   *Post-decommissioning phase: CO_2-water-rock interactions*
In the long-term, during the post-decommissioning phase, the conditions in the reservoir will slowly move towards a chemical equilibrium. This implies that silicate minerals will also have time to respond to the change in chemical equilibrium as a result of the high CO_2 partial pressure and partial CO_2 dissolution into the residual formation water beyond the dry-out zone. Since only residual (and thus immobile) formation water is present in the reservoir, a chemical equilibrium will only be obtained on the micro-scale; ions in the formation water can migrate by diffusion through the film of formation water as long as the film is connected. The scale on which formation water is connected is unknown and highly depends on the microstructural characteristics of the rock. Regardless of the scale of connection, diffusion of ions will be very slow, making it most likely to have chemical equilibrium on microscale only. The limited amount of water further slows down the reactions as water acts as a facilitator for the dissolution-precipitation reactions.

Tambach et al. (2015a) performed simulations with TOUGHREACT to predict long-term mineral reactions and sequestration of CO_2 in carbonate minerals for the P18 reservoir. A key uncertainty in the simulations is whether or not to include dawsonite as a secondary mineral. Dawsonite is a controversial carbonate mineral which, if included in geochemical simulations, is predicted to sequester a large part of the CO_2 in the long term. It is controversial as this mineral is only rarely found in natural CO_2-rich reservoirs, and if present, only in minor amounts. Most probably, the thermodynamic data in the chemical databases are incorrect, and therefore, dawsonite should not be included in geochemical modelling of CO_2 storage. Also the possibility of magnesite precipitation as a secondary mineral was questioned. In the chemical initialization of the reservoir formations, both dawsonite and magnesite were predicted to be present as initial minerals. Since they were both not measured

in any of the P18 reservoir samples analysed, it can be questioned whether the chemical database contains correct chemical constants for these minerals.

Simulations for long-term CO_2-water-rock interactions were performed with and without dawsonite and magnesite as secondary minerals. In both cases, long-term mineral reactions include the partial reaction of albite, K-feldspar and kaolinite to form illite. In the scenario which includes dawsonite and magnesite as secondary minerals the largest part of the CO_2 is predicted to be trapped in carbonate minerals within a few thousand years. In the simulation excluding dawsonite and magnesite as secondary minerals, leaving only calcite and dolomite as potential secondary carbonates, no CO_2 is predicted to be sequestered in carbonate minerals after equilibrium is reached within 10,000 years. Limited CO_2 partial pressure decrease from 365 bar after well closure to 300, 315 and 341 bar for the lower Detfurth, Upper Detfurth and Hardegsen Formation respectively is predicted after 10,000 years. This is related to a slight overall porosity increase due to dissolution-precipitation reactions. More than 95% of the CO_2 remains in the reservoir in the supercritical state.

Studies on natural analogues rarely report on the occurrence of dawsonite, and if present, it is only present in very small amounts. Natural analogues include occurrences of CO_2-rich gas reservoirs in which the CO_2 has had thousands to millions of years to reach chemical equilibrium with the reservoir formation water and mineralogy. These reservoirs therefore present a unique opportunity to study the long term fate of CO_2 in a depleted hydrocarbon reservoir and validate geochemical models. The absence of large amounts of dawsonite in natural analogues suggests that dawsonite precipitation in geochemical simulators is not well defined.

Two major studies on natural analogues in the US and the UK show that in most cases negligible trapping in carbonate minerals occurred (Baines and Worden, 2004; Gilfillan et al., 2009), which is most likely due to the slow dissolution of silicate minerals which is a rate-limiting step (Baines and Worden, 2004). The study by Gilfillan et al. (2009) identified solubility trapping as the primary sink for the natural CO_2 fields analysed, but this is only possible in case of sufficient availability of formation water, which is not the case in depleted hydrocarbon fields without strong aquifer supports such as the P18-2 reservoir. Based on the insights obtained from natural analogues, the scenario by Tambach et al. (2015b) excluding dawsonite and magnesite as secondary minerals provides a more realistic prediction of the long-term fate of CO_2. We can conclude that almost all of the injected CO_2 will remain in the supercritical state for thousands of years.

6.6 Conclusions

The injection simulations lead to the following conclusions.

Storage capacity.
The storage capacity of the P18-6 field is 1.3 Mt of CO_2, assuming a maximum bottomhole pressure during injection that is equal to the initial pressure (the pressure prior to production of the natural gas).

Containment.
CO_2 fills the pore volume that was previously filled with natural gas. The CO_2 only moves down-dip below the original gas-water contact in a small part of the reservoir. Even when the reservoir is overfilled, i.e. when the average reservoir pressure increases beyond the initial pressure, the CO_2 does not move far and will move back up the slope when injection is stopped. In the north-west corner of the reservoir where a spill point is, the CO_2 does not move beyond the original gas-water contact. Thus, the conclusion is that the reservoir contains the injected CO_2, without risk of spilling.

Near-well hydrate formation
Hydrate formation is not expected in P18-6, since the downhole pressure and temperature ranges expected are outside the possible hydrate formation window.

Near-well chemical clogging
Injection of CO_2 into the reservoir will cause drying out of the reservoir and the precipitation of salt. This is not expected to lead to clogging of the near-well area but should clogging occur, there is no impact on storage safety or security.

Temperature effects
The injection of CO_2 at low temperature into the P18-6 gas field must be modelled in detail prior to the start of injection as the cold CO_2 will affect bottomhole pressure during injection. The pressure in the reservoir will slowly increase as the CO_2 in the reservoir gradually reach initial reservoir temperature. The magnitude of these effects has been estimated in this study; a more detailed analysis is needed prior to the start of injection.

Long-term reservoir integrity
No significant interactions between the CO_2 and the reservoir are expected. CO_2 is expected to remain in supercritical state in the reservoir for a period of the order of thousands of years.

7 Fault stability

7.1 Introduction

This section focuses on the evaluation of the potential of destabilization of intra-reservoir faults identified in the seismic cube and mapped in the static and dynamic models.

The P18 reservoirs, including the P18-6 reservoir, that have been assigned as potential storage reservoirs are fault bounded. These faults are sealing: the compartments are hydraulically isolated from their surroundings due to juxtaposition of the reservoir against impermeable shales. This section investigates the stability of these faults, in both geomechanical terms and geochemical terms. Fault stability in relation to reservoir re-pressurisation is discussed in Section 7.2, then in relation to the low temperature of the injected CO_2 in Section 7.3 and finally in relation to geochemical effects of CO_2 in Section 7.4.

The overall conclusion from the work presented in this section is that the risk of fault reactivation due to the injection of CO_2 is low.

The increasing reservoir pressure, as a result of injecting CO_2 stabilizes the faults that bound the P18-6 field. CO_2-related geochemical effects in fault zones are unlikely to lead to reactivation of the faults, or to CO_2 migration along faults.

If low-temperature CO_2 (the temperature can be about 60 °C cooler than the reservoir temperature) reaches a fault, the fault can be locally destabilized. This risk can be mitigated by monitoring and, if necessary, reducing the injected amount of CO_2 through wells that are close to bounding faults. Further analysis is needed to define the risk and mitigation requirements in more detail.

7.2 Fault stability: pressure effect

To study the effects of pressure changes on intra-reservoir fault reactivation we use MACRIS (Mechanical Analysis of Complex Reservoir for Induced Seismicity), a TNO-developed semi-analytical approach which allows us to evaluate both the poro-elastic effect and the direct pressure effect on stresses along the mapped faults.

Details of MACRIS are given in Section 17.8. The required input for running MACRIS is the ECLIPSE reservoir grid with the flow simulations detailed in Section 6. Taking the ECLIPSE reservoir flow simulations as inputs MACRIS directly computes the stress induced by both the poro-elastic effect (i.e., the reservoir contraction/dilation due to depletion/injection of gas) and the direct pressure effect (i.e., the changes in effective normal stress due to the changes in pore pressure inside the faults). It is important to mention that MACRIS captures the effect of the differential compaction between two offset compartments. For the direct pressure effect, the average pore pressure between the two juxtaposed reservoir compartments at faults has been assumed.

It is not needed to rebuild a new geomechanical mesh with MACRIS as it directly works with the grid of the flow simulation (ECLIPSE). This way, MACRIS is extremely fast. Moreover, it allows the evaluation of stresses in 3D along all the mapped faults with high resolution.

For a simplified 3D single-fault tank reservoir model, the MACRIS stress solution has been compared with the solution given by the Diana FE (Finite Element) simulator. The results are presented in Section 17.8.1 and clearly demonstrate the almost perfect match between MACRIS and the FE solution. It is important to keep in mind that it would not be possible to use an FE approach for the 3D evaluation of the stresses along the multiple faults of the P18-6 field. Only 2D cross-sections, as performed in the previous P18 study (Vandeweijer et al., 2011), can be performed. Having access to the Coulomb stress distribution in 3D along the fault planes with MACRIS is extremely advantageous, since the along-strike variability is accessible and the area of excess Coulomb stress can be quantified. This area of excess Coulomb stress is key to evaluate the risk of fault reactivation.

All the input parameters used for MACRIS are listed in Table 6-1 and are the same as the ones used for the P18-2 field (Neele et al., 2019). One unique set of model parameters has been used in the present analysis and thus the parameter sensitivity search has not been performed. The stress changes computed in MACRIS must be added to the initial stress tensor. In the West Netherlands Basin the minimum in situ stress is horizontal and the stress regime is extensional or normal-faulting (i.e. the largest principal stress is vertical). The largest vertical stress ($S_v = S_{max}$) is calculated as the overburden weight from seawater, rock, and pore fluid densities (see Table 7-1). The orientation of the minimum horizontal stress Sh, determined from borehole breakouts and the World Stress Map, is 55° (N55E). The magnitude of Sh is defined by applying the ratio of horizontal-to-vertical effective stress Ko' = Sh'/Sv'; a value of Ko' = 0.63 is used for the analysis. Finally, the magnitude of the maximum horizontal stress SH is defined by the ratio Sh/SH=0.9. It is important to note, that a single unique value of each of the parameters controlling the in-situ stress conditions (notably the orientation of Sh, Ko' and Sh/SH) is used for the geomechanical analysis. In other words, a parameter sensitivity search has not been carried out. However, the input parameter values are aligned with the ones used in the geomechanical analysis of Vandeweijer et al. (2011) and the previous P18-2 study (Neele et al., 2019).

Table 7-1   Input model parameters used for the MACRIS semi-analytical approach.

MACRIS model parameters	
Sh orientation	N55E
Ko' = Sh'/Sv'	0.63
Sh/SH	0.9
ρ_{rock}	2260 kg/m^3
ρ_{water}	1150 kg/m^3
ρ_{gas}	200 kg/m^3
E_reservoir (Young's modulus)	18 GPa
E_overburden (Young's modulus)	25 GPa
E_underburden (Young's modulus)	28 GPa
υ *(Poisson's ratio)*	0.2
μ *(friction coefficient)*	0.6
α *(Biot's coefficient)*	1.0

From the new full stress tensor, including the induced stress changes, one can derive the shear stress τ and effective normal stress σ' for any fault orientations. In order to assess the potential reactivation of a fault, both stresses need to be combined, the shear stress promoting slip whereas the normal is clamping the fault. One convenient way to calculate this is using the Coulomb stresses C or the Fault Shear Capacity (FSC), respectively defined as:

$$C = \tau - \mu\sigma' \qquad\qquad (7\text{-}1)$$

$$FSC = \frac{\tau}{\tau_{max}} = \frac{\tau}{\mu\sigma'} \qquad\qquad (7\text{-}2)$$

where $\mu = 0.6$ is the friction coefficient. When C starts to be positive or alternatively FSC reaches unit, a pre-existing fault can be reactivated since the shear stress is larger than the frictional strength defined as $\mu\sigma'$.

Figure 7-1 displays the initial negative Coulomb stresses (see equation (7-1) for the definition of the Coulomb stress) computed by MACRIS before any pressure depletion. In MACRIS, the along-fault stresses are evaluated along fault pillars (see Section 17.8.1 for more details) as shown in Figure 7-1. In the previous P18-2 study (Neele et al, 2019), this along-pillar discrete stress distribution was interpolated over a regular grid; here the initial discrete stress distribution is displayed. For all the faults and at any locations along these faults, the initial Coulomb stresses are mostly negative and around minus 10-15 MPa (Figure 7-1). These negative Coulomb stresses represent the initial distance to failure, that is the required additional Coulomb stresses for the faults to be reactivated.
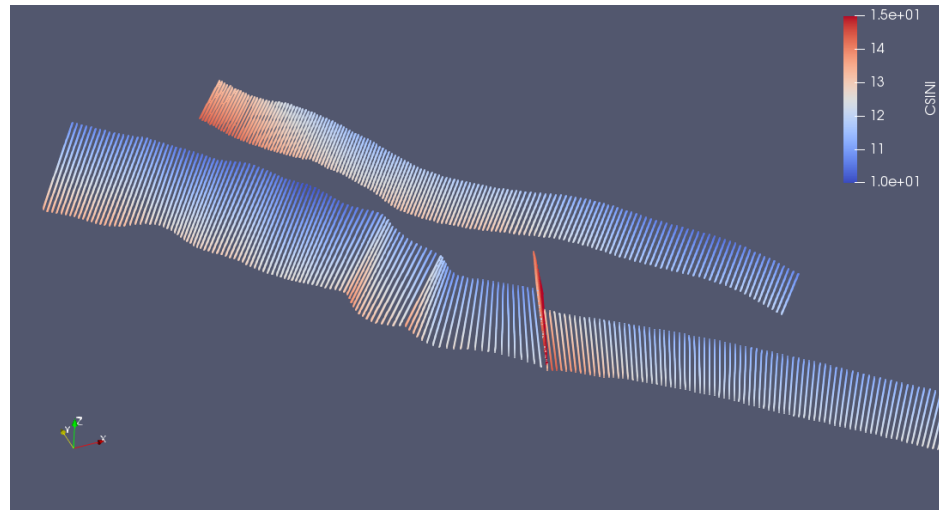
Figure 7-1   Initial distance to failure along the P18-6 faults. Colours indicate the negative Coulomb stress in units of MPa at the initialization of the MACRIS analysis, that is before any pressure depletion.

At the end of the depletion period elongated areas of large positive Coulomb stress changes along the strike direction can be localized at the reservoir edges (see Figure 7-2). These elongated areas of high positive Coulomb stress changes

reduces during the injection phase (see Figure 7-3). Figure 7-4 indicates that these elongated areas of high positive Coulomb stress changes (at the edge of the depleting part of the reservoir) exceed the failure line at the end of the production period, meaning that potentially the concerned fault could be reactivated. However, as observed in Figure 7-4, most of the Coulomb stress peaks exceeding the failure line are expected to disappear during the injection period. The fault pillar displayed in Figure 7-4 is of particular interest, because it is close to a well. This aspect is further discussed in Section 7.3 when the temperature effect is assessed.
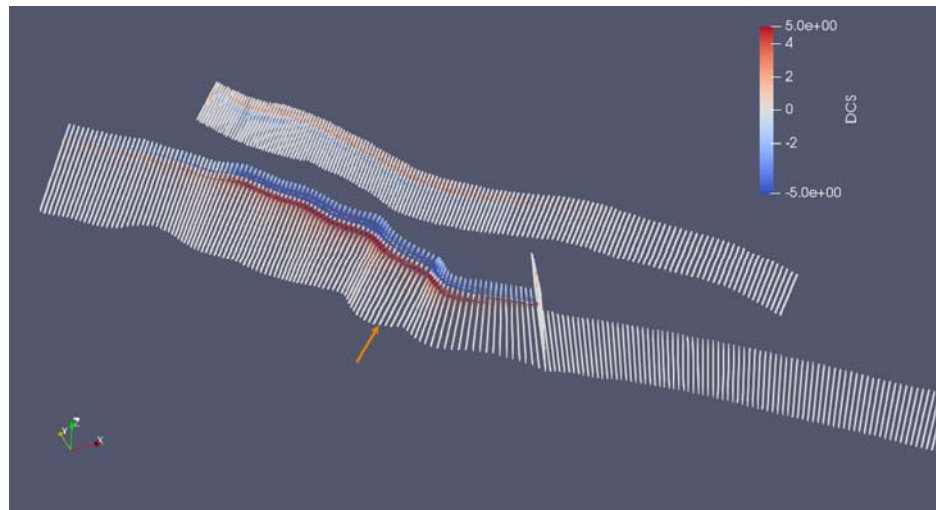
Figure 7-2   Changes in Coulomb stresses (MPa) along the P18-6 faults at the end of the production period inferred from MACRIS analysis. The orange arrow indicates the fault pillar where the stress and pressure changes are displayed in Figure 7-4.
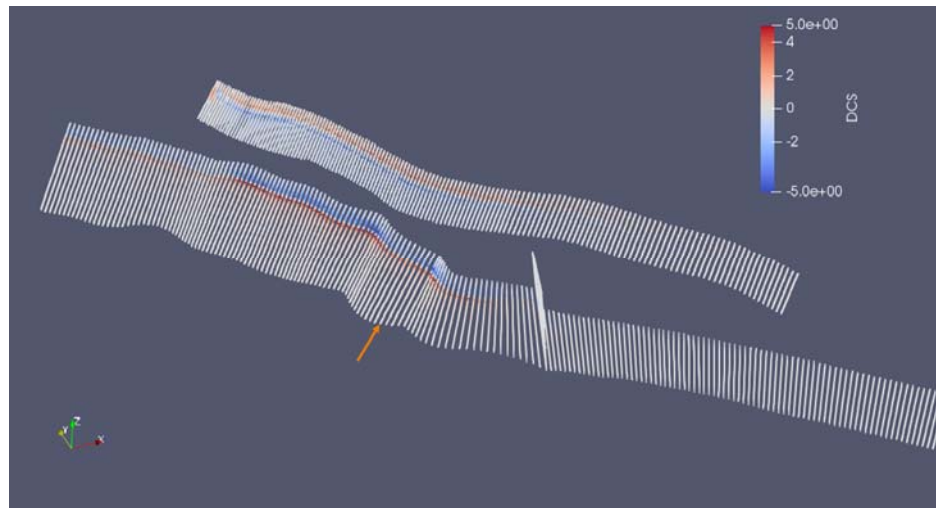
Figure 7-3   Changes in Coulomb stresses (MPa) along the P18-6 faults at the end of the injection period inferred from MACRIS analysis. The orange arrow indicates the fault pillar where the stress and pressure changes are displayed in Figure 7-4.
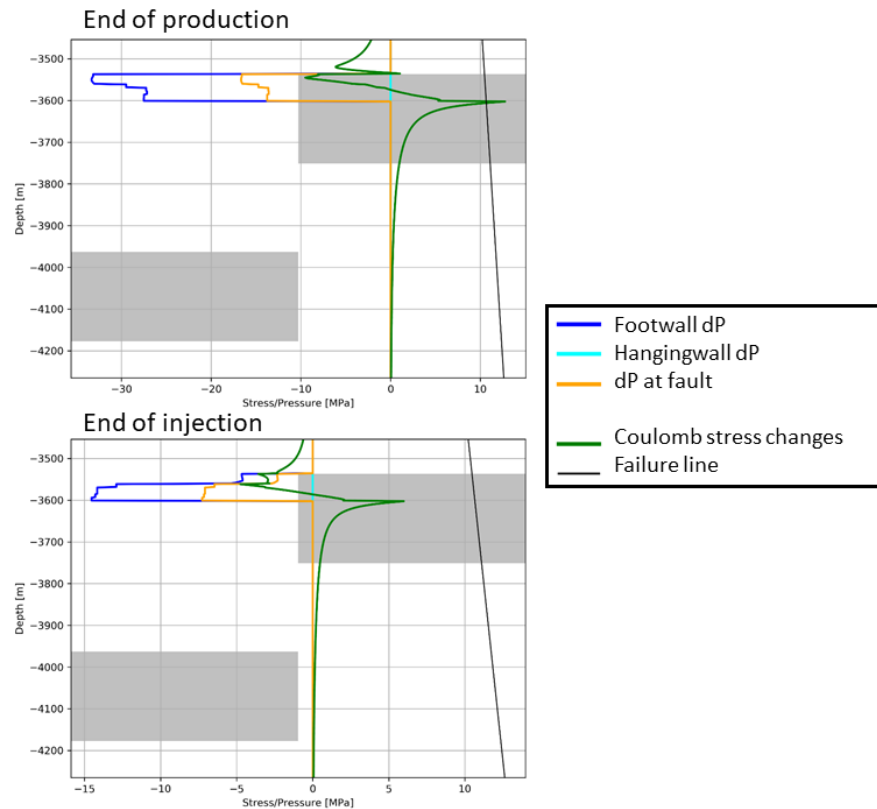
Figure 7-4 Changes in Coulomb stresses and pore pressures (inferred from MACRIS analysis) along one representative fault pillar (location of this pillar is indicated in Figure 7-2 and Figure 7-3. "Footwall dP" and "Hangingwall dP" represent the changes in pore pressure in the reservoir grid blocks juxtaposed to the fault in the footwall compartment and in the hanging wall compartment, respectively. "dP at fault" corresponds to the pore pressure inside the fault, taken as the average pressure between "Footwall dP" and "Hangingwall dP". The two grey rectangles delineate the two offset reservoir compartments. At the end of the production period, changes of Coulomb stresses exceed the failure locally at one reservoir edge. This Coulomb stress peak decreases during the injection period. For the sake of visibility, the ranges of the x-axis have been separately adjusted for each graphs.

Figure 7-5 is complementary to Figure 7-2 and Figure 7-3, giving access to the 3D along-strike variability of the likelihood of fault reactivation occurring. Figure 7-5 confirms that at the end of the injection period most (if not all) of the areas where the Fault Shear Capacity FSC (equation (7-2)) is exceeded, present at the end of the depletion period, disappear. Considering solely the pressure effect, the faults are thus expected to be stable at the end of the injection period. This conclusion would only be disputed in the case of either (1) direct injection inside a reservoir fault or (2) direct flow communication between the well and a reservoir fault. Assuming we are not missing pre-existing faults in the structural reservoir model, this study confirms that injection inside a reservoir fault is not occurring.
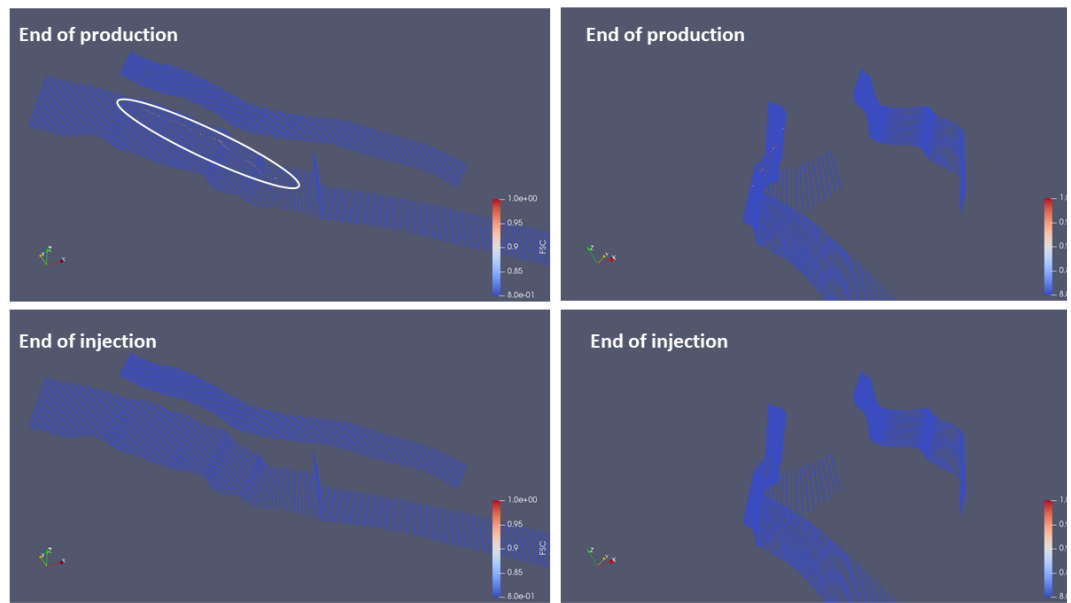
Figure 7-5	Fault Shear Capacity (FSC) along the P18-6 faults inferred from MACRIS analysis. At the end of the production period, the Fault Shear Capacity exceeds unity only very locally (at the reservoir edges and highlighted by the white ellipse) meaning that the shear stress is larger than the frictional shear strength ("max shear stress"). During the injection period, these very local areas of exceedance of the frictional shear strength disappear.

## 7.3	Fault stability : temperature effect

Up to this point, the results of the MACRIS analysis only take into account he pressure effect on fault stability. The temperature effect on the stability of the intra-reservoir faults is now addressed.

Table 7-2	Input model parameters used for the thermo-elastic semi-analytical approach.

Thermo-elastic model parameters	
ΔT	−90℃
Sh orientation	N55E
Ko' = Sh'/Sv'	0.63
Sh/SH	0.9
ρ_{rock}	2260 kg/m^3
ρ_{water}	1150 kg/m^3
ρ_{gas}	200 kg/m^3
E (Young's modulus)	18 GPa
υ (Poisson's ratio)	0.2
α_T (linear thermal expansion coefficient)	10^{-5} K^{-1}
μ (friction coefficient)	0.6
α (Biot's coefficient)	1.0

To answer this question, we used a TNO-proprietary geomechanical semi-analytical approach detailed in Section 17.8.2. The required input for this approach is the radially symmetric temperature field resulting from the TOUGH2 flow simulation introduced in Section 6. Table 7-2 outlines the input parameters required for this

analysis which are the same as used in the P18-2 study (Neele et al., 2019). The TOUGH2 flow simulation and the geomechanical semi-analytical approach should be seen as one-way coupled, and the temperature effect on the fluid viscosity is handled by the TOUGH2 simulator.

The temperature field after 5 years of injection is taken as representative for the amplitude and extent of the cooling in the reservoir (see Figure 7-6). The transient temperature field after 5 years of injection from TOUGH2 is first approximated as an homogenous cylindrical field at a temperature relative to that of the undisturbed reservoir of -50 °C, with a height equal to 45m, and with a radius of 200m (see Figure 7-6). This approximation of a sharp temperature front is often assumed for fast analytical approaches (Candela et al., 2018). The semi-analytical approach, detailed in Section 17.8.2, provides an estimate of the thermo-elastic stresses inside and around the cylindrical field which are induced by cooling.
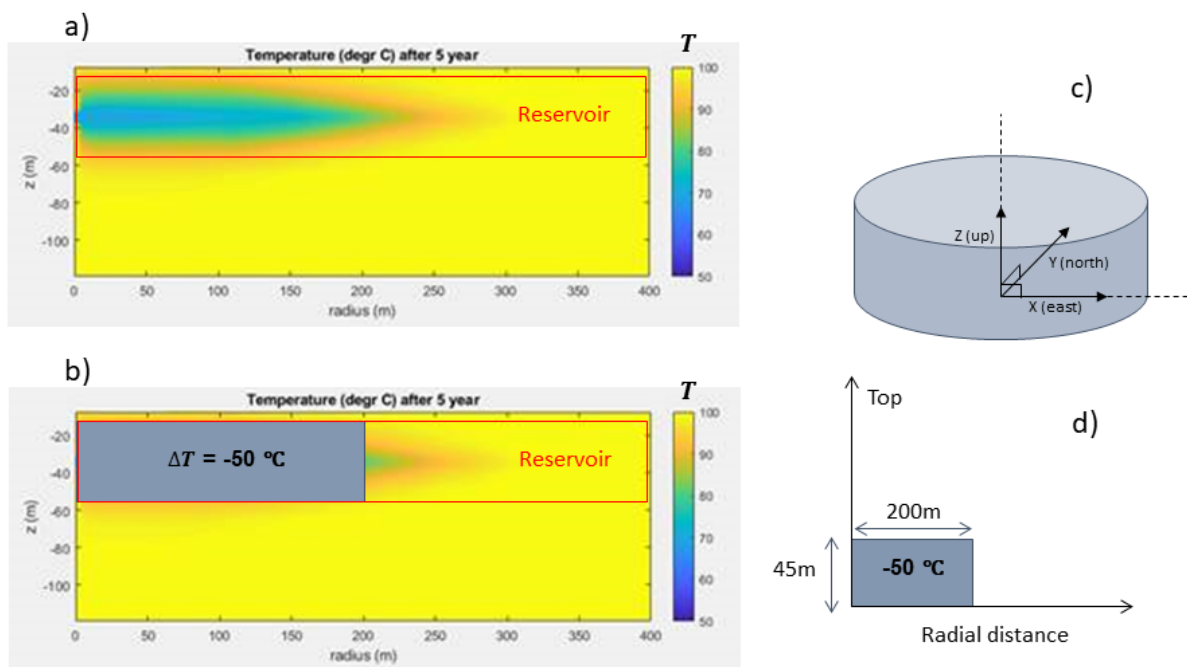
Figure 7-6   Temperature distribution and geometry of the geomechanical semi-analytical approach used to evaluate thermo-elastic stresses. a) Transient temperature field simulated by TOUGH2 (see Section 6.4). b) Cylindrical-shape approximation of the transient temperature field in a). For a) and b) the temperature change is homogeneously distributed and fixed at -50 ℃. c) and d) Geometry of the geomechanical semi-analytical approach.

Following the semi-analytical approach, faults are not explicitly modelled (as it was the case in the MACRIS analysis for the pressure effect) but the changes in stress which are induced by the reservoir cooling can be calculated at any location inside the reservoir and caprock. From equation (7-1) the changes in Coulomb stress induced by the temperature effect at any reservoir fault can be calculated. As soon as the cooling front reaches a fault, Figure 7-7 and Figure 7-8 show that the change in Coulomb stress can reach a value as high as 9 MPa. This result holds for a range of fault planes orientations which are relevant for the P18-6 field. Ahead of the cooling front, the thermally-induced Coulomb stresses rapidly decay and at 100 m

from the cooling front the Coulomb stresses are around 1.5 MPa. As concluded for the P18-2 study (Neele et al., 2019) the distance reached by the cooling front is the determining parameter for the fault stability analysis. Before reaching the fault, the increase in Coulomb stress in front of the cooling zone is minor, but as soon as the cooling front reaches a fault, the increase in Coulomb stress goes up to ~9 MPa, which is a magnitude capable of reactivating this fault. After 5 years of injection the cooling front is at 200 m from the well which means this scenario might occur (see Figure 7-6) and one of the P18-6 faults cross-cutting both the reservoir and caprock is at a distance of ~100m from a well (Figure 7-9).

However, in order to reach conclusions regarding fault reactivation, the changes in Coulomb stress in the initial stress situation before injection of cold CO_2 need to be added to the thermally induced Coulomb stress. Figure 7-2 and Figure 7-4 display this initial stress situation at the end of the production period and along the fault pillar closest to a well (a distance from well to fault of ~100m). As discussed before, the initial Coulomb stresses (at the end of the production period) are highly heterogeneous spatially along the fault pillar. At the reservoir edge the Coulomb stresses are already reaching the failure line but some other locations are at more than 10 MPa from the failure line. Adding the 9 MPa of thermally induced Coulomb stresses to the initial Coulomb stresses induced by the reservoir depletion, it can be estimated that almost three-fourths of the fault pillar would overreach the failure line (i.e.an along-dip fault section of 150m long might potentially be reactivated). It can therefore be concluded that for this particular fault which is close to a well, the likelihood of reactivation is high.

This last result will still hold, even if the cooling front reaches this fault later during the injection period. The simultaneous reduction in Coulomb stresses induced by pressure changes is expected to stabilize the fault. However this pressure-induced reduction in Coulomb stresses is weak relatively to the temperature-induced increase in Coulomb stresses. Indeed, later during the injection period and if we solely consider the pressure effect, the two-thirds of the fault pillar still remain at less than 9MPa from the failure line (see Figure 7-4). Therefore if we add up the 9 MPa increase of Coulomb stresses due to the temperature effect, two-thirds of the fault pillar will still overreach the failure line even if we combine both temperature and pressure effects.

Finally it is important at this stage to emphasise the limitations of TOUGH2 where the highest temperature that can modelled is 103 ℃ whereas the initial reservoir temperature was ~117℃. The change in temperature can therefore be expected to be more severe than the -50 ℃ used in our geomechanical semi-analytical approach which could result in the modelled change of Coulomb stress being even higher.

The cooling front modelled here represents a realistic scenario where the cooling is due to prolonged injection of CO_2 at a temperature of 70 °C. However, in reality a more gradual temperature front is expected and thus the area of excess Coulomb stress relative to the failure line will be more limited in space. In other words, the potential of reactivating a pre-existing fault inside the reservoir would be confined to a small area beyond the cooling front. Finally, a solution in this scenario is to adjust the injection rate at this particular well located close to a reservoir fault. This way,

the extent of the cooling front can be constrained to maintain a safe distance from the fault.
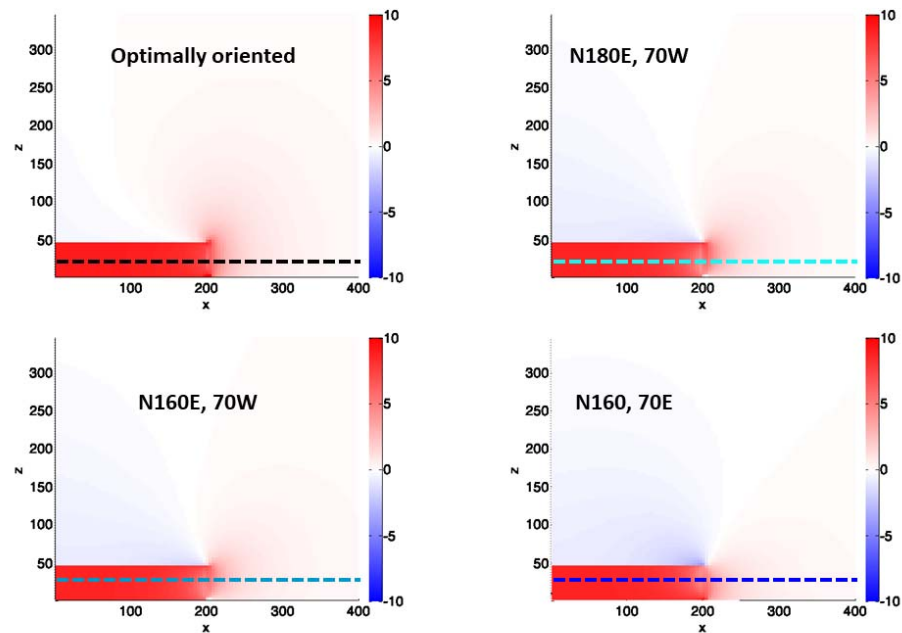
Figure 7-7   Thermo-elastically induced Coulomb stress changes in units of MPa for different fault orientation. Top left: fault planes with the highest Coulomb stress changes; Top right: fault planes with a North-South strike and dipping 70 degrees toward West; Bottom left: fault planes with a N160E strike and dipping 70 degrees toward West; Bottom right: fault planes with a N160E strike and dipping 70 degrees toward East. The model input used to generate these results is the homogenous temperature field presented in Figure 7-6. The horizontal dashed lines in the centre of the reservoir represent the stress profiles displayed in Figure 7-8.
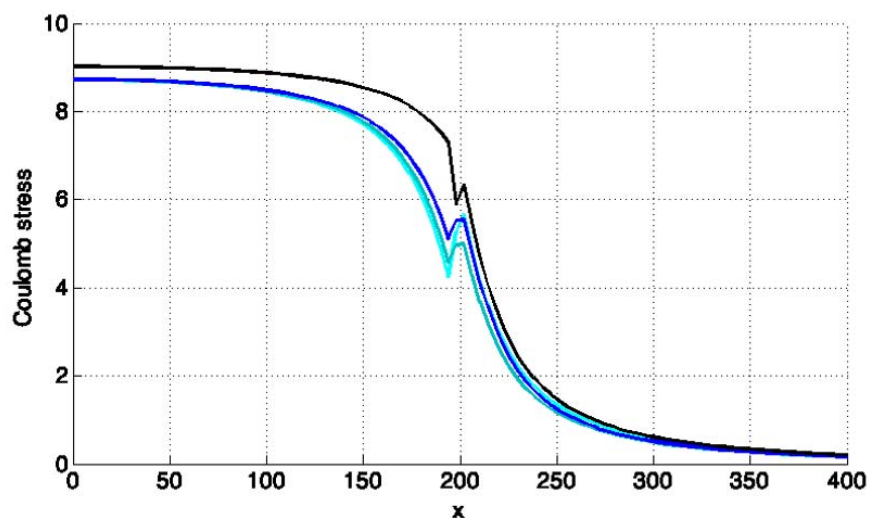
Figure 7-8   Profiles of thermo-elastically induced Coulomb stress changes in units of MPa. Each colour corresponds to each fault family presented in Figure 7-7.
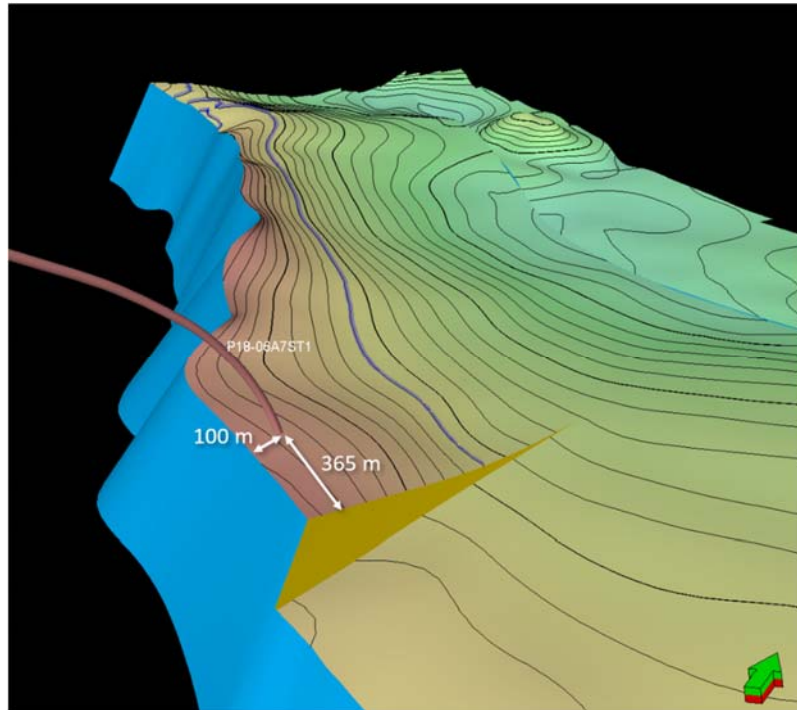
Figure 7-9 Schematic showing the distances from the faults to the wells.

Alongside fault reactivation another important consideration is regarding the potential magnitude of any induced earthquakes should fault reactivation occur. To answer this question additional modelling results are required. However this study can provide insight on the expected end-members in terms of event magnitude. One first end-member is the case where a rupture will remain confined to the perturbed zone and thus the induced event would be small (magnitude <1). The perturbed zone is the area of the fault already included in the cooled domain with the excess Coulomb stress.

The second end-member is the case where the rupture will propagate all the way through the fault area extent. In this case, the magnitude of the event would be large (magnitude well above 1). Note here that the case where the rupture could jump to another fault and extend even further is not considered. The reality is likely to occur between the first and the second end-member. One dominant factor that controls the event propagation and thus its final size is the initial Coulomb stress level at the start of the fault reactivation. This initial Coulomb stress is the one at the end of the production period and given by the MACRIS analysis (see Figure 7-2 and Figure 7-3). Due to the differential compaction effect, this initial Coulomb stress level is highly heterogeneous spatially with only some locations at the reservoir edge close to the failure line or already at the failure line. It can therefore be assumed that the propagation of an induced event will remain confined to the perturbed zone and will quickly die out outside due to the lack of high stresses to sustain its propagation. However it should be emphasised that to give a more definitive answer on the potential magnitudes of induced events, new geomechanical models focusing on this particular matter would need to be developed.

7.4   Fault stability: geochemical effects

7.4.1   Introduction

The P18 reservoir compartments that have been assigned as potential storage reservoirs are fault bounded. It is assumed that these faults are sealing; the compartments are hydraulically isolated from their surroundings due to juxtaposition of the reservoir against impermeable shales. Large-scale faults are generally surrounded by an area with a large number of smaller faults and fractures and matrix consisting of fault gouge. Instead of 'faults' we should refer to the 'fault (damage) zone' (Fisher, 2013). If porous rocks or sediments are faulted in early stages of consolidation, the damage zone generally has a lower permeability than the undeformed material (Fisher, 2013).

For storage integrity purposes, a difference should be made between sealing *across* and *along* the fault zone. Juxtaposition against a sealing formation can result in hydraulic isolation due to sealing across the fault. Yet, if the fault zone extends to above the caprock and the fault gouge is permeable, the risk of upward migration exists. In the P18-6 area, none of the faults extends upward outside the caprock. In a previous analysis of migration scenarios for P18, shallow gas pockets in the overburden were found, but these most probably originated in the overlying Jurassic Posidonia shales (Vandeweijer et al., 2011). No evidence was found for gas leakage from the P18 reservoir, supporting a conclusion that the fault zones of each of the faults penetrating the caprock are sealing. The question remains why upward gas migration did not occur along the non-sealing faults.

When CO_2 is injected in the reservoir, geochemical reactions between CO_2 and minerals within the fault might change the sealing capacity (in case of sealing faults) and/or cause reactivation. The geochemical effects of CO_2 on the faults, and the impact of these effects on its sealing integrity and reactivation potential need to be evaluated to assess the risk of leakage through the faults of the P18-6 reservoir and the potential of reactivation on the long term. These are described below based on recent literature.

7.4.2   Geochemical effects of CO_2 on sealing capacity

Due to juxtaposition of the reservoir against impermeable shales, it is assumed that the fault zone mineralogy of sealing faults is made up of crushed and mixed sandstone and shale components, whereas the non-sealing faults which did not juxtapose the reservoir against impermeable shales comprises crushed reservoir material only. Although the Triassic sandstones have a relatively high clay content, the non-sealing faults probably contain less clay minerals than the sealing faults. Yet, the sealing and non-sealing faults will have very similar mineralogy, with variable mineral contents consisting of quartz, feldspars, clay minerals, carbonates, anhydrite and accessory minerals.

Similar to geochemical effects of CO_2 on caprock integrity, the only migration mechanism for CO_2 into sealing faults is by diffusion in dissolved form. Therefore, horizontal and vertical penetration of the geochemically affected zone is of the same order of magnitude as the vertical penetration into the caprock (several meters after 10,000 years). Changes in mineralogy will include partial dissolution of silicate minerals and precipitation of carbonate and clay minerals. Corresponding porosity changes will be too small to affect the sealing capacity.

The non-sealing fault zones might allow migration of supercritical CO_2 but breakthrough across the fault zones is not an issue if the compartment across the fault is also used as storage reservoir. Upward migration could lead to enhanced chemical reactions. According to Fisher (2013), the most common type of fault gouge in Triassic reservoirs is cataclastic faults. For the 19 Triassic fault gouges studied, gas permeability values ranged from 0.0007 to 1.8 mD (Fisher, 2013). A non-sealing fault will have a permeability at the high end of this range, but it is still a low permeability. Low flow rates will enhance self-sealing of the leak path by carbonate precipitation, especially in the presence of sufficient clay minerals which can provide the required cations for reaction with dissolved CO_2 to form carbonate minerals. However, the rate of self-sealing is not well known and will probably be highly dependent on many variables and fault characteristics.

7.4.3   *Geochemical effects of CO_2 on reactivation potential*
Chemical interactions between the carbonized brine and fault zone mineralogy will result in slight mineralogical changes. These changes will only occur in the first few meters at the contact with the reservoir for sealing fault zones after thousands of years. In the case of non-sealing faults, mineral reactions might have occurred across the fault zone. The chemical reactions in the long-term are uncertain and will be affected by local differences in mineralogy. Overall, it is predicted that the carbonate content will increase because of the interaction with dissolved CO_2 with cations in the formation water, and on the long term with cations from silicate minerals. Few geomechanical studies have been conducted to investigate the effect of carbonate content on mechanical properties of faults. The studies that have been conducted concluded that with increasing carbonate content, fault gouge has an increased friction coefficient, indicating lower potential for fault reactivation (Samuelson et al., 2012; Adelinet et al., 2014; Bakker et al., 2016). In the case where fault reactivation *does* occur, higher carbonate contents increase the tendency for velocity weakening (which makes the fault weaker and sliding can continue, e.g. unstable slip) and can therefore increase the probability of microseismicity to occur (Samuelson et al., 2012). This is supported by an experimental study in which fault gouge from an outcrop which was very heavily altered by CO_2 interactions showed unstable slip at reservoir temperatures, whereas less heavily altered fault gouge resulted in stable slip (Bakker et al., 2016). The permeability of fault gouge material shows a tendency to decrease by orders of magnitude upon displacement during slip (Bakker et al., 2016), although it is not clear whether this occurs for both stable and unstable slip.

7.4.4   *Evidence of leakage from field data*
In Arizona, USA, CO_2 leakage through faults from a large natural CO_2 reservoir was studied in order to quantify leakage rates (Miocic et al., 2019). In this specific area, faults extended from the reservoir up to the surface, and CO_2 rich fluids have been leaking for 420,000 years through fractures present in the damage zones around the faults. It was estimated that the average leakage rate through the faults is up to 36 kt/yr, which is less than 0.01% leakage per year for this reservoir. In case of the P18-6 storage site, the faults do not reach the surface, but end in the Cretaceous aquifers. In a worst case, that the non-sealing faults turn out to be leakage paths, and self-sealing by carbonate precipitation does not occur, supercritical or gaseous CO_2 would migrate up to the Cretaceous aquifers and dissolve into the formation water. From the Arizona study it was concluded that leakage along faults does not

negatively impact the suitability of a reservoir from the point of view of CO_2 emission reductions (Miocic et al., 2019).

7.5   Conclusions

Pressure effect on fault stability
The 4D distribution of Coulomb stresses has been computed along the mapped faults. Following the MACRIS approach, these Coulomb stresses combined (1) the poro-elastic effect, (2) the direct pressure effect at faults and (3) the effect of the fault offset. This analysis indicates that these Coulomb stresses only exceed the failure line very locally at the reservoir edge and the risk of fault reactivation due to pressure effect is considered low. The fact that none of the faults in the P18-6 storage site extend to above the caprock reduces the impact of any fault destabilisation.

Temperature effect on fault stability
In order to model the temperature effect on fault stability a TNO-proprietary geomechanical semi-analytical approach has been used. The distance reached by the cooling front is the determining parameter for the fault stability analysis. When the cooling front reaches a fault, the induced Coulomb stresses by the temperature effect can be such that locally, at this particular location, the fault can be reactivated. Given this distance criteria, one P18-6 fault close to a well has been identified as potentially locally reactivated by the coupled temperature and pressure effect. Adjusting the injection rate at the particular well close to this fault can be a solution to maintain the distance of the cooling front at a safe distance from the fault.

Geochemical effects on fault stability
The impact of geochemical alterations in fault zones is unlikely to lead to CO_2 migration along faults. Currently the migration of methane along faults cannot be ruled out but if it happens the cumulative volumes of methane migrating along the fault remain below the detection limit in seismic data, strongly suggesting that flow rates are insignificant, if occuring at all. This, in turn limits the speed and depth of penetration of CO_2 into a fault zone, rendering the impact of chemical alterations insignificant.

8   Caprock integrity

8.1   Introduction

This section focuses on the potential reactivation of faults in the caprock due to pressure increase during CO_2 injection (Section 8.2), to temperature effects from the injection of low-temperature CO_2 (Section 8.3). Changes in pressure and temperature inside the reservoir can induced different stress changes between intra-reservoir section of the pre-existing faults and their caprock section. Section 8.4 discusses geochemical effects of interaction between CO_2 and the caprock.

The caprock overlying the P18-6 field has a thickness of more than 450 m. None of the faults that exist in the field or that bound the field extend to above the caprock. This means that the consequences of fault reactivation are likely to be limited.

The conclusion from the results presented below is that the risk of reactivation of faults in the caprock due to the injection of CO_2 is very low. The interaction between CO_2 and the caprock is expected to be insignificant.

8.2   Pressure effect on caprock integrity

This section considers the potential destabilization of pre-existing faults inside the caprock due to the pressure effect. These faults are the ones present inside the reservoir flow model that extend upward into the caprock. The pressure-induced Coulomb stress changes along the pre-existing fault planes are thus calculated following MACRIS analysis and is detailed in Section 7.1; implicitly it is also assumed that generating a new fault will require larger stress changes.

Figure 7-2, Figure 7-3 and Figure 7-4 show that the Coulomb stresses rapidly decay near the top of the reservoir within the caprock. The pressure effect is thus not expected to contribute to the risk of fault reactivation in the caprock.

8.3   Temperature effect on caprock integrity

A temperature decrease of the reservoir due to the injection of relatively cold CO_2 induces contraction of the rock mass and a change in total stress, dependant on the boundary conditions. The induced stress changes take place inside the reservoir, but also within the caprock on top of it. The present section addresses the magnitude and distribution of temperature-related stress changes in the caprock. The main question addressed in this section is: what are the risks of reactivating a pre-existing fault in the caprock due to the temperature-induced stress changes?

To answer this question we used a TNO-proprietary geomechanical semi-analytical approach detailed in Section 17.8.2 and already introduced in Section 7.3. The same temperature field as the one considered for intra-reservoir fault reactivation after 5 years of injection is taken as input (see Figure 7-6).

According to the semi-analytical approach, and as mentioned previously, faults are not explicitly modelled but the changes in Coulomb stress which are induced by the reservoir cooling can be calculated for any fault orientation and at any location

within the caprock. The Coulomb stress changes are thus defined for any fault plane in the caprock; generating a new fracture will require larger shear stress than those for reactivating a fault plane. The fault planes should therefore be seen as "potential fault planes" since faults have not explicitly been identified in the seismic cube.

The results achieved (see Figure 8-1 and Figure 8-2) indicate that on top of the cooled part of the reservoir, the changes in Coulomb stress are negative. On these locations in the caprock, therefore, there is no risk of fault reactivation due to cooling of the reservoir below it. Only on top of the reservoir beyond the edge of the cooling front, the changes in Coulomb stress start to be positive (see Figure 8-1 and Figure 8-2). For this analysis the optimally oriented fault planes were chosen, i.e. for any location the fault orientations where the Coulomb stress changes are maximum were selected. Consequently, the current approach in terms of risk quantification can be seen as conservative, or worst case. However, Figure 8-2 shows that instead of considering the optimally oriented fault planes but the orientations of the P18 faults cross-cutting both the reservoir and caprock, it would have led to similar changes in Coulomb stress.

To summarize, the potential risk of reactivating a pre-existing fault in the caprock is very low.
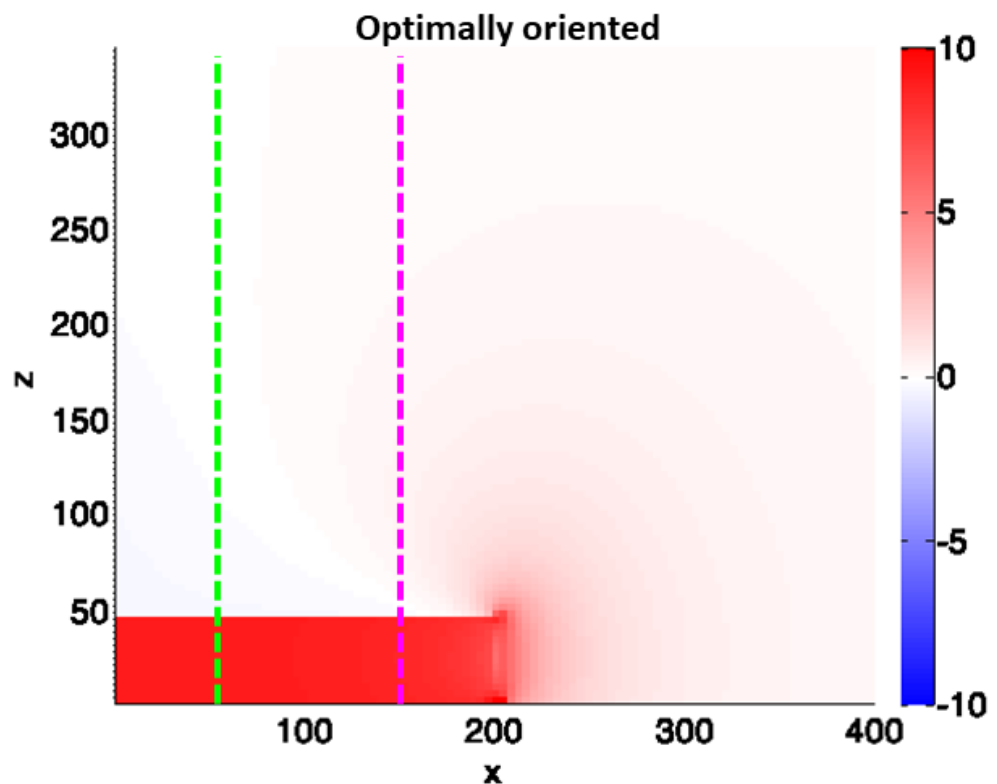
Figure 8-1   Thermo-elastically induced Coulomb stress changes in units of MPa along optimally oriented fault planes. The vertical dashed lines represent the stress profiles displayed in Figure 8-2.
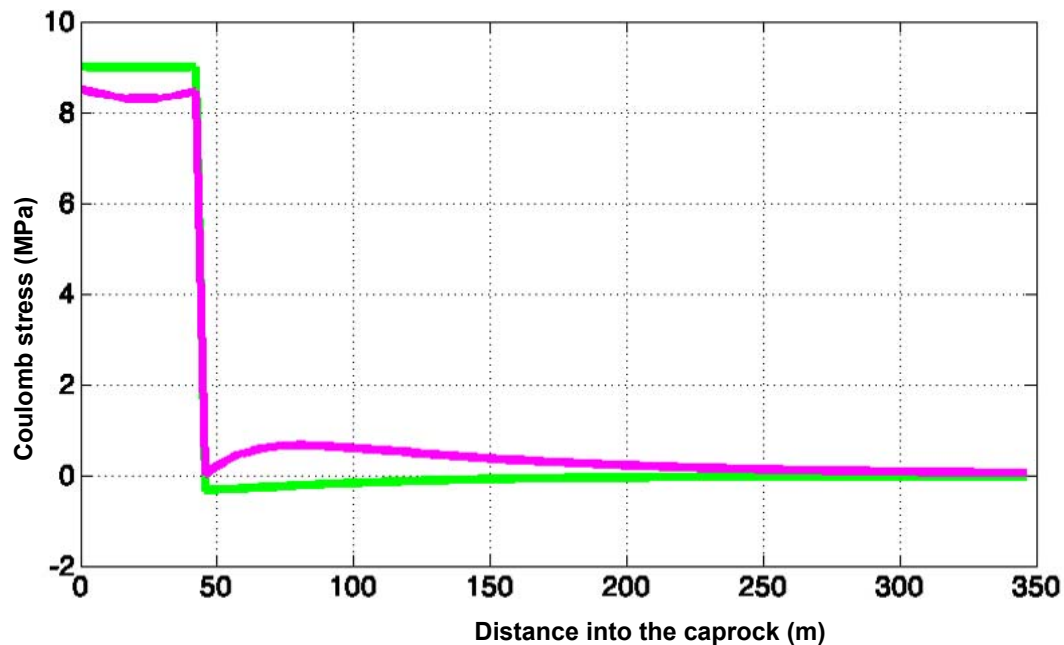
Figure 8-2   Profiles of thermo-elastically induced Coulomb stress changes in units of MPa. Each colour corresponds to different vertical cross-sections for the stress profiles as displayed in Figure 8-1.

8.4   Geochemical effects

8.4.1   Introduction

Geochemical reactions between CO_2 and the caprock minerals can change the sealing capacity. The geochemical effects of CO_2 on the caprock, and the impact of these effects on its sealing integrity need to be evaluated to assess the risk of leakage through the caprock of the P18-6 reservoir on the long term. These are described below based on recent literature.

8.4.2   Geochemical effects of CO_2 on caprock integrity

The caprock of the P18 reservoirs comprises the Solling Claystone Member with the Röt Claystone and Main Evaporite Members situated above. Caprock material of the P18 reservoirs has not been obtained during drilling operations. Caprock material of the nearby Q16 reservoir as analogue for P18 caprock was characterized by Peach et al. (2019). Eight caprock samples from the Solling and Röt Formations were measured for gas permeability and porosity. All permeability values were below 0.1 mD and porosity ranged between 0.02 and 5.3%. Four samples from the Röt Formation were analysed by XRD and eight samples of Solling and Röt Formations were analysed by optical microscopy. The samples were carbonate-rich mudrocks with a mineralogy mainly made up of carbonates (ankerite or dolomite), phyllosilicates (mica and clay) and quartz (Peach et al., 2010).

The caprock of both the P18 and the Q16 gas fields has a proven sealing capacity for natural gas yet, CO_2 behaves differently than natural gas, both from physical

and chemical perspective. The low permeability measured for the Q16 caprock samples justifies the assumption that penetration of supercritical CO_2 ($scCO_2$) into the caprock will not occur, as long as the CO_2 pressure in the reservoir remains well below the pre-production gas pressure. The only way for the CO_2 to migrate into the caprock is by upward diffusion in a dissolved state. The diffusion is driven by an increased concentration of dissolved CO_2 in the reservoir pore and at the contact with the caprock. Tambach et al. (2012, 2015b) report on 1D reactive transport simulations that were performed with PHREEQC to assess the interaction of dissolved CO_2 during upward migration into the caprock. Due to the lack of detailed caprock mineralogical analysis, the mineralogy was based on samples from the adjacent P15 field, analysed and reported by Spain and Conrad (1997). The detailed analysis showed a much higher quartz content than the analyses by Peach et al. (2010). Dolomite, illite and anhydrite are present in moderate amounts, and small amounts of K-feldspar, albite, siderite and pyrite were identified. The simulation results showed that the upward diffusion of dissolved CO_2 and the associated pH decrease is very slow. During the upward migration, mineral reactions occur to buffer the pH and convert the dissolved CO_2 into carbonate minerals. This further slows down the upward migration of the dissolved CO_2. After 10,000 years some mineral reactions and a minor porosity increase was simulated only in the 5-10 metres above the reservoir-caprock contact (Figure 8-3). A sensitivity study on mineral types and reactive surface areas predicted a porosity increase in the bottom part of the caprock of no more than 0.7%. Only one simulation predicted a porosity decrease of 1.8% in the first metre and porosity increase up to 5 metres into the caprock (Tambach et al., 2012).

Gaus et al. (2005) found similar orders of magnitude for the extent and scale of geochemical reactions in shale caprock at the Sleipner injection site in Norway. The authors predicted either a porosity increase or decrease in the lowest few metres of the caprock, depending on the mineralogical composition of the rock, 3,000 years after injection. The predicted porosity increases are below 0.05%, porosity decreases are up to 2.6%. For two different mineral compositions, the migration of dissolved CO_2 reached either 1.5 or 10 meters into the caprock after 3000 years (Gaus et al., 2005). In the first scenario, a more reactive mineral composition was able to sequester the CO_2 in carbonate minerals much faster, thereby retarding the upward migration of dissolved CO_2. Wang et al. (2019) also predicted minor mineral reactions and porosity increase in shale caprock after 1,000 years and concluded that mineral dissolution and precipitation reactions have 'small to negligible impact on the permeability of the caprock'.

In a more detailed reactive transport simulation, assessing the impact of heterogeneities in shale caprock, local penetration of supercritical CO_2 was predicted in areas of a caprock with lower sealing capacity (Tian et al., 2019). Local changes in porosity and permeability (both positive and negative) were predicted, related to variations in mineral compositions. Vertical migration of the CO_2, in those areas that penetration occurred, reached almost 50 m into the caprock after 500 years (Tian et al., 2019). With a total caprock thickness for the P18-6 reservoir of several hundreds of meters, migration of small amounts of CO_2 out of the storage would take > 1,000 years. Such a scenario represents a worst case condition, as exploration data for the P18-6 did not show any evidence for penetration of gas into the caprock, providing evidence for the overall sealing capacity of the P18-6 caprock.
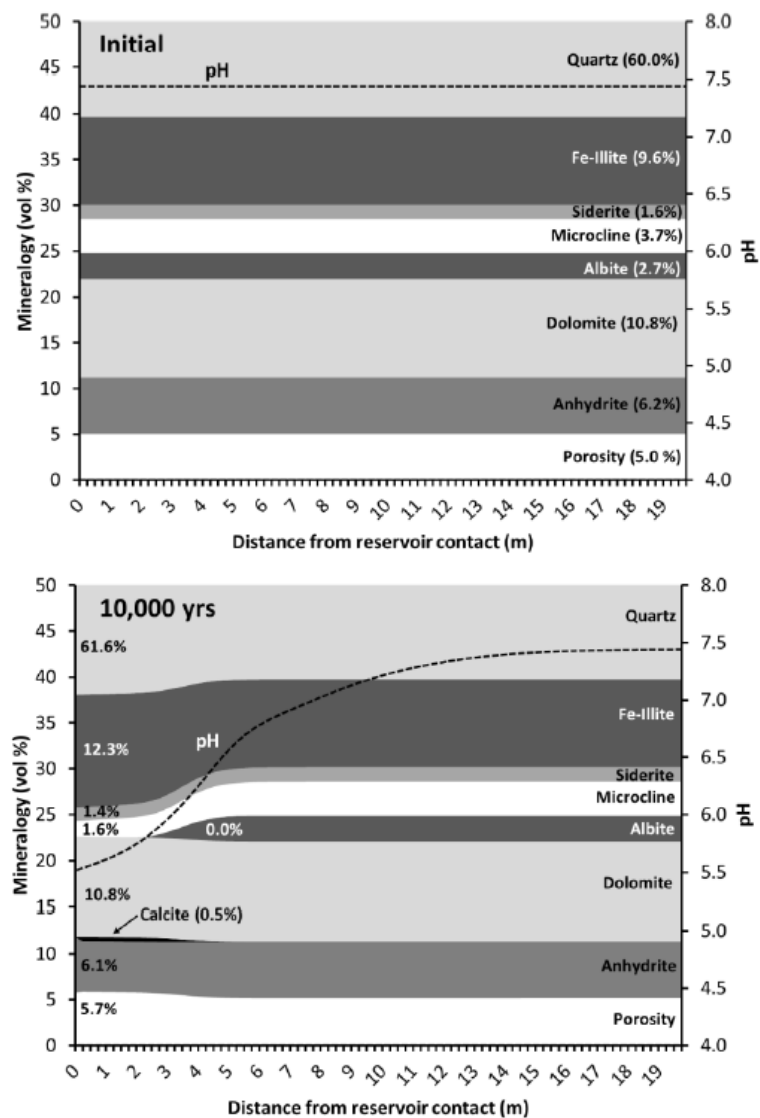
Figure 8-3: Initial mineralogy of the caprock and mineralogy after 10,000 years of simulation as a function of the distance from the reservoir contact. Up to 50 vol% is shown, the remaining part is made up of quartz. From Tambach et al. (2012).

8.5   Conclusions

Pressure effect on caprock integrity
Following the MACRIS approach, both induced Coulomb stresses along the intra-reservoir part of the faults and those along the intra-caprock part of the faults have been assessed. These Coulomb stresses rapidly vanish on top of the reservoir inside the caprock; the intra-caprock mapped faults are thus not expected to be reactivated by the pressure effect.

Temperature effect on caprock integrity
In order to model the temperature effect on pre-existing faults in the caprock, a TNO-proprietary geomechanical semi-analytical approach has been used. The geomechanical analysis shows that the changes in Coulomb stresses in the

caprock due to reservoir cooling are negative. The risk of intra-caprock fault reactivation is thus very low.

Geochemical effects on caprock integrity
CO_2 is not expected to significantly interact with or migrate into the caprock.

9 Well integrity

9.1 Introduction

This section presents the analysis of the integrity of the well in the P18-6 field. Well integrity is considered at in the following sections at four levels:
- The integrity of the well in its current state (Section 9.2);
- The effect of injecting cold CO_2 on the integrity of the well (Section 9.2.2);
- Geochemical processes acting on the cement (Section 9.3.4);
- Well decommissioning (Section 9.4).

The conclusions from the well integrity analysis are the following:
- *Well integrity.* The P18-6 well has the potential to be used safely as CO_2 injection. Appropriate mitigation measures are proposed to make the well fit for storage operations.

- *Effects of injecting cold CO_2 on well integrity.* It is highly likely that de-bonding of cement interfaces will take place upon cold CO_2 injection, creating microannuli. The characteristics of the microannuli and pressure conditions determine whether upward CO_2 migration would actually take place. Keeping the CO_2 pressure in the reservoir below hydrostatic pressure conditions will reduce the likelihood of leakage through microannuli.

- *Well decommissioning.* Appropriate methods should be used for the decommissioning of the well. Given the likelihood of microannuli forming during the injection of cold CO_2, decommissioning methods that remove these potential leakage paths could be considered. As an example, full-bore pancake like plugs would provide formation-to-formation closure of the injection well.

9.2 Status of the well barriers

9.2.1 Well Integrity assessment approach

Currently there are no specific industry standards for CO_2 injection wells. Therefore the approach followed in this well integrity assessment is to utilize existing oil and gas industry standards that address well integrity for injectors and complement any specific gaps for CO_2 injection wells if required.

The standards on which this well integrity assessment is based are:
1. Norsok Standard D10, rev. 4 June 2013 - Well integrity in drilling and well operations (NORSOK, 2013);
2. ISO standard 16530-1:2017, March 2017 - Petroleum and natural gas industries - Well integrity, Part 1: Life cycle governance (ISO/TC 67/SC 4 Drilling and production equipment, 2017);
3. NOGEPA industry standard no. 45, 12 October 2016 - Well decommissioning (NOGEPA - OPCOM, 2016).

The reports related to well integrity and CO_2 storage and used for this assessment are:
4. MiReCOL report, February 2015 - D8.1 Description of leakage scenarios for consideration in the work in SP3 (Vrålstad, et al., 2015);

5. Dutch State Supervision of Mines (SSM/SodM), January 2019 – The integrity of onshore wells (SodM, 2019).

For the sake of completeness some relevant sections of the above mentioned standards and reports are presented.

1. The Norsok D10 standard refers to well integrity by:
    -   General principles: A two well barrier concept of primary barrier and secondary barrier for wells penetrating into hydrocarbon bearing formations and/or formations with the potential to flow to surface.
    -   Structural integrity: the key components (conductor, guide base, risers) that provide structural integrity of the well during its service life shall be evaluated with respect to loads, wear and corrosion.
    -   Injection / disposal wells: The well shall be constructed such that the injected media will be contained within the targeted formation zone (reservoir) without risk of out of zone injection.
    -   WBS examples: Permanent well decommissioning (abandonment) is illustrated by a primary well barrier at caprock, secondary well barrier at intermediate section and an open hole to surface barrier.

2. The ISO well integrity standard refers to the Norsok D10 standard and considers:
    -   Structural integrity monitoring: The well operator should establish suitable systems to model or measure degradation in the structural well operating limits. The conductor, surface casing (and supporting formations) and wellhead assembly typically provide structural support for the well. Failure of these structural components can compromise well integrity and escalate to a loss off containment. For each well the well operator should assess the risk of failure of such structural components.

3. The NOGEPA no. 45 standard on well decommissioning has the following statements on well decommissioning.
    -   Summarised mandatory requirements for Well Decommissioning:
        o   A permanent barrier shall extend across the full cross section of the well covering all annuli.
        o   The depth of the permanent barrier shall be selected to be adjacent to the caprock of adequate thickness with an estimated formation fracture pressure that exceeds the maximum anticipated pressure at depth.
        o   In case of cement, the permanent barrier length inside the inner wellbore shall be:
            ▪   At least one hundred meters long (100 m), or
            ▪   At least fifty meters (50 m) when placed on top of a tested mechanical support in cased hole.

4. The MiReCOL D8.1 report refers to Norsok D10 and includes the following information on well integrity:
    -   The report considers well barrier breaches (CO_2 migration along the well bore) and includes the in-situ formation of the previous casing behind the liner lap as a barrier element to mitigate the risk of out of zone injection (which is conform Norsok D10).

- Aging issues with cement degradation, casing corrosion and wear, and thermal loads imposed on the well infrastructure are examples of the most likely causes for well leakages.

5. SodM (2019) categorizes CO_2 storage wells as gas wells from a well integrity perspective with the associated well failure model identifying potential leak paths, see Figure 9-1 (this is based on the ISO 16530 well failure model).

   It should be noted that SodM defines the Surface tree (also known as the X-mass tree) as a secondary barrier element and the Surface Controlled SubSurface Safety Valve (SCSSSV) as primary barrier element, which is conform the Norsok D10 standard. However, they do define failures of the tubing above the SCSSSV, the control line, tubing hanger and feedthroughs (blue items 3, 16 and 17 in Figure 9-1) as primary leakage elements, which is a variation on the Norsok D10 standard.
   In this report Norsok D10 is primarily followed, as a result all elements above the SCSSSV are considered to be secondary barrier elements (because they are isolated in the event of an SCSSSV closure).

Faalmodel gasput

1	Tubing Hanger/Seal Leak (i/o)
2	Wellhead Seal Leak
3	Tubing Leak above SSSV (i/o)
4	Intermediate Casings Leak (i/o)
5	SSSV Leak
6	External leak Or Seep Outside Conductor
7	Corrosion leak at Shallow Aquifer level (i/o)
8	Production Casing Leak (i/o)
9	Tubing Leak Below SSSV (i/o)
10	Leak through SPM Accessory (i/o)
11	Leak Casing Shoe vs. an Outer Annulus (i/o)
12	Leak Casing Shoe vs. B-annulus (i/o)
13	Production Packer Leak (i/o)
14	Leak through Poor Cement or Micro Annulus (i/o)
15	Leak through the Liner Hanger or Liner Cement (i/o)
16	a: Leak Hydraulic Line vs. A-annulus (i/o) b: Leak Other Line vs. A-annulus (i/o)
17	a: Leak Hydraulic Line at Xmas Tree Void/Tubing Hanger (i/o) b: Leak Other Line at Xmas Tree Void/Tubing Hanger (i/o)
18	a: Leak Hydraulic Line at Wellhead Outlet b: Leak Other Line at Wellhead Outlet
19	Leak Xmas Tree or Wellhead Valves vs. Process Facilities (i/o)
20	Stem Packing Leak
21	Bonnet Seal Leak
22	X-Mas Tree Flange Leak
23	Xmas Tree Body Leak
24	Xmas Tree Valve Leak
25	Xmas Tree Connector Leak
26	Leak through Geological Pressure Seal / Cap Rock

Figure 9-1 Well failure model for gas wells, including storage wells. (SodM, 2019). The blue numbers are primary barrier element failures and the red numbers are secondary barrier element failures.

9.2.1.1 Well integrity assessment concept

Based on the reviewed standards and reports, the scope of the well integrity assessment in this report includes and reviews the following elements:

a) The primary and secondary well barrier elements from reservoir caprock to surface, conform NORSOK D10.

b) The risk of out of zone CO_2 injection due to a failure of a primary and/or a secondary barrier, with supporting in-situ formation of the previous casing below the liner lap.
c) Structural integrity of the load bearing surface casing, conductor or riser.

The definition of the barrier elements for this assessment comes from Norsok D10.
  − Primary well barrier: first well barrier that prevents flow from a potential source of inflow.
  − Secondary well barrier: second well barrier that prevents flow from a potential source of inflow.
The structural integrity assessment of the load bearing surface casing is for this assessment limited to a review of the "as built" status, identifying the potential well integrity risk.

It should be pointed out that the assessment of the influence of fatigue or corrosion on well integrity, with the structural load effects and associated thermal and pressure cycles, is not in the scope of the current work. This should be considered as the next fundamental step in assessing the structural well integrity lifecycle for the CO_2 injection program.

9.2.2 *P18-6 well integrity analysis*
The P18 fields have been subjected to CO_2 storage assessment and well integrity evaluations in the CATO-2 R&D programme (Akemu, et al., 2011). The previous well integrity assessment focused on the P18-4 field and identified and evaluated barriers of wells relevant for the foreseen storage operation and identified gaps or uncertainties about barrier status in general. Based on this previous study it was not possible to decide on the suitability of the P18-6 well for CO_2 injection and storage given the new operating envelope. The present assessment is based upon the previous work and addresses the gaps that where identified earlier. It considers new findings, as well as information that was not available at the time of the first studies.

The present study includes:

− An assessment of well penetrating the P18-6 reservoir P18-A-07-S1);
− An assessment of earlier identified gaps, by detailed review of the end-of-well reports (EOWR)[7], newly obtained records and quantification of the relevant barrier elements for the primary, secondary and structural barriers in place;
− Illustration of well barrier envelope status in a well barrier diagram combined with the potential risks for each barrier, with the aim to assist on assessing the suitability of the well for injection of CO_2 in the P18-6 reservoir.

9.2.3 *General well integrity P18-6 and well status issues*
The status of the P18-A-07-S1 well, penetrating the P18-6 reservoir, that emerges from the review of previous work is as follows:
  a) The well has not been assessed for the well completion load case for CO_2 injection with respect to temperature and pressure.
  b) No assessment records were found on the lifecycle assessment of load bearing surface casing and conductor. External corrosion due to corrosive fluids and Metocean induced fatigue of the load bearing casing could reduce

---

[7] Two end of well reports were used. Well P18-A-04 is the bottom (20" and 30") of well P18-A-07-S1. The well report for well P18-A-04 is Amoco (1993); the EOWR for well P18-A-07 is BP (2003).

its lifecycle load capacity. This is a fundamental requirement to assess the lifecycle of the well and the risk of loss of well integrity.

c) The expected final CO_2 reservoir pressure for P18-6 is maximised at initial pressure (see Section 5.5); this has been considered in the assessment of individual barriers.

d) The material specifications of the flow wetted barrier elements like surface tree, tubing hangers, completion accessories and seals / elastomers need to be validated against the CO_2 injection operating envelope.

9.2.4   Well P18-A-07-S1

The P18-A-07-S1 well was drilled and completed in the P18-6 block in 2003. The Glomar Adriatic III installed a 20" casing in 1993 in slot 6 with the casing shoe at 416 m MD (reported MDBRT); the well name at that time was P18-2A4. In 2003 a 17 ½" pilot hole was drilled at this slot to 1014 m MD, which was subsequently enlarged to 22" (target depth at 1009 m MD) with an underreamer. A 17" liner was installed with the liner shoe at 1007 m MD.
The original 16" hole was drilled from 1007 m to 1883 m MD. Due to borehole instabilities the drill string got stuck and was cut, the original hole was abandoned. The 16" hole was side tracked from 1025 m MD and completed as a gas producer with a 4 ½" 13Cr-L80 completion. It has been assessed in view of CO_2 storage with the following results (see also Figure 9-2 and Table 9-1).

Primary barrier
- The 7" liner is made of P110 (carbon steel) material, it is reported to be successfully cemented, no CBL has been executed. The liner was tested as part of the full (combined) 9 5/8", 7" and 5" well pressure test to 3800 psi (262 bar). The 7" liner shoe was drilled out and a successful FIT of 13 ppg was conducted.
- The 5" liner was installed and cemented with an early bumped plug, most probably due to the top dart/plug bypassing some of the cement. The liner was tested to 3800 psi (262 bar). The 5" liner shoe was drilled out (hard cement) and a successful FIT of 12 ppg was conducted.
- The 5" top of liner was set approximately 35 meters above the cap rock.
- The Aalburg shale that covers part of the 5" liner has natural formation sealing potential. This could improve the sealing performance over time.
- The 5" liner is made of 13Cr-L80 and has no risk for corrosion. It is set in the 7" liner creating a double barrier for the 105 m long section between the top of the 5" liner and the 7" liner shoe, which is set in the cap rock.
- The production packer is located above the caprock and set in the 7" carbon steel liner, the 96 meter section of 7" liner between top of 5" liner and bottom of packer is flow wetted and is exposed to potential corrosion. Failure of this 7" liner section would result in leakage into the overburden (single barrier event).
- The well has a stable 6 bar pressure reported on the production annulus.
- The well has a 3 ½" pre-drilled liner installed, this is uncemented and is therefore not part of the primary barrier.

Secondary barrier
- The 7" liner was installed within 68 meters of the cap rock and successfully cemented and tested to 3800 psi (262 bar), combined with the 5" liner test. There has been no CBL executed.
- The 7" liner is covered by the Vlieland shale that has the potential of NFS (natural formation sealing). The 7" shoe track was drilled out and a successful FIT of 13 ppg was conducted in the top of the cap rock.
- The 9 5/8" casing was run and cemented with 175 barrels of cement, with 30 barrels losses during the pumping of the cement. An additional 199 barrels were reported to be lost during displacement. The top of cement (TOC) is calculated to be at 1840 m MD (which corresponds to 1570 m TVD). No CBL has been executed. The casing is tested to 3800 psi (262 bar) combined with the 5" and 7" liner test.
- The 9 5/8" shoe track was drilled out and a successful FIT of 12.3 ppg was conducted.

Structural well integrity
- The 13 3/8" casing is placed at 2290 m MD and has a poor cementation, several cement squeezes have been executed after drilling out the shoe, this resulted in a leak off test (LOT) of 9.7 ppg.
- The section between 17" casing shoe at 1007 m MD and the 13 3/8" casing shoe at 2290 m MD is uncemented. The 17" liner was run without a hanger and set on bottom of the 17 ½" x 22" hole and cemented from the 17" shoe at 1007 m to the top of the 17" liner at 369 m MD.
- The 20" casing shoe is placed at 416 m MD and was cemented to surface (cement returns at spider deck reported in EOWR; Amoco (1993), p.236). Cement has been placed from 351 m to 200 m MD between the 20" and 13 3/8" casings on top of an 13 3/8" inflatable external casing cement packer.
- The conductor is piled to 131 m MD. The conductor is coated underwater and in the splash zone (Amoco (1993), p. 234)..

Discrepancies
- The CATO-2 report on the well integrity assessment (Akemu et al., 2011). did not address the discrepancy of the 7" carbon steel liner below the production packer and the associated risk.

Summary
- From Table 9-1 it can be seen that the primary and secondary barrier elements could be validated, although no CBL's were executed.
- For the primary barrier the production packer is situated above the caprock, exposing the 7" carbon steel liner to well fluids and thereby introducing the risk of corrosion. This may cause failure and leakage to the overburden above the cap rock, which needs to be evaluated and potentially mitigated.
- The 7" liner shoe is set and cemented in the caprock and tested. The 5" liner is set, cemented and tested, providing a good seal in the caprock.
- The secondary barrier is formed from top of production packer with a 7" liner and 9 5/8" casing string to surface with the 7" liner lap and the 9 5/8" cemented and tested.
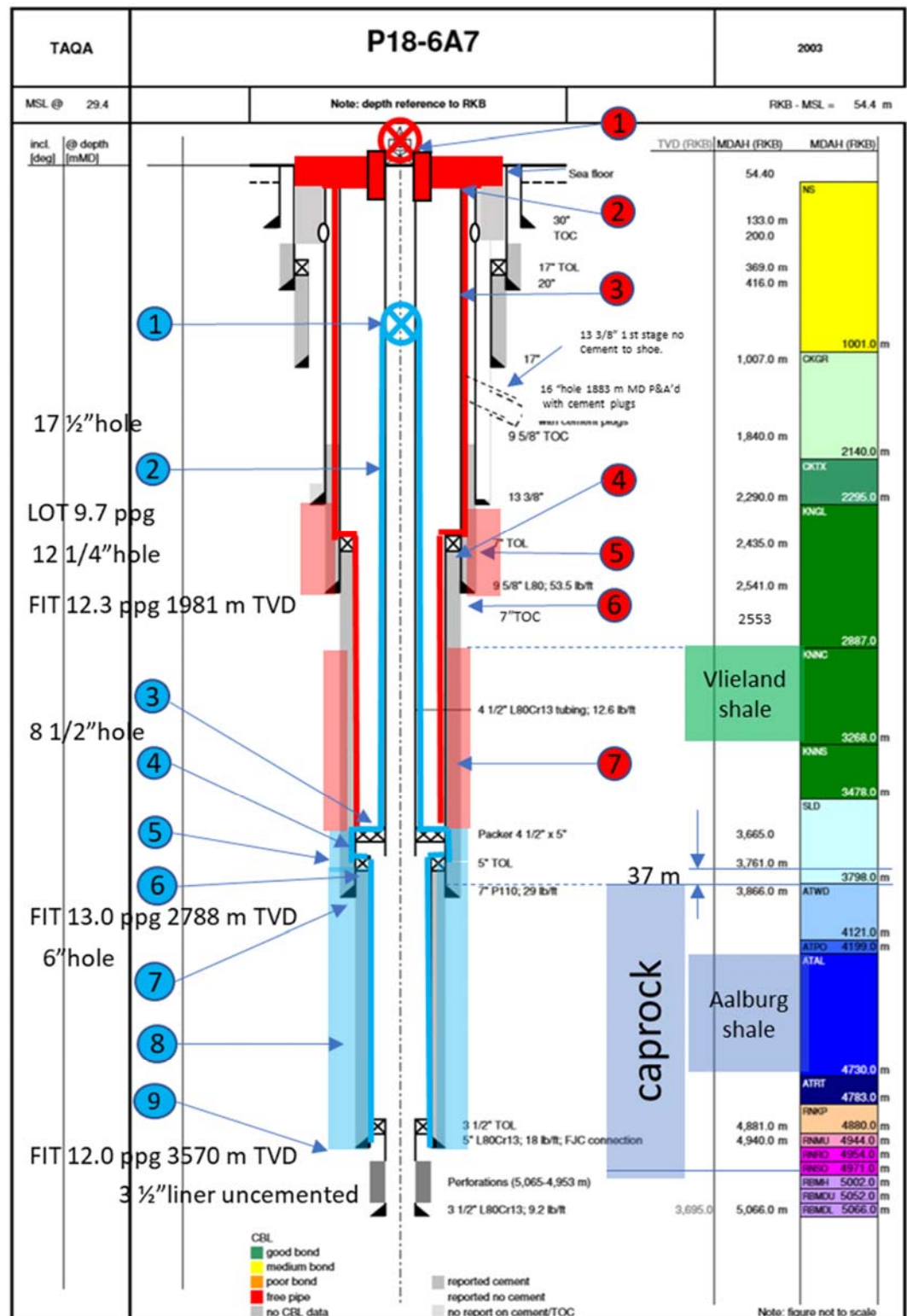
Figure 9-2. Well P18-A-07-S1 barrier diagram with barrier elements defined. See Table 9-1 for a discussion of the barrier elements (indicated by the numbered circles).

Table 9-1 Well P18-A-07-S1 barrier element assessment based on current data set. The numbers
in the first column correspond with the numbers in coloured circles in Figure 9-2.

no	P18 6A7	As built	Monitor	Barrier validated	Validation Criteria
					Primary well barrier
1	4 1/2" Scsssv		Maintained	Yes	Tested & maintained
2	4 1/2" Tubing	Tested to 4050 psi	Annular pressure records	Yes	Tested
3	7" Production packer	The permanent packer is set at 3665 m MD and tested, it is postioned 133 m above the caprock	Annular pressure records	Yes	Tested, set 133 m above caprock
4	7" Liner	The 7" liner is flow wetted over 96 meter between the production packer and the 5" liner lap	Annular pressure records	Yes	Pressure tested to 3800 psi. The flow wetted section is a single barrier to the overburden with a length of 96 m, this is above the caprock
5	7" Liner cement	Good cement report, the calculated TOC is at 2553 m MD (118 m below the 7" top of liner) and tested to 4050 psi, no CBL has been executed	NA	Yes	Good cement report and tested
6	5" Liner + liner lap	Tested to 3800 psi. The top of liner is at 3761 m MD, that is 37 m above caprock.	NA	Yes	Tested - installed 96 m below the production packer
7	In-situ formation (Caprock) at 7" liner shoe	FIT 13.0 ppg at 2788 m TVD	NA	Yes	A FIT of 13.0 ppg at 2788 m TVD has been reported
8	5" Liner cement	It is cemented with 14 bbl short of cement due to the wiper plug bypassing cement. It was tested to 3800 psi and there was no CBL executed	NA	Yes	It has a good cement report Identified NFS potential - Aalburg shale
9	In-situ formation (Caprock) at 5" liner shoe	FIT 12.0 ppg 3570 m TVD	NA	Yes	FIT 12.0 ppg 3570 m TVD reported
					Secondary well barrier
1	Surface tree + tubing hanger	Tested to 3800 psi	Maintained	Yes	Tested & maintained
2	Well head + Casing hanger	Tested to 3800 psi	Maintained	Yes	Tested & maintained
3	9 5/8" Casing	Tested to 3800 psi with 7" & 5" liners	Annular pressure records	Yes	Tested to 3800 psi with 7" & 5" liners
4	7" Liner + liner lap	Tested to 4050 psi. The top of liner is at 2435 m MD.	NA	Yes	Tested to 4050 psi
5	9 5/8" Casing cement	Cement report with some losses reported, the TOC of the 9 5/8" casing is calculated to be at 1840 MD (1570 m TVD). No CBL has been executed. It is tested to 3800 psi	Annular pressure records	Yes	Cement report with some losses reported, it has been tested to 3800 psi
6	In-situ formation	FIT 12.3 ppg at 1981 m TVD	NA	Yes	FIT 12.3 ppg at 1981 m TVD reported
7	7" Liner cement	Good cement report, the calculated TOC is at 2553 m MD (118 m below the 7" top of liner). It is tested to 4050 psi, no CBL has been executed	Annular pressure records	Yes	Good cement report and tested Identified NFS potential - Vlieland shale

9.2.5 Conclusion on current well status

The P18-A-07-S1 well is relevant in the context of CO$_2$ injection into the P18-6 reservoir and has been evaluated regarding its current status and well integrity risks. The well has the potential to be used safely as CO$_2$ injector. Appropriate mitigations can make it fit for CO$_2$ storage operations as given below.

9.2.5.1 Summary

The P18-A-07-S1 well could be re-used safely for CO$_2$ injection if the risks identified are mitigated properly; see overview in Table 9-2.

Table 9-2 Overview of P18-6 CO_2 injector well.

Well	Status	Integrity for CO_2 injector	Remarks
P18-A-07-S1	Producer	Yes	The production packer is placed above the caprock, this extends the 7" liner from above the caprock past the production packer. The 7" liner is made of P110 carbon steel and is exposed to corrosion of well bore fluids, with a potential risk of failure and leakage to the overburden. Repositioning of production packer to inside caprock should be considered.

9.3 Influence of cooling on well integrity

Injection of CO_2 at a lower temperature than the temperature of the surrounding rock can cause thermal contraction of the materials and associated stress reduction of the surrounding rock in the near-well area that may affect the structural integrity of the well barriers. The operating envelope of P18-6 CO_2 injection well needs to consider cooling effects, which are not part of the current operating envelope designed for natural gas production.

In this section we provide an estimate of the effects of cooling due to cold CO_2 injection on the structural integrity of the injection well, focussing on the integrity of annular cement behind the casing, and discuss the risk of leakage along the outside of the well. Potential failure modes of the sealant (cement sheath) that can create potential continuous leakage pathways up the well across the caprock are of primary interest (Figure 9-3). The most likely leakage mechanism is related to the flow of fluids along a microannulus formed by de-bonding of the cement-casing interface or the cement-formation interface.
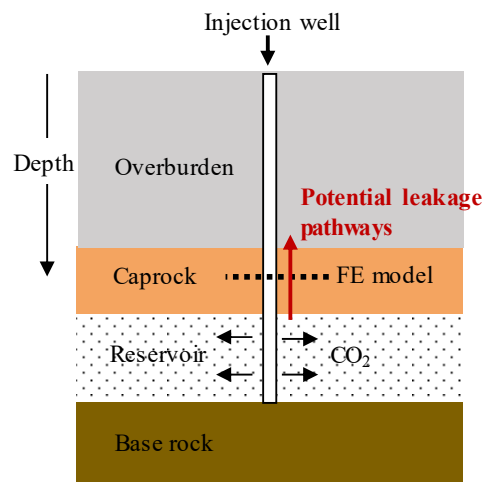
Figure 9-3: Sketch of an injection well showing the location of a finite element (FE) model for well integrity analysis at the caprock level. The model represents a cross-section of the near-wellbore area normal to the well axis at the analysis depth (see Figure 9-6). Please note that the relative sizes of reservoir, caprock and overburden are not to scale.

Note that, in order for CO_2 to migrate and eventually leak to the overburden through a microannulus, several events have to take place and several constraints with regard to subsurface conditions have to be met. The likelihood of cement-casing or cement-rock debonding to take place during injection of cold CO_2 in the P18-6 well is investigated using a numerical model based on the DIANA finite elements[8]. Subsequently, the likelihood that a continuous microannulus forms along the entire caprock level towards the overburden, and the conditions that need to be met for CO_2 to migrate through a microannulus into the overburden are discussed. For a worst-case scenario where all events occur and all conditions are met, an estimate of the leakage rate will be given and this will be discussed in the context of the total storage capacity in P18-6.

9.3.1   Pressure and temperature in the CO_2 injection well

Section 6.4.3 presents the results of a limited study of the CO_2 conditions in the well during injection. Figure 9-4 and Figure 9-5 show the pressure and temperature profiles for the storage and discharge scenarios, respectively. Figure 9-5 shows that CO_2 temperatures at bottomhole will be about 50 °C (for the storage scenario) or about 70 °C (for the discharge scenario) below reservoir temperature. The figures show pressure and temperature profiles for steady-state conditions; the temperature in the well during a non-steady-state operation (such as a shut-in procedure) may lead to lower temperatures of the CO_2 in the well, but the heat capacity of the well system (such as liner and annulus fluid) prevents those short-lived low-temperature events from significantly changing the temperature of the cement and casing in the deeper parts of the well [9]. The profiles shown in the figures can be used as a reliable estimate of the conditions in the well.
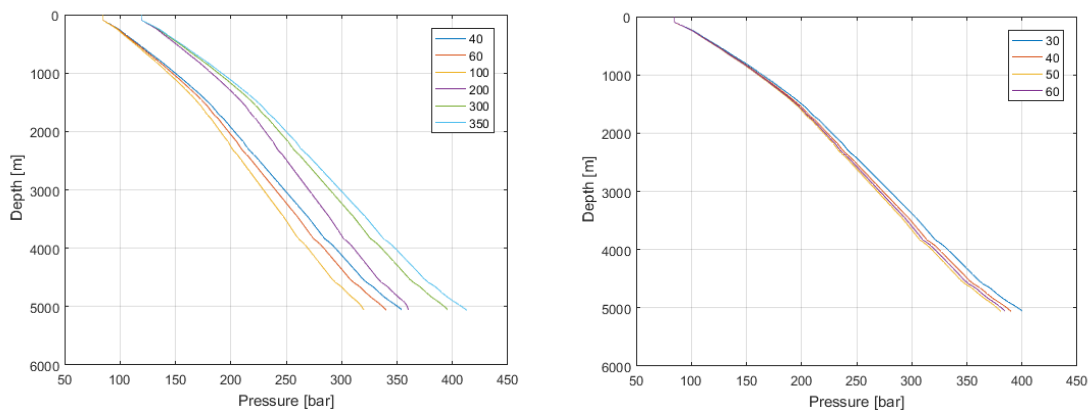
Figure 9-4: Pressure profiles as a function of the along hole depth for the cases of steady-state CO_2 injection from Table 6-1 (left) and pipeline discharge from Table 6-2 (right). Depth along the vertical axis is measured along the borehole.

---

[8] See dianafea.com.
[9] S. Belfroid, personal communication, 2019.
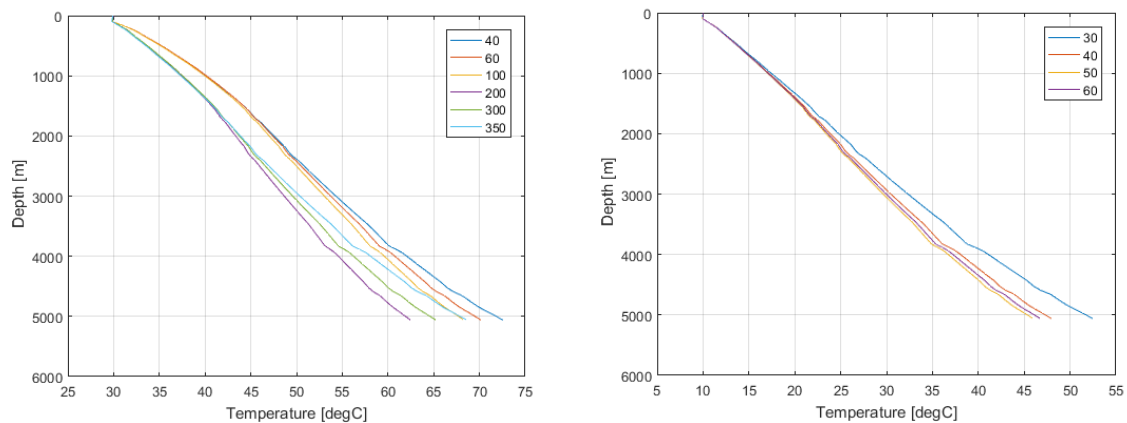
Figure 9-5: Temperature profiles as a function of the along hole depth for the cases of steady-state CO_2 injection from Table 6-1 (left) and pipeline discharge from Table 6-2 (right). Depth along the vertical axis is measured along the borehole. The temperature of the reservoir is 117 °C.

9.3.2 Numerical modelling of the effects of cold CO_2 injection on well cement integrity

A numerical model was developed to investigate the impact of thermal effects on well integrity, in particular on the integrity of annular cement behind the casing. Thermo-mechanical non-linear finite element analyses considered a section of a CO_2 injection well across the caprock (Figure 9-6), to evaluate whether failure of the well barriers could result in debonding of the annular cement with the casing and/or rock interfaces at caprock level, thereby creating a microannulus. In a worst case scenario, when such a microannulus is continuous from reservoir to above the caprock, a leakage path is formed.
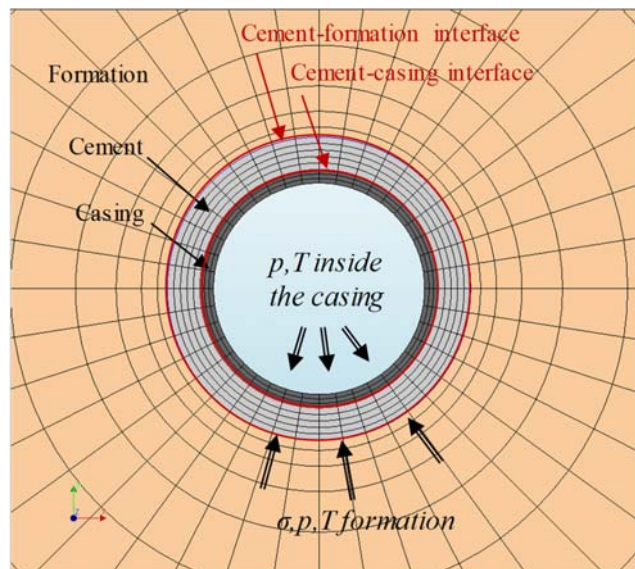
Figure 9-6: Mesh for a 2D finite element model of a cross-section of the near-well area.

Table 9-3: Model input parameters.

Parameter	Unit	Caprock	Cement	Casing	Interface
E Young modulus	GPa	26	8.3	200	rigid
v Poisson coefficient	-	0.3	0.1	0.3	-
Thermal expansion coeff.	K^{-1}	$1 \cdot 10^{-5}$	$1 \cdot 10^{-5}$	$1.3 \cdot 10^{-5}$	-
Volumetric specific heat	$Jm^{-3} K^{-1}$	$2.24 \cdot 10^{6}$	$4 \cdot 10^{6}$	$4 \cdot 10^{6}$	-
Thermal conductivity	$Wm^{-1} K^{-1}$	2.3	0.87	15	-

The non-linear finite element simulator DIANA was used to generate meshes for 2D numerical models of the well system and run simulations. The workflow for well integrity analysis is automated through a dedicated user interface called the DIANA SEALEC application. Based on the user input in DIANA SEALEC, meshes of the well system can be generated automatically and well integrity analyses mimicking the entire lifetime of a well can be conveniently defined and executed.

The numerical model of the near-well area was developed on a cross-sectional area normal to the well axis. The model comprises well casing(s), cement sheath(s) and the surrounding rock formation. Two models with different well completion geometries were developed: completion with a single casing (Figure 9-7a) and completion with a double casing (or a liner lap; (Figure 9-7b). Chosen sizes and characteristics of casings in the models are representative of the P18-6 well. The possible injection well is completed over the caprock depth interval with a 9 5/8" casing and a 7" liner, and in some cases with a 5" liner.

Complete plane strain elements are used for bulk materials and zero-thickness interface elements are used for the casing-cement and the cement-formation interfaces. All materials in the model are assumed to be elastic and the well material interfaces are assumed to be rigid. The model input parameters are given in Table 9-3.
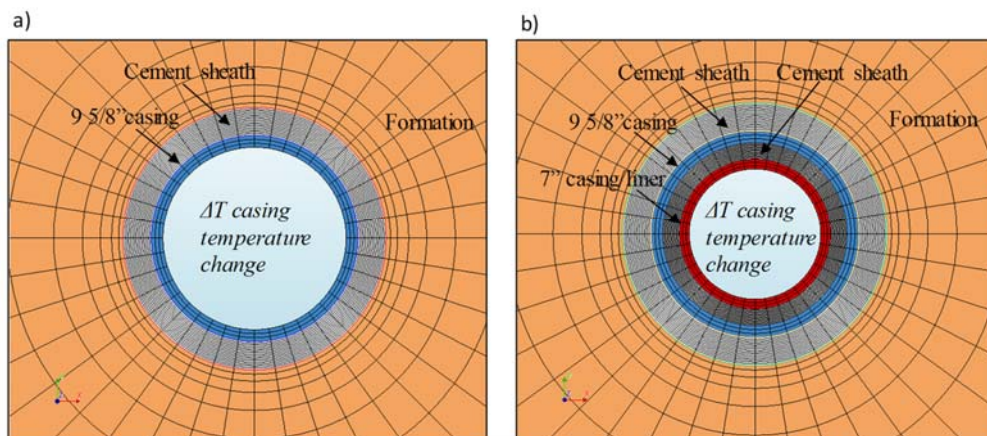
Figure 9-7: Meshes for 2D finite element models of the near-well area at the level of caprock for well sections completed with (a) a single casing and (b) a double casing (liner lap).
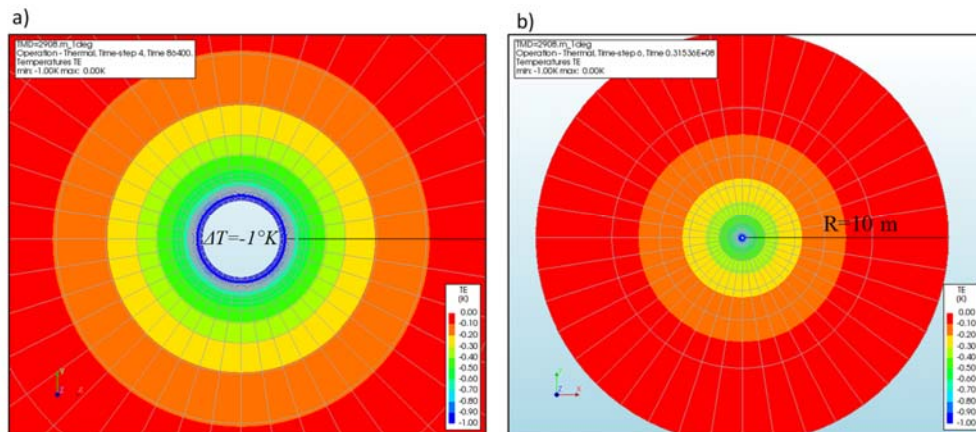
Figure 9-8: Contours of temperature change in the near-well area due to a casing temperature change of -1°K (or -1°C) after (a) 1 day and (b) 1 year. The contour interval is 0.1°K.

The effects of cooling were assessed by applying a temperature load of -1°K (- 1°C) on the inner side of the casing instantly at the start of the analysis. As all the well materials in the model were assumed elastic, the magnitude of induced thermo-mechanical stresses ($\sigma_{\Delta T}$) scales linearly with the degree of cooling (ΔT), i.e. the stress magnitude due to cooling by $\Delta T < -1°K$ is obtained simply by multiplying ΔT with the stress magnitude predicted by the model ($\sigma_{\Delta T}$ = -1 K). A staggered heat flow and mechanical analysis is then performed. First a transient temperature field is calculated for a change in temperature of -1°K (- 1°C) and then the related thermo-mechanical stresses caused by this temperature change.

Note that the model is initially stress-free, i.e. the initial stress state in the cement sheath is set to zero as our aim is to estimate the net thermo-mechanical stress induced by cooling. Estimating the initial, i.e. present day (compressive) stress in annular cement of gas producing wells is difficult: direct in-situ measurement of stress in cement at downhole conditions is not possible; stress estimates can only be obtained by modelling the entire well history, taking into account the different phases in the lifetime of a well, cement material properties, quality of executed cement job, interactions with the surrounding rock formation, etc.. Modelling well histories is beyond the scope of this task, which focusses on the thermo-mechanical effects of cooling on well cement integrity.
Simulation results show gradual extension of the cooled area radially into the surrounding rock (Figure 9-8 and Figure 9-9). After 1 year of injection, the radial extent of cooled area is about 10 m and has reached the edge of the model. The largest drop in temperature occurs within a radius of 1-3 m from the injection well (Figure 9-9).

Temperature profiles for 1°K cooling
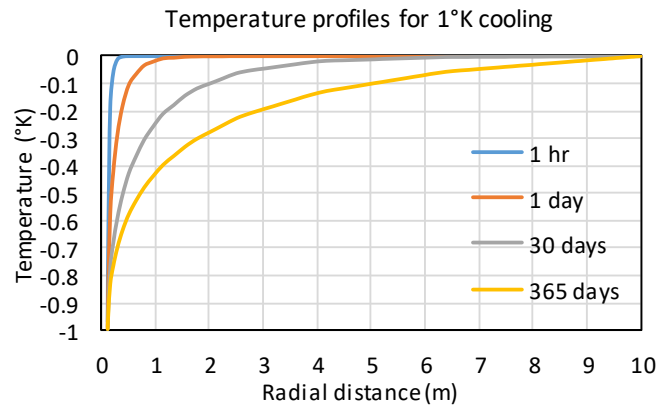
Figure 9-9: Profiles of temperature change as a function of radial distance from the well due to a casing temperature change of -1°K (or -1°C) for different times.

Cooling induces thermal contraction which in turn induces thermo-mechanical tensile stresses in the radial direction. As expected, the magnitude of tensile stress increases with time, as the cooling front propagates deeper into the surrounding formation, and decreases with the radial distance from the well casing.

For a single casing well model, the magnitude of tensile stresses is larger at the casing-cement interface, which is closer to the inner side of the casing than at the cement-formation interface (blue bar and orange bar, respectively in Figure 9-10). The magnitudes of tensile stresses range between 0.1 and 0.17 MPa/1°C. For a decrease of casing temperature by 50°C, tensile stresses at the interfaces will be thus 50 times higher and can reach 5 to 8.5 MPa. If the initial stress in cement is less than these values, de-bonding of the interfaces will occur.
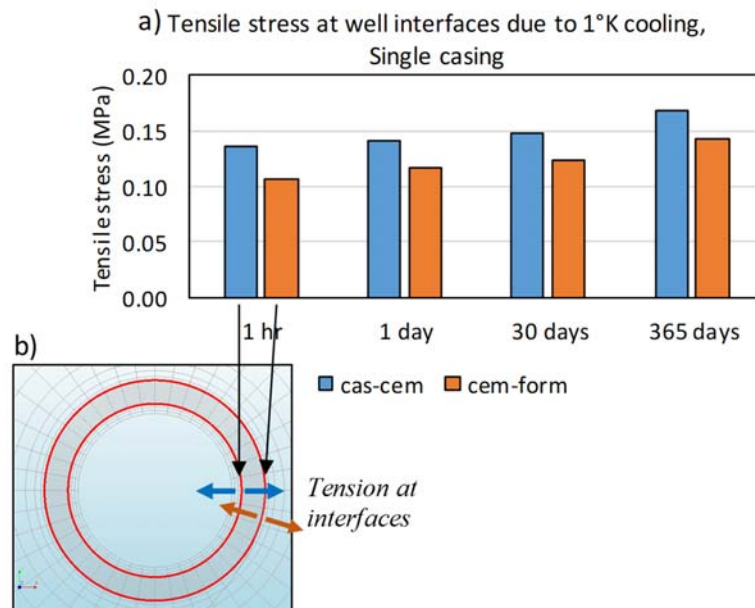
Figure 9-10: (a) Tensile stresses at the well interfaces due to a casing temperature change of -1°K (or -1°C) after 1 hour, 1 day, 30 days and 365 days. (b) Sketch showing locations of the monitoring points at the two interfaces in a single casing well model.
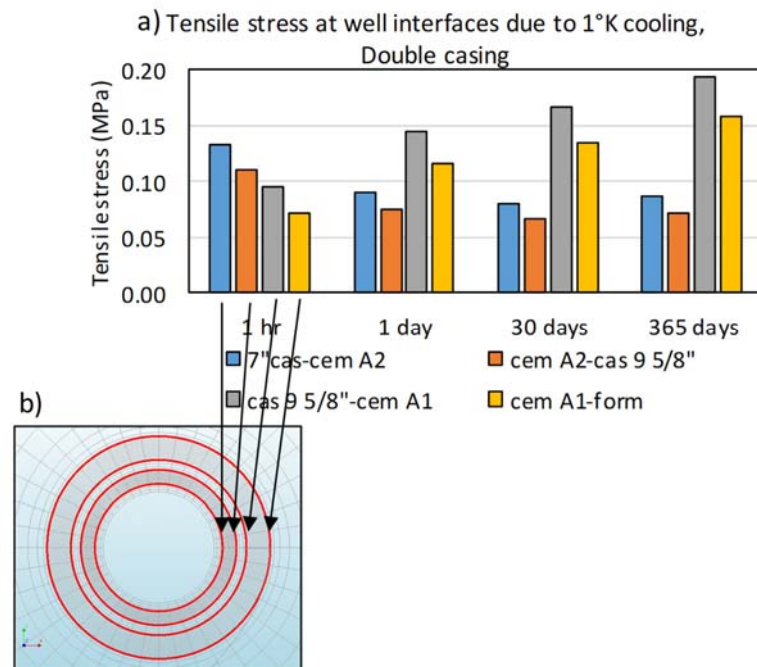
Figure 9-11: (a) Tensile stresses at the well interfaces due to a casing temperature change of -1°K (or -1°C) after 1 hour, 1 day, 30 days and 365 days. (b) Sketch showing locations of the monitoring points at the four interfaces in a double casing well model.

In a double casing well model there are four well interfaces and the evolution of tensile stresses at the interfaces with time is more complex (Figure 9-11). Initially, just after the start of cooling, the magnitude of tensile stresses at the interfaces decreases with the distance from the inner casing (Figure 9-11, 1hr). This pattern was also observed in the single casing well model. However, for longer cooling times, from 1 day onwards, the largest magnitude of tensile stresses occurs at a more distant interface between the 9 5/8" casing and cement (grey bar in Figure 9-11). These magnitudes of ~0.19 MPa per 1°C cooling are larger than in the case of a single casing well model (grey bar for 365 days in Figure 9-11). Overall, the magnitude of thermal stresses is dependent on the values of elastic and thermal properties for the well materials (casing, cement and rock) and their interfaces.

9.3.3   *Implications of debonding on formation of potential leakage pathway*
Annular cement across the caprock in the P18-6 well could only be assessed with cement reports, no CBLs were run. Based on the P18-2 assessments the well is expected to have sections with good cement and sections with poor/absent cement.Sections with poor cement are not considered to be sealing. Sections with good cement, which are in many cases a few tens of meters long, are most sensitive to debonding. For creation of a leakage pathway from reservoir to overburden, across the entire caprock thickness, de-bonding needs to occur along all sections with good cement, in order to connect sections with poor cement. Debonding of good cement is possible to occur at the level of caprock due to cooling by 50-70°C because of:
–   large induced thermo-mechanical tensile stresses, which tend to cause de-bonding (~5-10 MPa);

- very low tensile strength of the well cement interfaces (that counteracts the tensile stress) of 0.1-3 MPa for a good cement bond and ~0 MPa for a poor cement bond;
- possibly low, largely uncertain magnitudes of the radial compressive stress in the annular cement (that counteracts the tensile stress).

The actual permeability and therefore also the flow rate is stress-dependent. The microannulus may be open and act as a conduit or closed and act as a seal. The permeability of circumferential microannuluscreated by debonding depends on the effective normal stress acting on that fracture (σ_n') and the fluid pressure inside the microannulus (p); when $p > \sigma_n$', the microannulusis open and acts as a conduit, when $p < \sigma_n$' the microannulus is closed and acts as a seal.
The effective normal stress σ_n' is either:

- The radial stress in annular cement (σ_n'-cem) acting on the casing-cement interface. The σ_n'-cem is largely uncertain and could be low especially in the case of cement sheath located in-between two casings. The σ_n'-cem could possibly be lower than the hydrostatic stress (< 0.10-0.11 bar/m). This implies that the hydrostatic fluid pressure inside the microannulus could keep the leakage path at the casing-cement interface open.
  Although a microannulus at the casing-cement interface can be kept open under a pressure lower than the hydrostatic pressure, the hydrostatic pressure conditions will still exist at the tip of a microannulus transecting the caprock. Keeping the CO_2 pressure in the reservoir below the hydrostatic pressure conditions will prevent the CO_2 from displacing the brine in the micro-annulus, as discussed in more detail in the next section.
- The radial stress in the rock formation (σ_n'-rock) acting on the cement-rock interface. The σ_n'-rock could be:
  (i) lower than the minimum in-situ horizontal stress *Shmin (0.17-0.18 bar/m),* but likely larger than the hydrostatic pressure (~0.10 to 0.11 m/bar), if a plastic zone was formed in the (brittle) rock formation surrounding the wellbore;
  (ii) close to the *Shmin* (0.17-0.18 bar/m) if the wellbore is surrounded by naturally sealing formations, which are either ductile (Aalburg Shales) or viscous (Röt salt, halitic parts). Potential advantage of naturally sealing formations is that they can improve annular sealing around non-cemented or poorly cemented parts of casing strings simply by moving or creeping onto the casing strings. Additional advantage is an increase in the compressive stresses in the near-well area, which could become equal to the far-field stresses in these naturally sealing formations (0.17-0.18 bar/m in shales and 0.21 bar/m in halite). This implies that the hydrostatic fluid pressure inside the microannulus cannot keep the leakage path at the cement-formation interface open. The microannulus is closed and acts as a seal. Several shale layers and potentially salt layers in the caprock of the P18 reservoir have been identified as natural sealing formations. Local sealing of a microannulus could make the leakage path discontinuous and therefore prevent leakage.

9.3.4   Leakage risk and the effect of chemistry
The well integrity simulations demonstrated that de-bonding of the well interfaces could possibly occur at the good cement sections of the P18-6 well due to the mechanical stress related to cooling on the well materials and interfaces. In a worst case scenario, de-bonding could result in the formation of a leakage path (a

microannulus), connecting the storage reservoir with the overburden, as discussed in the previous Section.

Figure 9-12 gives a schematic representation of the pressure evolution in the reservoir and overburden in the various stages of the reservoir from initial (pre-production or virgin pressure) to post-CO_2 injection. The initial reservoir conditions at the start of the gas production phase show the equilibrium of the water and gas pressure as developed during the geologic time of its existence. The hydrocarbon buoyancy pressure anywhere in the reservoir above the water-gas contact, equal to the average capillary pressure, is higher than the water pressure. Because of the capillary entry pressure of the caprock, which is higher than the prevailing buoyancy pressure if leakage does not occur, the gas remains in the reservoir.

In the gas production phase, both the water and the gas pressure in the reservoir decrease to low and sometimes very low levels. In case of a 'tank reservoir' where (strong) aquifer support is absent, the pressure remains low after production has ceased.
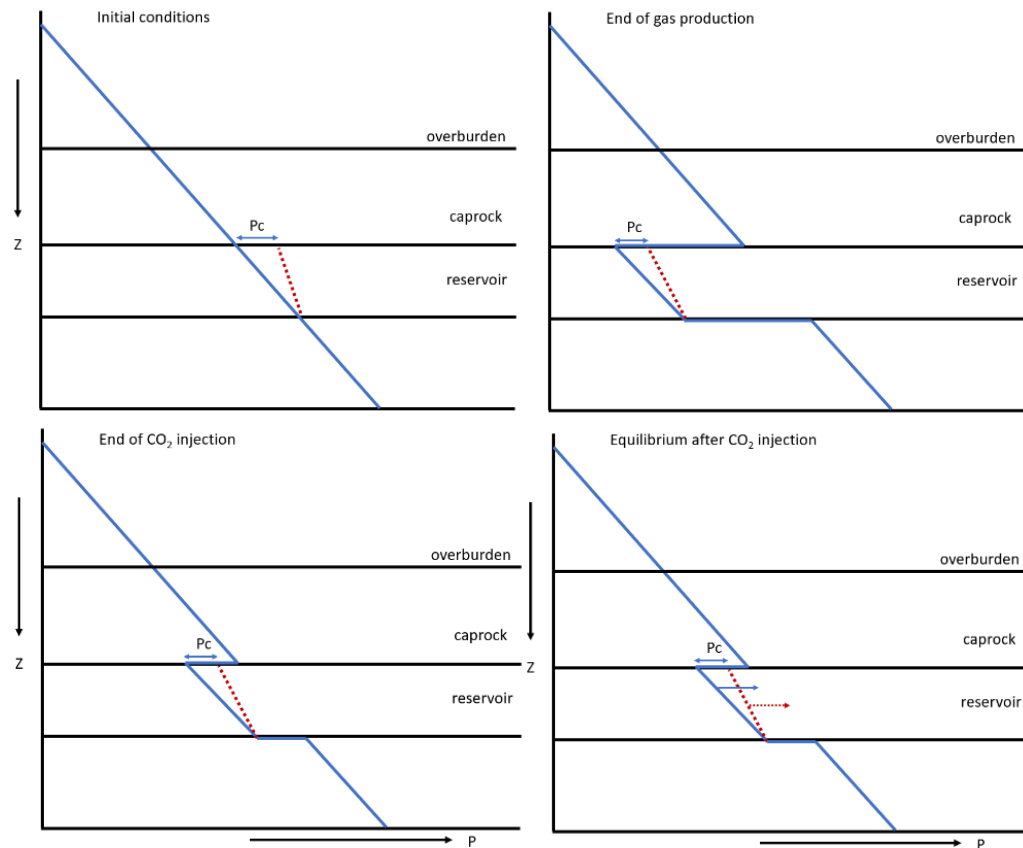
Figure 9-12: Pressure conditions in the various stages of the reservoir.

At the reservoir-caprock interface, a sharp water pressure transition exists because the water in the caprock is practically immobile on the time scale of hydrocarbon production and CO_2 injection. During CO_2 injection, both the water and gas pressure in the reservoir increase. As long as the gas pressure remains below the hydrostatic conditions at the base of the caprock, the gas will not be able to

displace the water column in the overburden and leakage will not occur, even if a leakage path such as a microannulus exists. With time, the reservoir conditions will move towards an equilibrium state due to water influx from the over- and underburden into the reservoir, implying re-pressurisation of the reservoir. In case of a tank reservoir, this influx is very small and it will take thousands of years before the gas pressure in the reservoir will become higher than the overlying hydrostatic column. This implies, that even if a leakage path such as a microannulus exists, a CO_2 leakage mechanism is absent.

In the unfortunate event that the gas pressure does increase to above the hydrostatic pressure, it is still uncertain whether CO_2 would migrate through a microannulus. Microannuli with small apertures will have a capillary entry pressure, similar to caprocks. The gas pressure has to be higher than the sum of the hydrostatic pressure at the base of the caprock and the entry pressure.

If CO_2 could displace the water column within the microannulus and starts migrating upwards, chemical interaction will take place with the cement. Assuming that the cement is of good quality, horizontal migration of CO_2 into the cement will take place by diffusion in dissolved state. Cement, which has a very high pH, is susceptible to interaction with carbonized water as cement minerals can quickly dissolve when the pH of the pore water decreases. The complex chemical interaction between cement minerals and carbonized brine is described in many publications (e.g., Kutchko et al., 2007; Rimmelé et al., 2008; Duguid et al., 2010). The most important reactions involve the dissolution of portlandite ($CaOH_2$), the de-calcification of Ca-silicate hydrate (CSH) and the precipitation of calcite ($CaCO_3$) (Figure 9-13). Depending on the location of calcite deposition, complete pore clogging of the cement can occur, preventing further diffusion of carbonized brine and thereby further degradation of the cement.
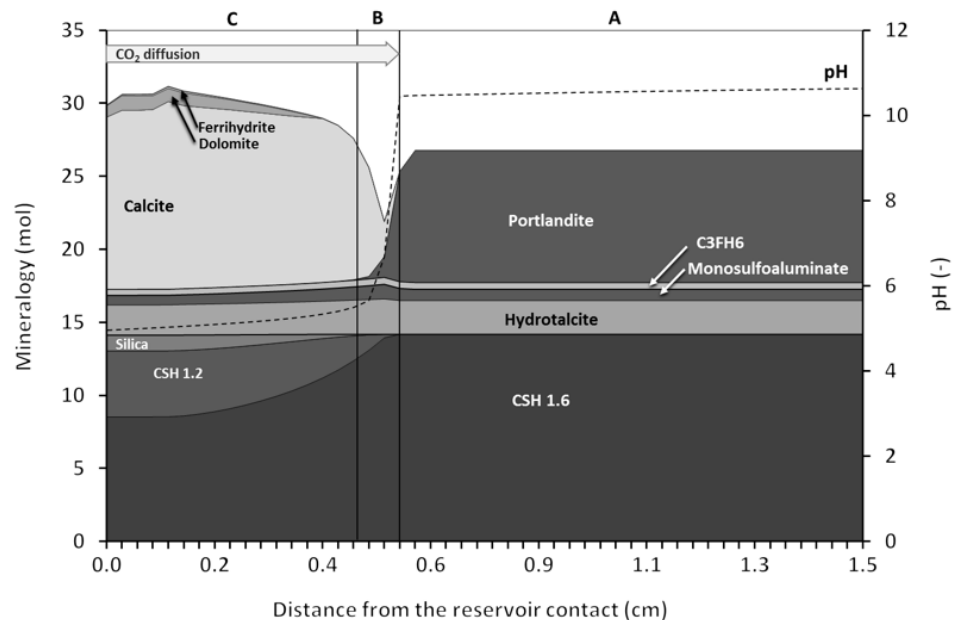
Figure 9-13: Simulated cement mineralogy with distance from the reservoir (or brine) contact after 300 days of inward diffusion of dissolved CO_2 and kinetic mineral reactions (PHREEQC software). Three zones develop: A: original cement, B: dissolution front, C: carbonated zone. The porosity of the cement decreases in the carbonated zone. From Koenen et al. (2014).

The upward flow of CO_2 through the microannulus adds another complicated component to the process, and has been described in Koenen and Wasch (2018). Instead of calcite precipitation in the pore spaces of cement, the calcite can accumulate within the microannulus and block the leakage path. The potential presence of sulfate in the caprock formation water can result in anhydrite precipitation in the microannulus, supporting the microannulus clogging by calcite (Koenen and Wasch, 2018). Whether clogging occurs depends on the upward flow rate of the CO_2 and the width of the microannulus. A low flow rate and/or small microannulus will allow calcite (and anhydrite) deposit to grow and block the leakage path. A high flow rate and/or large microannulus will not allow calcite growth, and instead, the leakage path will get worse in time due to cement mineral dissolution.

This is illustrated in Figure 9-14. The worst case conditions for a microannulus of 100 micron and a CO_2 pressure 10 bar above hydrostatic conditions give a migration rate of CO_2 towards the overburden in the order of 10^{-6} kg/s, adding up to slightly more than 30 kg per year (Koenen and Wasch 2018). Compared to the storage volume of ~1.3 Mtonne, this amount of leakage can be considered as negligible.
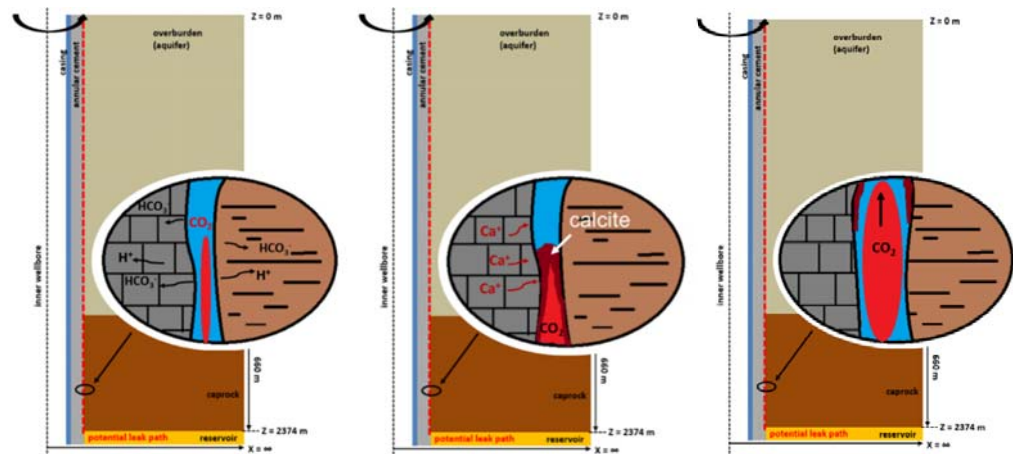
Figure 9-14: Schematic overview of CO_2 migration through a microannulus (red dotted line in between the annular cement and the surrounding rock). Left: initial state of microannulus and CO_2 migration. Middle: at low flow rate and/or small microannulus dissolved calcium migrates to the microannulus and is deposited as calcite, thereby blocking the leakage path. Right: at high flow rate and/or large microannulus the leakage path is enhanced as fast cement dissolution and CO_2 flow prevent calcite deposition. From Koenen & Wasch (2018).

9.3.5   *Conclusions*

Well dynamics simulations provided input on the temperature evolution along the wellbore with time. They showed that the CO_2 inside the injection well is 50 °C to 70 °C colder than the surrounding caprock formation, with largest temperature differences occurring in the initial phase of injection when the reservoir pressure is low (~60 bar) and the temperature of CO_2 at bottom hole is 60-70 °C.

Based on performed simulations, debonding of well interfaces in the P18-6 CO_2 injection well is possible to occur due to cold fluid injection, thermal contraction and associated stress reduction in the near-well area. Debonding can, in principle, occur

over lengths of tens of meters of caprock sections with good CBL. However, for migration of CO_2 with eventually leakage to occur, a continuous microannulus along the well cemented sections need to connect poorly cemented sections towards the overburden before we can speak of a leakage path. The presence of shale and potentially salt layers in the P18-6 caprock, identified as natural sealing formations could locally interrupt the leakage path. Even if a continuous leakage path would exist, it depends on the microannulus characteristics and pressure conditions whether upward CO_2 migration would actually take place. If the pressure conditions in the reservoir are high enough to overcome the capillary pressure within the microannulus, and migration does take place, the chemical interaction between CO_2 and cement can either prevent or enhance leakage towards aquifers overlying the caprock or towards the surface, also depending on the microannulus characteristics and pressure conditions. Keeping the CO_2 pressure in the reservoir below or at the hydrostatic pressure conditions will prevent the CO_2 from displacing the brine in the microannulus. In that case adequate monitoring during injection operations is required. The decommissioning method and procedures should result in well plugging from formation-to-formation (pancake plug or similar) in case microannulus formation is likely and poorly bonded annulus cement is not accepted as a leakage barrier.

Overall, the likelihood of CO_2 leakage through microannuli is small. De-bonding of cement-casing and cement-rock interface is very likely, but a leakage path requires a continuous microannulus from reservoir to overburden which is less likely. The presence of that natural sealing formations in the caprock could locally seal a microannulus, disconnecting the reservoir from the overburden. If a leakage pathway does exist, the CO_2 pressure in the reservoir should be high enough to displace the water in the microannulus. For a pressure below or at hydrostatic conditions, as is the plan for CO_2 storage in P18-6, this would not happen. In case the CO_2 pressure would be high enough to migrate through the microannulus, chemical interaction between the CO_2 and the cement would stimulate self-sealing of the leakage path by calcite precipitation. In a worst case scenario that self-sealing would not occur, leakage rates would be very low; e.g. <0.00001% of the total amount of CO_2 that can be stored in P18-6 on an annual basis.

9.4　Well decommissioning

9.4.1　*Decommissioning after the end of injection*
After completing the CO_2 injection through the P18-6 injection well, it needs to be decommissioned in a way that conforms to good practice and meets required standards for a CO_2 storage site. After decommissioning, the well should ensure permanent and safe containment of the CO_2 in the reservoir.

Currently cement is the material of choice for annular seals and decommissioning of oil and gas wells. The abandonment plug has to extend across the full cross section of the well ("rock-to-rock"), whilst covering all annuli. If the cement behind the casing(s) is good, this can be achieved by placing a cement plug in the casing. If the quality of the annular seal is not sufficient or cannot be confirmed, pancake plugs have to be installed. This is achieved by removing the casing(s) and potentially cement and thereby creating a so called 'window'. These are standard O&G practices, clearly described in the decommissioning standards.

Reaction of CO_2 with wellbore cement is a slow process if good construction practices and proper cement materials were used (IEAGHG, 2018). Degradation rates have been found to be proportional to temperature, pressure and the square root of time (Shell, 2015). According to literature the degradation of Portland cements could be up to about 12 m in 10.000 years. It is also reported that the permeability that can be created by the degradation is such that it still is within API criteria for cement (EPA, 2012).

Previous work (Vandeweijer et al., 2011) recommended placing pancake-type abandonment plugs. This approach to the P&A of CO_2 wells was also proposed in the permit application for the P18-4 reservoir. Whether pancake-type plugs will be the method of choice for decommissioning of the P18-6 injection well, and which materials to be used for the plug, depends on future developments until time of decommissioning.

9.5   Conclusions

Well integrity
The P18-A-07-S1 well has been evaluated in the context of CO_2 injection into the P18-6 reservoir regarding its current status and integrity risks. The reviewed well has the potential to be used safely as CO_2 injector. Appropriate mitigation measures have been proposed to make it fit for CO_2 storage operations.

Effects of injecting cold CO_2 on well integrity
It is possible that de-bonding of cement interfaces will take place upon cold CO_2 injection, creating microannuli. In the unlikely case that the microannulus forms a continuous leakage path from reservoir to overburden, the characteristics of the microannuli and pressure conditions determine whether upward CO_2 migration would actually take place. Keeping the CO_2 pressure in the reservoir below or at hydrostatic pressure conditions will prevent the CO_2 from migrating through the microannulus. This justifies the choice of keeping the reservoir pressure below or at hydrostatic conditions. However, if for some reason the reservoir pressure would be high enough to displace the water column in the microannulus, the chemical interaction between CO_2 and cement can either prevent or enhance leakage, also depending on the microannulus characteristics and pressure conditions. For worst-case conditions, if CO_2 would migrate from the reservoir to the overburden through a microannulus, leakage rates would still be very low; i.e. <0.00001% on an annual basis. Overall, the likelihood and effect of leakage through microannuli is very low and can be considered insignificant.

Well decommissioning
Appropriate methods should be used for the decommissioning of the well. Given the likelihood of microannuli forming during the injection of cold CO_2, decommissioning methods that remove these potential leakage paths would be preferred. As an example, full-bore pancake like plugs would provide formation-to-formation closure of the well.

10   P18-6 storage site and storage complex

10.1   Introduction

The assessment of leakage risks for CO_2 storage in the P18-6 field relies on a robust definition of the storage site and storage complex. In this Section these definitions are discussed, based on definitions in the EU Storage Directive and insights from the detailed reservoir, fault, caprock and well evaluations in Sections 6 to 9.

10.2   Definitions in the Netherlands Mining Law and the EU Storage Directive

The EU Storage Directive (EU, 2009) introduced the concept of the 'storage complex' when defining rules for environmentally sound and safe geological storage of CO_2. The directive states that safe storage is to be accomplished by the characterization and assessment of the storage complex.

The following definition is given of the storage complex, *op. cit.*:
> 'storage complex' means the storage site and surrounding geological domain which can have an effect on overall storage integrity and security; that is, secondary containment formation

According to the Netherlands Mining Law (Mijnbouwwet, 10 April 2019):
"*CO_2-opslagcomplex: opslagvoorkomen voor CO_2 en de omringende geologische gebieden die een weerslag kunnen hebben op de algehele integriteit van de opslag en de veiligheid ervan*". The definition of "storage complex" in the Netherlands Mining Law does not explicitly refer to "secondary containment formation" like in the EU Storage Directive.

For the definition of "storage site" the Netherlands Mining Law uses the term "*opslagvoorkomen van CO_2*". Although it seems that this term can be linked to "storage site" in the EU Directive it is not clear if this will include "the associated surface and injection facilities" as well, like is defined in the EU Storage Directive (see below). For this report it is assumed that these facilities are part of the storage site. "*Opslagvoorkomen is: een voorkomen dat gebruikt wordt voor opslag*" according to the Netherlands Mining Law meaning "an occurrence which is used for storage".

The storage site according to the EU Directive is defined as, *op. cit.*:
> "storage site" means a defined volume area within a geological formation used for the geological storage of CO_2 and associated surface and injection facilities

Leakage then means "*any release of CO_2 from the storage complex*" and migration stands for "*the movement of CO_2 within the storage complex*" according to the EU Directive.

The Storage Directive (EU, 2009: Article 4, para 4) also says:
> "*4. A geological formation shall only be selected as a storage site, if under the proposed conditions of use there is no significant risk of leakage, and if no significant environmental or health risks exist.*".

The hydraulically connected pore space bordered by flow barriers together representing a physical trap is considered, and the dispersion of CO_2 inside the physical trap is predicted by dynamic modelling. Our predictions will be tested by operational monitoring. This implies that monitoring activity should be focused particularly on providing the evidence for the effectiveness of the geological and engineering barriers that prevent significant risk of leakage (migration out of the storage complex).

Note that Guidance document no 2 (EC, 2011) suggests to allow for changes in the specific boundaries of the storage complex during the storage permit review and updating process.

CO_2 movement out of the storage site but remaining in the storage complex is called migration (in the Storage Directive). Movement of CO_2 out of the storage complex is called leakage under the Storage Directive, and if the CO_2 then reaches the atmosphere it is called emission under the implementing regulation of the ETS Directive (ETS Directive, 2009; EU 2018) and emission allowances need to be returned by the storage permit holder to the state. Leaks cannot be measured, they can only be estimated. From the monitoring plan and plan for corrective measures it needs to be defined how to recognise such movement of CO_2 and what actions or corrective measures to take.

10.3 Definition of the storage site

The storage site is what contains the CO_2 (i.e. the reservoir), the injecting or not yet decommissioned wells, the associated surface installations (wellheads) and injection facilities (tubing in wells). More specifically, the P18-6 storage site comprises the following:

- P18-6 Triassic reservoir rocks of the Volpriehausen Sandstone, Lower and Upper Detfurth Sandstones and the Hardegsen Formation. The lower 3 units are vertically hydraulically disconnected by the presence of low permeable zones in between (baffles). Strongly restricted flow is possible between the Upper Detfurth sandstone and the Hardegsen Formation (see Figure 17-11). The reservoir is bounded by faults on the SW and SE sides and dip closure on the NW and NE sides downdip of the GWC (see Figure 10-1; more details are in Section 12.1).
- Well P18-A-07-S1 penetrating the storage site up to the wellheads;
- Related wellheads, measurement equipment and christmas tree.

10.4 Definition of the storage complex

In addition to the components of the storage site mentioned in Section 10.3, the storage complex also includes the formations that seal off CO_2 in the reservoir and any surrounding formation that could contain CO_2.

The Porthos P18-6 storage complex is proposed to include the following spatial compartments in addition to the storage site components:

- Massive caprock on top of the reservoir consisting of impermeable rocks of the Upper Germanic Triassic Group and Altena Group with a total thickness of 450 to 750 m;

- The formations below the storage reservoir consisting of the Triassic Rogenstein and Main Claystone Members.
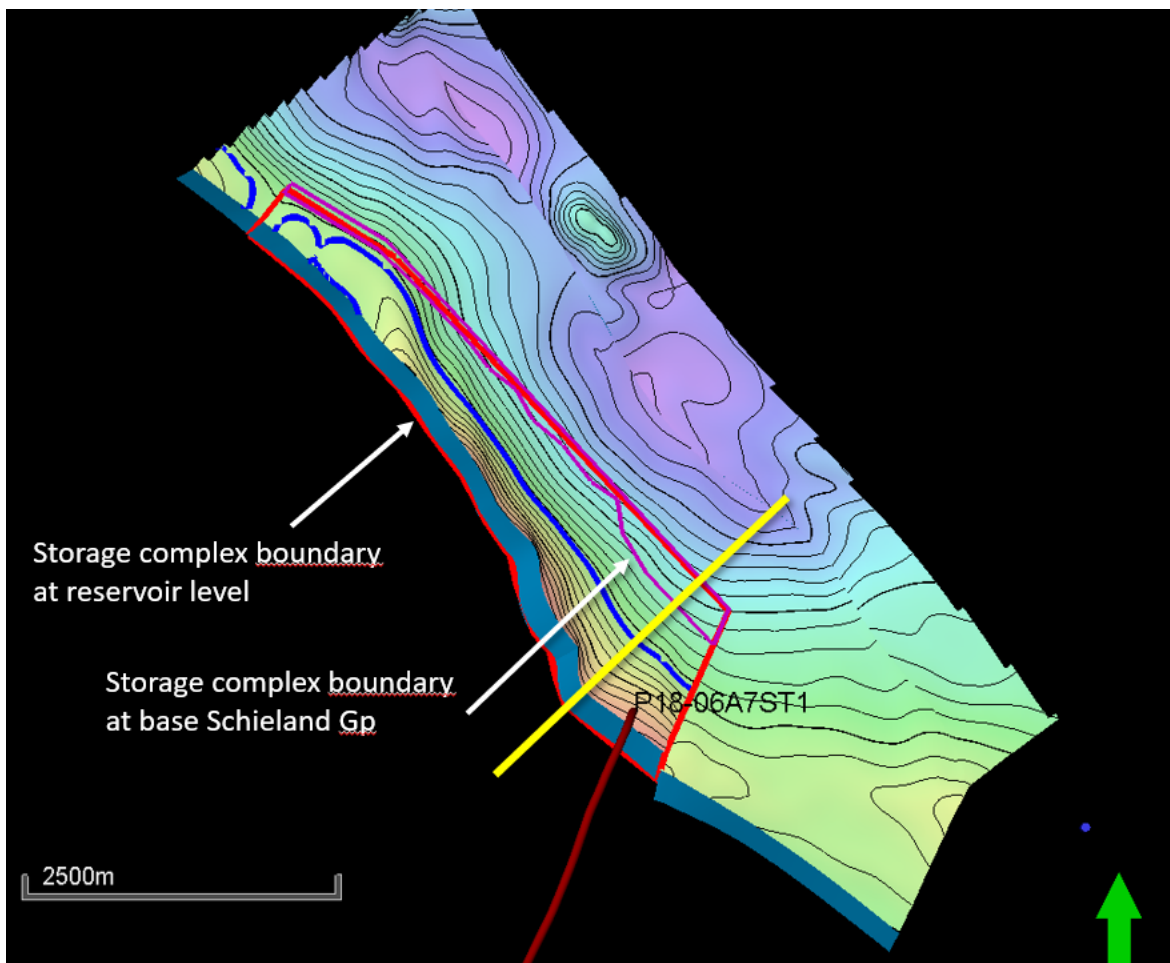
Figure 10-1 Depth map of the top of the reservoir with the proposed boundary of the storage complex at top reservoir level (red line) delimited by the bounding faults and an open boundary downdip of the GWC to the north; purple line indicates storage complex boundary at the top of the caprock (Base Schieland Gp). Yellow line represents the location of the geological cross section shown in Figure 10-2.
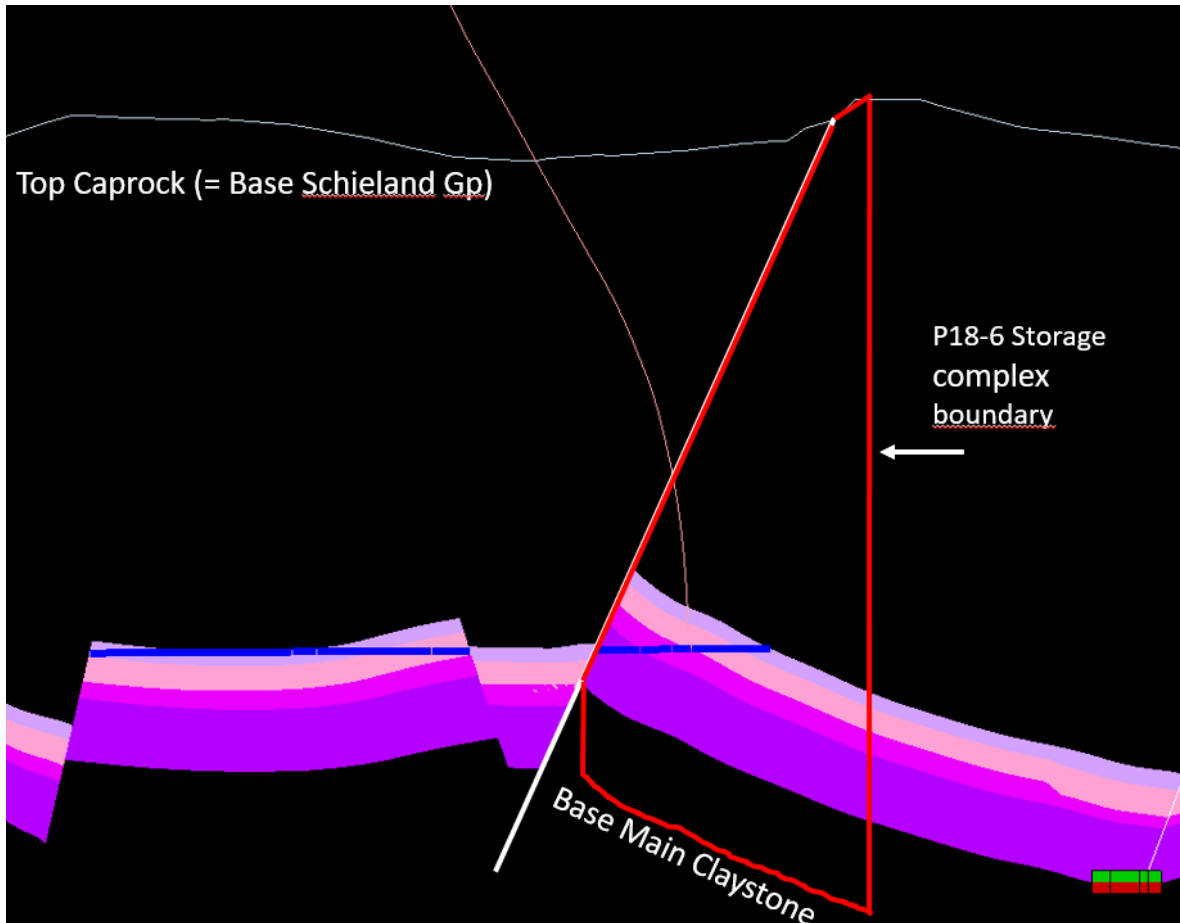
Figure 10-2 Geological cross section of the reservoir and the overburden with indication of the vertical extension of the geological compartments and the wells determining the storage complex); location of cross section is shown in Figure 10-1.

10.5 Barriers

10.5.1 Barriers in the storage complex

The storage complex includes the principle barriers for the permanently stored CO_2 in the P18-6 depleted gas reservoir.

The *geological barrier system* consists of:
- Massive caprock, consisting of Triassic and Jurassic shales, directly located above the reservoir rocks (see also Section 4.3);
- Sealing, reservoir-bounding faults;
- Structural relief trapping of CO_2, e.g. at the NW and NE boundaries of the reservoir.

The *well engineering barrier system* consists of the two barriers described in Section 9.
-

10.5.2 Evaluating barrier integrity

The various barriers have been evaluated in detail to further qualify the P18-6 reservoir for permanent CO_2 storage:

- The initial condition of the caprock and the faults is characterized in Section 4 and Section 17.
- The risk of lateral migration (spilling) from the reservoir compartment to the North was assessed in more detail in Section 6.
- The stability of the fault zone under the influence of chemical, mechanical and thermal processes were investigated (see Section 7).
- The possible effects of fracturing and chemical degradation on the integrity of the caprock have been evaluated with semi-analytic thermomechanical modelling and following a literature study, respectively (see Section 8).
- The integrity of the well P18-A-07-S1 penetrating the reservoir have been evaluated and recommendations for qualifying the well for CO_2 storage have been defined (see Section 9).

The results of these investigations have been used to characterize the risks for loss of containment and to propose measures to lower the risk level if necessary (see Section 12). Section 13 describes the monitoring plan, which enables the early identification and intervention of potential issues for CO_2 containment.

11   Migration paths

11.1   Introduction

The EU storage directive requires an analysis of potential leakage pathways (EU, 2009, Annex I). The results presented in sections 6 through 9 support the conclusion that leakage of CO_2 (i.e. CO_2 moving out of the storage complex) along wells, faults or through the caprock is highly unlikely, if the injection process is conducted within safe limits (see Sections 12 and 13). Overfilling the reservoir (i.e., spilling of the CO_2 across a spill point) does not occur as long as the average reservoir pressure is kept below initial gas pressure.

Nevertheless, with this starting point, an analysis was made of pathways that CO_2 would take in case of a hypothetical leak out of the reservoir, along one of the wells, or through the caprock. The analysis includes the identification of possible secondary containment at the level of the reservoir formations, or in the overburden.

A static overburden model was assembled, based on both 2D and 3D seismic surveys and well information. On the basis of the overburden model and the selected migration pathways, an evaluation of possible migration scenarios was developed. The scenarios shown below focus on (hypothetical) migration paths relevant for the P18-6 field.

The conclusions are that in the case of overfilling of the reservoir and migration through the Buntsandstein (reservoir formations level), the CO_2 remains trapped and finally will migrate towards the adjacent gas reservoirs. In the case of migration of CO_2 into the aquifers of the overburden, caused by a shortcut along the wellbore, it will remain trapped within these aquifers. However, migration of CO_2 along faults in the overburden (above the Altena Group) to a shallower aquifer level cannot to be excluded.

Overall, given the results presented in the previous sections, the conclusion from the analysis presented in this section is that the only potential pathway to the surface of CO_2 stored in the P18-6 field is via leaking wells, leaking directly into the atmosphere and not indirectly via pathways originating in deeper parts of the overburden.

11.2   Available data and workflow

A geological model was constructed with Petrel modelling software (Schlumberger). The model comprises an area with a 14 km minimum radius surrounding the P18 gas fields. In vertical direction the model spans the total overburden of the reservoir.

The workflow for building the model is described in *CATO-2-WP3.1-Geological report P18 (December 2010)*: seismic interpretation of the overburden was performed, and subsequently the model was built on the basis of a fault model with a grid cell size of 250m x 250m. The model was converted from time to depth, and tied to the wells.

Figure 11-1 shows the location of the P18 fields, with neighbouring fields and wells.
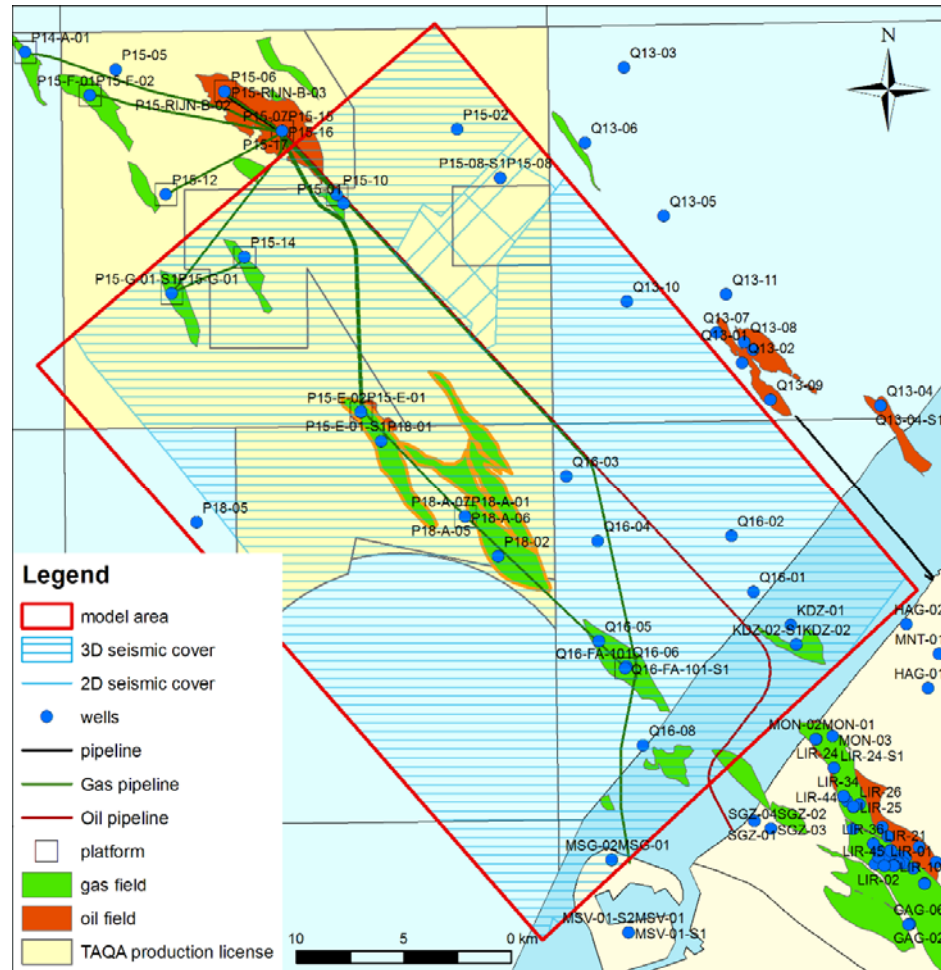
Figure 11-1: Location map of P18 model area. Target P18 gas fields are indicated with an orange boundary.

11.3 Geological model of the overburden

11.3.1 Overburden

The primary seal, made up of the Upper Germanic Trias and Altena Groups is successively overlain by (see also Figure 11-2):

- The Schieland Group, which consists of shales and (stacked) channel sands of the Nieuwerkerk Fm. (Delft sandstone equivalent). The lateral continuity of the individual sand bodies (thickness 2-5m) is probably very limited.
- Lower Cretaceous Rijnland Group, which consist of marine sandstones, shales and marls. At the base of the Rijnland Group, the Rijn / Rijswijk Fm. is present. This sandstone is widely distributed in the P18 area. It is also known for its oil (P15) and gas (onshore) accumulations within the West Netherlands Basin. The sandstones are interpreted as transgressive sheet sands, with good lateral continuity. In the upper part of the Rijnland succession, the Holland Greensand Member is present. It consists of argillaceous sands and silts. The distribution is limited to the southern margin of the West Netherlands Basin. Although the Holland Greensand has good lateral continuity, permeability is general low.

− Upper Cretaceous Chalk Group, which consist at the base of the formation of sands and marls and a thick layer (900 m) of limestones (Chalk). The distribution of the basal Texel Greensand is limited to the southern basin margin.
− The North Sea Group, which consists of siliciclastic sediments. Two major aquifers cam be distinguished; the Dongen sand, a basal transgressive sandstone, and the marine Brussels Sand Member.

Figure 11-2: Composite well log (GR, DT) of P18-02 with main stratigraphic units and aquifer intervals

11.3.2   *Faults*

Faults present at reservoir level (Buntsandstein) in general continue till the Schieland group (white line) or base Rijnland Group (dark green line in Figure 11-3). Late Cretaceous inversion caused faulting of the sediments above the Base Cretaceous Unconformity (base Rijnland) These faults (dashed lines Figure 11-3) have limited displacement, but continue to the Upper North Sea Group.
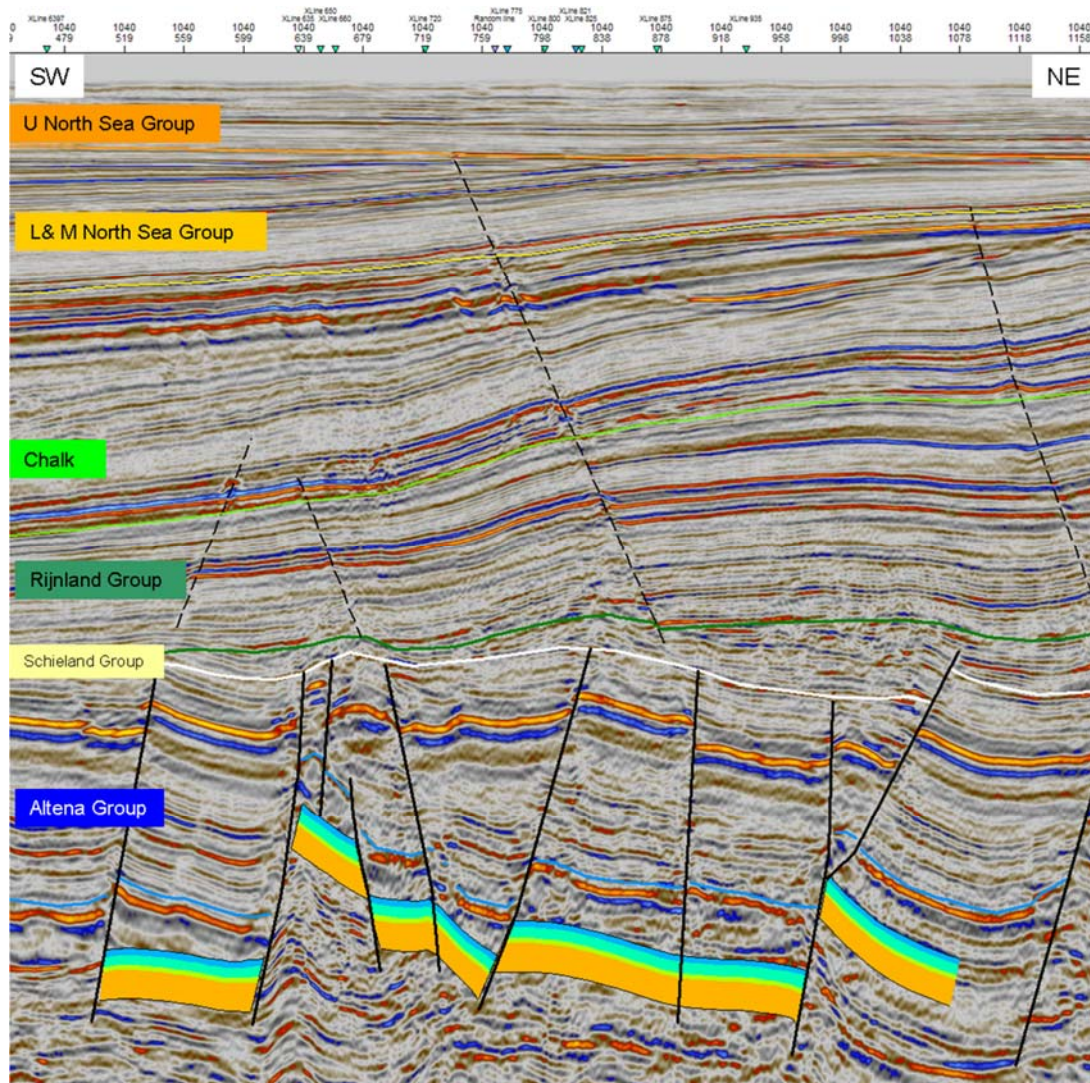
Figure 11-3: Seismic cross-section (inline 1040 of P15P18 seismic cube) through the P18 field, displaying the reservoir interval (coloured layering), the main bounding faults to the reservoirs (bold lines), the main stratigraphic units in the overburden and the faults in the overburden (dashed)

11.4   Migration scenarios

For the qualitative analysis three migration scenarios were considered.

1. Spilling out of the gas reservoir, due to overfilling. This leads to migration within the Bundsandstein formations beyond the boundaries of the storage complex (hence, this would be classified as leakage). See Section 11.6.1.

2. Leakage through the caprock due to fracture formation. This leads to CO_2 entering the Rijn/Rijswijk Sandstone (Section 11.6.2).
3. A wellbore shortcut, opening pathways for CO_2 into formations overlying the caprock.
   - Migration into Rijn/Rijswijk Sandstone (Section 11.6.2);
   - Migration into Holland Greensand (Section 11.6.3);
   - Migration into Texel Greensand (Section 11.6.4);
   - Migration into Dongen & Brussel Sandstone (Section 11.6.5).

The sections below investigate the consequences of these scenarios occurring, in spite of their low to very low probability, given the results presented in Sections 6 (spilling out of the reservoir), 8 (caprock integrity) and 9 (well integrity).

11.5 Methods

Potential CO_2 migrations pathways were analyzed using the rapid trapping assessment tool PetroCharge Express of IES. With this tool a rapid analysis of the migration pathways based on the layer geometry is performed. The layer geometry was provided by the exported horizons from Petrel (regional scale model). The program uses the input top layer as bounding elements assuming these layers to be impermeable. Although in reality the layers are not completely impermeable the goal is to create a concept model from which migration routes within the layer can be deducted.

It should be noted that PetroCharge only looks at the geometry and does not describe various other aspects of flow. It was therefore decided to "inject" large amounts of CO_2 in the considered leakage scenarios and to focus on the migration paths and final accumulation structures.

11.6 Results

11.6.1 Migration scenario: Buntsandstein
In case of "overfilling" the gas reservoir with CO_2 it might be possible that the CO_2 will pass by the original closure defined by the initial gas water contact (GWC).
- Overfilling the P18-6 reservoir could lead to migration towards the Q16-4 structure (Figure 11-4, arrow 1);
- Overfilling the P18-6 compartment could lead to migration towards the P15-10 field (Figure 11-4, arrow 2).

It must be noted that in the structure drilled by the (dry) exploration wells Q16-04 and Q16-03, only minor amounts of gas were encountered. If the containment were to fail by a mechanism described above, the most probable failure would that be of an absence of a side-seal in combination with reservoir juxtaposition with Jurassic sandstones from for instance the Nieuwerkerk Formation.

Figure 11-4 Structure map of Top Buntsandstein. Black lines indicate faults. Also shown are boundaries of gas accumulations and location of wells.

11.6.2   *Migration scenario: Rijn/Rijswijk sandstone*

In the case of fault reactivation or a shortcut occurring via a wellbore, CO_2 can hypothetically migrate into the Rijn/Rijswijk sandstone aquifer.

- Spill originating from well P18-A-07-S1 will migrate towards Q16-03 & Q16-04 structure (Figure 11-5, arrow 1).

11.6.3   *Migration scenario: Holland Greensand*

In the case of a shortcut via a wellbore, CO_2 can hypothetically also migrate into the Holland Greensand aquifer

- Spill originating from well P18-A-07-S1 will migrate towards Q16-03, Q16-04 structure (Figure 11-6, arrow 1)

Figure 11-5: Structure map of the Base Rijnland Group. Black lines indicate faults. Also shown are boundaries of gas accumulations and location of wells.
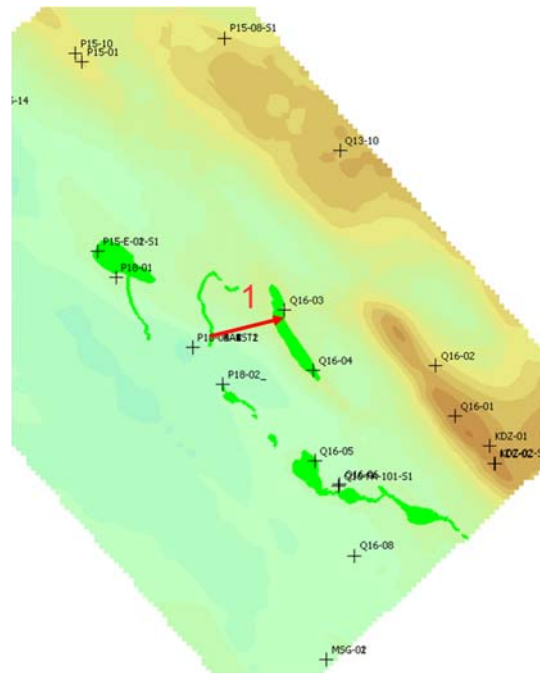
Figure 11-6: Structure map Holland Greensand.

11.6.4 Migration scenario: Texel Greensand

In the case of a shortcut via a wellbore, CO_2 can also hypothetically migrate into the Texel Greensand aquifer

- Spill originating from P18-A production wells will migrate towards Q16-3 structure and finally Q16-02 (Figure 11-7, arrow 1).
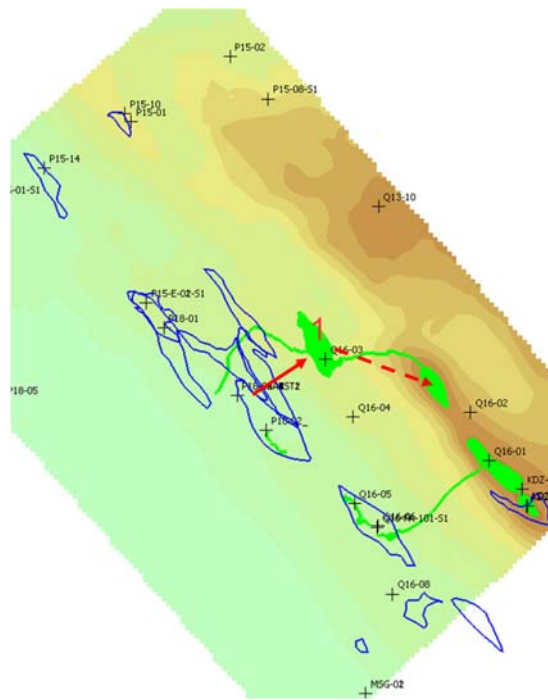
Figure 11-7: Structure map base Chalk Group.

11.6.5   *Migration scenario: Dongen sand & Brussel sandstone*
In the case of a shortcut occuring via a wellbore, CO_2 can hypothetically migrate into the North Sea Group aquifer
- Spill originating from P18-A production wells will migrate towards Q13-10 structure (Figure 11-8, arrow 2).
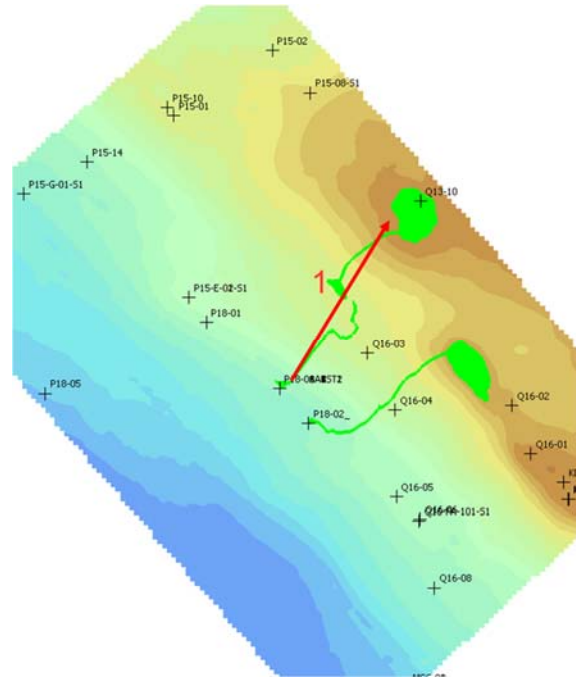
Figure 11-8: Structure map base North Sea Group.

11.7   Present day hydrocarbon migration

Inspection of the overburden revealed the possible existence of shallow gas pockets. (*CATO-2-WP3.1-D01-Geological report P18 (December 2010).* The gas is most probably sourced from Jurassic Posidonia shales (van Balen et al., 2000). The Posidonia shales are situated stratigraphically above the Bunter reservoir and seal, so this hydrocarbon migration provides no proof of seal failure/leakage within the P18 Bunter reservoir.

Figure 11-9 shows a seismic section of the overburden, to illustrate hydrocarbon migration, and to illustrate a possible migration pathway for CO_2. Gas is sourced from the Posidonia shale (the strong reflector at the base of the lowest arrow), and migrates via a fault into the sands of the North Sea Group. The red ellipses indicate bright spots, which suggest the presence of gas. Migration is also possible within the Brussels sand and is indicated by the arrows in Figure 11-9. At the location where the Brussels sand toplaps against the Upper North Sea Group (Mid Miocene Unconformity, orange line), an increase of amplitudes in observed, which suggest migration from the Brussels sand into the Upper North Sea Group.
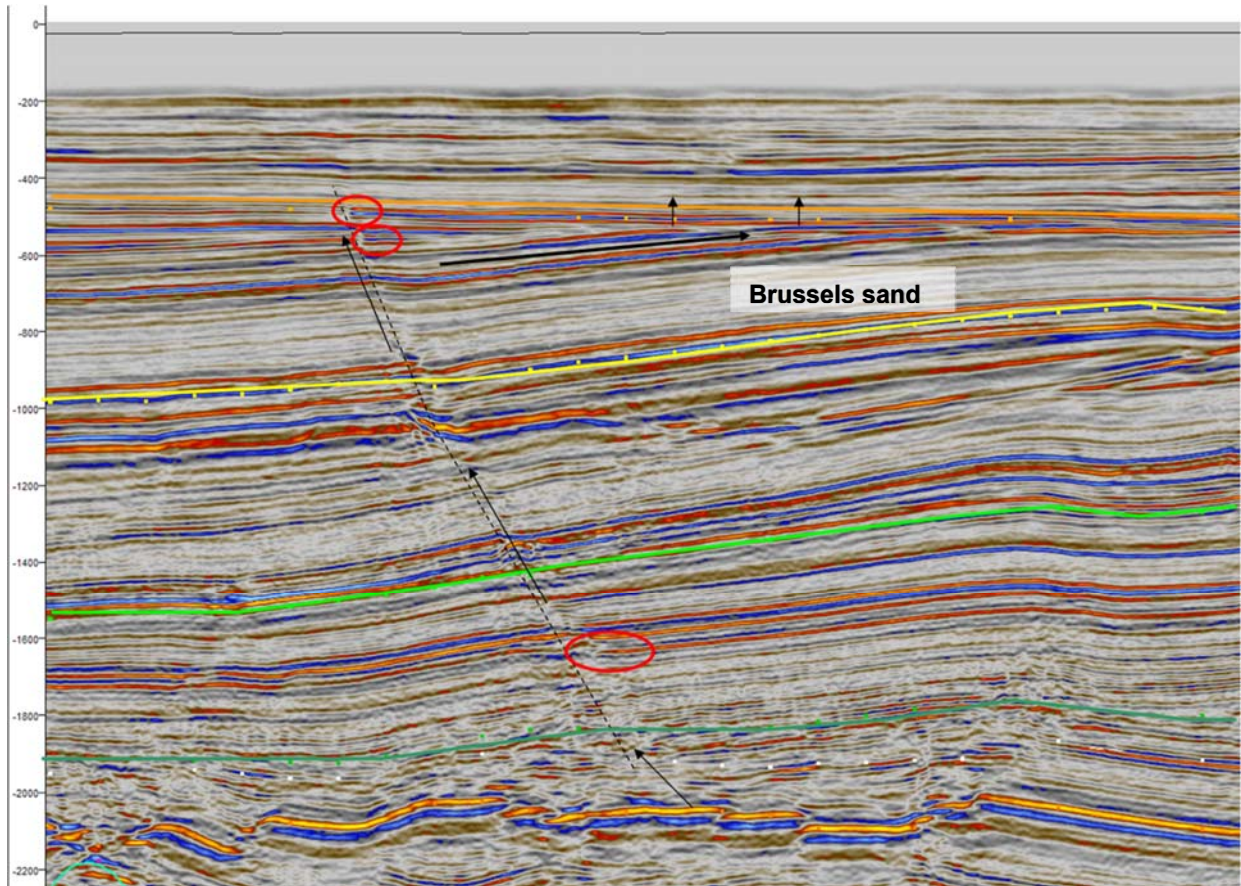
Figure 11-9: Seismic section of the P18 overburden. Arrows indicate hydrocarbon migration along a fault (dashed line). Red ellipses mark bright spots on the right side of the fault. Dark green line: base Rijnland (BCU), bright green line: base Chalk, yellow line: base North Sea, orange line: base Upper North Sea (MMU).

11.8   Conclusions

A Petrel model of the overburden has been constructed, using publicly available data and data provided by TAQA. Based on the geological model and selected hypothetical migration scenarios a qualitative evaluation of the possible pathways was developed.

This assessment was based on the results presented in sections 6 through 9, which support the conclusion that leakage of CO_2 (i.e., CO_2 moving out of the storage complex) along wells or faults is highly unlikely. If the injection process is conducted within safe limits (see Sections 12 and 13), the conclusions from this assessment are that in case of overfilling of the reservoir the CO_2 remains trapped in the Buntsandstein (reservoir formations level) and finally will migrate towards the adjacent gas reservoirs. Also, in case of migration of CO_2 into the aquifers of the overburden, caused by a shortcut along the wellbore, it will remain trapped within these aquifers. However, migration of CO_2 along faults in the overburden (above the Altena Group) to a shallower aquifer level cannot to be excluded in the unlikely case that leakage along the well does occur.

Overall, given the results presented in the previous sections, the conclusion from the analysis presented in this section is that the only potential pathway to the surface of CO_2 stored in the P18-6 field is via leaking wells, leaking directly into the atmosphere and not indirectly via pathways originating in deeper parts of the overburden.

12 Risk assessment and preventative measures

The current study on the feasibility of CO_2 storage in the P18-6 reservoir made optimal use of earlier work done on the P18 reservoirs, a large part of which was carried out as part of the national CATO2 programme until 2011 and specific work on the P18-2 field (Neele et al., 2019). The risk assessment work for P18-6 was built on the assessment for P18-2 and where relevant the assessment was adjusted or expanded. The risks identified for CO_2 storage in the P18-6 reservoir are based on detailed investigations which are presented in Chapters 6 through 9, and on earlier work for the P18 reservoirs (Vandeweijer et al., 2011; Neele et al., 2019). The central question is where the CO_2 is at any given point in time and whether it could (partially) flow out of the storage complex. In Section 10 the delimitations of the storage site and the storage complex which includes the intended storage reservoir, have been presented.

After the identification and evaluation of the risks, measures were defined to diminish the risk level. The present chapter provides an extensive summary of this risk management exercise. The risk evaluations are presented for the individual spatial compartments, e.g. reservoir, caprock, fault zones and wells, which together make up the storage complex including the flow barriers. A summary of the risks and their evaluation is provided in the risk register (see Section 18).

The assessment presented here is based on a number of technical conditions which are presented in Chapter 5.5. The assessment is focused on the functioning of the P18-6 reservoir as a suitable 'container' for the injected CO_2 to prevent significant leakage from the storage complex as required under the EU Storage Directive (EU, 2009). The permanent containment of CO_2 is provided by a number of geological and technical barriers. It is of great importance that any risk to this containment function is small, can be managed and is acceptable.

The risk of loss of containment relates to possible existing or future defects in the reservoir (pressure evolution and fluid flow leading to lateral flow or spilling of CO_2), in the caprock (migration pathways, e.g. fractures), bounding faults (re-activation and increased likelihood for CO_2 migration) or the wells (migration pathways as a result of defects in well cement or casing).

The results from the risk assessment represent a main building block for the Environmental Impact Assessment which is required for the storage permit application.

12.1 Reservoir

The P18-2 reservoir is bounded by sealing faults on SW and SE sides and is marked by dip closure on the NE and NW sides, where there is direct contact with the low permeable water saturated part of the Triassic reservoir rocks more downdip (see Figure 4-2). In the zones with dip-closure there is a risk of lateral migration of CO_2 or spilling. In addition there may be flow between the P18-2 and P18-6 reservoirs, which was already assessed for in the feasibility study for the P18-2 reservoir (Neele et al., 2019).

In summary, three locations with potential hydraulic connections to permeable rocks outside the reservoir have been evaluated in more detail:

- Tip of bounding cross fault (F600) to the SE;
- Dip-closure at NW edge of reservoir;
- Small section along fault F57 between reservoirs P18-2 and P18-6.

12.1.1   *Evaluation of spilling at the tip of the bounding cross fault to the SE*

Information from nearby wells indicate that the aquifer has a low permeability due to illitisaton. Dynamic reservoir simulations show no spilling, even in the case of strong over-pressurization, although the CO_2 may migrate beyond the gas-water contact (see Chapter 6).

Keeping the average reservoir pressure at or below the hydrostatic pressure at the end of injection and the robustness of flow simulations indicate a very low likelihood that a negligible amount of CO_2 migrates out of the reservoir (risk classification A-1; see also Section 18 and Figure 12-1).

12.1.2   *Evaluation of spilling at the NW edge of reservoir*

A saddle is present at the NW edge of the P18-6 reservoir. The robustness of flow simulations indicate a very low likelihood that a negligible amount of CO_2 migrates out of the reservoir. Keeping the average reservoir pressure at or below hydrostatic pressure at the end of injection will decrease this likelihood, although the reservoir simulations do not suggest this is necessary.

12.1.3   *Evaluation of CO_2 flow between reservoirs P18-2 and P18-6*

Both the static model used during the CATO2 work and the new model for the current feasibility study indicate that there is a small section across the fault zone with juxtaposition of the low-permeable Volpriehausen Sandstone (see Section 6.3.6). The P18-6 reservoir is located directly to the NE of Compartment 2-IV of the P18-2 reservoir. Geological reservoir modelling and pressure history observations indicate that this compartment represents a separate hydraulic unit from the P18-2 reservoir, which implies that no CO_2 will migrate in this part of the reservoir and thus will not end up in the P18-6 reservoir.

The pressure in P18-06 was at the initial level of 377 bar when pressure had already dropped to about 100 bar in the P18-2 reservoir in June 2003. Apparently, this pressure difference could exist, which indicates absence of both flow and pressure equilibration between the two reservoirs on production time scales. Any pressure communication would only be expressed on geological time scales in the order of 10^3 to 10^6 years.

An analysis of the P18 faults revealed that between P18-02 and P18-6 the faults have a high (to very high) probability of having sealing characteristics due to the high probability of impermeable fault gouge formation or cataclasis (Nieuwland, 2012).

The pressure difference of about 277 bar between the two reservoirs and the very low permeability of the Volpriehausen Sandstone show that there is a very low likelihood that even a negligible amount of CO_2 will migrate from P18-2 to P18-6 or no CO_2 is flowing out of P18-2 to P18-6 at all (risk class A-1; see Figure 12-1).

Likelihood ->		A	B	C	D	E
	Containment function	Very low	Low	Medium	High	Very high
1	Nill or negligible amount of CO2 migrates out of the reservoir.			C-1	D-1	E-1
2	Very small amount of CO2 migrates out of the reservoir but stays in the storage complex.	A-2	B-2	C-2	D-2	E-2
3	Small amount of CO2 migrates out of the reservoir and partly ends up outside the storage complex.	A-3	B-3	C-3	D-3	E-3
4	Large amount of CO2 migrates out of the reservoir and partly ends up outside the storage complex.	A-4	B-4	C-4	D-4	E-4
5	Very large amount of CO2 migrates out of the reservoir and out of the storage complex.	A-5	B-5	C-5	D-5	E-5

NW edge
P18-2 <> P18-6
Cross fault

Spilling of CO_2 out of the reservoir

Figure 12-1   Geological risk matrix for the reservoir compartment with inclusion of appropriate risk reduction measures

12.2   Caprock

Impermeable shales of the Upper Trias and Altena Groups with a thickness of 450 m to 750 m overlie the P18-6 reservoir, which represent a good seal for the natural gas reservoir. The sealing capacity is evident from the presence of gas in the reservoir below the seal with a gas column of about 170 m.

12.2.1   Initial condition
As the evidence for the initial sealing capacity of the caprock is very strong, it is a good seal for CO_2 storage as well and consequently the risk of CO_2 migration out of the reservoir is low to even negligible (see Figure 12-2).

12.2.2   Fracturing due to pressurizing the reservoir
Fractures in the seal may be caused by local stress variations due to initial gas production, subsequent CO_2 injection and associated pressure changes. Fractures represent a potential conduit for CO_2 loaded fluids depending on their connectivity and continuity (see also Fault zone).

Semi-analytic modelling has shown that Coulomb stresses as a consequence of pressure build-up due to injection quickly decay on top of the reservoir inside the

caprock. The pressure effect is thus not expected to contribute to the risk of fracture or fault reactivation in the caprock. New fractures or faults will not be generated as they would require even higher Coulomb stresses.

Considering the huge thickness of the caprock and the very rapid decay of the pressure near the top of the reservoir and the basis of the caprock, the likelihood of fracturing the complete caprock is nil and consequently the risk is very low to negligible (Figure 12-2).

12.2.3   *Fracturing due to cooling of the reservoir*
Fractures in the seal may be caused by local stress variations due to initial gas production, subsequent CO_2 injection and associated temperature changes. Fractures represent a potential conduit for CO_2 loaded fluids depending on their connectivity and continuity (see also Fault zone).

Temperature-induced Coulomb stresses in the caprock due to reservoir cooling are negative, and thus do no lead to re-activation of faults or fractures in the caprock nor will they result in new fractures in the caprock. The likelihood of re-activating a pre-existing fault or fracture in the caprock is thus very low.

Temperature drop in the reservoir is very unlikely to lead to re-activation of fractures (or formation of new fractures) and thus will not lead to the migration of CO_2 out of the reservoir. The risk is very low to negligible (Figure 12-2).

12.2.4   *Chemical degradation*
DissolvedCO_2 may react with minerals in the caprock near the interface with the CO_2 reservoir. Since the caprock has proven to be a seal for gas, the only way of upward migration is via diffusion of the dissolved CO_2, which is a very slow process. Chemical interaction between dissolved CO_2 and caprock minerals is very slow and has minor effects on porosity and permeability. Hence, no migration path is expected to be formed. The affected zone of migration of dissolved CO_2 and chemical interaction is in the order of several meters in thousands of years (Gaus et al., 2005; Tambach et al., 2012).

Chemical degradation will only marginally influence the sealing properties of the caprock and thus will the overall integrity of the caprock stay intact. The likelihood of degrading the caprock is very low and its consequence will be nil or negligible (Figure 12-2).

Likelihood ->		A	B	C	D	E
Consequence ->	Containment function	Very low	Low	Medium	High	Very high
1	Nill or negligible amount of CO2 migrates out of the reservoir.			C-1	D-1	E-1
2	Very small amount of CO2 migrates out of the reservoir but stays in the storage complex.	A-2	B-2	C-2	D-2	E-2
3	Small amount of CO2 migrates out of the reservoir and partly ends up outside the storage complex.	A-3	B-3	C-3	D-3	E-3
4	Large amount of CO2 migrates out of the reservoir and partly ends up outside the storage complex.	A-4	B-4	C-4	D-4	E-4
5	Very large amount of CO2 migrates out of the reservoir and out of the storage complex.	A-5	B-5	C-5	D-5	E-5

Initial condition
Fracturing by repressurizing
Fracturing by cooling
Chemical degradation

Migration through the caprock

Figure 12-2   Geological risk matrix for the caprock compartment with inclusion of appropriate risk reduction measures

12.3   Fault zones

12.3.1   Initial condition

Bounding faults F430 (main fault) and F600 (cross fault; see also Chapter 17.1) are effective seals as evident from the presence of juxtaposed gas reservoirs and sealing rock. As reservoir rocks next to bounding faults are sealed off by very low permeable rocks on the other side of the fault zone, it has a very low likelihood that a negligible amount of CO_2 will migrate across or along the fault and sealing rock (see Figure 12-3).

12.3.2   Chemical degradation

Chemical alteration of the fault zone may enhance migration of CO_2 along the fault. Currently, there is no evidence for gas migration from the P18-6 reservoir along the faults to overlying formations. In general, the geochemical reactions between CO_2, formation water and fault gouge mineralogy will result in precipitation of carbonate minerals. In the longer term, silicate minerals might react, providing additional cations for carbonate precipitation. Porosity and hence permeability effects are predicted to be negligible. Increase of carbonate content in the fault gouge is known to increase the friction coefficient and to decrease potential for fault re-activation (Samuelson et al., 2012; Adelinet et al., 2014; Bakker et al., 2016). It is therefore

highly unlikely that chemical degradation in itself leads to the migration of CO_2 across the fault zone (see Figure 12-3). See also Section 7.4.

12.3.3   *Fault stability: effects of re-pressurising P18-6*
Due to pressure changes during production and/or injection faults may be re-activated (Vandeweijer et al., 2011: par 6.7, p109) and potentially act as conduits for CO_2.

No seismic activity was encountered during production, based on the KNMI database.[10] Semi-analytic modelling has shown that at the end of the injection period most (if not all) of the areas where positive Coulomb stresses which are present at the end of depletion, have disappeared. The faults are thus expected to be stable at the end of the injection period.

Based on the results from the semi-analytic modelling it appears to be highly unlikely that faults will be re-activated due to the increased pressure by CO_2 injection and consequently will not lead to migration of CO_2 along the fault. The risk is characterized as low (Figure 12-3).

12.3.4   *Fault stability: effects of injecting low-temperature CO_2*
Injection of a cold CO_2 stream could re-activate a nearby fault and change its fluid transport properties. Well P18-A-07-S1 is at a distance of about 100 m from the main bonding fault. Initial TOUGH2 simulations have shown that the cooling front with a temperature drop of about 50 ºC could extend to 200 m from the injector after 5 years of injection. Semi-analytic thermomechanical modelling indicates that the Coulomb stresses may reach up to 9 MPa at the edge of the cooling front, which can be sufficient to re-activate the fault. The cold CO_2 from injection wells at less than 200 m from a fault may thermo-mechanically influence its stability.

With time reservoir pressure will increase and the bottomhole injection temperature will increase which will result in making the cooling effect less prominent. Furthermore, the cold area around the well will warm up due to the higher ambient temperature. The pressure increase in itself has a stabilizing effect on the faults. The well P18-2-A1 which is close to a fault, has the worst injectivity and consequently a less pronounced cooling effect. All this will reduce the risk of fault re-activation. On the other hand the effect of cooling may be underestimated as the TOUGH2 simulator has a limit to the temperature of 103 ºC whereas the ambient reservoir temperature is 14 ºC higher.

The advancement of the cold front near faults can be managed by adjusting the injection rate of well P18-A-07-S1, which is in close distance of the main bounding fault.

Additional simulations with TOUGH2 for a limited period of time of injection (content of pipeline as defined in the discharge scenario) show that the advance of the cold front is strongly limited to 20 m from the well and thus cannot thermo-mechanically reactivate a fault at 100 m from the well. This is considered to be a more representative case for the use of P18-06 field as a backup injection site.

---

[10] KNMI Seismic and Acoustic Data Portal, 2 Oct 2019: doi:10.21944/e970fd34-23b9-3411-b366-e4f72877d2c5).

With inclusion of appropriate management of the injection rate in the well faults the likelihood of thermomechanical fault re-activation leading to the migration of a negligible amount of CO_2 out of the reservoir will be very low or no migration of CO_2 out of the reservoir at all. (Figure 12-3).

Likelihood ->		A	B	C	D	E
	Containment function	Very low	Low	Medium	High	Very high
1	Nill or negligible amount of CO2 migrates out of the reservoir.			C-1	D-1	E-1
2	Very small amount of CO2 migrates out of the reservoir but stays in the storage complex.	A-2	B-2	C-2	D-2	E-2
3	Small amount of CO2 migrates out of the reservoir and partly ends up outside the storage complex.	A-3	B-3	C-3	D-3	E-3
4	Large amount of CO2 migrates out of the reservoir and partly ends up outside the storage complex.	A-4	B-4	C-4	D-4	E-4
5	Very large amount of CO2 migrates out of the reservoir and out of the storage complex.	A-5	B-5	C-5	D-5	E-5

Initial condition
Chemical degradation
Pressure re-activation
Thermal re-activation

Migration along faults

Figure 12-3   Geological risk matrix for the fault zones with inclusion of appropriate risk reduction measures.

12.4   Wells

The P18-6A-07-S1 well penetrating the P18-6 reservoir, was evaluated in detail:

12.4.1   Outer casing inside conductor
The surface casing in the conductor might be subjected to external corrosion or fatigue induced by metoceanic movement. The presence and quality of the cementation of the conductor and the 20" casing could not be fully ascertained. After evaluation of the presence and quality of the cementation and the implementation of any additional measures, the likelihood that a negligible amount of CO_2 will migrate out of the reservoir; is characterized as low (see Figure 12-4).

12.4.2 Production packer in 7" liner

A short stretch of the 7" liner (and cement) above the 5" Top of Liner (TOL) and below the production packer in the 7" liner is just above the caprock in the Schieland Group and may be exposed to corrosive fluids. The 7" liner is P110 carbon steel and is exposed to well bore fluids and represents a single barrier in this small depth window. In the event of presence of water or brine in the wellbore fluids, the risk of corrosion may lead to loss of the primary barrier with potential leakage to the overburden.

With the implementation of adequate measures, leakage from the well will be prevented. The likelihood will be low that a negligible amount of CO_2 will migrate out of the reservoir (see Figure 12-4).

12.4.3 Cooling

Injection of cold CO_2 leads to thermal contraction of the wells. The induced tensile stresses can exceed the bonding strength and thus lead to debonding at the well-cement interface. The resulting micro-annuli represent a potential pathway for CO_2 migration which could be further enhanced by chemical interaction of CO_2 and the cement around the micro-annuli (see Sections 9.2.2 and 9.3.4). The effect of cooling at P18-6 will be less than at P18-2 because of the higher pressure and lower temperature drop in P18-6.

Although the creation of micro-annuli is considered to be likely, the migration of CO_2 is prevented by the pressure of CO_2 which is to be maximised at the hydrostatic pressure (at datum level of 3400 m). At the end of the injection phase an appropriate formation-to-formation plug is recommended.

After appropriate decommissioning of the injector wells the risk will be reduced to a low likelihood that a small amount of CO_2 migrates out of the reservoir (risk class B-1; see Figure 12-4).

	Likelihood ->	A	B	C	D	E
Consequence ->	Containment function	Very low	Low	Medium	High	Very high
1	Nill or negligible amount of CO2 migrates out of the reservoir.	A-1	**Cooling** **Packer in 7"liner** **Casing inside conductor**		D-1	E-1
2	Very small amount of CO2 migrates out of the reservoir but stays in the storage complex.	A-2	B-2	C-2	D-2	E-2
3	Small amount of CO2 migrates out of the reservoir and partly ends up outside the storage complex.	A-3	B-3	C-3	D-3	E-3
4	Large amount of CO2 migrates out of the reservoir and partly ends up outside the storage complex.	A-4	B-4	C-4	D-4	E-4
5	Very large amount of CO2 migrates out of the reservoir and out of the storage complex.	A-5	B-5	C-5	D-5	E-5

Migration along injection well

Figure 12-4   Risk matrix for well P18-6A-07-S1 after implementation of appropriate risk reduction measures including any workover activities.

12.5   Conclusion

All risks can be reduced to acceptable, low levels
All geological and subsurface well engineering risks in the P18-6 field can be reduced to acceptable, low levels, with no significant environmental impacts if the storage site is properly designed, managed and decommissioned. The conclusion is that there are no prohibitive risks to storing CO_2 in the P18-6 field. All risks can be managed so that their risk level is low and acceptable.

Well workovers required
Well P18-A-07-S1 will require workover activities to some degree to qualify as a CO_2 injector. Proper management of injection rate and temperature is necessary to prevent undesired effects of cooling on wells and nearby wells. For that purpose pressure, temperature and flow rate of injected CO_2 should be monitored (see Section 13).

Reservoir pressure after injection
As mentioned above, all risks identified here can be reduced to acceptable, low levels if the storage site is properly designed, managed and eventually closed. This will require the development of safe injection scenarios and the management of pressure and temperature in the wells and reservoir. It should be noted that the simulation of the injection of CO_2 into the reservoir, the behaviour of CO_2 inside the reservoir, the integrity of the caprock and the stability of faults do not result in limits

to the average reservoir pressure at the end of injection (apart from the maximum given by the initial pressure, which represents the maximum pressure at which the reservoir, caprock and faults have proven containment). Safe and secure storage is possible for reservoir pressure up to initial pressure (i.e., the pressure that existed in the field prior to production).

However, the study did identify a risk that requires reservoir pressure to be maximised at hydrostatic pressure. The potential migration of CO_2 through micro-annuli formed between casing (liner) and cement due to the low temperature of the injected CO_2 becomes small to negligible when reservoir pressure is kept below hydrostatic pressure.

13   Monitoring and corrective measures plan

13.1   Introduction

A thorough risk based approach to monitoring is adopted. This means that the elaboration of the plan depends on the results of the location-specific risk assessment, which is laid out in the previous sections.

A risk-based monitoring plan will:
- Aim to ensure the safety and integrity of the storage complex;
- Reveal the necessary information for transfer of responsibility to government after the end of injection;
- Be able to supply and incorporate additional learning with respect to large-scale CCS;
- Be able to prove the effectiveness of corrective measures;
- Provide a balance between efficiency and costs.

New techniques and equipment will be included whenever judged appropriate, provided that these techniques do not add to the complexity associated with operating an offshore unmanned installation.

The monitoring and corrective measures plans are part of a set of related plans that are part of the storage permit. The location specific risk assessment (Section 12) is the main input for the corrective measures and closure plans. The development of the monitoring plan is also based on a location specific risk analysis and has strong links with the corrective measures plan. Figure 13-1. illustrates the links and the consistency between the plans.

Figure 13-1. Consistency between risk management, monitoring an corrective measures plans.

Monitoring requirements of the CCS Directive 2009/31/EC and OSPAR are framed around enabling the operator to understand and to demonstrate understanding of

ongoing site processes, to predict future site behaviour and to identify any leakage. Further requirements of the monitoring include early identification of deviations from predicted site behaviour, provision of information needed to carry out remediate actions and the ability to progressively reduce uncertainty.

13.1.1   *Reading Guide*
In the following section the monitoring and corrective measures plan is outlined. The foundation of the plan is given first which refers to the legislation, regulations and other preconditions that have been taken into account. Then the philosophy of the monitoring plan is explained. Finally, the elaboration of the operational monitoring plan is explained, while the detailed monitoring plan is documented in Section 19. The cross-references to the corrective measures plan are explicitly indicated.

The plan described here represents the draft monitoring plan, to be updated and detailed prior to the start of injection.

13.2   Foundation of the monitoring and corrective measures plan

For the P18-6 storage project the monitoring plan needs to comply with the following regulations and requirements:
- Provisions of two key regulatory treaties governing CO_2 storage in the European offshore area, which are the OSPAR Guidelines (OSPAR, 2007) and the European Storage Directive (EU, 2009) and its implementation in the Dutch Mining Law.
- Requirements of the EU Emissions Trading System (ETS), as defined under the EU Monitoring and reporting Guidelines (EC, 2018), which deals with the accounting of leaked emissions from storage sites.
- Specific requirements to the P18-6 storage project as a first of a kind project for The Netherlands.

The starting point for developing the monitoring and corrective measures plan is an adequate characterization and risk assessment. Although the monitoring and corrective measures plan presented here also makes optimal use of earlier work done on the P18 reservoirs.

The general requirements for both site characterization and risk assessment are given in the Dutch mining law, the EC Storage Directive and its Annexes. Clarifying details are provided in the EU guidance documents.

The detailed site characterization benefited from the fact that the storage reservoir is part of a larger natural gas field which has been produced for more than two decades. This has led to an abundance of information on the site.

The monitoring plan must relate to preventative and corrective measures. In the adopted template in this report, potential risks, monitoring techniques and mitigation measures are all linked together.

With respect to the phases of a storage operation, the plan describes a 'workflow' for monitoring activities during the pre-injection (site qualification), injection (operation), post-injection (closure and post-closure) phases and after transfer of

responsibility (long-term stewardship). However, monitoring in the different stages of a project is not fundamentally different. The philosophy of the monitoring plan is that it must be complete, transparent, consistent, and verifiable.

An additional requirement for the P18-6 storage project is that the monitoring plan may also serve the first of a kind character of the project, in combination with CO_2 injection in the P18-4 field and, potentially, the P18-2 field. This could mean gathering more data for a deeper understanding of the storage process, learning of findings.

13.2.1 *General requirements from Directive 2009/31/EC*
A monitoring plan should meet the requirements according to the EU CCS Directive (EU, 2009; Annex II), as listed below.

Initial plan
The monitoring plan shall provide details of the monitoring to be deployed during the main stages of the project, including baseline, operational and post-closure monitoring.

The following shall be specified for each phase:
1. Parameters monitored;
2. Monitoring technology employed and justification for technology choice;
3. Monitoring locations and spatial sampling rationale;
4. Frequency of application and temporal sampling rationale.

For the purpose of:
- Comparing actual and modelled behaviour of CO_2 and brine
- Detecting significant irregularities
- Detecting CO_2 migration
- Detecting CO_2 leakage
- Detecting significant negative effects for environment, drinking water, nearby residents, the biosphere
- Evaluating the effectiveness of corrective measures taken in case of leakage
- Proving safety and integrity of the storage complex, including the assessment of complete and permanent storage.

The parameters to be monitored are identified so as to fulfil the purposes of monitoring. However, the plan shall in any case include continuous or intermittent monitoring of the following items:
- Fugitive emissions of CO_2 at the injection facility;
- CO_2 volumetric flow at injection wellheads;
- CO_2 pressure and temperature at injection wellheads (to determine mass flow);
- Chemical analysis of the injected material;
- Reservoir temperature and pressure (to determine CO_2 phase behaviour and state).

The choice of monitoring technology shall be based on best practice available at the time of design. The following options shall be considered and used as appropriate (texts taken from the Directive):

- Technologies that can detect the presence, location and migration paths of CO_2 in the subsurface and at surface;
- Technologies that provide information about pressure-volume behaviour and areal/vertical saturation distribution of CO_2 to refine numerical 3-D-simulation to the 3-D-geological models of the storage formation established pursuant to Article 4 and Annex I of the Storage Directive (EU, 2009);
- Technologies that can provide a wide areal spread in order to capture information on any previously undetected potential leakage pathways across the areal dimensions of the complete storage complex and beyond, in the event of significant irregularities or migration of CO_2 out of the storage complex.

Updated plan

The monitoring system initially installed and its related procedures need to be updated on the basis of the evaluation and modelling activity, or the verification of results. Monitoring plans must be updated, at least every five years, to take into account changes to the assessed risk of leakage, changes to the assessed risks to environment and human health, new scientific knowledge, and improvements in the best available technology. National authorities may set a more stringent frequency.

According to Annex II of the Storage Directive one has the following updating requirements:

a. The data collected from the monitoring shall be collated and interpreted. The observed results shall be compared with the behaviour predicted in dynamic simulation of the 3-D-pressure-volume and saturation behaviour undertaken in the context of the security characterization.

b. Where there is a significant deviation between the observed and the predicted behaviour, the 3-D-model shall be recalibrated to reflect the observed behaviour. The recalibration shall be based on the data observations from the monitoring plan, and where necessary to provide confidence in the recalibration assumptions, additional data shall be obtained.

c. Steps 2 and 3 of Annex I of the Storage Directive shall be repeated using the recalibrated 3-D model(s) so as to generate new hazard scenarios and flux rates and to revise and update the risk assessment.

d. Where new CO_2 sources, pathways and flux rates or observed significant deviations from previous assessments are identified as a result of history matching and model recalibration, the monitoring plan shall be updated accordingly.

Post-closure monitoring shall be based on the information collected and modelled as in a) through d). The plan must now also provide information needed for the transfer of responsibilities to the competent authority (long-term stewardship). Especially the site's permanent containment must be indicated, based on all available evidence.

13.2.2   *Emissions accounting for ETS*

The Monitoring and Reporting Guidelines for CCS under the ETS describe the method for quantifying potential CO_2 emissions from a storage project.

Potential sources for CO_2 emissions from the geological storage of CO_2 include

- Fuel use at booster stations and other combustion activities such as on-site power plants;
- Venting at injection or at enhanced hydrocarbon recovery operations;
- Fugitive emissions at injection;
- Breakthrough CO_2 from enhanced hydrocarbon recovery operations;
- Leakage from the storage complex.

Quantitative monitoring for ETS will only be required if there is an indication of leakage. There is no requirement for emissions accounting as long as there is no evidence that the site leaks. However, in case irregularities are observed (for example in the downhole pressure and temperature measurements) the need for additional monitoring to detect migration pathways out of the storage complex becomes stringent.

The key question for quantitative monitoring is to what extent the state-of-the-art technology allows for an accurate quantification. In that perspective NSBTF (2009) suggests choosing a combination of a model-driven approach in combination with a monitoring strategy to best estimate the leakage for ETS purposes.

In the unlikely event that there is evidence for CO_2 flow out of the storage complex, or that irregularities occur that give rise to the need to check for anomalies outside of the storage reservoir, a strategy would be to detect leakage to the surface by geophysical methods like seismic data (detection of gas chimneys) or sea-bottom sonar techniques (detection of pockmarks) and then carry out in situ gas measurements and/or sample these leakage areas for direct CO_2 detection. Based on these observations an estimate can be made of leakage rates for the area. However, it should be noted that in the case of CO_2 storage in depleted gas fields, seismic methods have limited value. Most currently operational CO_2 storage projects use saline aquifers, such as Sleipner and Snøhvit in Norway, in which case seismic methods provide an efficient way to monitor the development of the CO_2 plume in the storage reservoir and verify containment by the caprock (e.g., Furre *et al.*, 2017). Seismic methods cannot be used to monitor the distribution of CO_2 in a depleted gas field, as seismic waves cannot discriminate between CO_2 and residual natural gas in the reservoir. In addition, gas fields offer high certainty that CO_2 will be contained in the depleted reservoir (as shown here in Sections 4 through 8), effectively removing the need to check for anomalies above the caprock. Only in case of evidence of unforeseen circumstances or non-conformance would seismic methods be considered as monitoring tool for CO_2 in depleted gas fields.

13.2.3   *Specific requirements for the P18-6 storage project*
CO_2 storage is the main objective of the P18-6 storage project. For the project, and the storage permit in particular, the monitoring plan serves to make supported statements about the following:
- Safety and integrity, regarding possible damage to the environment or the soil. Monitoring will have to support that the CO_2 remains stored in the reservoir and does not end up in the biosphere. The lasting quality of the structure of the reservoir and the sealing layer must also be clear. Monitoring offers the opportunity to take action if anomalies occur.
- Demonstration character of the project, learning of findings, some situations can be better understood through measurements.

- Commercially, regarding the ETS and the amounts stored. Monitoring must show that the captured CO_2 is in fact permanently out of circulation and no emission rights for this CO_2 need to be surrendered.
- Legally, regarding the delineation of the storage location. Monitoring must show that the CO_2 does not enter other reservoirs for which no storage permit has been issued.
- Offer a foundation to support the transfer of responsibility after injection is concluded.

13.3 Philosophy of the monitoring plan

Besides meeting all legal requirements, the monitoring plan should be based on a balance between efficiency and costs.

13.3.1 Regular measurements
A significant part of the monitoring program is measuring primary operational parameters and verifying the underlying model of the subsurface.

A plan has been devised that includes regular measurements, such as flow, pressure and temperature. These parameters will be used to test whether the injection program is proceeding according to plan and the extent to which anomalies occur with respect to the modelled behaviour.

Traffic light model
The measurement program uses the so-called traffic light model. This means that for the measurements, the expected values are indicated in ranges: green, yellow and red. Quantification of these monitoring value ranges is a key element of the monitoring plan update prior to the start of injection.

In the traffic light model, a green zone is given for each operational parameter; the value of the parameter falls within this range, when the operation is proceeding as expected. Outside of this range, threshold 1 (see Table 19-1), a yellow zone exists, indicative of a deviation from the predicted behaviour, without a direct need for corrective measures. When values fall within this range, it is important that insight is gained into the cause of the anomalous results. For that reason, additional measurements should be taken (extra measurements and/or the use of other measuring techniques, depending on the circumstances). Finally, there is a red zone, threshold 2 (see Table 19-1), indicating measurements that are so far outside of the expected range that corrective measures are probably necessary. If such an unexpected event occurs, undesired effects may develop. In order to limit such consequences as much as possible, corrective measures may be deployed. The monitoring program serves to indicate the effectiveness of these corrective measures.

Business as usual
When the injection proceeds as predicted, with measured values consistent with predicted values (green zone), the frequency of measurements could gradually be decreased.

Scale-up
If the measurements deviate from the expected values (yellow zone), this will lead to a higher frequency of measurements, or the introduction of other types of measurements. If this does not provide sufficient illumination of the situation, the monitoring program will be expanded further.

Adjusting the model
Monitoring data can also provide (new) information and insights about the subsurface; this information should be used to adjust and calibrate any models used. The adjusted models can be used to predict future behaviour with higher reliability, so that the behaviour of the CO_2, the well, the reservoir and the sealing layer can be predicted more accurately as the injection process proceeds.

13.3.2   *Special measurements*
Pre- injection, injection and post-injection monitoring do not differ in intent. Risks may be deemed higher in (parts of) the injection phase, notably the beginning of the injection activities. The monitoring plan reflects higher degrees of risk through more frequent and / or different monitoring techniques. Besides the measurements for the verification of predicted behaviour during injection, there are a number of special measurements included in the monitoring program. These concern baseline measurements, measurements before closure and transfer, as well as measurements under special circumstances during the injection process.

Baseline measurements
In the pre-injection phase there will be a period of monitoring in order to determine the current status of the storage site. During this period baseline data will be gathered. It is of key importance to identify all possible baseline data that might be required later in the injection and post-injection phases both for required monitoring and for contingency monitoring.

The baseline data will serve as a reference for monitoring during and after the injection process.

Baseline and repeat measurement acquisition, processing and interpretation are part of the monitoring plan (Table 19-1), where the relation with risk assessment and preventive/corrective measures is also described.

Measurements before closure and transfer
Measurements should be made before the closure of the reservoir and before the transfer to the competent authority. Their purpose is:
  • to determine whether the behaviour of the CO_2 stored in the reservoir is such that the well can be decommissioned.
  • to establish whether the CO_2 stored is in or moving towards a stable situation, after the conclusion of injection, so that it is possible to transfer responsibility to the government.

Measurements under special circumstances
During CO_2 injection, the pressure in the reservoir increases; the temperature, pressure and flow rate through each well are chosen such that injection can take place safely. During the injection process, the injection rates of CO_2 will vary, with

occasional interruptions. Part of the monitoring program is to measure the conditions that arise during such transient operations.

The period required for monitoring after decommissioning of the wells and prior to decommissioning of the platform is not defined yet, neither is the period between decommissioning of the platform and transfer of liability to the state authorities. The required lengths of these periods need to be established in agreement with State Supervision of the Mines (SodM).

13.3.3   *Direct and indirect determination of possible leakage*
Two ways can be distinguished to enable verification of the points above. On the one hand, there are direct detection methods that can be used to demonstrate the presence of CO_2 migration from the reservoir. An example of this can be CO_2 measurements at wells.

On the other hand. there are also indirect detection methods available, which can be used to verify that the CO_2 injected is behaving as predicted. The predictions are derived from static and dynamic models created beforehand, but also from updates to these models based on available monitoring data (such as pressure measurements in the reservoir). For this reason, important parameters have been included in the monitoring plan for the purpose of indirect monitoring. These include:
- pressure and temperature measurement in the wells;
- annular pressures of the wells;
- volume of injected CO_2;
- composition of the injected gas;
- well integrity measurements ;
- measurements of irregularities at the seabed.

13.3.4   *Different stages*
Different stages can be distinguished throughout the lifetime of the CO_2 storage project. This leads to different monitoring requirements through the lifetime of the project. The different stages are listed below.
- Pre-injection
Prior to actual injection, the monitoring focuses on recording the starting situation (baseline monitoring).
- Injection
In the operational phase CO_2 is injected until the reservoir is filled to an extent that further injection is not desired or allowed, or until no more CO_2 is delivered and a decision is made to conclude CO_2 injection.
- Post-injection
After CO_2 injection has stopped, there is a period of observation. During this period it will be decided whether a stable end situation will be reached. If this is the case, the well will be closed with a plug. If the plug is shown to be of an acceptable quality, the wells will be sealed.
- Post-injection — decommissioning
If the seal is shown to be of acceptable quality, the wells will be permanently decommissioned. Later, responsibility can be transferred to the government.
- Post-injection — transfer of liability
Once a stable situation is achieved, the responsibility of the filled reservoir may be transferred to the competent authority. After the transfer, the developments

in the reservoir will be followed periodically. The competent authority is responsible for a monitoring period of 30 years from the moment of transfer.

For each stage, the monitoring plan (Table 19-1) indicates the parameters to be measured, the frequency, the technology used and the location for each activity. The expected duration of each monitoring period is also indicated.

13.3.5   *Report monitoring results*
Prior to the start of injection activities a baseline report will be compiled, describing the starting state of the wells and the storage site. This is the basis that will be used to map any changes.

An annual report of the monitoring results will be presented to the competent authority. The report should hold operational information, possible anomalous situations and information towards closure and transfer.

Prior to both site closure and site transfer a report is compiled, recording the state of both the well and the subsurface.

13.3.6   *Conclusion*

Deviations from expectations
Deviations from any expected behaviour of the storage complex may indicate migration or leakage of the injected CO_2. In the P18-6 case the main activities in determining such deviations from the expected behaviour consist of monitoring the CO_2 pressure and temperature.

A thorough and reliable history match has been established. Deviations from the expected pressure development (p/Z curve) throughout and after the operational phase, could be an indicator of migration of CO_2 from the reservoir or leakage from the storage complex. To this end the pressures at the top of the wells are measured in any case (in the wellhead) as well as the pressures at the bottom of the wells (downhole).

Should unexpected deviations be measured and migration of CO_2 from the reservoir be suspected, measures need to be taken. Taking into account the comments about the application of seismic methods in the case of CO_2 storage in depleted gas fields given in Section 13.2.2. These may include time-lapse seismic monitoring, which allows possible migration paths or shallow CO_2 accumulations to be detected with an expected observation threshold of several tens of kilotons. The detection limit and measurement precision will be specified with the submission of the revised monitoring plan prior to injection and after detailed engineering.

The shallower the gas accumulation occurs, the better the chance that it can be detected. Baseline monitoring prior to injection will be used to make an inventory of pockmarks already present. This will allow the change with respect to the initial situation to be determined in case of a possible migration or leakage.

Well integrity
Various techniques are used to monitor the integrity of the (injection) wells. These include:

- Logging across the depth of the well:
- Measurement of the pressures in the annuli;
- Periodic analysis of the liquids in the annuli, in order to test for the presence of CO_2.

Prior to the commencement of CO_2 injection, each injection well will be worked over and its state will be recorded as the baseline for later determinations of the integrity of the well. After injection, the well will be safely sealed and permanently decommissioned. However, before the well is entirely decommissioned, there will first be a period in which the integrity of the plug (FFP) is measured at seal level. These measurements consist of tests monitoring the annular pressures, logs and taking samples of the liquids from the well above the seal in order to analyse for the presence of CO_2.

Monitoring of the seabed

Finally, there is monitoring of the seabed. This is mainly in order to show that there are no changes and therefore there is no migration of CO_2 to the seabed. Various acoustic technologies (multibeam echo sounding, side scanning sonar, etc.) can be used to identify changes in and at the seabed as a result of changes in the deep underground (often in the shape of pockmarks) and possible CO_2 bubble streams in the water column. In addition, seabed samples (via coring) can be used to establish the presence or absence of leaking CO_2.

13.4 Interpretation

Abovementioned aspects have led to the monitoring plan presented here. The following aspects will be monitored:
- Injection process
- Well integrity
- Reservoir integrity
- Environmental monitoring {for leakage of CO_2 from the storage complex)

13.4.1 Categories

Monitoring of CO_2 storage can be achieved either by measuring the absence of any leakage through direct detection methods, or by verifying indirectly that the CO_2 is behaving as expected in the reservoir based on static and dynamic modelling and updating thereof corroborated by monitoring data. The main challenge for measuring absence of any leakage consists of spatial and temporal coverage of the monitoring method, i.e. "Where and when do we need to monitor in order to be sure that no leakage occurs". The strategy should therefore be based on identified risks.

For the indirect model-based monitoring the emphasis is more on scenario confirmation. As long as monitoring data demonstrates that the storage system is behaving according to the predictive models, the understanding of both the processes occurring and the behaviour of the storage complex can be considered sufficient. In case of significant deviations, one should find the causes of the deviations and where necessary recalibrate the models and perform new predictive simulations. If however the deviations fall well beyond the uncertainty ranges of the predictive models, then additional monitoring and possibly contingency measures need to be taken.

In practice often a combination of approaches is applied required and the optimum monitoring plan will be guided by the risk assessment and the site characterization.

Following the NSBTF (2009) and the draft EU guidance documents (2010), the following categories for monitoring are identified:

1. Mandatory monitoring: in any case for all sites. A number of parameters to be monitored is mandatory based on the EU storage directive (EU, 2009).
2. Required monitoring: site specific. This monitoring group is directed to gathering evidence for containment in the reservoir and to demonstrate integrity of seal, fault and wells in case of regular development.
3. Contingency monitoring. The third group refers to a contingency monitoring system which will only be installed if irregularities show up. In the CCS Directive a "significant irregularity" is defined as '…any irregularity in the injection or storage operations or in the condition of the storage complex itself, which implies the risk of a leakage or risk to the environment or human health'.

It is to be noted that these three categories as such have not been implemented in Dutch legislation, therefore the term *mandatory* should be read as "mandatory following the CCS Directive". Similar for the term *required*, which is not as such defined in legislation. Required in the context of this report means a preliminary proposal of essentially risk-based monitoring with the current state of knowledge.

The quantification of a leakage at the sea bottom for ETS purposes is considered as part of the contingency monitoring. Quantitative monitoring for ETS will only be required, if there is an indication of leakage. For the North Sea the strategy suggested by NSBTF (2009) would be to detect leakage to the surface by geophysical methods like seismic data (detection of gas chimneys) or sea-bottom echo-sounding (detection of pockmarks) and then sample these leakage areas for direct CO_2 detection repeatedly. Based on the sampling profiles an estimate can be made of leakage rates over time for the area. In case of wellbore leakages an additional monitoring program in and around the well is suggested.

In the operational execution, the following categories are distinguished, and for each category the measurements performed for general testing are indicated, as well as the measurements that relate to gaining insight into deviations and to conclusion and transfer.

13.5 The monitoring plan

Following NSBTF (2009) and the draft EU guidance documents (EU, 2011), Table 13-1 lists the categories for monitoring that have been identified, as well as the aspects to be monitored. Table 13-2 gives a summary of the monitoring plan describing the equipment or method that can be used to measure certain processes.

Table 13-1. Summarized monitoring classification table.

	Mandatory (Mandatory monitoring according to Annex II of the EU directive)	**Required** (Preliminary estimation of required monitoring)	**Contingency monitoring**
Injection process	Flow, pressure, temperature and composition of injected CO_2		
Well integrity	Various Integrity measurements, well head pressure & temperature	Various baseline measurements, plug integrity measurements	
Reservoir integrity	Flowing pressure and temperature measurements	Stabilized pressure and temperature measurements	Seismic survey in case of irregularities
Environmental monitoring		Various baseline measurements, Microseismic monitoring	Various surveys in case of irregularities

The complete monitoring plan for P18-6, in the form of a table, is given in Table 19-1. Below is a description of the parameters mentioned in the table. These parameters follow both from the mandatory monitoring obligations as stipulated by the storage directive and the risk assessment.

Column 1
The first column describes the parameters to be monitored. These parameters follow both from the mandatory monitoring obligations as stipulated by the storage directive and from the risk assessment.

Column 2
The second column indicates the proposed technique adopted to measure the parameter. A more detailed description of the technique is provided outside the table.

Column 3
The third column indicates the category of monitoring (mandatory according to the EU directive, required, contingency).

Column 4 and 5
The fourth and fifth columns give a description of both the temporal frequencies (column 4) and spatial coverage (column 5) of the data acquisition foreseen in the different phases of the project (pre-injection, injection and post-injection including long-term stewardship after transfer of responsibility). The rationale behind the monitoring strategy related to the identified risks is described in the following section.

Column 6
Column six provides a description of the expected values that indicate normal behaviour and of the expected accuracy of the monitoring method. Expected values and therefore this column is coloured green.

Table 13-2. Summary of specific monitoring equipment and methods to be used for monitoring of certain processes.

	Injection process	Measurement equipment / method
1	Injection rate	Flow meter
2	Injection stream CO_2 concentration	Samples & analysis: online system
3	Injection stream composition	Samples & analysis: Additional samples for calibration
4	Water measurement	Water measurement
5	Discontinuous emissions through leakage, venting or incidents	Combination of techniques
	Well integrity	
6	Annular pressure	Pressure device (with alarm value)
7	Well integrity	Wireline Logging (selection of tool: CBL, PMIT, EMIT, USIT, WAF, optical)
8	Well head pressure	Pressure device
9	Well head temperature	Temperature device
10	Plug integrity	Pressure test and additional inspections
	Reservoir integrity	
11	Reservoir pressure (FBHP) (see also line 8)	pressure device
12	Reservoir Temperature (FBHT) (see also line 9)	thermometer or DTS
13	Stabilized pressure (CIBHP) (gradient) during shut-in period	pressure device combined with shut-in
14	Stabilised temperature (CIBHT) (gradient) during shut-in period	thermometer or DTS combined with shut-in
15	Suspected leakage	Surface seismic survey
	Environmental monitoring	
16	Pockmarks at the seabed	Multi-beam echosounding
17	Presence of shallow gas or gas chimneys in the subsurface	Baseline seismic data
18	Migration pathways for gas in the shallow subsurface	Time-lapse seismic data acquisition (2D or 3D)
19	CO2 in soil at pockmarks	Gas samples using vibrocore + lab analysis
20	Bubble detection at wellhead	Acoustic bubble detector
21	Microseismic monitoring	Permanent geophones or DAS in monitoring wells

Column 7

The seventh column indicates threshold values, where normal behaviour as anticipated stops and where irregularities start. As long as the measured values remain below these threshold values, no actions are required (green column). In case threshold values exceeded, the seventh column (coloured orange) defines specific actions. Upon exceeding threshold values, monitoring data suggest that the behaviour of the storage system starts to deviate from expectations. This could for example lead to recalibration of the models, but when persisting to more stringent measures.

Column 8

In case the monitor values exceed the threshold defined in the eighth column (coloured red), the highest alert phase starts and immediate actions (or contingency measures) as defined in the second sub column of column eight are required.

Items to be monitored

The next part of the monitoring plan describes the different items or events to be monitored (Injection process, Well integrity, Reservoir Integrity, Environmental Monitoring) and over which time frame (Pre-injection, Injection, Post-injection, etc). See Table 19-2.

It is noted that the timing for monitoring of the post injection period including the decommissioning of the wells and the decommissioning of the platform and the period to the transfer of liability to the state have not been defined in this plan. The definition of these periods will be subject of discussion with State Supervision of the Mines (SodM).

13.5.1   Proposed monitoring methods

This section provides more detailed background information on the rationale behind the selection of the proposed monitoring techniques. For each section corresponding to an identified actor in the risk analysis the primary relevant monitoring techniques are referred to between brackets by their number as appearing in the first column in Table 19-1. Monitoring techniques for contingency monitoring are not given between the brackets, this to not overcomplicate the overview below. Techniques relevant for contingency monitoring are indicated in Table 19-1.

13.5.1.1   Reservoir / injection process (1,2,3,4,5,8,9,11,12,13,14)

The risk identified from leakage of CO_2 out of the reservoir / storage site where:

- Spilling (via spill point), or
- Sealing capacity of fault zone between P18-2 and P18-6.

Based on the history match of the P18-6 reservoir the field can be considered as a "tank model", without an active aquifer drive. Therefore CO_2 is expected to disperse throughout the original gas reservoir.

Often – and this applies only to storage of CO_2 in saline aquifers - the key tool for reservoir / CO_2 plume imaging is 3D surface seismic, however this technique is not deemed suitable for P18-6. This is because of the considerable depth of the P18-6 storage reservoir, which renders surface seismic methods less effective. Additionally, for P18-6 the presence of (residual) gas within the reservoir makes the feasibility of repeated seismic surveys for the monitoring of CO_2 dispersion questionable, as seismic data cannot discern between CO_2 and residual gas.

The main components for monitoring deviations in expected behaviour indicating potential migration out of the reservoir or storage complex consist of pressure (and temperature) monitoring. After proper history matching, a deviation from the expected pressure trend (P/z curve) during and after the operational phase is an indicator for potential migration out of the storage complex. As for the P18-6 reservoir, pressure monitoring has the potential to be a powerful tool, since there is no strong aquifer drive masking potential deviations. A rough estimation of the threshold of the mass of CO_2 migration out of the reservoir that can be detected is in the order of 2-10 kt of CO_2. The exact value depends on the quality of the P/z curves with proper and reliable pressure measurements. Factors like water influx, communication with neighbouring compartments or CO_2 dissolution in water have a

negative effect on the detectability. In addition, the measurement accuracy of inflow rates should be taken into account.

Proper pressure measurements can be obtained from the injection well after a shut-in, or continuously from a "monitoring" well. The latter is the preferred option allowing a continuous measurement of the reservoir pressure in equilibrium, but for the P18-6 reservoir hardly an option. In case the reservoir pressure is measured in the injection well after a shut-in, pressure equilibration should be measured over a time interval in the order of days. Based on the latter, the equilibrium pressure can be extrapolated (if it has not already been reached in this period).

Migration in the reservoir can be followed by additional geophysical logs (RST logs) well tests and downhole fluid samples at monitoring wells in the same reservoir to detect CO_2 breakthrough. During the injection phase, microseismic monitoring (not necessarily from a well in the same reservoir, but in the direct vicinity of the reservoir). and innovative pulse testing techniques may provide data on the location of the advancing CO_2 temperature front by detecting thermal fracking (if any), and density/viscosity differences. The latter is not considered as an absolutely required measurement for CO_2 tracking, but is recommended. Furthermore the CO_2 can be traced as it closes in on boundary faults or moves toward spill points.

13.5.1.2   *Well integrity (6,7,8,9,10,11,12,13,14,16)*

The key tool for monitoring well integrity is logging, aimed both directly at the wellbore (cement bond logging, etc.), but also at the surrounding formations (saturation logging). Pressure-temperature logging and downhole fluid chemistry are also potentially very useful. Non-well-based tools include 2D or 3D surface seismic for volumetric imaging of the overburden around the wellbores and multibeam echosounding to detect surface changes around the wellbore. During the injection stage, well-based microseismic monitoring can also provide information on flow and degradation processes around the wellbores.

13.5.1.3   *Caprock/overburden (11,12,13,14,16,17,21)*

Caprock integrity is assumed intact as long as no abnormal behaviour of the pressure is observed. In case significant deviations are observed, contingency monitoring is required; potentially useful techniques include time-lapse seismic surveys to detect migration pathways (chimneys) or shallow gas accumulations. 2D surface seismic surveys may be a cost-effective alternative to full 3D, but will not provide full areal coverage of the top seal.
The threshold value of seismically detectable shallow accumulations of CO_2 is in the order of 10's of ktonnes under the condition that CO_2 accumulates as a concentrated gas pocket. The shallower the CO_2 accumulates, the better the chances of picking up the signal.
During the injection phase, microseismic monitoring could provide data on whether the top seal is being geomechanically compromised. The feasibility of using wells as monitoring wells for microseismic monitoring has not been thoroughly explored yet, but may be regarded as a option, especially now DAS systems become ever more sensitive.

13.5.1.4   *Faults (11,12,13,14,21)*

Thermal reactivation of faults is identified as a risk with risk classification B-2 (Section 12.3). If the cold front of the injected CO_2 reaches a fault, the likelihood of

activation increases. In order to reduce this risk, the advancement of the cold front from the injector wells to nearby faults needs to be managed and monitored. Pressure and temperature monitoring data needs to be used in combination with non-isothermal reservoir simulations to assess whether the cold front stays away from the faults within and bounding reservoir blocks.

During the injection phase, microseismic monitoring as well as advanced well tests (pulse testing) may provide data on the location of the migrating CO_2 front. Geophysical logs would not provide reliable indications of generalized CO_2 migration, except where free CO_2 accumulates in very close proximity to the wellbores.

The threshold value of seismically detectable accumulations of CO_2 in the overburden is in the order of 10's of ktonnes, depending on the depth and geophysical properties of the reservoir and surrounding rocks. In the P18-6 case this is considered a contingency measurement. Just like sampling fluids of shallower aquifers can show traces of leaking CO_2. To detect the absence of migration to the seabed, various types of surveys are an option. These will be able to identify pockmarks or bubbles and check for composition and origin.

13.5.1.5 *Calibration of flow simulations (1,2,3,4,5,8,9,11,12,13,14)*

The calibration of flow simulations combines aspects of several of the above aims, effective reservoir management, accurate pressure and temperature monitoring and insights into fine-scale and geochemical processes. Likely tools are downhole pressure/temperature measurements, RST logs and monitoring breakthrough in monitoring wells. For P18-6 where 3D seismic imaging of CO_2 in the reservoir is considered difficult if not impossible, downhole pressure/temperature is the key technology. As in a number of cases above, microseismic monitoring and pulse testing (an advanced way of well testing) may be useful in the injection phase.

13.6 Conclusion

The adopted monitoring approach for CO_2 storage in P18-6, builds on the results of the site characterization and the risk assessment. The reservoir has been classified as suitable for CO_2 storage; the reservoir offers stable long-term containment. This conclusion is essentially based on a) the fact that natural gas has been contained in these reservoirs for millions of years, b) the knowledge of the reservoirs obtained during exploration and production of the fields, c) the fact that at the end of injection the pressure in the reservoir will be lower than that of surrounding formations.

The monitoring plan proposed is designed to verify CO_2 containment and storage reservoir integrity while and after the storage facility is in operation. This is achieved by both measuring the absence of any leakage through direct detection methods (for example at the wells), and by verifying indirectly that the CO_2 is behaving as expected in the reservoir by collecting pressure, temperature and injection rate data that feed in to static and dynamic modelling. The design includes therefore the collection of data such as representative storage pressures and annuli pressures, injected volumes and gas qualities, well integrity measurements, reservoir conditions, micro seismicity and sea bottom measurements.

The main component for monitoring deviations in expected behaviour indicating potential migration out of the reservoir consists of pressure and temperature monitoring. After proper history matching any deviations from the expected

pressure trend (P/z curve) during and after the operational phase is a potential indicator for migration out of the storage reservoir. Reservoir pressures will be determined regularly via shut-in of injection wells or monitoring wells. Downhole pressure tests are envisaged to verify the storage pressures and to verify the conversion of the wellhead pressures to downhole pressures.

Only in case irregularities are observed in seismicity pressure, or the temperature behaviour and when migration in the overburden is suspected, additional monitoring is proposed, like time-lapse seismic monitoring to detect possible migration pathways (chimneys) or shallow gas accumulations. The threshold value of seismically detectable accumulations of CO_2 is of the order of 10's of ktonnes under the likely condition that CO_2 accumulates as a concentrated gas pocket in shallower aquifers. The shallower the CO_2 accumulates, the better the chances of picking up the signal.

The key tools for monitoring well integrity consist of (repeated) logging, measuring the annuli pressures and regular analysis of the annuli fluids for the presence of gas or CO_2. Prior to CO_2 injection a proper assessment of the current state of the existing wells is carried out, as well as work-overs. Before decommissioning, wells will be suspended for a period of time to verify the quality of the plugs at caprock level by gas tests, monitoring of annuli pressures and possibly sampling of fluids from the well to monitor for the presence of CO_2.

Finally, shallow monitoring, to detect the absence of migration to the seabed, in the form of multi-beam echosounding, side scanning sonar or high-resolution 3D surveys can be considered for identifying pockmarks or bubbles. Furthermore, sampling fluids in the soil at the sea bottom (via cores) can be used to verify the absence of traces of migrating CO_2. The locations of the sampling will essentially be associated with the well positions, but additional locations can be selected based on multi-beam echosounding results.
In both cases, echosounding and fluid sampling, these types of monitoring should be performed when there is reason to suspect loss of containment and significant leakage out of the storage complex.

14   Conclusions

The identified risks that are related to the potential leakage of CO_2 out of the P18-6 storage complex during or after CO_2 injection have been studied in detail and classified in a risk register. Most of the risks have been classified as 'very low', with 'very low likelihood' that a small ('nil to negligible') amount of CO_2 could migrate out of the reservoir'; this corresponds with the lowest possible risk class. The risks associated with the injection well have been classified as 'low', with a 'low likelihood' and a small ('nil to negligible') amount of CO_2 could migrate out of the reservoir.

The risks assessed are related to (1) lateral CO_2 migration out of the storage reservoir, (2) the integrity of the well in the field, (3) the stability of the faults in the storage system and integrity of the caprock.

(1) Simulation of the flow of CO_2 during injection into the storage formations shows that the injected CO_2 will be retained within the confines of the original gas field. There is no risk of CO_2 spilling, even when the pressure in the reservoir is brought back to the initial pressure.

(2) Analysis of available data on the integrity of the well in the P18-6 field shows that a workover is required for the existing well, P18-A-07-S1. Once this is performed, the risk of CO_2 leaking along the well, based on pre-injection status, is considered low.

The initial low reservoir pressure leads to low temperature of the CO_2 at the bottom of the well, causing significant temperature gradients in the well. These might to lead to de-bonding of well liner (casing) and cement, potentially allowing leakage pathways to form (micro-annuli) for CO_2. However, only when the pressure in the reservoir is above hydrostatic pressure could CO_2 enter these micro-annuli and potentially migrate into overlying aquifers. Therefore, the pressure in the reservoir is to be maximized at hydrostatic pressure, to reduce the likelihood of CO_2 flowing through these micro-annuli to 'low', with an amount of CO_2 that is 'small to negligible'.

(3) The cold CO_2 is injected into the reservoir formations, where it will create a low-temperature zone around the injection well. In case injection into the P18-6 reservoir on a continuous basis, this zone could reach faults that are present in the reservoir, affecting fault stability; however, at the same time, faults become more stable during the injection process due to increasing reservoir pressure. If the P18-6 reservoir is only used to store the cold contents of the surface transport pipeline after a shut-in period, the mass of injected (colder) CO_2 is small and the low-temperature front does not reach faults near the well. In both modes of operation, monitoring of injection rate and temperature is recommended to measure the pressure and track the temperature development in the reservoir and ensure that faults remain stable. However, all analysis points to small to negligible impact of fault reactivation; none of the faults in the P18-6 reservoir extend to above the caprock of 450 m to 750 m thick. This ensures that, fault destabilization, if any, will not lead to CO_2 movement through the caprock.

The likelihood that CO_2 injection in the P18-6 reservoir affects caprock integrity is very low.

Recommendations

(1) In the study presented here the modelling of the injection process was performed with an isothermal reservoir simulator that could not simultaneously handle pressure and temperature variations in the reservoir. The impact of the low temperature of the injected CO_2 was estimated through the use of an additional simulator and analytical approaches. While the results obtained thus far are considered sufficient for the assessment of the risks associated with CO_2 storage, detailed coupled modelling of pressure and temperature in the storage formations is required prior to the start of injection. This is needed for pressure and temperature predictions that are sufficiently reliable for the management of the injection process and for the interpretation of monitoring data.

(2) The aim of the present study was to provide the basis for a storage permit application, by understanding the current status of the storage formations, the caprock, the faults and the wells, and their response to the injection of CO_2. The study established that conditions can be established under which CO_2 can be injected and stored safely and securely in the P18-6 field. The study did not aim to arrive at a complete and detailed description of these conditions. Such an 'operational plan' for CO_2 injection into the P18-6 field will be required prior to the start of injection, as a basis for the detailed monitoring plan and for the operational management of the injection process. The present study is the first step towards the P18-6 operational plan.

15 References

Adelinet M., Nauroy J-F., Graham C.C., Cuss R.J., Wiseall A.C., Bakker E., Spiers C.J. and Hangx S.J.T. (2014). Progress report with data on processes, constitutive relations and parameters for modelling work. EU FP7 UltimateCO$_2$ Deliverable D4.5.

Akemu, O., Miersemann, U., Benedictus, T., Nepveu, M., Desroches, J. (2011). Well integrity assessment of the P18 gas field (TAQA), CATO2 report WP3.4-D22.

Ames R., Farfan P.F. (1996). The environments of deposition of the Triassic Main Buntsandstein Formation in the P and Q quadrants, offshore the Netherlands. In: Rondeel H.E., Batjes D.A.J., Nieuwenhuijs W.H. (eds) Geology of Gas and Oil under the Netherlands. Springer, Dordrecht. pp 167-178.

AMOCO (1993). Final well report, well P/18-2A3(z) & well P/18-2A4.

Bacci G., Korre A. and Durucan S. (2011). An experimental and numerical investigation into the impact of dissolution/precipitation mechanisms on CO$_2$ injectivity in the wellbore and far field regions. International Journal of Greenhouse Gas control 5, 579-588.

Baines S.J., and Worden R.H. (2004). Geological Storage of Carbon Dioxide. Geological Society, London, Special Publications 233, 59-85.

Barnes, J. and Hut, P. (1986). A hierarchical O(N log N) force-calculation algorithm. Nature, 324, 446-449.

Bakker E., Hangx S.J.T., Niemeijer A.R. and Spiers C.J. (2016). Frictional behaviour and transport properties of simulated fault gouges derived from a natural CO2 reservoir. International Journal of Greenhouse Gas Control 54, 70-83.

Baumann G., Henninges J. and De Lucia M. (2014). Monitoring of saturation changes and salt precipitation during CO$_2$ injection using pulsed neutron-gamma logging at the Ketzin pilot site. International Journal of Greenhouse Gas Control 28, 134-146.

Belfroid, S. (2019). Porthos – CO$_2$ injection, TNO report TNO 2019 R10335.

BP (2007). P/18 Field Petrophysical Study. Company report, 13 p.

BP (2003). End of well drilling & completion report – P18-6A7, Feb – June 2003.

Candela, T., van der Veer, E.F., Fokker, P.A. (2018). On the importance of thermo-elastic stressing in injection-induced earthquakes, Rock Mechanics and Rock Eng., 51 (12), 3925-3936.

Duguid A. and Scherer G.W. (2010). Degradation of oilwell cement due to exposure to carbonated brine. International Journal of Greenhouse Gas Control 4, 546-560.

Energy Institute (2019). Hearts and Minds toolkit – Risk assessment matrix. website, version 15 Oct 2019.
https://publishing.energyinst.org/heartsandminds/toolkit/RAM

EPA (2012). Geologic Sequestration of Carbon Dioxide Underground Injection Control (UIC) Program Class VI Well Construction Guidance (May 2012).

ETS directive, 2009: DIRECTIVE 2009/29/EC OF THE EUROPEAN PARLIAMENT AND OF THE COUNCIL of 23 April 2009 amending Directive 2003/87/EC so as to improve and extend the greenhouse gas emission allowance trading scheme of the Community EU Guidance Document 2 (draft 2010): Site Characterisation, CO$_2$ Stream Composition, Monitoring and Corrective Measures. Draft document for consultation version June 17, 2010.

EU, 2009: DIRECTIVE 2009/31/EC OF THE EUROPEAN PARLIAMENT AND OF THE COUNCIL of 23 April 2009 on the geological storage of carbon dioxide and amending Council Directive 85/337/EEC, European Parliament and Council Directives 2000/60/EC, 2001/80/EC, 2004/35/EC, 2006/12/EC, 2008/1/EC and Regulation (EC) No 1013/2006.

EU (2011). Implementation of Directive 2009/31/EC on the Geological Storage of Carbon Dioxide. Guidance document 2: Characterisation of the storage complex, CO_2 Stream Composition, Monitoring and Corrective Measures.

EC (2018). II (Non-legislative acts) Regulations – Commission implementing regulation (EU) 2018/2066 of 19 December 2018 on the monitoring and reporting of greenhouse gas emissions pursuant to Directive 2003/87/EC of the European Parliament and of the Council and amending Commission Regulation (EU) No 601/2012, Official Journal of the European Union, L 334/1-93

Fisher Q. (2013). Collection of petroleum field analogues data and description of risks of CO2 leakage along faults. EU FP7 UltimateCO2 Deliverable D4.1.

Fischer, H., Orlic, B., Osinga, S., Hopmans, P., Wollenweber, J., Geel, K. (2016). Options to initiate and enhance ductile properties of shale for well bore sealing. "TKI Plugging wells by enhanced formation ductility" - Deliverable report D5.1; TNO report 2016 R10970

Gaus I., Zazroual M. and Czernichowski-Lauriol I. (2005). Reactive transport modelling of the impact of CO_2 injection on the clayey cap rock at Sleipner (North Sea). Chemical Geology 217, 319-337.

Geel, C.R. (2016). Geological screening of ductile formations. "TKI Plugging wells by enhanced formation ductility" - Deliverable report D4.1; TNO report 2016 R10273.

Geertsma, J. (1973). A basic theory of subsidence DUE to reservoir compaction: The homogeneous case. Verhandelingen Koninklijk Nederlandsch Geologisch Mijnbowkundig Genootschap 2S, 43-61.

Gilfillan S.M.V., Lollar B.S., Holland G., Blagburn D., Stevens S., Schoell M., Cassidy M., Ding Z., Zhou Z., Lacrampe-Couloume G. and Ballentine C.J. (2009). Solubility trapping in formation water as dominant CO_2 sink in natural gas fields. Nature 458, 2 April 2009, doi:10.1038/nature07852.

Grude S., Landrø M. and Dvorkin J. (2014). Pressure effects caused by CO_2 injection in the Tubåen. Fm., the Snøhvit field. International Journal of Greenhouse Gas Control 27, 178-187.

Hulten, F.F.N. van (2006) Reservoir quality distribution as tool for better exploration prospect evaluation and estimation of the resource base in the Netherlands. In: Hulten, F.F.N. van & Lutgert, J.E. (comp.). Tight gas fields in the Netherlands, workshop EBN-TNO, September 19, Utrecht (The Netherlands), 13 p.

IEAGHG (Greenhouse Gas Programme) (2016). Impact of impurity on CO_2 compression, liquefaction and transportation, Report 2016/01.

IEAGHG (2018). Well Engineering and Injection Regularity in CO2 Storage wells, IEAGH Technical Report, 2018-08.

ISO/TC 67/SC 4 Drilling and production equipment. (2017). *ISO 16530-1:2017: Petroleum and natural gas industries - Well integrity - Part 1: Life cycle governance* . bsi.

Kim K.-Y., Han W.S., Oh J., Kim T. and Kim J.-C. (2012). Characteristics of salt precipitation and the associated pressure build-up during CO_2 storage in saline aquifers. Transport in Porous Media 92, 397-418.

Koenen M., Wasch L., Wollenweber J. and Tambach T. (2014). CATO-2 Deliverable WP3.4-D12. Experimental and modelling study into chemical degradation mechanisms and rates of cement subjected to aqueous and supercritical CO_2 at in-situ reservoir conditions.

Koenen M. and Wasch L. (2018). The potential of CO_2 leakage along de-bonded cement-rock interface. 14th International Conference on Greenhouse Gas Control Technologies, GHGT-14. 21st – 25th October 2018, Melbourne, Australia.

Kutchko B.G., Strazisar B.R., Dzombak D.A., Lowry G.V. and Thaulow N. (2007). Degradation of well cement by CO under geologic sequestration conditions. Environmental Science and Technology 41 (13), p4787-4792

Loeve, D., Hofstee C. and Maas J.G.,(2014). Thermal effects in a depleted gas field by cold CO_2 injection in the presence of methane, Energy Procedia, Volume 63, p. 5378-5393.

Mijnbouwwet, https://wetten.overheid.nl/jci1.3:c:BWBR0014168&z=2019-04-10&g=2019-04-10

Mindlin, R.D. (1936). Force at a point in the interior of a semi-infinite solid, Physics, 7(5), 195–202.

Miocic J.M., Gilfillan S.M.V., Frank N., Schroeder-Ritzrau A., Burnside N.M. and Haszeldine R.S. (2019). 420,000 year assessment of fault leakage rates shows geological carbon storage is secure. Scientific Reports, DOI:10.1038/s41598-018-36974-0.

Miri R. and Hellevang H. (2016). Salt precipitation during CO_2 storage – A review. International Journal of Greenhouse Gas Control 51, 136-147.

Myklestad, N.O. (1942). Two problems of thermal stress in the infinite solid, Journal of Applied Mechanic, 9, 136-143.

Neele, F., Delpart-Jannaud, F., et al. (2013). Site characterization workflow, SiteChar report D1.4.

Neele, F., Wildenborg, T., Geel, K., Loeve, D., Peters, L., Kahrobaei, S., Candela, T., Koenen, M., Hopmans, P., van der Valk, K., Orlic, B. and V. Vandeweijer, CO_2 storage feasibility in the P18-2 depleted gas field, TNO report, 2019.

Nepveu, M, Neele, F, Delprat-Jannaud, F, Akhurst, M, Vincké, O, Volpi, V, Lothe, A, Brunsting, S, Pearce, J, Battani, A, Baroni, A, Garcia, B, Hofstee, C, And Wollenweber, J. (2015). CO_2 storage feasibility: a workflow for site characterization, Oil and Gas Science and Technology 70, 4, 555–566.

Nieuwland, D. A. (2012) Fault Seal Prediction in Sandstone Reservoirs - A quantitative and calibrated geomechanical method, 3rd International Conference on Fault and Top Seals - From Characterization to Modelling, Montpellier, France 1-3 October, 2012.

NOGEPA - OPCOM (2016). Industry Standard no. 45 - Well Decommisioning. NOGEPA.

NORSOK (2013). *Norsok standard D-010: Well integrity in drilling and well operations.*

North Sea Basin Task Force (NSBTF), 2009, Monitoring Verification Accrediting and Reporting (MVAR) Report for CO_2 storage deep under the seabed of the North Sea.

Okada, Y. (1992). Internal deformation due to shear and tensile faults in a half-space, Bull. Seism. Soc. Am., 82(2), 1018–1040.

OSPAR (2007). OSPAR Guidelines for Risk Assessment and Management of Storage of CO_2 Streams in Geological Formations (Reference Number: 2007-12), Meeting of the OSPAR Commission, Ostend, 25-29 June 2007.

Peach C.J., de Bresser J.H.P., van der Kroef R.F.M., Mols A., Verberne B.A. and Samuelson J. (2010). Site-representative caprock and fault rock samples acquired and characterised (1st Year Progress Report). CATO-2 Deliverable WP 3.03-D06.

Pruess, K., (2011). ECO2M: A TOUGH2 Fluid Property Module for Mixtures of Water, NaCl, and CO2, Including Super- and Sub-Critical Conditions, and Phase Change Between Liquid and Gaseous CO2. LBML, Uni. Berkeley, Berkeley, CA (Updated Sept 2013).

Rimmelé G., Barlet-Gouédard V., Porcherie O., Goffé B. and Brunet F. (2008). Heterogeneous porosity distribution in Portland cement exposed to CO_2-rich fluids. Cement and Concrete Research 38, 1038-1048.

ROAD (2018). Rotterdam capture and storage demonstration project, https://ccsnetwork.eu/projects/road-project-rotterdam.

Roels S.M., Ott H. and Zitha P.L.J. (2014). μ-CT analysis and numerical simulation of drying effects of CO_2 injection into brine-saturated porous media. International Journal of Greenhouse Gas Control 27, 146-154.

Samuelson J., Spiers C., Koenen M. and Tambach T. (2012). Lab evaluation of the reactivation potential of simulated faults under CO2 storage conditions – implications for system integrity and seismic risk. CATO-2 Deliverable WP 3.3 – D13.

Shell (2015). Peterhead CCS Project, Well Technical Specification, Doc No.: PCCS-05-PT-ZW-7770-00001, 20/05/2015.

SodM (2019). *De integriteit van onshore putten.* SodM

Tambach T., van Bergen F., Gutierrez-Neri M., Hostee C., Koenen M., Kooi H., Loeve D., Maas J., Plug W-J., Ranganathan P., Roels S., van der Meer B., Wasch L. and Zitha P. (2012). Models describing near-well clogging and mineralization to support feasibility and long-term integrity. CATO-2 Deliverable WP3.02-D13.

Tambach T.J., Loeve D., Hofstee C., Plug W.-J. and Maas J.G. (2015a). Effect of CO_2 injection on brine flow and salt precipitation after gas field production. Transport in Porous Media 108, 171-183.

Tambach T.J., Koenen M., Wasch L.J. and van Bergen F. (2015b). Geochemical evaluation of CO_2 injection and containment in a depleted gas field. International Journal of Greenhouse Gas Control 32, 61-80.

TAQA (2009) CO_2 Offshore Storage Source to Sink. Presentation given by TAQA Energy B.V., 3 July 2009.

TAQA (2018) Geophysical Evaluation P18. TAQA Internal report, 6 p.

Tian H., Xu T., Zhu H., Yang C. and Ding F. (2019). Heterogeneity in mineral composition and its impact on the sealing capacity of caprock for a CO_2 geological storage site. Computers and Geosciences 125, 30-42.

Van Balen, R.T., Van Bergen, G., De Leeuw, C., Pagnier, H.J.M., Simmelink, H., Van Wees, J.D., Verweij, J.M. (2000). Modeling the hydrocarbon generation and migration in the West Netherlands Basin, the Netherlands. Netherlands Journal of Geosciences 79, 29-44.

Van Eijs, R., Kuijper, M. and Bisschop, R. (2011). Containment demonstration for the Barendrecht CO_2 storage project, Energy Procedia, 4, 4092-4099.

Vandeweijer V. et al. (2011). Feasibility study P18 (final report). CATO2-WP3.01-D06.

Vrålstad, T., Todorovic, J., Wollenweber, J., Abdollahi, J., Karas, D., & Buddensiek, M. (2015). *D8.1 - Description of leakage scenarios for consideration in the*

work in SP3. https://mirecol-co2.eu/download/D08.1%20-
%20Description%20of%20leakage%20scenarios.pdf.

Wang Y., Zhang L., Soong Y., Dilmore R., Liu H., Lei H. and Li X. (2019). From
core-scale experiment to reservoir-scale modeling: A scale-up approach to
investigate reaction-induced permeability evolution of CO_2 storage reservoir
and caprock at a U.S. CO_2 storage site. Computers and Geosciences 125,
55-68.

Williams, S., T. Carlsen, K. Constable, & A. Guldahl (2009) Identification and
qualification of shale annular barriers using wireline logs during plug and
decommissioning operations. SPE paper 119321, 15 p.

Zang, W., (2013) Effect of modeling factors on the dissolution-diffusion-convection
process during CO2 geological storage in deep saline formations, Front.
Earth Sci. 2013, 7(2): 238–256 DOI 10.1007/s11707-013-0359-x.

16 Appendix A: compliance with EU Storage Directive site characterisation and assessment

This appendix presents the links between the site characterisation and assessment elements in the EU Storage Directive (EU, 2009) and the site characterisation elements of the P18-6 feasibility study. Annex I of the EU Storage Directive, used here as a reference, consists of three steps, each of which consists of a list of items. The Guidance Document #2 to the EU Storage Directive provides an explanation of all the list elements; this is not repeated here. The tables below are modified after the Site characterisation workflow in Appendix I of the SiteChar report D1.4 (Neele *et al.*, 2013).

16.1 Data collection (step 1)

	Storage Directive elements in step 1	Sections of the P18-6 feasibility study	Comments
(a)	Geology and geophysics	17 Appendix B	
(b)	Hydrogeology (in particular existence of ground water intended for consumption)	-	n.a.
(c)	Reservoir engineering (including volumetric calculations of pore volume for CO_2 injection and ultimate storage capacity)	17 Appendix B	
(d)	Geochemistry (dissolution rates, mineralisation rates)	-	Based on earlier studies
(e)	Geomechanics (permeability, fracture pressure)	17 Appendix B	
(f)	Seismicity	17 Appendix B	Related to fault stability in 12.3.3, 12.3.4
(g)	Presence and condition of natural and man-made pathways, including wells and boreholes which could provide leakage pathways	17 Appendix B	
(h)	Domains surrounding the storage complex that may be affected by the storage of CO_2 in the storage site	-	Based on earlier studies
(i)	Population distribution in the region overlying the storage site	-	n.a.
(j)	Proximity to valuable natural resources (including in particular Natura 2000 areas pursuant to Council Directive 79/409/EEC of 2 April 1979 on the conservation of wild birds(1) and Council Directive 92/43/EEC of 21 May 1992 on the conservation of natural habitats and of wild fauna and flora(2) ,	-	Addressed in EIA

	potable groundwater and hydrocarbons)		
(k)	Activities around the storage complex and possible interactions with these activities (for example, exploration, production and storage of hydrocarbons, geothermal use of aquifers and use of underground water reserves)	-	Addressed in EIA
(l)	Proximity to the potential CO_2 source(s) (including estimates of the total potential mass of CO_2 economically available for storage) and adequate transport networks	-	Not known at time of study; assumptions provided by client

16.2   Building the 3-D static geological earth model (step 2)

	Storage Directive elements in step 2	Sections of the P18-6 feasibility study	Comments
(a)	Geological structure of the physical trap	4.2, Appendix B: 17.1-17.5	
(b)	Geomechanical, geochemical and flow properties of the reservoir overburden (caprock, seals, porous and permeable horizons) and surrounding formations	4.1, 4.2, 4,4, 8.2, 8.3 Appendix B: 17.4	Geochemical properties based on earlier work
(c)	Fracture system characterisation and presence of any human-made pathways	4.2, 4.5, 9 Appendix B: 17.4	
(d)	Areal and vertical extent of the storage complex	10	
(e)	Pore space volume (including porosity distribution)	Appendix B: 17.4.3-17.4.5	
(f)	Baseline fluid distribution	Appendix B: 17.7	
(g)	Any other relevant characteristics	Appendix B: 17.6.5, 17.7.2, 17.7.3, 17.7.6	Gas production data, PVT, RFT and PLT data
(all)	The uncertainty associated with each of the parameters used to build the model shall be assessed by developing a range of scenarios for each parameter and calculating the appropriate confidence limits. Any uncertainty associated with the model itself shall also be assessed.	6.3.5 6.3.6 6.5.4 9.3 17.7.5	Fault sealing, salt precipitation, mineral assemblage, cement bonding, well cross flow

16.3 Characterisation of storage dynamic behaviour, sensitivity characterisation, risk assessment (step 3)

Step 3 consists of several parts, which are discussed separately.

16.3.1 Characterisation of the storage dynamic behaviour (step 3.1)

	Storage Directive elements in step 3, characterisation of the storage dynamic behaviour	Sections of the P18-6 feasibility study	Comments
(a)	Possible injection rates and CO_2 stream properties	5.2, 5.3, 6.2	
(b)	Efficacy of coupled process modelling (that is, the way various single effects in the simulator(s) interact)	6.3, 6.4 7.2, 7.3, 8.2, 8.3, 9.3	Thermohydraulic Thermomechanical
(c)	Reactive processes (that is, the way reactions of the injected CO_2 with in situ minerals feedback in the model)	6.5, 7.4, 9.3	
(d)	Reservoir simulator used (multiple simulations may be required in order to validate certain findings)	6.3.3, 6.4.2	
(e)	Short and long-term simulations (to establish CO_2 fate and behaviour over decades and millennia, including the rate of dissolution of CO_2 in water)	6.3 6.5	Short term Long term geochem.

16.3.2 Insights from dynamic modelling (step 3.1)

	Storage Directive elements in step 3, insights from dynamic modelling	Sections of the P18-6 feasibility study	Comments
(f)	Pressure and temperature of the storage formation as a function of injection rate and accumulative injection amount over time	6.3, 6.4	
(g)	Areal and vertical extent of CO_2 vs time	6.3	
(h)	Nature of CO_2 flow in the reservoir, including phase behaviour	6.3, 6.4	
(i)	CO_2 trapping mechanisms and rates (including spill points and lateral and vertical seals)	4, 6.3, 10	
(j)	Secondary containment systems in the overall storage complex	10, 11	
(k)	Storage capacity and pressure gradients in the storage site	6.3, 6.4	
(l)	Risk of fracturing the storage formation(s) and caprock	7.2, 7.3, 8.2, 8.3, 12.2, 12.3	
(m)	Risk of CO_2 entry into the caprock	4.3, 8.3, 8.4, 12.2	

	Storage Directive elements in step 3, insights from dynamic modelling	Sections of the P18-6 feasibility study	Comments
(n)	Risk of leakage from the storage site (for example, through decommissioned or inadequately sealed wells)	12	
(o)	Rate of migration (in open-ended reservoirs)	11, 12.1	
(p)	Fracture sealing rates[11]	12.3.2	Qualitative; no rates
(q)	Changes in formation(s) fluid chemistry and subsequent reactions (for example, pH change, mineral formation) and inclusion of reactive modelling to assess affects	6.5, 7.4, 8.4, 9.3.4	
(r)	Displacement of formation fluids	-	
(s)	Increased seismicity and elevation at surface level	7	

16.3.3 Sensitivity characterisation (step 3.2)

This element of the EU Storage Directive reads: "*Multiple simulations shall be undertaken to identify the sensitivity of the assessment to assumptions made about particular parameters. The simulations shall be based on altering parameters in the static geological earth model(s), and changing rate functions and assumptions in the dynamic modelling exercise. Any significant sensitivity shall be taken into account in the risk assessment.*"

Sections of the P18-6 feasibility study: 6.3.5, 6.3.6, 6.3.5, 8.4.2

Comments: Sensitivity to temperature, injection rate, mineral types

16.3.4 Risk assessment: hazard characterisation (step 3.3.1)

This element of the SDEU reads: "*The hazard characterisation shall cover the full range of potential operating conditions to test the security of the storage complex. Hazard characterisation shall be undertaken by characterising the potential for leakage from the storage complex, as established through dynamic modelling and security characterisation described above. This shall include consideration of* [the items in the table below]. *The hazard characterisation shall cover the full range of potential operating conditions to test the security of the storage complex."*

	Elements of Storage Directive Risk assessment: hazard characterisation (step 3.3.1)	Sections of the P18-6 feasibility study	Comments
(a)	potential leakage pathways	9, 11, 12	
(b)	potential magnitude of leakage events for identified leakage pathways (flux rates)	7.4.4	Mostly qualitative

---

[11] The EU Guidance Document #2 does not offer an explanation as to the meaning of 'fracture sealing rates'. Here, fracture sealing is assumed to be a combination of chemical reactions (resulting in mineral deposition in injection-induced fractures) and geomechanical processes (resulting in fractures closing).

	Elements of Storage Directive Risk assessment: hazard characterisation (step 3.3.1)	Sections of the P18-6 feasibility study	Comments
(c)	critical parameters affecting potential leakage (for example maximum reservoir pressure, maximum injection rate, temperature, sensitivity to various assumptions in the static geological Earth model(s))	12	
(d)	secondary effects of storage of CO_2, including displaced formation fluids and new substances created by the storing of CO_2	6.5, 7.4, 8.4	New substances
(e)	any other factors which could pose a hazard to human health or the environment (for example physical structures associated with the project)	-	n.a.

16.3.5   *Risk assessment: exposure assessment (step 3.3.2)*
This element of the SDEU reads: "*Based on the characteristics of the environment and the distribution and activities of the human population above the storage complex, and the potential behaviour and fate of leaking CO2 from potential pathways identified under Step 3.3.1.*"

The site characterization study will yield probability density functions for CO_2 fluxes, times… as deemed necessary by experts in HSE research and industrial safety. See 4.10 for details.

Sections of the P18-6 feasibility study: -

Comments: Not in scope of present study

16.3.6   *Risk assessment: effects characterisation (step 3.3.3)*
This element of the SDEU reads: "*Based on the sensitivity of particular species, communities or habitats linked to potential leakage events identified under Step 3.3.1. Where relevant it shall include effects of exposure to elevated CO2 concentrations in the biosphere (including soils, marine sediments and benthic waters (asphyxiation; hypercapnia) and reduced pH in those environments as a consequence of leaking CO2). It shall also include an assessment of the effects of other substances that may be present in leaking CO2 streams (either impurities present in the injection stream or new substances formed through storage of CO2). These effects shall be considered at a range of temporal and spatial scales, and linked to a range of different magnitudes of leakage events.*"

Sections of the P18-6 feasibility study: -

Comments: Not in scope of present study

16.3.7   *Risk assessment: risk characterisation (step 3.3.4)*
This element of the EU Storage Directive reads: "*This shall comprise an assessment of the safety and integrity of the site in the short and long term, including an assessment of the risk of leakage under the proposed conditions of use, and of the worst-case environment and health impacts. The risk characterisation shall be conducted based on the hazard, exposure and effects assessment. It shall include an assessment of the sources of uncertainty identified during the steps of characterisation and assessment of storage site and when feasible, a description of the possibilities to reduce uncertainty.*"

The site characterization study will yield probability density functions for CO_2 fluxes, times, as deemed necessary by experts in HSE research and industrial safety. See 4.10 for details.

Sections of the P18-6 feasibility study: Section 12

Comments: Directed to characterisation of subsurface hazards

17 Appendix B. Subsurface model descriptions

17.1 Static model

17.1.1 New geological model – reasons

Since the completion of the storage feasibility assessment for the P18-4 field (Vandeweijer et al., 2011) , which produced a 3D reservoir model of all P18 fields, a number of developments necessitated the building of a new 3D reservoir model. Around 2014, the operators and co-owners of the P15-P18 blocks had the P15-P18 3D seismic survey reprocessed. A pre-stack, depth migrated (PSDM) version of the cube was now available, both in time and depth, as well as a velocity cube. An initial comparison of the Top Bunter interpreted from that cube with the one from the P18-4 study (Vandeweijer et al., 2011) revealed several important differences, enough to justify a new seismic interpretation, as well as a new geological reservoir model.

It was therefore decided to build a new reservoir model, based on a seismic interpretation on the new, reprocessed 3D cube.

17.2 Seismic interpretation

A substantial part of the Top Bunter and Top Keuper had already been interpreted by TAQA. Only a few blank areas needed to be done. After a review of the TAQA horizon and fault interpretations, the remaining uninterpreted areas of the reprocessed cube were interpreted. This was mostly the southeastern tip of the P18-2 field and P18-6 in its entirety (Figure 17-1).
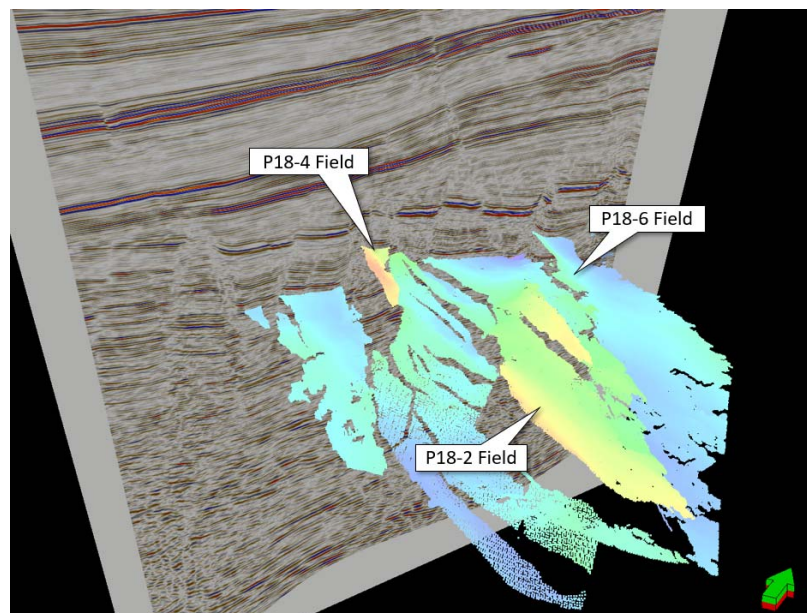

Figure 17-1 Oblique view on seismic interpretation of Top Bunter on the reprocessed P15-P18 3D cube.

Faults interpreted by TAQA were inspected and generally found to agree with the seismic data, although in some instances modifications were made on some of the faults. The P18-6 faults were completely newly interpreted (Figure 17-2). None of the P18-6 boundary faults extends upward to the Base Cretaceous Unconformity.
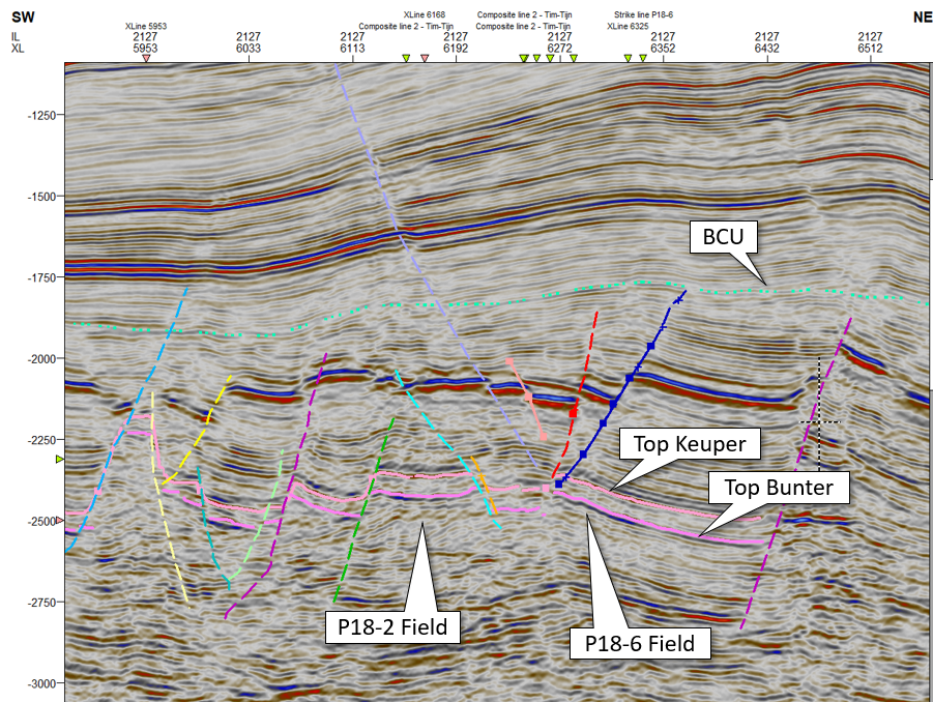

Figure 17-2: Seismic inline 2127 showing the top Bunter (purple horizon), Top Keuper (pink), and Base Cretaceous Unconformity (light green). Note that P18-6 Boundary Fault 400 (dark blue) does not extend upward into the Base Cretaceous Unconformity (BCU).

17.3 Time-depth conversion

After consulting TAQA, it was found that the reprocessed P15-P18 cube came with a strongly improved velocity cube. It was therefore decided to adopt TAQA's velocity model which for the current project only contains two horizons: Top Keuper and Top Bunter (Table 17-1). In contrast to the velocity model that was used in the 2011 CATO study which was based on VELMOD and used six horizons, in the present model the entire overburden velocities above the Triassic are taken from the velocity cube (TAQA, 2018). For the Upper Germanic Trias Group itself a constant velocity of 4568 m/s was applied.

Table 17-1: Velocity model from TAQA as used in the current study

Interval	Top	Base	TZ conversion method
Overburden	MSL	Top Keuper	PSDM velocities
Upper Triassic	Top Keuper	Top Hardegsen	Constant velocity: 4568 m/s
LowerTr.–Perm.	Top Hardegsen	Top Carboniferous	Constant velocity: 4694 m/s

17.4   Petrel model building

Although initially a model was populated with porosity, permeability, and water saturation from upscaled logs, during the history matching process it became apparent that the reservoir properties away from well P18-A-07-S1 needed major changes in order to match produced volumes, rates, and pressures (see below). Therefore, only the values at the well position were retained in the reservoir simulation model. Since the original static property model was not used for the final model, only the properties resulting from the history match are described here.

17.4.1 Fault model, gridding

The P18-6 Field consists of a NW-SE elongated, tilted fault block. It is bounded to the SW by a large-offset fault (Fault 400 and 430) and on the SE by a smaller, transverse fault (Fault 500). All in all, it is a straightforward structure, and no difficulties were encountered during the gridding process.

Figure 17-3 shows the end result of the fault construction and pillar gridding process. Names of the faults used in the current model are also shown in Figure 17-3. For the pillar gridding (Figure 17-4) an average X and Y increment of 50 m was specified.
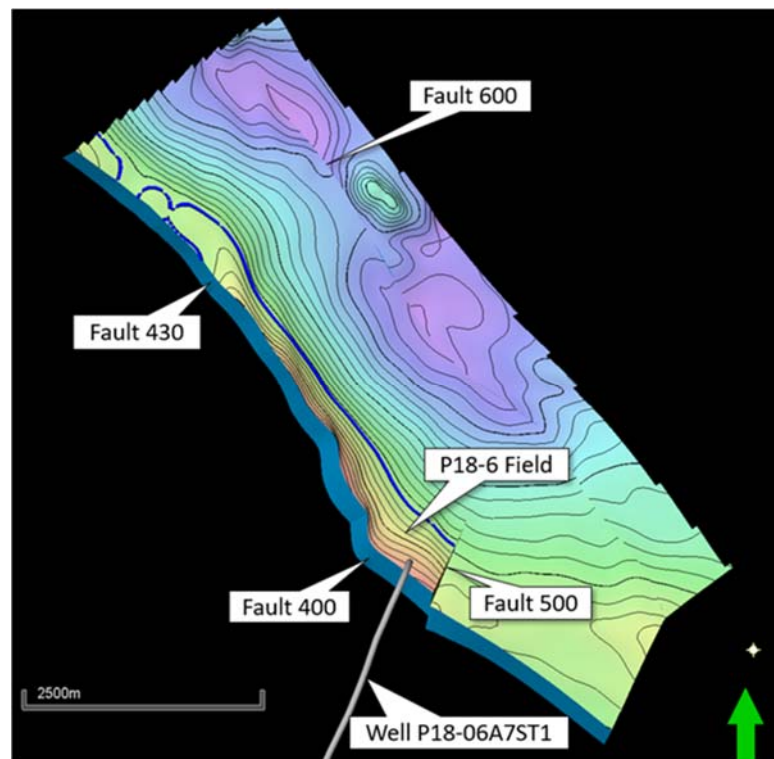

Figure 17-3: Map view of all faults that have been incorporated in the pillar grid of the P18-6 Petrel reservoir model.
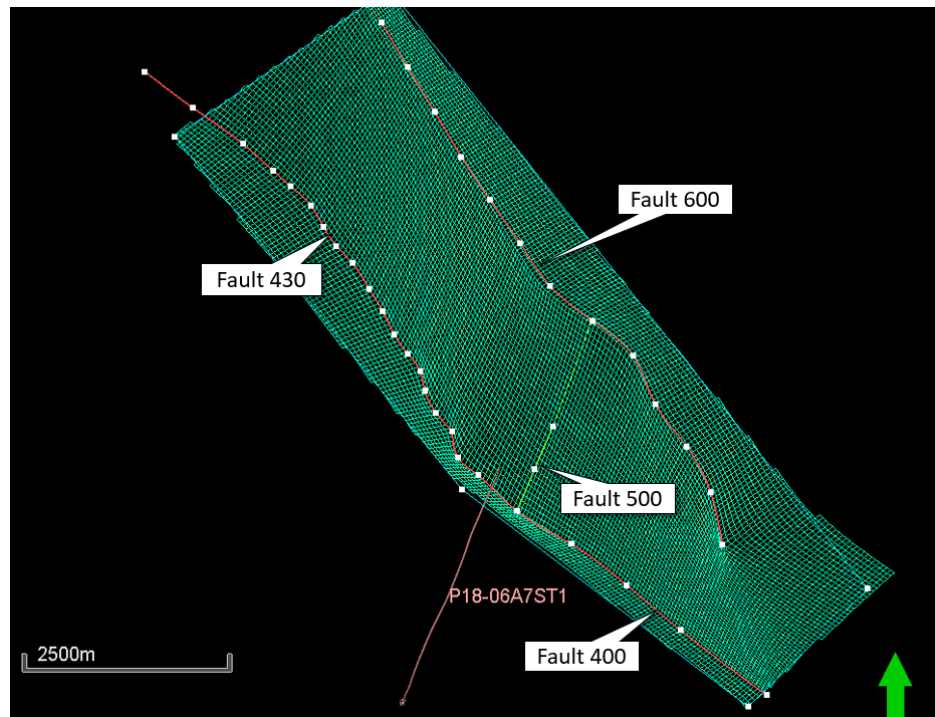
Figure 17-4: Map view of all faults and trends used in the pillar gridding, and the resulting grid.

17.4.2 Make Horizons / Make Zones

The new model has a different approach towards the construction of the reservoir formations compared to the P18 model from 2011. In the previous model, all Lower Triassic formation tops had a separate horizon as input in the 'Make Horizons' process. In combination with the many faults this led to geometrical problems such as rapidly thinning and thickening formations. The current model utilises only one horizon for the reservoir formations (Top Bunter; Figure 17-5).

The 2011 P18 model subdivision into formations was maintained, from top to base: Hardegsen, Upper Detfurth, Lower Detfurth, and Volpriehausen Formation.
The rest of the horizons were created using isopachs (Figure 17-6, Figure 17-7, Figure 17-8). The result is a smooth reservoir model where formation thickness changes across the field are kept to a minimum.
The layering was done as follows: Hardegsen 20, Upper Detfurth 5, Lower Detfurth 5, and Volpriehausen 3 layers. All layers were assigned the type 'proportional'.
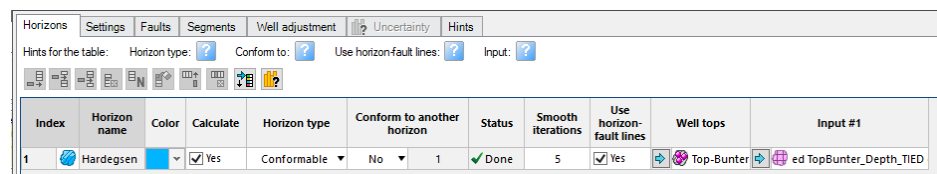
Figure 17-5: Dialog box of the 'Make Horizons' process of the Petrel reservoir model.
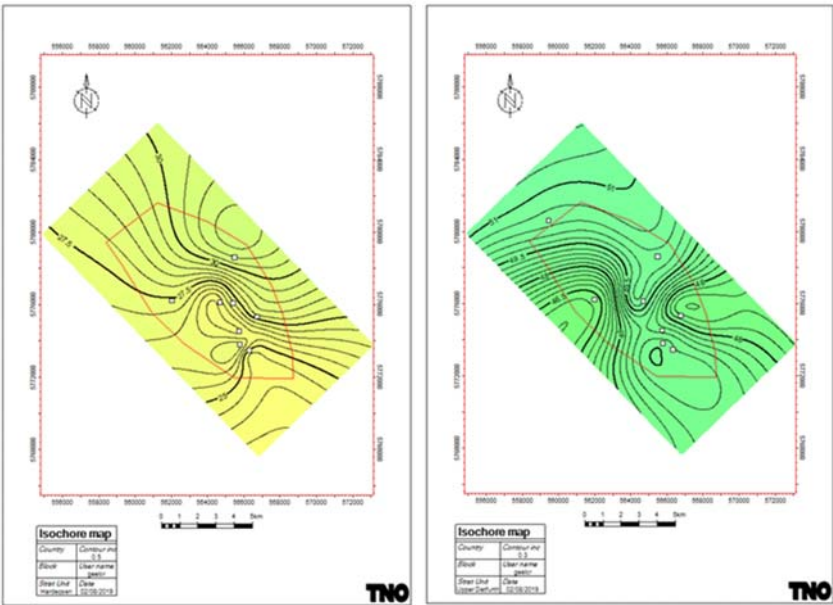
Figure 17-6: Isochore maps of the Hardegsen Fm (left) and the Upper Detfurth Fm (right). Well values on which the isochore maps are based are shown as white squares.
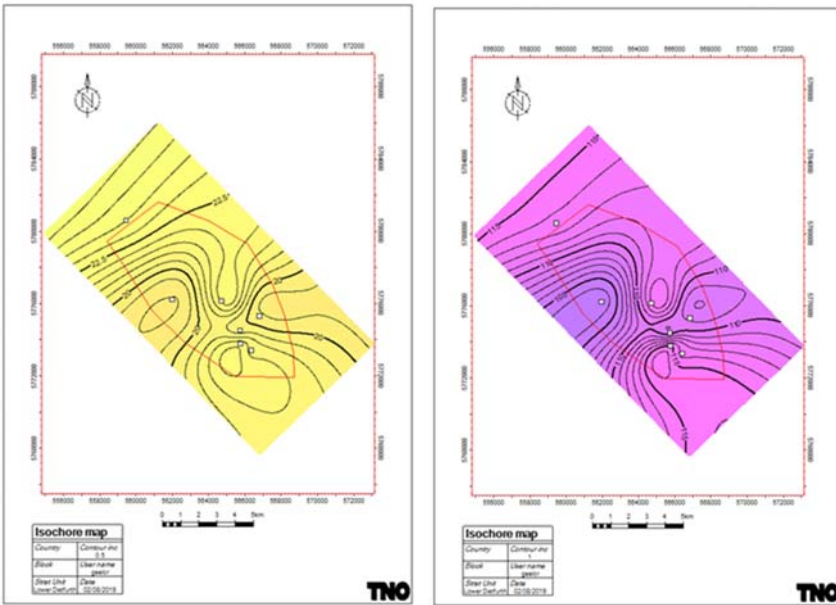
Figure 17-7: Isochore maps of the Lower Detfurth Fm (left) and the Volpriehausen Fm (right). Well values on which the isochore maps are based are shown as white squares.
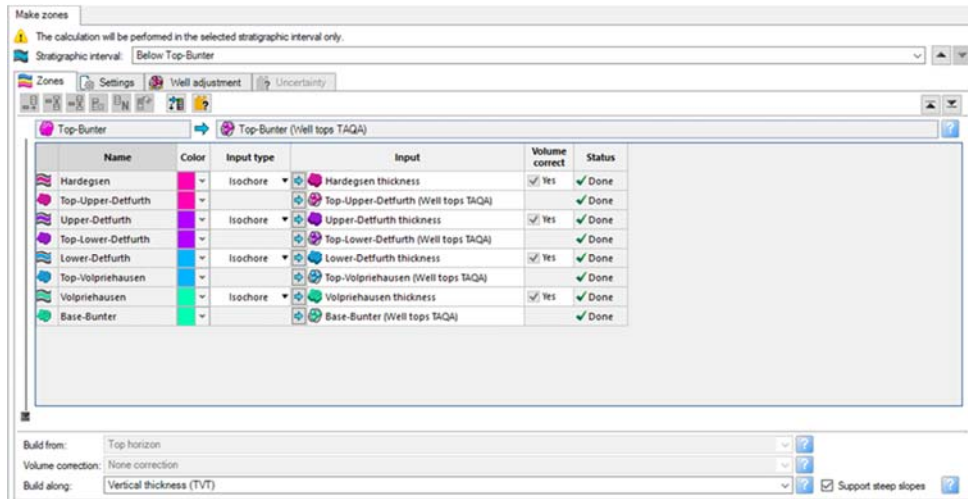
Figure 17-8: Creation of the various reservoir zones in the Petrel reservoir model.

17.4.3 Reservoir properties

A detailed petrophysical study on the P15-P18 area was done by BP (2007). Relationships between porosity and permeability in this study were established on the basis of rock types (lithofacies). The origin of these rock types is not readily apparent from this study but seems to have been generated by the Baker Hughes "Horizon" software package (see Ames & Farfan, 1996). On the basis of well log readings, this software package classifies depth intervals into rock types that have been calibrated against lithofacies from core descriptions.

For the P18 area these rocktypes are:
− Rock Type 1: Eolian Dune
− Rock Type 2: Interdune
− Rock Type 3: Eolian Dolomitic
− Rock Type 4: Shales

For each of these rock types a separate porosity-permeability relation has been established (BP, 2007).
− Rock Type 1: Kcalc = 10^ (-3.3+0.58* PHIcalc - 0.01229(PHIcalc)**2)
− Rock Type 2: Kcalc = 10^ (-2.75+0.464* PHIcalc - 0.011(PHIcalc)**2)
− Rock Type 3: Kcalc = 10^ (-3.003+0.358* PHIcalc - 0.0068(PHIcalc)**2)
− Rock Type 4: Kcalc = 0.01
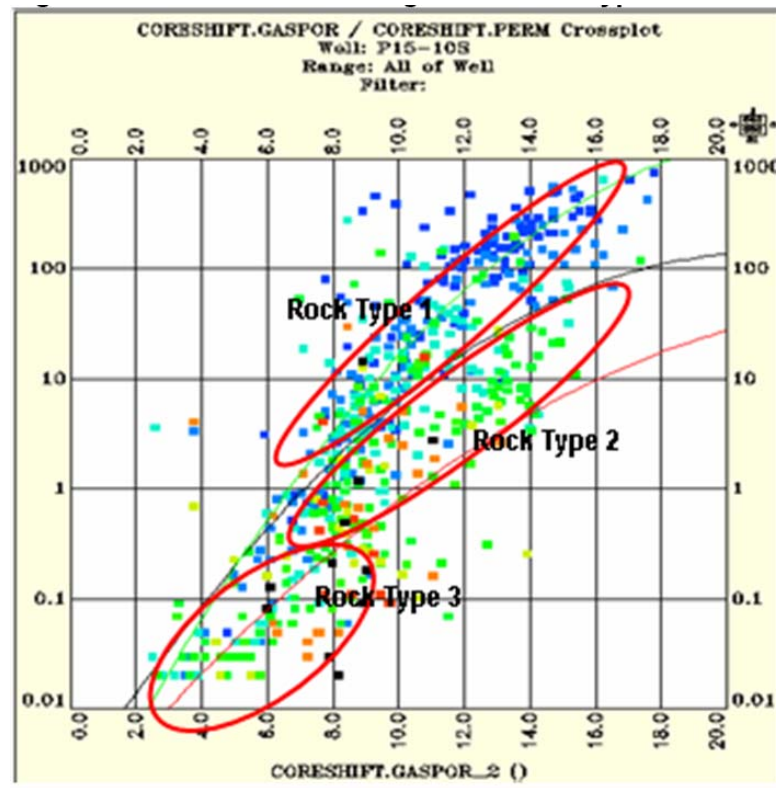
Figure 17-9: Relationship between porosity and permeability for three rock types (lithofacies): 1 = Aeolian Dune, 2 = Interdune, 3= Aeolian Dolomitic. Not shown in this graph is rock type 4 = shales. From BP (2007).

For the P18-6 field, because the rock type distribution was not present and for simplicity (see also "modelling of reservoir properties") a single relation between porosity and permeability was used, which is based on the BP relations (see Figure 17-10). The final relationship was adjusted during the history match (PHIE in %):

$$Kcalc = 10^{\wedge} (-3.5+0.57* PHIE - 0.0129(PHIE)**2)$$

In the P18-2 field, two field-wide no-flow boundaries or baffles were identified, between Upper and Lower Detfurth Fm, and between Lower Detfurth and Volpriehausen (Figure 17-11). It is assumed that these also exist in P18-6 and again these were implemented in the ECLIPSE reservoir model by using transmissibility multipliers between the lowermost layer of Upper Detfurth and uppermost layer of Lower Detfurth, and between the lowermost layer of Lower Detfurth and uppermost layer of Volpriehausen Fm. Also a barrier was identified between the Hardegsen Fm and the Upper Detfurth. The value of this barrier was set in the history match
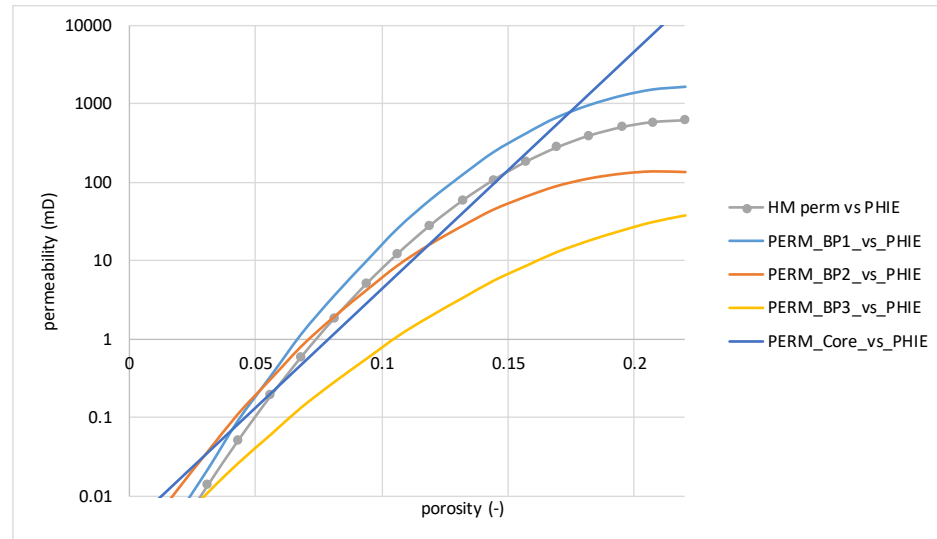
Figure 17-10: Relationship between porosity and permeability used in the history match (HM perm) and for comparison the relationships for the three rock types (lithofacies from BP) on which the used relationship is based.
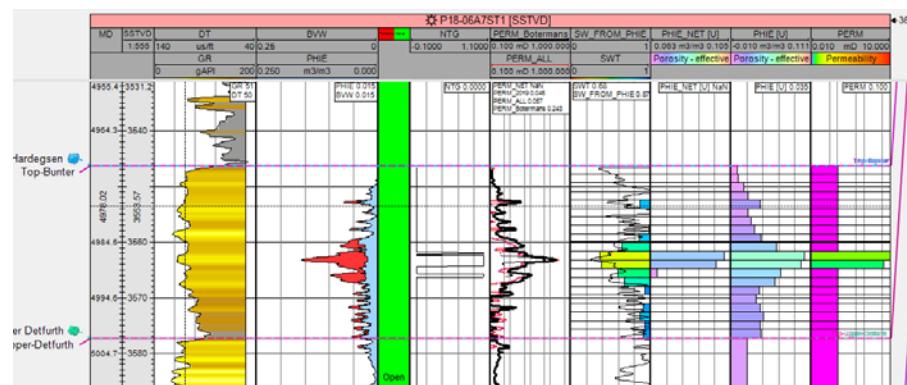
Figure 17-11: Well P18-06-A7 showing the presence of a barrier between the Hardegsen and Upper Detfurth Fm.

17.4.4 Modelling of reservoir properties

For the P18-6 model, for the distribution of the reservoir properties a different approach was used, because:

- The properties observed at P18-A-07-S1 are not representative for the rest of the field, because the observed GIP is far larger than can be expected based on the porosity from the well log.
- The field has only a single well.

Therefore a simplified model approach is chosen in which properties are defined homogeneous per layer (layer-cake model). The layering is based on the upscaled well log and different zones. The advantage of this approach is that a good history match to the dynamic data can be achieved. The disadvantage is that sharp boundaries are implemented that might not be realistic.

Three zones were identified:
− a near well zone with poor properties, which were based on the upscaled well log.
− the gas field which has much better properties than the near-well zone. It is assumed that the high-perm layer present in the well extends also in the gas field.
− the aquifer which has very poor properties. Although the well is drilled close to the aquifer, no significant water production has been observed, indicating low mobility of water in the aquifer. In view of the substantial depth of the aquifer (>3680 m), a reduced permeability is expected due to autigenic illite growth (Van Hulten, 2006).

The properties and distribution of the zones was also part of the history match and will in part be discussed there.
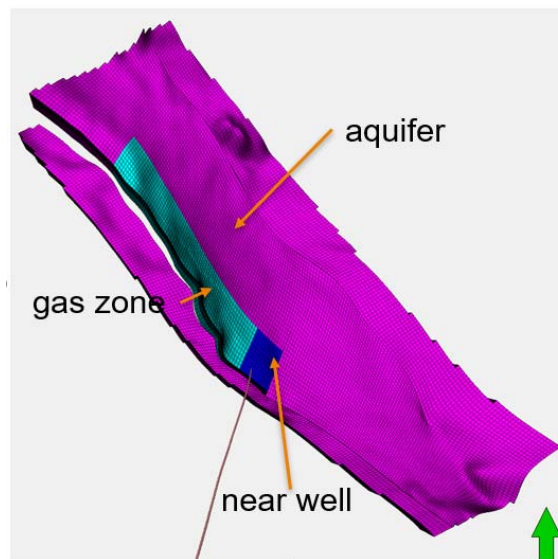
Figure 17-12: distribution of the three zones defined in the P18-6 model.

The log of PHIE (effective porosity) was arithmetically upscaled to the grid resolution of the dynamic model. Figure 17-13 shows the histograms of the upscaled porosity. The upscaled porosity was used for the porosity in the near-well zone (see Table 17-2 for the details). Because the high porosity values were lost due to upscaling, the highest porosity layer (layer 11) was increased to 0.15.

(a)

(b)
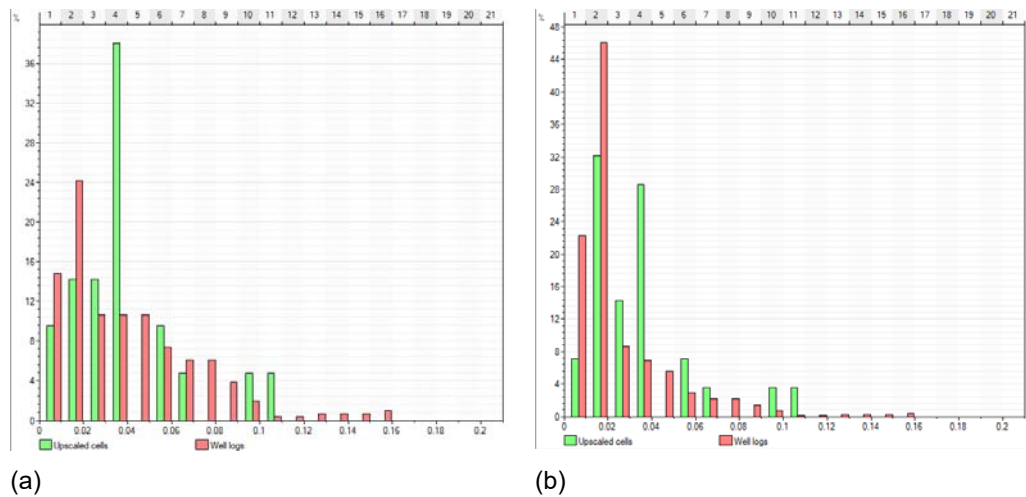
Figure 17-13: Comparison of the distributions of effective porosity (PHIE) in well log and upscaled well log for Hardegsen Fm (a) and the entire well (b).

Table 17-2. Porosity in the different layers and zones (Figure 17-12) of the reservoir model of P18-6.

Model layer	Formation	Por near well	Por gas zone	Por aquifer
1-4	Hardegsen	0.023	0.14	0.07
5-9	Hardegsen	0.023	0.07	0.07
10	Hardegsen	0.059	0.2	0.07
11	Hardegsen	0.15	0.2	0.07
12	Hardegsen	0.097	0.2	0.07
13	Hardegsen	0.066	0.2	0.07
14	Hardegsen	0.057	0.2	0.07
15-20	Hardegsen	0.023	0.07	0.07
21	Upper Detfurth	0.015	0.07	0.07
22-23	Upper Detfurth	0.015	0.12	0.07
24-25	Upper Detfurth	0.015	0.07	0.07
25-33	Lower Detfurth + Volpriehausen	0.015	0.06	0.06

In order to compare the static gas in place with the dynamic gas in place, it is necessary to calculate the water saturation in the field. A Lambda saturation-height function was developed by matching the water saturation logs from resistivity logs with a water saturation log calculated from porosity and height above free water level. The best match yielded the following Lambda saturation-height function (Figure 17-14):

$$Sw = 0.001 + 2.8\, HAFWL^{-2.9\, Phie - 0.14} \qquad (17\text{-}1)$$
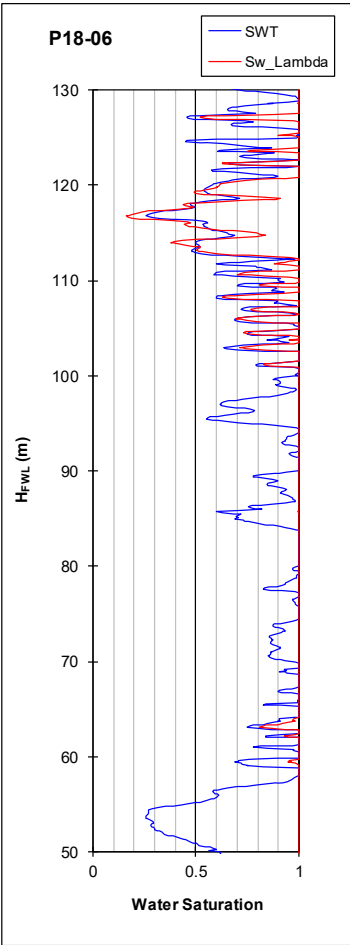
Figure 17-14: Comparison of log-derived water saturation (STW; blue line) and water saturation calculated with a saturation-height function (SW_Lambda; red line).

17.4.5 GIIP

The actual volumetrics are done during the ECLIPSE history match, but to see whether the geometry and properties of the reservoir model are sufficiently close, the GIIP was calculated. GIIP was calculated without cutoffs on PHIE or VSH, so with a Net to Gross of 1.0, The gas expansion factor Bg was set to 0.0040. The GIIP is only calculated for segment 3 in Figure 17-15, which is the only segment which contains gas.

Table 17-3: Result of static GIIP calculations for P18-6 for segment 3 (Figure 17-15).

Formation	HC pore volume [M rm^3]	GIIP [M sm3]
Hardegsen	2.090	522
Upper Detfurth	1.120	280
Lower Detfurth	0.106	26
Volpriehausen	0.006	2
Total	3.322	831
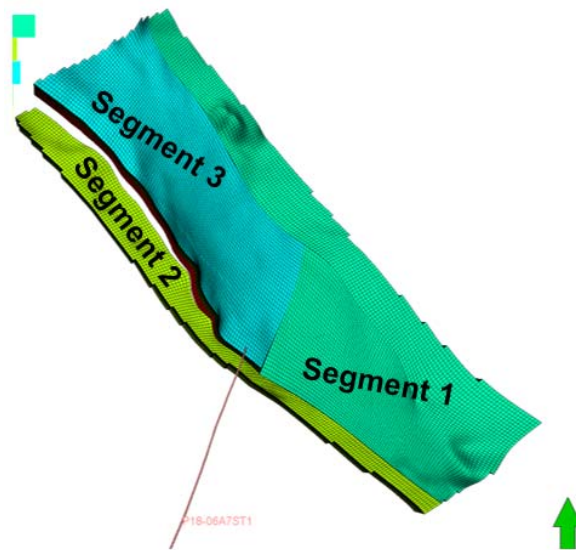
Figure 17-15: Definition of segments for the GIIP calculation.
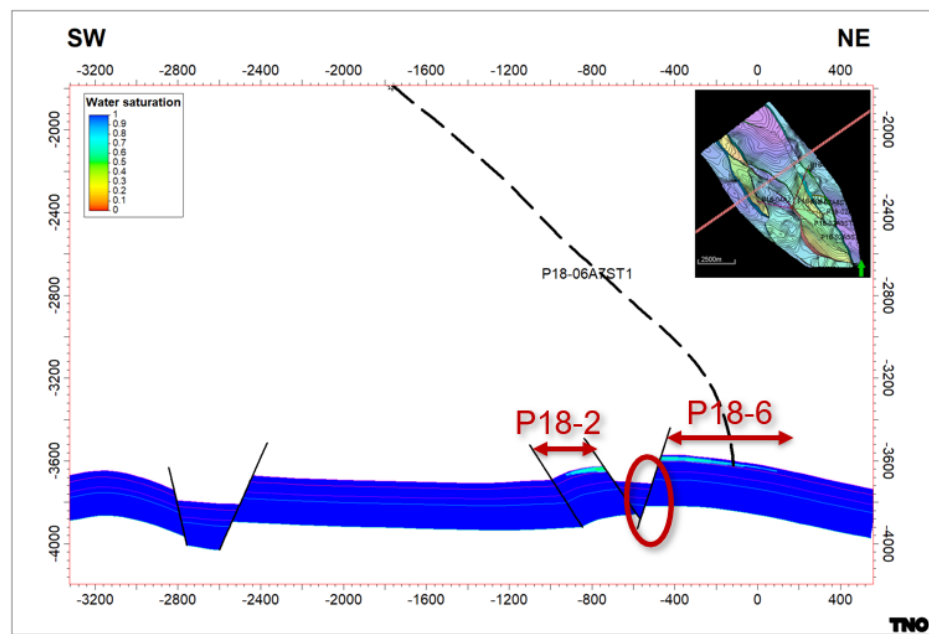
Figure 17-16: Model cross-section through P18-6 and P18-2 showing the original water saturation in the two accumulations. Note that Volpriehausen Fm in P18-6 is juxtaposed against Hardegsen and Detfurth Fm in P18-2.
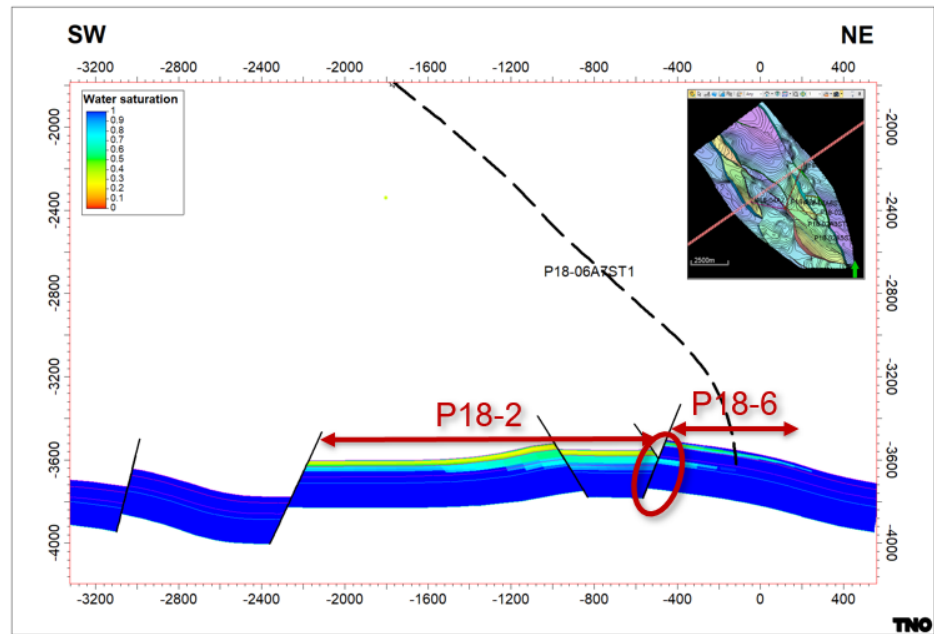
Figure 17-17: Model cross-section through P18-6 and P18-2 showing the original water saturation in the two accumulations. Note that Lower Detfurth in P18-6 is juxtaposed against Upper Detfurth in P18-2, and Hardegsen in P18-6 is juxtaposed against Upper Triassic seal in P18-2.
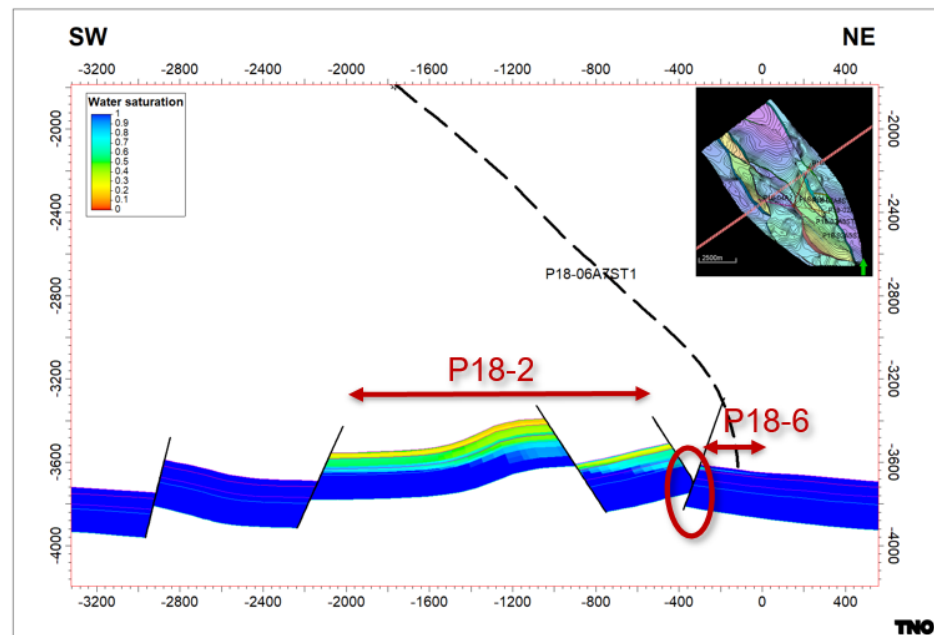
Figure 17-18: Model cross-section through P18-6 and P18-2 showing the original water saturation in the two accumulations. Bunter in P18-6 is juxtaposed against Upper Triassic seal, or Volpriehausen.

17.5 Adjustments made to the static model

In the geological model, the fault on the eastern side of the model (Fault 600) is not extended to the boundaries of the model area. Therefore in the north part of the model, the fault is extended in the reservoir model using pore volume multipliers. The southern part of the model is removed, to make sure that the faults extend to the boundaries of the model and because the erroneously high elevations cause gas accumulations in the aquifer which are not real.
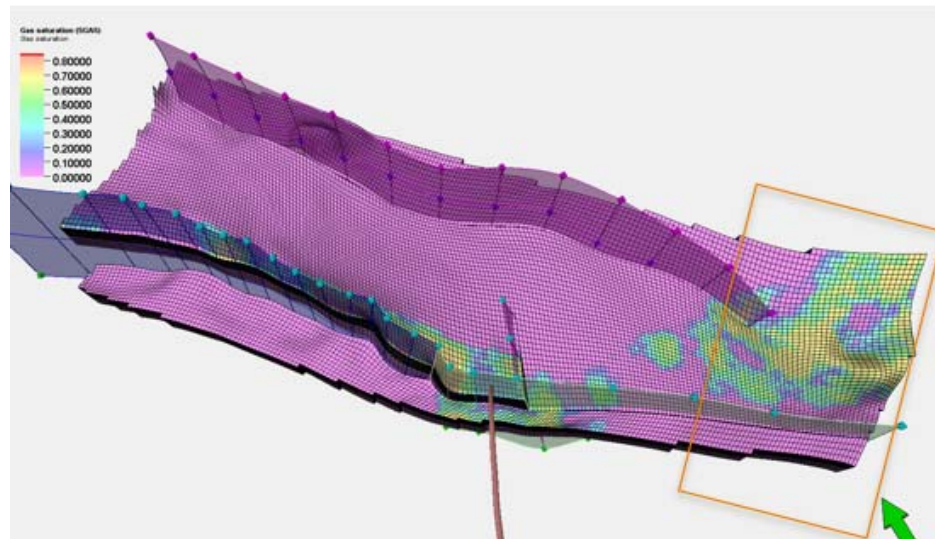
Figure 17-19: Geological model with initial gas saturation. Orange frame indicates the part of the model that is removed.

17.6 Dynamic model

17.6.1 Reservoir simulator

For the dynamic modelling Eclipse 300 was used. Alternatives were to use the Eclipse 100 simulator or the Shell proprietary reservoir simulator MoReS. The compositional Eclipse simulator was used for the following reasons:

- A black oil simulator cannot handle gas to gas interactions, which is needed for CO_2 injection into a gas (methane) reservoir.
- MoReS was used for P18-2 and P18-4 modelling in a previous study (Vandeweijer et al (2011). Since that study, the workflow Petrel-Eclipse-Macris has been developed and is considered to be state of the art.

17.6.2 Data

For any dynamic reservoir simulation, including Eclipse, the following sets of data are required:

- General run data: grid dimensions, phases present, components present.
- Grid geometry data: specification of geometry of computational grid (location of grid block corners).
- Reservoir rock properties: porosity, net-to-gross, absolute permeability in each grid block.
- PVT data: properties of reservoir and stock tank fluids such as density, viscosity and saturation pressure.

- Saturation and pressure dependent rock properties: relative permeabilities and capillary pressures as function of phase saturations, and rock compressibility.
- Initial conditions in the reservoir: pressure, temperature, phase saturations and phase compositions.
- Regions: specification of regions that splits the computational grid into regions for calculation of PVT properties, saturation properties, initial conditions, and fluids in place.
- Operations data: specification of the wells (location, productivity index, etc.) and the operations to be simulated (production and injection controls and constraints).

These data describe the dynamic characteristics of the P18-6 reservoir. Each of these sets of data will be discussed in the following sections

17.6.3　General simulation data

As mentioned in section 17.6.1 the Eclipse 300 simulator is used with two reservoir fluid phases namely water and gas, and five components in the gas phase namely N_2, CO_2, C_1, C_2, C_{3P}.

As explained in Section 17.4, the geological grid was not upscaled to the dynamic 2019 model, however directly from the logs a new dynamic grid was generated. Table 17-4 below gives an overview of the grid dimensions. The size of the grid blocks do vary in size in each individual direction but are in the order of 50x50 m (XY). The layer thickness changes per formation: ~1.2 m for Hardegsen, ~8 m for Detfurth and ~37 m for Volpriehausen.

Table 17-4 – Overview of grid dimensions in the geological model and in the simulation model.

	Number grid blocks x-direction NX	Number grid blocks y-direction NY	Number grid blocks z-direction NZ	Total number of grid blocks	Number active grid blocks
Simulation grid model	63	197	33	409563	300135

17.6.4　Reservoir Rock properties

This was described in Section 17.4.3.

17.6.5　PVT data

17.6.5.1　Gas PVT data

An equation of state is generated for Eclipse 300 with the composition at 1 m depth listed in Table 17-5. The same values were used as in P18-2.

Table 17-5 – Overview of composition at 1 m depth (mole fractions).

	Composition
N_2	0.01508
CO_2	0.01288
C_1	0.8765
C_2	0.02376
C_{3P}	0.0718

17.6.5.2 Water PVT data

The water formation volume factor is 1.0223 rm³/Sm³ at a reference pressure of 215 bar. The water compressibility is $4.1483 \cdot 10^{-5}$/bar and water viscosity is 0.32929 cP, also at reference pressure of 215 bar.

17.6.6 Saturation and pressure dependent rock properties

Relative permeability and capillary pressure (Special Core Analysis - SCAL - data) are not available for P18 field. In this study the final parameters used to described the individual curves are described in Table 17-6 and Figure 17-20 and were part of the history match study. Mobility of water was reduced considerably compared to the values used for P18-2, because otherwise well P18-6-A07 produced water prematurely.

The most used description of the relative permeability curves is the Corey parametrization according to equation

$$k_{r,i}\left(S_i\right) = k_{r,end,i}\left(\frac{(S_i - S_{irr,i})}{(1 - S_{irr,i} - S_{irr,j})}\right)^{n_i} \qquad (17\text{-}2)$$

where
$k_{r,i}$ = relative permeability of phase i
$k_{r,end,i}$ = end-point relative permeability of phase i
S_i = saturation of phase i
$S_{irr,i}$ = irreducible or connate saturation of phase i
n_i = Corey exponent for phase i

The values used to describe the relative permeabilities are listed in Table 17-6.

Table 17-6 – Parameters for calculation of gas-water relative permeabilities

Parameter	Description	Value used in dynamic model
S_{wc}	Connate water saturation (Hardegsen/Detfurth + Volpriehausen)	0.10/0.25
S_{grw}	Residual gas saturation in gas/water system	0.05
$n_{w,}$	Corey exponent for water	4
n_o	Corey exponent for gas	1.5
k_{rwor}	Water end-point relative permeability	0.05
k_{rgcw}	Gas end-point relative permeability	1
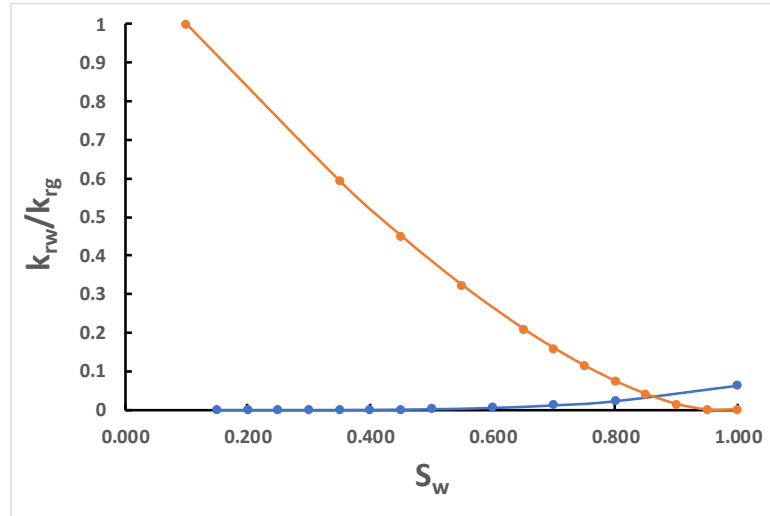
Figure 17-20: Relative permeabilities used in the P18-6 study.

The capillary pressure curves were based on a Leverett J-function corresponding to equation (17-3). The J-function itself was based on the saturation-height functions in Section 17.4.4. P_c was calculated based on HAFWL and the phase densities. The J-function values (shown in Figure 17-21) were calculated based on the following equation:

$$J(S_w) = \frac{P_c \times \sqrt{\frac{k}{\varphi}}}{\sigma U_c} \qquad (17\text{-}3)$$

Where
P_c = capillary pressure [bar]
σ   = surface tension [dyne/cm] (water gas) set to 72 dynes/cm (is 72 milli N/m) (typical value for water gas system, petrowiki)
U_c = constant (0.318316 for the given units, Eclipse reference manual)
φ   = porosity [-]
k   = permeability [mD]

A function was fitted to the cross-plotted values of J and Sw (Figure 17-21) to parametrize the J-function used in Eclipse (Eq. (17-3.):
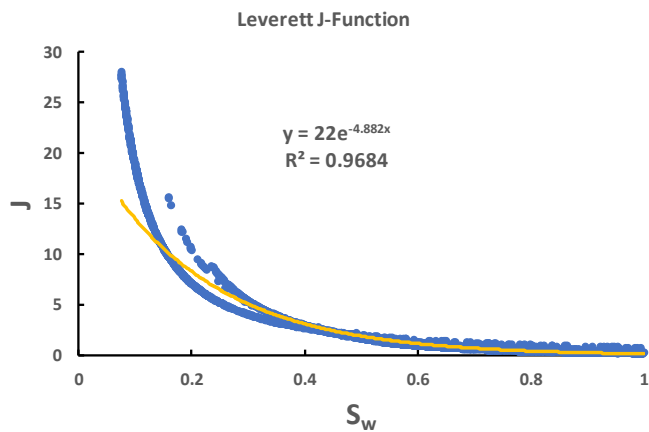
Figure 17-21: The J-function used (orange line) and the saturations of the P18 reservoir (blue dots).

After initialisation with these saturation functions the modelled water/gas saturations were compared to the total water saturations based on the logs (Figure 17-22).
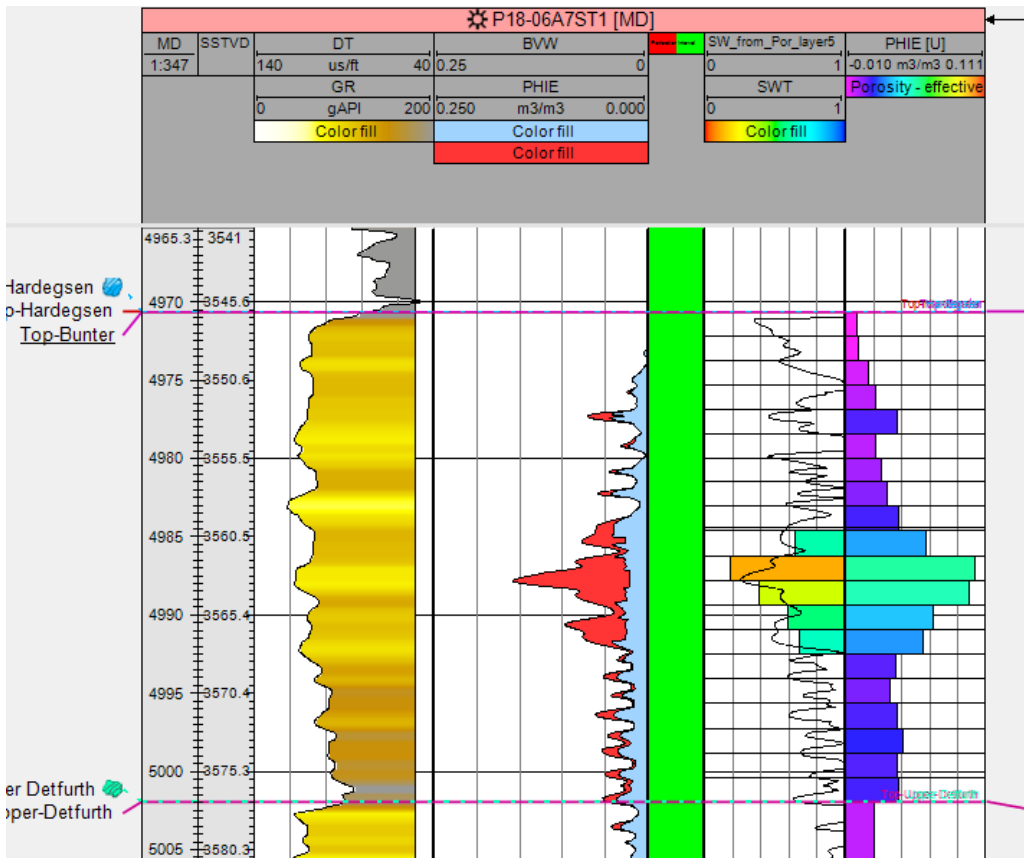
Figure 17-22: Total water saturation based on logs (SWT) and synthetic log based on the j-function (Sw_from_Por_layer5).

17.6.7 Pore compressibility

As no pore compressibility measurements are available for the P18-2 field, a correlation is used[12]. The compressibility is (also) dependent on the porosity according to:

$$Cr(\Phi) = 7.248 \cdot 10^{-6} / (\Phi + 0.000001) - 0.26 \cdot 10^{-5}$$

Where
    Cr   = pore compressibility,
    Φ = porosity.

Note: in the final review phase, it was discovered that the distribution of the rock compressibility was not updated to the final porosity distribution. Since on average the rock compressibility is correct, this has only minor impact (~2-3 bar) on the history match.

17.6.8 Regions

In the dynamic model regions are specified based on porosity classes for rock properties described in section 17.6.6. and to split the computational grid into regions for calculation. Furthermore regions are used to evaluate the gas initial in place (GIIP) for the different compartments separated by faults or boundaries (see Figure 17-15) .

17.6.9 Initial condition in the reservoir

The reservoir is a mechanical and thermodynamic system and hence its (initial) conditions are fully defined by the following state variables at any point in the reservoir or grid block in the simulator:

- Temperature;
- Pressure;
- phase compositions;
- phase saturations.

Initialization of these variables is discussed below.

17.6.9.1 Temperature

Since an isothermal model is used, all temperature dependent fluid and rock properties are assume to be specified at the reservoir temperature of 117 °C degrees.

17.6.9.2 Pressure

Reported initial pressure is 377 bar at 3500 m TVDSS. In the simulator, the initial (gas) reservoir pressure is 380.9 bar at datum depth 3680 m TVDSS. It is important to note that in fact each phase has its own pressure and that each phase pressure is assumed to be in hydrostatic equilibrium. Phase pressures and phase saturations are coupled through capillary pressure between phases. The capillary pressure is based on the J-function defined in equation (17-3).

---

[12] Personal communication, NAM.

17.6.9.3 Gas water Contact

The gas water contact (taken as free water level, i.e. P_c = 0) is at 3680 m depth in segment 2 (see Figure 17-15 for the definition of the segments). In the other two segments the gas water contact is defined above the reservoir, to ensure that no gas is present in the aquifer. Because the gas water contact was not observed in well P18-A-07-S1, the same contact as in P18-02 was used.

17.6.10 General remarks

Petrel 2018 was used to generate an input deck for the dynamic model. The reservoir engineering module offers options such as specification of fluid and rock properties, specification of historic production data.
There a few manual adaptations in the input files:
− PVT data generated by Petrel are overwritten by TNO's PVT data, in other words an equation of state is used;
− Saturation functions generated by Petrel are overwritten by TNO's saturation functions;
− History match multipliers.

17.7   History Match of the dynamic model

17.7.1 Introduction

In the previous chapter the data required to describe the reservoir have been described. In this chapter the data required to define the operations and resulting reservoir behaviour will be discussed. These data are:
•   Specification of wells: location, trajectory, casing data, perforation data, productivity index, etc.;
•   Production and injection data:
     •   Water and gas production rates;
     •   Bottom hole pressures;
     •   Reservoir pressures.

Next the adaption of the reservoir parameters to arrive at an acceptable history match is discussed in detail.

17.7.2 Well data and production data

17.7.2.1 Well Location and trajectory

For all wells well head coordinates and deviation data have been received and imported in Petrel. (see section 17.4).

17.7.2.2 Well completions and perforations

Based on the received well test reports the completion perforation and skin data was gathered shown in Table 17-7.

Table 17-7 Well test, completion and perforation data.

Well name	Completion size (inch)	Productivity index (Nm³/day)/bar	Perforations (m)	KH (mDm) from well test	Skin from well test
P18-02-A-01	4 ½	26.72	3580-3695	1847	0.6-0.9
P18-02-A-03S2	4 ½	31.89	4070-4209	-	2.1-3.3
P18-02-A-05S1	7	37.33	4798-4980	25249	3.19
P18-02-A-06	4 ½	14	4488-4633	3686	2
P18-02-A-06ST1	4 ½	22.28	3376-3936	-	-
P18-4A-02	4 ½	40.95	4085-4199	8208	-
P18-A-07-S1	4 ½	6.83	4975-5065	-	-

17.7.2.3 RFT and PLT data
For well P18-A-07-S1 no RFT or PLT data are available.

17.7.2.4 Historic Well Production data
Daily gas and condensate production data was provided by the operator.
In Figure 17-23 the daily gas production data of the production well is shown. The received data was recalculated from Nm³ to sm³ which is required for Eclipse and upscaled to monthly time steps (using Petrel).
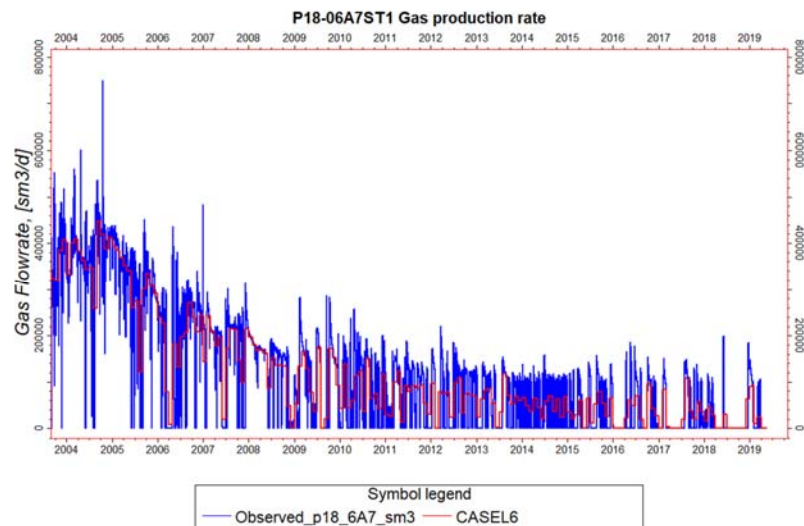
Figure 17-23: Gas production of well P18-A-07-S1 showing the observed daily values and the monthly values used for the simulator (CASEL6).

17.7.2.5 Historic pressure data
Daily tubing head pressure (THP) data and on irregular basis shut in pressure data was provided. A bottom hole pressure (BHP) is generally not measured directly. Instead, the (THP) is measured and BHP is calculated from this THP and reported production or injection rates using a well bore flow model. To be able to calculate

the BHP from the THP a number of parameters, including completion data and production rates, have to be accurately known. By absence of Vertical Lift Performance Relationship (VLP) of each production well the opportunity to convert THP to BHP is not performed. The measured initial pressure of 377 bar in 2003 suggests there is no pressure communication with the P18-2 field (Figure 17-16).
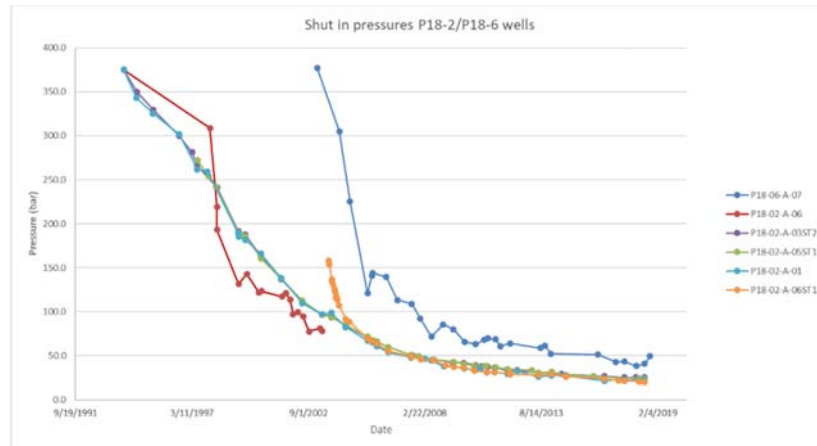
Figure 17-24: Pressure profiles of the production wells over time.

17.7.3 P/Z curves

The standard method to estimate the GIIP and driving mechanism (e.g. natural water drive, volumetric depletions) is material balance analysis applied on the production and pressure history. The most used method is the p/Z plot shown in Figure 17-25. This p/Z plot is based on extrapolated build-up profiles rather than direct pressure observations, due to the slow build-ups observed in this well. The GIIP estimated from this curve is 800 MNm^3 (844 M sm^3).
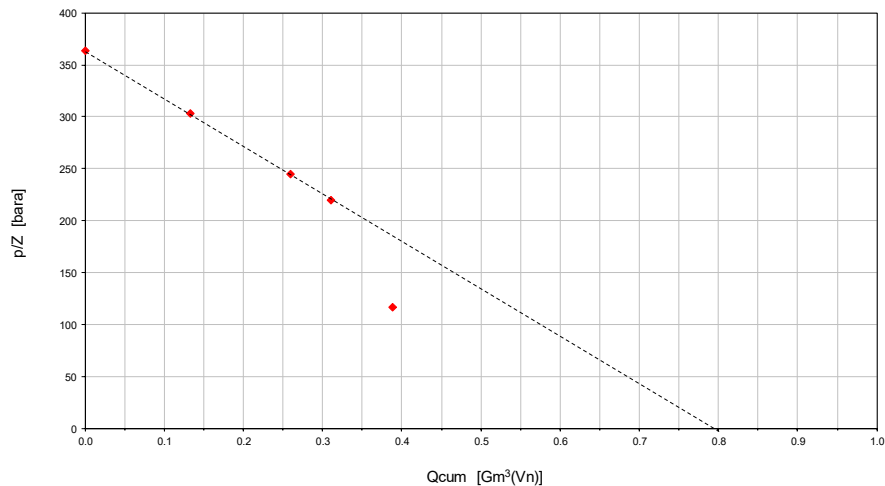
Figure 17-25: P/Z curve of P18-6 field.

17.7.4 History matching approach

As discussed in a previous section (17.7.2.5) no BHP observations are available, therefore the measured shut-in pressures is matches with the 9-point pressure of each individual well. The history match approach is done according to the following procedure:

- The simulations were performed under rate constraint conditions
- Change the GIIP by adjusting the J-function
- Change the permeability of the dynamic model based on porosity – permeability relationship, since no well test data (KH) is available.
- Match the measured shut-in pressures with the 9-point pressure by adjusting the multipliers on flow barriers.

17.7.4.1 History Match of GIIP

The result of the history matching the GIIP is summarized in Table 17-8 for segment 3 (Figure 17-15). The other segments don't contain gas. The gas present in Lower Detfurth and Volpriehausen is not producible. Connected GIIP in the dynamic model is 826 Msm^3 which is close the GIIP estimate of 844 M sm^3 from the p/Z curve.

Table 17-8: GIIP results for segment 3 (Figure 17-15).

Formation	Pore volume [M rm^3]		HC pore volume [M rm^3]		GIIP [M sm^3]	
	static	dynamic	static	dynamic	static	dynamic
Hardegsen	20	20	2.091	2.102	523	541
Upper Detfurth	30	30	1.120	1.122	280	289
Lower Detfurth	24	24	0.106	0.091	26	23
Volpriehausen	69	69	0.006	0.006	2	2
Total	143	142	3.324	3.321	831	856

17.7.4.2 History match on pressure data

In the initial models, connectivity in the gas zone was too large and permeability near the well was too small. Water production occurred too fast in the initial models compared to actual observations (no significant water production has been observed in the well). To achieve a history match on the pressure data, the following adjustments were made:

- To reduce water inflow into the well low porosity and permeability in the aquifer has been assumed and water mobility in the relative permeability has been reduced.
- Increase in permeability in the near well zone by increasing porosity in the highest porosity layer to 0.15, increasing permeability in the near well area in the high permeability layer by 1.5 and a PI multiplier of 2.
- Permeability in vertical direction was set to 0.01 x permeability in horizontal direction.
- The multiplier between the Hardegsen Fm and Upper Detfurth Fm was adjusted to a final value of 0.08. Gas from the Upper Detfurth Fm is produced via the Hardegsen. Although the well has perforations in the Upper Detfurth, due to the low permeability in the near-well zone, the gas flow to the well via the Hardegsen.
- The pressure behaviour in well P18-A-07-S1 shows a very rapid decline initially and a much slower tail. This was interpreted as 300 to 400 M Nm^3 of fast gas and the rest of the gas is available at a much lower rate (interpretations

received from TAQA). Since the amount of gas present in the (well-connected) Hardegsen is more than 500 M sm³, an intra-Hardegsen flow barrier is inferred. After evaluating both a vertical and a horizontal barrier, finally a vertical barrier was implemented by a using a multiplier on the horizontal flow of 0.0015 (Figure 17-26).
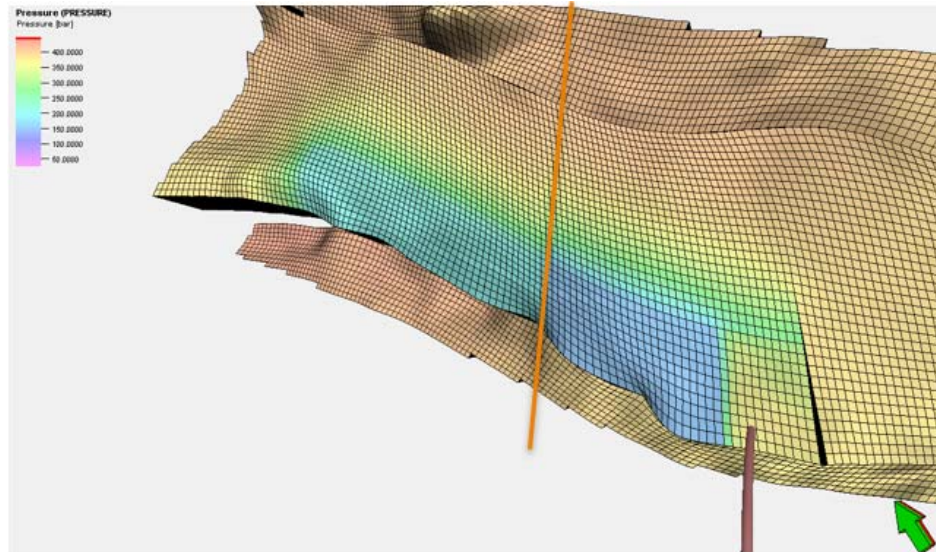
Figure 17-26: Position of the intra-Hardegsen flow barrier indicated by the orange line.

The match of the near well permeability for well P18-A-07-S1 is uncertain because no estimate of the KH from well tests is available. Only one estimate of the Productivity Index (PI) from 2010 (~2500 d after start of production) is available: 6830 Nm³/day/bar. The PI from the final history matched Eclipse model is presented in Figure 17-27. These PI values are higher, however the definition is also somewhat different.
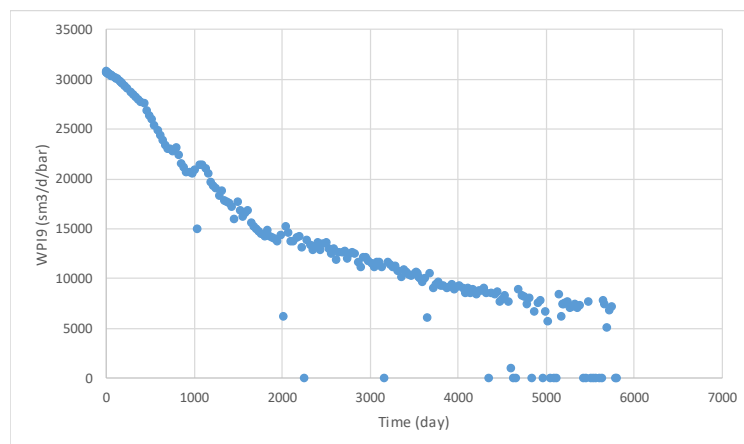
Figure 17-27. Productivity Index of well P18-6-A7-ST1 estimated by Eclipse using the 9-point pressure during production.

When comparing P18-A-07-S1 to the wells in P18-2 and P18-4 (Table 17-7), it is clear that P18-A-07-S1 is the poorest well and that the PI is a factor 2 to 6 lower than the others. However, the initial values for the KH from the model were 40 mDm, which is almost two orders of magnitude lower than for the other wells. The history matched KH from the Eclipse model is 216 mDm (excluding the PI multiplier of 2), which is more in line with the other wells.

17.7.5 Result of the history match
Based on the parameters described in the previous section the following production and pressure match is achieved (Figure 17-28 and Figure 17-29). The observed gas production was fully matched.
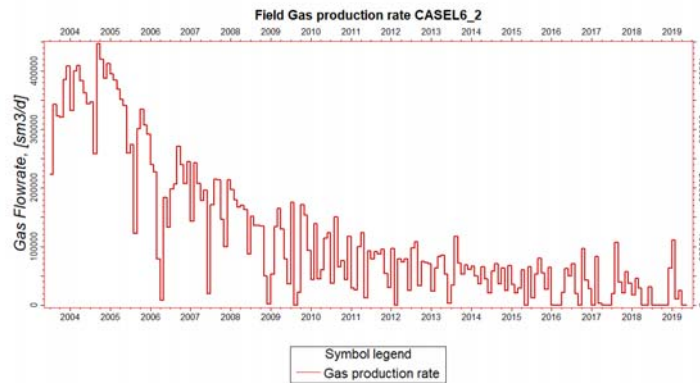
Figure 17-28: History matched production data well P18-A-07-S1.
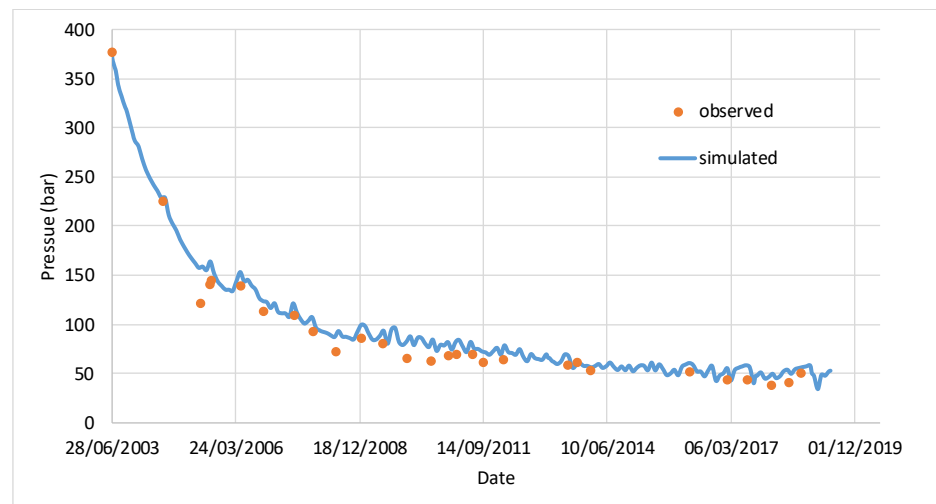
Figure 17-29: History matched pressure data well P18-A-07-S1.

No RFT or PLT data were available for matching. However, three build-ups were extrapolated by TAQA to estimate the reservoir pressure. The observed build-ups had not stabilized yet, because of the slow response of the field. Table 17-9 shows the pressure values estimated by TAQA from the extrapolated build-up profiles and simulated using the Eclipse model. The simulated values are higher than the extrapolated ones. Since the GIIP in the model is the same as the GIIP estimated

from the p/Z curve based on these extrapolated build-up profiles (Figure 17-25), the discrepancy might be due to aquifer support in the simulation model. This is not represented in the extrapolated build-up profiles. From the currently available data it is not possible to verify whether this aquifer support is realistic or not.

Table 17-9. Estimated pressure (at datum depth of 3500 m SSTVD) from extended (extrapolated) build-ups and from Eclipse simulation.

Date	Qcum	P extrapolated	Simulated P*
	Gm^3	bar	bar
Initial	0	377	
15/08/2004	0.13	301	305
26/08/2005	0.26	232	242
29/04/2006	0.31	206	223

* Value depends on the duration of the simulated build-up
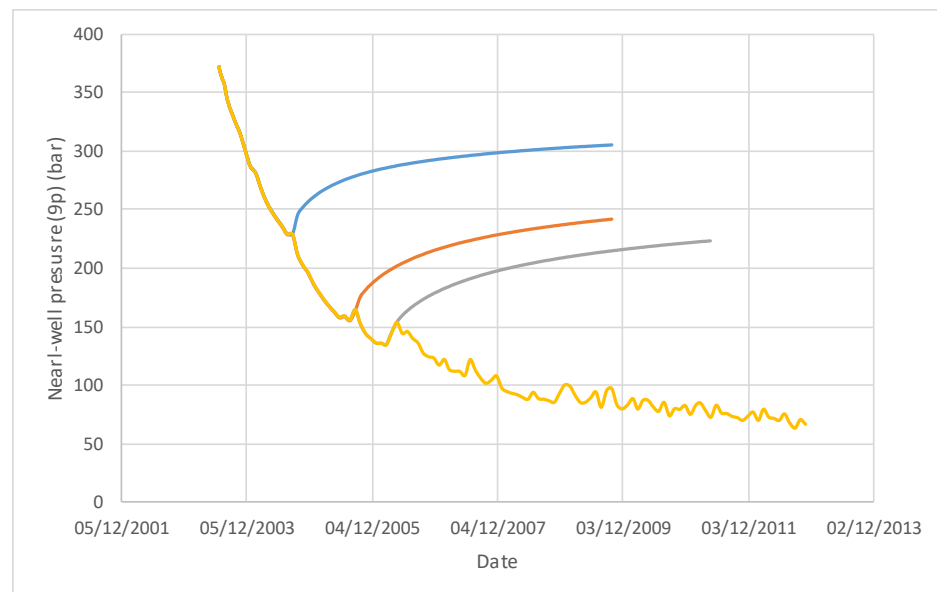
Figure 17-30. Simulated near well pressure for three extended pressure build-ups.

17.7.6 History match conclusion
- The dynamic model reproduces production rates and most of the pressure data.
- An intra-Hardegsen flow barrier was required to achieve a history match on the pressure data (fast initial response and slow tail).
- Aquifer permeability and water mobility were both reduced compared to the initial estimates to reduce water inflow into the well.

17.7.7 Simulation of final production phase
The proposed CO_2 injection will not start at the end of the history match period. To start the injection scenarios at the right initial conditions, a further simulation period is required, namely the final production phase. For P18-6, this final production phase is simulated using a rate constraint of $6 \cdot 10^4$ sm^3/d and BHP constraint of 1

bar. Although in reality well P18-A-07-S1 is produced intermittently, the simulation assumed continuous production for simplicity. The production was continued for another five years to 1 April 2024. At the end of this production period, the rate has dropped to $1.8 \cdot 10^4$ sm^3/d, the near well pressure is 20.4 bar (after 15 days of shut-in), the field average gas pressure is 62 bar (or 52 bar if only the connected gas is considered). These conditions will be used for the start of injection.
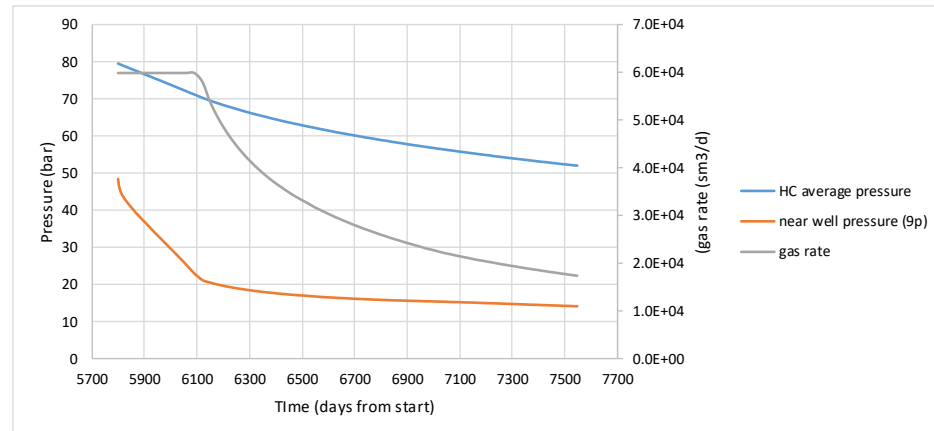
Figure 17-31. Near well pressure, field average gas (HC) pressure of the connected gas and gas rate during the simulated final production phase.

17.8   Geomechanical model

17.8.1   MACRIS – Poro-elastic model

We detail here the TNO-developed semi-numerical approach (MACRIS, Mechanical Analysis of Complex Reservoirs for Induced Seismicity) to handle pressure effects along multiple faults. More specifically MACRIS is designed to compute 3D stress changes along faults induced by: (1) poro-elastic effect (contraction/inflation of the reservoir due to fluid pressure depletion/injection), (2) direct pressure effect (changes of the fluid pressure intra-faults can induce changes in effective normal stress), (3) differential compaction effect due to the fault offset.
MACRIS is a mesh-free approach where there is no need to build a dedicated grid for the geomechanical analysis. MACRIS takes directly as input the grid of the reservoir flow simulation; in our case: the 3D pressure fields of the P18-6 field at a yearly sampling rate. Each grid block of the reservoir flow simulation is considered as a compacting nucleus of strain (center of compression; Mindlin 1936; Geertsma, 1973; Okada, 1992). The contribution of each of these nuclei is integrated to compute the poro-elastic stress changes along each fault of the P18-6 field with a meter-scale spatial resolution. The restriction that we presently still have is that only one-way coupling is considered. We deem this acceptable for gas reservoirs, where the effect of compaction on the gas pressures in the pores is small. The Barnes-Hut algorithm (Barnes & Hut, 1986) is used for re-discretizing the initial reservoir grid for two purposes: (i) clustering the nuclei of strain close to the faults in order to increase the spatial stress resolution, and (ii) shortening the computation time.

MACRIS thus computes the poro-elastic normal and shear stress changes induced by the reservoir compaction for every observation point along each fault.

Observation points are placed on fault pillars (i.e. sub-vertical lines along the fault dip direction), which in turn make up the 3D geometry of a fault (see Figure 17-32).
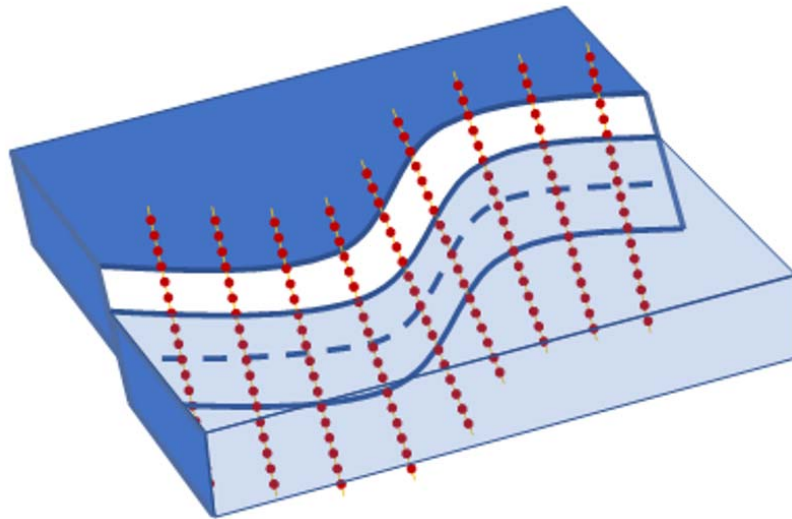
Figure 17-32: Schematic of the distribution of the observation points (where the stress solution is evaluated) along fault pillars.

In order to account for the direct pressure effect, we still need to define the pore pressure changes inside the faults to calculate the effective normal stress changes and derive the Coulomb stress changes. This intra-fault pore pressure is defined as the average fluid pressure between the two juxtaposed reservoir compartments.

MACRIS has been validated by comparison with relatively slow finite-element (FE) numerical computations (DIANA), with excellent results (van Wees et al., 2018). This benchmarking exercise has been carried on using single-fault tank models; for MACRIS it was a 3D model and for DIANA it was a 2D plane strain model. For the present study we extended this benchmarking exercise by comparing the 3D MACRIS model with this time a full 3D DIANA model. Results of this exercise are presented in Figure 17-33. The 3D single-fault model mimics the P18-6 field at the end of the depletion period, that is with an initial pressure of 330 bars and a decrease of pressure of -300bars at the end of the depletion period. The MACRIS results closely match the FE DIANA solution. Deviations between both solutions are less than 3%.
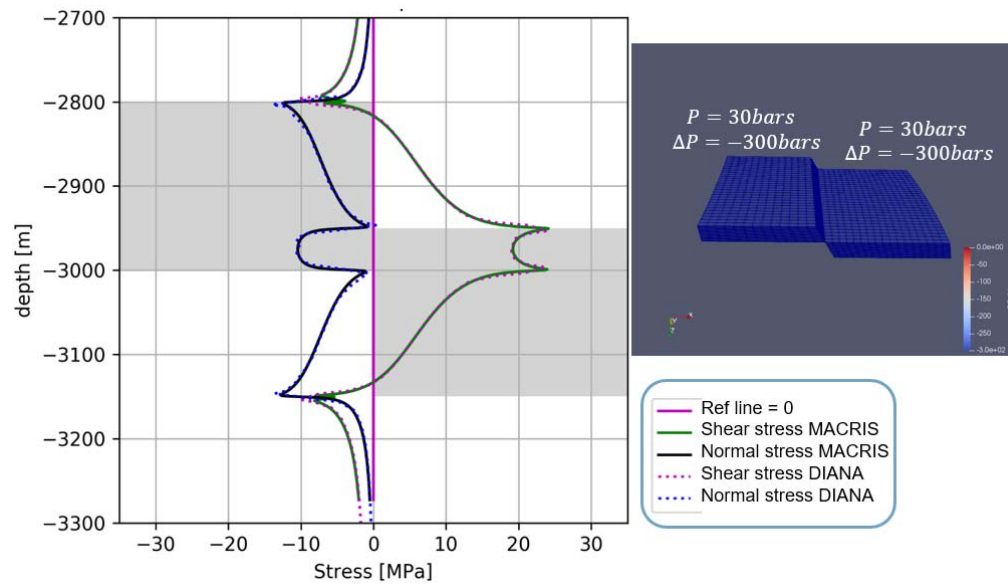
Figure 17-33: Comparison MACRIS vs. Diana FEM package. Right: 3D single-fault model with offset. Both compartments start with the same initial pressure (330 bars) and are depleted of the same amount (-300 bars). Left: Stress solution along the central pillar of the model. The changes in shear and normal stresses induced by the poro-elastic effect are almost identical between both solutions. For this particular example, the pore pressure inside the fault remains at the initial pore pressure.

17.8.2 Thermo-elastic model

The TNO-developed semi-analytical approach to model thermo-elastic stresses due changes in temperature of reservoir rock is based on Myklestad (1942). Myklestad (1942) derived equations for all the components of the stress tensor as induced by heating a semi-infinite cylinder to a constant temperature difference with respect to the ambient reservoir temperature using elliptical integrals in a cylindrical coordinate system. Candela et al. (2018) contains all the details of the derivation.

This approach gives us the tensor of stress changes inside and outside the reservoir in the cylindrical coordinate system. This tensor of stress changes thus needs to be translated to Cartesian coordinates using standard cylindrical coordinate transformation. The initial stress state is then added to the tensor of stress changes to obtain the stress tensor in Cartesian coordinates (see Figure Figure 17-34 and Figure 17-35).

We consider faults uniformly distributed in our model. In other words, each location inside and outside the reservoir (in the caprock) can potentially host a fault. More specifically, from the stress tensor, at each location, one can calculate the Coulomb stress changes for any fault plane orientations.
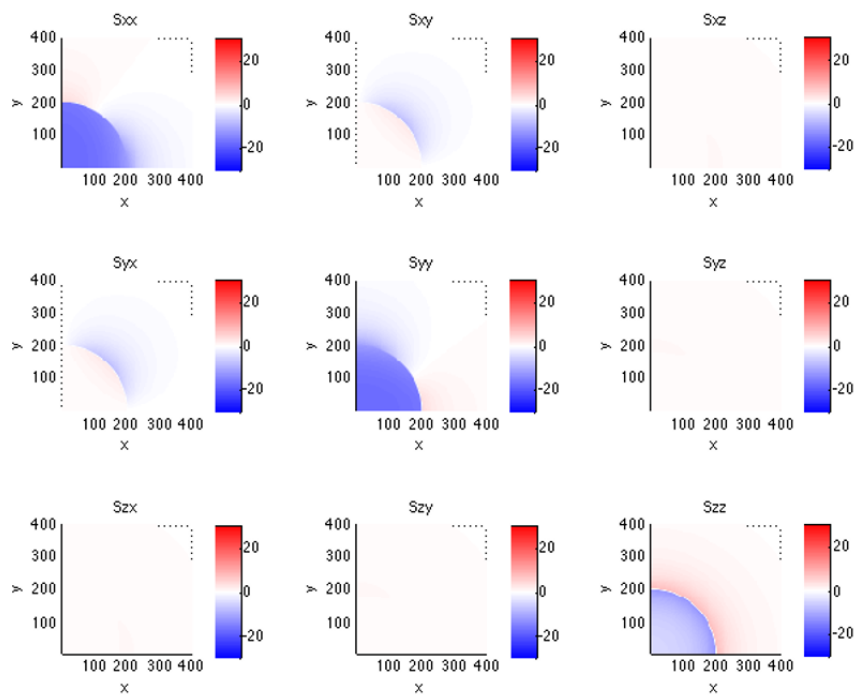
Figure 17-34: Horizontal [XY] spatial distribution of each component of the tensor of stress changes.
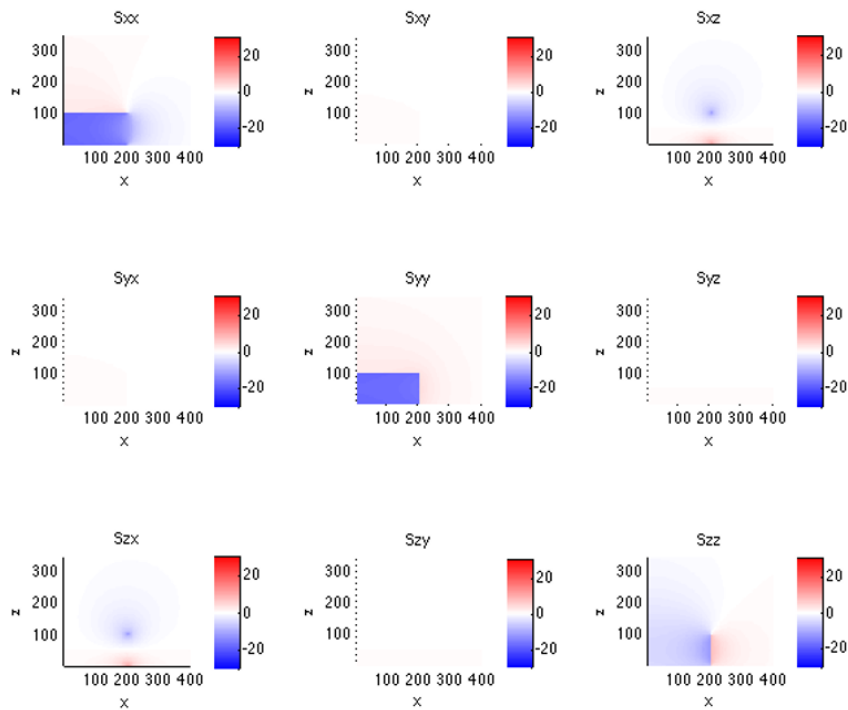
Figure 17-35: Vertical [XZ] spatial distribution of each component of the tensor of stress changes.

17.9   Well degradation model

The nonlinear finite element simulator DIANA[13] is used to generate meshes for 2D numerical models of the well system and run structural and heat transfer simulations. The workflow is automated by a dedicated user interface DIANA SEALEC: the user-defined input and model parameters are used to generate meshes and define the complete non-linear (phased, staggered) analysis, which mimics the different loads acting on the well system throughout the entire lifetime of a well, from the drilling phase, well completion, testing, operations and decommissioning (Figure 17-36).
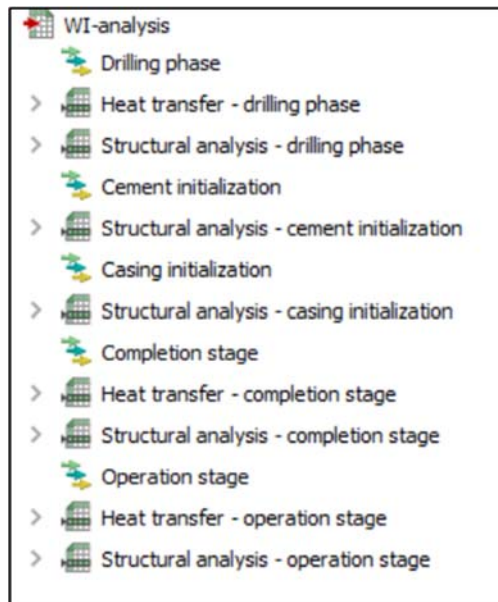
Figure 17-36: Example of steps in the wellbore integrity analysis.

The model of the well system, representing a cross-section normal to the well axis, comprises the casing, the cement and the surrounding rock formation. The chosen 2D modelling approach is computationally efficient and simulations can easily be repeated for various depths along the wellbore. Complete plane strain elements are used for bulk materials. Zero-thickness interface elements are used for the casing-cement and the cement-formation interfaces. The well materials can be modelled with different constitutive models; for example a von Mises elasto-plastic material model for the steel casing; a combination of the Mohr-Coulomb elasto-plastic model and the multi-directional fixed crack model for the cement; a Mohr-Coulomb elasto-plastic model for the rock formation; and the Coulomb friction model with a tension cut-off for the interfaces between materials. Different failure modes can be simulated, for example: plastic deformation of casing, plastic deformation and cracking of the cement sheath, plastic deformation of formation and debonding of cement interfaces (Figure 17-37). Specific deformational behaviour of materials can be modelled such as shrinkage of cement and the creep behaviour of viscous rock salt formation.

---

[13] See dianafea.com.

Structural, heat transfer and fluid flow analyses are typically needed for wellbore integrity assessment. Results from finite element analyses are typically displacements, stresses and strains in different formulations.
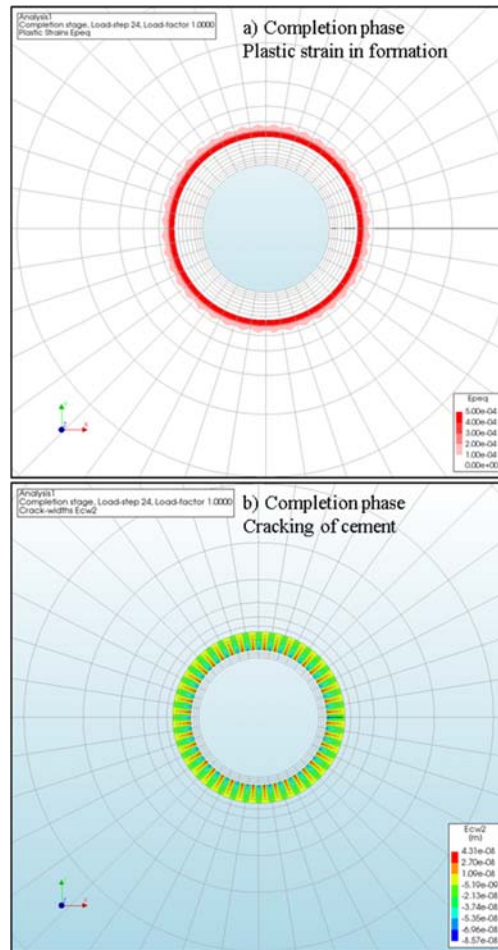
Figure 17-37: (a) Plastic strain in the formation and (b) cracking of annular cement in the completion phase.

18   Appendix C. Risk Register

Caprock

Identified risk	Description	Positive evidence for integrity	Risk reduction measures	Risk characterisation	Risk classification
Initial condition	Impermeable shales of the Upper Triassic and Altena Groups overlie the P18-06 reservoir, which represent a good seal for the natural gas reservoir.	Effective seal as evidenced by the presence of gas in reservoir below the seal with a total thickness between 450 and 750 m and gas column of about 170 m (the latter based on a GWC at 3680 m SSTVD, assumed to be similar to P18-2)	Avarage reservoir pressure at the end of CO2 injection equal to or lower than hydrostatic pressure	As the evidence for the initial sealing of the gas reservoir is very strong, it is a good seal for CO2 storage as well and consequently the risk of migration out of the reservoir is low to even negligible when the pressure is kept at or below the hydrostatic pressure.	A-1
Pressure fracturing	Fractures in the seal may be caused by local stress variations due to initial gas production, subsequent CO2 injection and associated pressure changes. Fractures represent a potential conduit for CO2 loaded fluids depending on their connectivity and continuity (see also Fault zone).	Semi-analytic modelling has shown that Coulomb stresses as a consequence of pressure build-up due to injection quickly decay on top of the reservoir inside the caprock. The pressure effect is thus not expected to contribute to the risk of fault reactivation in the caprock. New fractures or faults will not be generated as they would require even higher Coulomb stresses.	Keep the pressure below fracturing condition	Considering the huge thickness of the caprock and the very rapid decay of the pressure near the top of the reservoir and the basis of the caprock, the likelihood of fracturing the complete caprock is nil and consequently the risk is very low to negligible.	A-1
Thermal fracturing	Fractures in the seal may be caused by local stress variations due to initial gas production, subsequent CO2 injection and associated temperature changes. Fractures represent a potential conduit for CO2 loaded fluids depending on their connectivity and continuity (see also Fault zone).	Temperature-induced Coulomb stresses in the caprock due to reservoir cooling are negative, and thus do no lead to re-activation of faults or fractures in the caprock nor will they result in new fractures in the caprock. The likelihood of re-activating a pre-existing fault or fracture in the caprock is thus very low.	Appropriate management of thermal effects	Temperature drop in the reservoir is very unlikely to lead to re-activation of fractures (or formation of new fractures) expected to lead will occur and thus will not lead to the migration of CO2 out of the reservoir. The risk is very low to negligible.	A-1
Chemical degradation	CO2 if dissolved may react with minerals in the caprock near the interface with the CO2 reservoir.	Since the caprock has proven to be a seal for gas, the only way of upward migration is by diffusion of dissolved CO2, which is a very slow process. Chemical interaction between dissolved CO2 and caprock minerals is very slow and has minor effects on porosity and permeability. Hence, no migration path is expected to form. The affected zone of migration of dissolved CO2 and chemical interaction is in the order of several meters in thousands of years (Gaus et al., 2004; Tambach et al., 2012).	Reservoir pressure after CO2 injection at or lower than initial gas reservoir pressure, to prevent CO2 from entering the caprock in gaseous/supercritical state thereby enhancing geochemical reactions.	Chemical degradation will only marginally influence the sealing properties of the caprock and thus will the overall integrity of the caprock stay intact. The likelihood of degrading the caprock is very low and its consequence will be nil or negligible.	A-1

Cont. improvement
ALARP
Intolerable

Fault zone

Identified risk	Description	Positive evidence for integrity	Risk reduction measures	Risk characterisation	Risk classification
Initial condition	Sealing capacity of main reservoir bounding fault to the SW and bounding cross fault to the SE mainly determined by juxtaposed reservoir rocks and sealing rocks	Bounding faults F430 (main fault) and F600 (cross fault) are effective seals as evidenced by presence of juxtaposed gas reservoirs and sealing rock.	Manage pressure gradient across fault	As reservoir rocks next to bounding faults are sealed off by very low permeable rocks on the other side of the fault zone, it has a very low likelihood that a negligible amount of CO2 will migrate across or along the fault and sealing rock.	A-1
Chemical degradation	Chemical degradation of material in fault zone	Currently, there is no evidence for gas migration from the P18-02 reservoir along the faults to overlying formations. In general, the geochemical reactions between CO2, formation water and fault gouge mineralogy - if present - will result in precipitation of carbonate minerals. On the longer term, silicate minerals might react, providing additional cations for carbonate precipitation. Porosity and hence permeability effects are predicted to be negligible. Increase of carbonate content in the fault gouge is known to increase the friction coefficient and to decrease potential for fault re-activation.		Chemical degradation leads to lowering of the porosity and permeability of the fault gouge and increases the friction coefficient of faults. Therefore it is highly unlikely that chemical degradation in itself leads to the migration of CO2 across the faul zone.	A-1
Pressure re-activation	Due to pressure changes during production and/or injection faults may be re-activated (Vandeweijer et al., 2011: par 6.7, p109) and potentially act as conduits for CO2.	No seismic activity was encountered during production, based on the KNMI database (KNMI Seismic and Acoustic Data Portal, 2 Oct 2019: doi:10.21944/e970fd34-23b9-3411-b366-e4f72877d2c5). Semi-analytic modelling has shown that at the end of the injection period most (if not all) of the areas where positive Coulomb stresses which are present at the end of depletion, have disappeared. The faults are thus expected to be stable at the end of the injection period.	Injection of CO2 is a mitigation measure in itself as it reduces the underpressure in the reservoir and consequently the risk of fault re-activation.	Based on the results from the semi-analytic modelling it appears to be highly unlikely that faults will be re-activated due to the increased pressure by CO2 injection and consequently will not lead to migration of CO2 along the fault. The risk is characterized as low.	A-1
Thermal re-activation	Cold injection stream could re-activate a nearby fault and change its fluid transport properties.	Well P18-6A-07-S1 is at a distance of about 100 m from the main bounding fault. Initial TOUGH2 simulations have shown that the cooling front with a temperature drop of about 50 °C could extend to 200 m from the injector after 5 years of injection. Semi-analytic thermomechanical modelling indicates that the Coulomb stresses may reach up to 9 MPa at the edge of the cooling front, which can be sufficient to re-activate the fault. The cold CO2 plume from injection wells at less than 200 m from a fault may thermomechanically influence its stability. Note that the actual temperature drop cold be about 14 °C lower due to limitations of the TOUGH2 simulator.	Managing the advancement of the cold front near faults by adjusting the injection rate of well P18-6A-07-S1, which is in close distance of the main bounding fault. Additional simulations with TOUGH2 for a limited period of time of injection (content of pipeline as defined in the discharge scenario) show that the advance of the cold front is strongly limited to 20 m from the well and thus cannot thermomechanically reactivate a fault at 100 m from the well. This is considered to be a more representative case for the use of P18-06field as a backup injection site.	With inclusion of appropriate management of the injection rate in the well faults the likelihood of thermomechanical fault re-activation leading to the migration of a negligible amount of CO2 out of the reservoir will be very low or no migration of CO2 out of the reservoir at all.	A-1

Cont. improvement
ALARP
Intolerable

Reservoir

Identified risk	Description	Positive evidence for integrity	Risk reduction measures	Risk characterisation	Risk classification
Spilling in SE at tip of cross fault	Overfilling could lead to lateral migration (spilling) of CO2 to neighbouring Buntsandstein aquifers and gas reservoirs. Subsequently, CO2 may migrate to Lower Cretaceous or Lower Tertiary aquifers via a non isolatd wells or faults if any A potential spill zone is identified at the northern tip of the SE boundary fault of the P18-6 field.	Information from nearby well indicate that the aquifer has low permeability due to illitisaton. Dynamic reservoir simulations show no spilling, even in the case of strong overpressurization. although the CO2 may migrate beyond the GWC.	Spilling prevented by keeping the reservoir pressure at or below the initial pressure and by limiting the total mass of injected CO2. Proper zonal isolation of wells and preventing re-activation of faults to avoid vertical migration (see also Fault compartment).	Keeping the average reservoir pressure at or below the initial pressure at the end of injection and the robustness of flow simulations indicate a very low likelihood that a negligible amount of CO2 migrates out of the reservoir.	A-1
Spilling at NW edge near saddle	Overfilling could lead to lateral migration (spilling) of CO2 to neighbouring Buntsandstein gas reservoirs and aquifers. Subsequently, CO2 may migrate to Lower Cretaceous or Lower Tertiary aquifers via a non isolated wells or permeable faults if any. A potential spill zone is identified at the NW edge of the P18-6 field, represented by a saddle.	Information from nearby well indicate that the aquifer has low permeability due to illitisaton. Dynamic reservoir simulations show no spilling, even in the case of strong overpressurization. although the CO2 may migrate beyoud the GWC.	Spilling prevented by keeping the reservoir pressure at or below the initial pressure and limit the total mass of injected CO2. Proper zonal isolation of wells and preventing re-activation of faults to avoid vertical migration (see also Fault zone compartment)	Keeping the average reservoir pressure at or below initial pressure at the end of injection and the robustness of flow simulations indicate a very low likelihood that a negligible amount of CO2 migrates out of the reservoir.	A-1
Flow between P18-2 and P18-6 reservoirs	Over a small section across the fault zone between the P18-2 and P18-6 reservoirs, reservoir rocks of the Volpriehausen Sandstone are juxtaposed, which may lead to migration of CO2 fom P18-2 to P18-6.	As the permeability of the Volpriehausen Sandstone is very low, the migration and pressure equilibration will be very slow. An assessment of the fault zone indicates that there is a very high probability of an impermeable gouge being present in the fault zone (Nieuwland, 2011). The pressure in P18-6 was at 378 bar before starting injection whereas at he same time pressure has dropped to about 100 bar in the producing P18-2 reservoir (June 2003). Apparently, this enormous pressure difference could exist indicating that there is virtually no flow and pressure equilibration between the two reservoirs on production time scales. Geological information indicates that Block 2-IV, which is directly adjacent to the P18-6 reservoir is a separate hydraulic unit.		The pressure difference of about 278 bar between the two reservoirs, the very low permeability of the Volpriehausen Sandstone and the hydraulic isolation of Block 2-IV show that the likelihood of a negligible amount of CO2 migrating from P18-2 to P18-6 is very low.	A-1

Low: Cont. improvement
Medium: ALARP
High: Intolerable

Well

Identified risk	Evaluation of integrity	Risk characterisation (before workover)	Risk classification (before workover)	Risk reduction measures	Risk characterisation (after workover)	Risk classification (after workover)
P18-6A-07-S1: production packer in 7"liner	A short stretch of the 7" liner (and cement) above the 5" TOL and below the production packer in the 7" liner is just above the caprock in the Schieland Group and may be exposed to corrosive fluids.	The 7" liner is P110 carbon steel and is exposed to well bore fluids and represents a single barrier in this small depth window. In the event of presence of water or brine in the wellbore fluids, the risk of corrosion may lead to loss of the primary barrier with potential leakage to the overburden. The likelihood that a small amount of CO2 leaks to the overburden is estimated to be medium.	C-3	Appropriate measures, to reinstate the dual barrier function at the level of the 7" liner above the caprock	With the implementation of adequate measures, leakage from the well will be prevented. The likelihood will be low that a negligible amount of CO2 will migrate out of the reservoir.	B-1
P18-6A-07-S1: status outer casing inside conductor	The surface casing in the conductor might be subjected to external corrosion and/or fatigue induced by metoceanic movement.	As the cementation of the conductor and 20" casing could not be sufficiently ascertained, the likelihood that a small amount of CO2 leaks to the overburden is estimated to be medium.	C-3	Verification of the presence and quality of cementation of the conductor and 20"casing and adequate measures if needed.	With the implementation of adequate measures, leakage from the well will be prevented. The likelihood will be low that a negligible amount of CO2 will migrate out of the reservoir.	B-1
P18-6A-07-S1: cooling	Injection of cold CO2 may lead to the creation of a micro-annulus at the casing-cement interface which may be enhanced by chemical interaction with CO2.	Although the pressure and temperature conditions are more favourable than for P18-2, a micro-annulus may still be formed. A medium likelihood exists that a small amount of CO2 migrates along the micro-annulus and partly ends up outside the storage complex.	C-3	Logging during operations, appropriate management of the temperature in the wellbore zone and keeping the reservoir pressure below the hydrostatic pressure (at datum level of 3,400 m)	Low likelihood remains that a negligible amont of CO2 migrates out of the reservoir	B-1

Low: Cont. improvement	
Medium: ALARP	
High: Intolerable	

19 Appendix D. Monitoring Plan

Table 19-1 – P18-6 Base case monitoring plan

No.	Parameter to be Monitored*	Proposed Technique adopted	Category of monitoring (Mandatory according to EU directive)	Category of monitoring (Required (preliminary estimation))	Category of monitoring (Contingency)	Pre-inj	Inj	Post-Inj	Post-Inj (abandonment)	Long-term stewardship	Location	Normal situation (Expectation value)	Normal situation (Accuracy)	Alert value (> Threshold 1)	Alert value (Action**)	Contingency value (> Threshold 2)	Contingency value (Contingency measures***)
	Injection proces																
1	Injection rate	Flow meter	x				Cont				Near well head or Compressor station	Max rate = 105 ton CO2/uur (30 kg/s or 1 Mton CO2/year) and no fluctuations at constant pressure, expected value t.b.d.		Fluctuations at constant pressure or value above max. rate	Verify compressor, find cause of increased rate	Fluctuations at constant pressure or value above max. safety margins	Find cause, solve problem and if necessary reduce injection until flow < threshold 1 value again
2	Injection stream CO2 concentration	Samples & analysis: online system	x				Cont or 1-3 hourly sampling combined with online analysis system				Near well head or Compressor station	Defined % for the CO2 concentration of the stream		Allowed fluctuations reached	Additional measurements	Above allowed fluctuations	Adapt stream composition, reduce injection temporarily
3	Injection stream composition	Samples & analysis: Additional samples for calibration	x				Quarterly				Near well head or Compressor station	Defined % for the composition of the gas		Allowed fluctuations reached	Additional measurements, find cause, adapt gas composition, potentially reduce injection rate	Above allowed fluctuations	Find cause, adapt stream composition, potentially reduce or stop injection temporarily
4	Water measurement	Water measurement	x				Cont				Near well head or Compressor station	Specification value		In case specification value is reached	Consultation with the CO2 provider, check dehydration system	In case value is above specification value and creates a safety issue	Stop CO2 delivery, investigate at the CO2 provider the cause, start delivery if value OK again
5	Discontinous emissions through leakage, venting or incidents	Combination of techniques	x				Yearly				Potential leakage points like joints or ventstacks						

No.	Parameter to be Monitored*	Proposed Technique adopted	Mandatory according to EU directive	Required (preliminary estimation)	Contingency	Pre-inj	Inj	Post-Inj	Post-Inj (abandonment)	Long-term stewardship	Location	Expectation value	Accuracy	> Threshold 1	Action**	> Threshold 2	Contingency measures***
	Well integrity																
6	Annular pressure	Pressure device (with alarm value)		X		Baseline date prior to operations	Continuously with remote system for online reading			-	At the well head	Constant pressure		Increase or decrease in pressure within safety margins	Additional measurements like logging or sampling + analysis of fluids to detect CO2	Increase or decrease in pressure above safety margins	Investigate causes (sampling) and options to remediate (in the extreme case well abandonment)
7	Well integrity	Wireline Logging (selection of tool: CBL, PMIT, EMIT, USIT, WAF, optical)	X	X		Baseline	Frequency should be determined and adapted during the course of the project				Well	Measurements within the expected range		Measurements above expectation values	Additional measurements (such as repeat) to corroborate observations, potentially seismic contingency measurements in case values large enough to be detected by seismics	Measurements significantly above expectation values	Stop injection, additional measurements and seismic contingency measurements to identify shallow gas accumulations, investigate options to remediate (in the extreme case well abandonment)
8	Well head pressure	Pressure device	X			Baseline	Continuous	Continuous	Continuous		At the well head (injection skid)	Measurements within the expected range, no large fluctuations expected at constant flow rates		Loss or increase of pressure with respect to expected values	Additional measurements to determine the cause	No recovery of injection pressure after lowering or increasing injection flow	Stop injection, investigate the cause and evaluate whether conditions are safe
9	Well head temperature	Temperature device	X			Baseline	Continuous	Continuous	Continuous		At the well head (injection skid)	Determine operational limits for temperature range		In case temperature reaches the determined operational limits (high or low)	Additional measurements to determine the cause	In case temperature reaches the determined operational limits	Stop injection until the cause of the temperature change is clarified and safe
10	Plug integrity	Pressure test and inspection		X					Test during abandonment to assess the quality of the plug		In the well above the plug	No pressure changes		Minimal pressure changes	Investigate cause with other measurements (e.g. check deformation of the wellbore, fluid sample)	Significant pressure changes	Redo the plug

No.	Parameter to be Monitored*	Proposed Technique adopted	Mandatory according to EU directive	Required (preliminary estimation)	Contingency	Pre-Inj	Inj	Post-Inj	Post-Inj (abandonment)	Long-term stewardship	Location	Expectation value	Accuracy	> Threshold 1	Action**	> Threshold 2	Contingency measures***
	Reservoir integrity																
11	Reservoir pressure (FBHP) (see also line 8)	pressure device	(x)			Baseline data	Cont (TH cont, BH cont or monthly in case memory gauges)	Cont (TH cont, BH cont or monthly in case memory gauges) as long as the well is not suspended			Calculated from FTHP continuous, AND downhole permanent sensor (large risk of failure) OR downhole memory gauges	Flowing bottomhole pressure in agreement with simulations		Deviation from expected values	Recalibration of the reservoir simulation model until satisfactory history match	Significant deviation from expected values	Re-evaluate reservoir model, in case no explanation can be provided, stop injection
12	Reservoir Temperature (FBHT) (see also line 9)	thermometer or DTS	(x)			Baseline data	Cont (TH cont, BH cont or monthly in case memory gauges)	Cont (TH cont, BH cont or monthly in case memory gauges) as long as the well is not suspended			Calculated from FTHT AND potentially downhole permanent sensor (large risk of failure) or downhole memory gauges	Flowing bottomhole temperature in agreement with well model		Deviation from expected values	Recalibration of the well model until satisfactory history match	Significant deviation from expected values	Re-evaluate well model, in case no explanation can be provided, stop injection
13	Stabilized pressure (CBHP) (gradient) during shut-in period	pressure device combined with shut-in		x		Baseline data	Every year	Every year as long as the well is not suspended			Calculated from THP, AND permanent downhole sensor (large risk of failure) or downhole memory gauges, combined with shut in	Pressure date in agreement with expected simulation model and P/z curve		Deviation from expected values	Recalibration of the reservoir simulation model until satisfactory history match	Significant deviation from expected values	Re-evaluate reservoir model, in case no explanation can be provided, stop injection
14	Stabilised temperature (CBHT) (gradient) during shut-in period	thermometer or DTS combined with shut-in		x		Baseline data	Every year	Every year as long as the well is not suspended			DTS for permanent installation or memory gauges combined with shut-in AND if available in monitoring well	Temperature data in agreement with expected well model		Deviation from expected values	Recalibration of the well model until satisfactory history match	Significant deviation from expected values	Re-evaluate well model, in case no explanation can be provided, stop injection
15	Suspected leakage	Surface seismic survey			x	Baseline data already available	Only when other monitoring indicates leakage	Only when other monitoring indicates leakage	Only when other monitoring indicates leakage	Survey can be considered for the transfer of liability	Marine vessel (seismic acquisition using streamers)	No changes in the presence of shallow gas pockets or gas chimneys	~10's of Ktonnes of CO2	Shallow gas pockets	Determine the origin of the gas		

Environmental monitoring

No.	Parameter to be Monitored*	Proposed Technique adopted	Category of monitoring: Mandatory according to EU directive	Required (preliminary estimation)	Contingency	Pre-inj	Inj	Post-Inj	Post-Inj (abandonment)	Long-term stewardship	Location	Normal situation: Expectation value	Accuracy	Alert value: > Threshold 1	Action**	Contingency value: > Threshold 2	Contingency measures***
16	Pockmarks at the seabottom	Multi-beam echosounding		x		Baseline				survey prior to transfer of liability and every 5 years after handover of liability	Acquisition from a ship	No pockmarks		Pockmarks	Additional gas sampling + analysis to identify the origin of potential seepage or leakage. In case of leakage, identify the pathway with time-lapse seismic data.	Detection of bubbles	Additional gas sampling + analysis to identify the origin of potential seepage or leakage. In case of leakage, identify the pathway with time-lapse seismic data. Mitigation to...
17	Presence of shallow gas or gas chimneys in the subsurface	Baseline seismic data		x		Baseline data					Available baseline seismic data	No bright spots or chimneys in the subsurface		Bright spots and/or gas chimneys	Investigate origin of the gas, in case a leakage pathway is suspected, apply time-lapse seismic data	Bright spots and/or gas chimneys to the surface	Additional gas sampling + analysis to identify the origin of potential seepage or leakage. In case of leakage, identify the pathway with time-lapse seismic data. Mitigation to potential leaks.
18	Migration pathways for gas in the shallow subsurface	Time-lapse seismic data acquisition (2D or 3D)			x		Contingency	Contingency	Contingency	Contingency	Marine acquisition from a vessel	No changes in bright spots or chimneys in the subsurface		Changes in bright spots and/or gas chimneys	Investigate origin of the gas, in case a leakage pathway is suspected, apply time-lapse seismic data	Changes in bright spots and/or gas chimneys to the surface	Additional gas sampling + analysis to identify the origin of potential seepage or leakage. In case of leakage, identify the activeness of the pathway with time-lapse seismic data. Mitigation to potential leaks.
19	CO2 in soil at pockmarks	Gas samples using vibrocore + lab analysis			x	Contingency	Contingency	Contingency	Contingency	Contingency	Sampling from a vessel			In case of leakage detection at the seabottom by geophysical methods	Investigate origin of the gas, in case a leakage pathway is suspected, apply time-lapse seismic data	In case of leakage detection at the seabottom by geophysical methods	Investigate origin of the gas, in case a leakage pathway is suspected, apply time-lapse seismic data
20	Bubble detection at wellhead	Acoustic bubble detector			x	Contingency	Contingency	Contingency	Contingency	Contingency	Install at the seabottom	No bubbles		In case of few bubbles	Investigate origin of the gas, in case a leakage pathway is suspected, apply time-lapse seismic data	Significant bubble stream	Well remediation (workover)
21	Microseismic monitoring	Permanent geophones or DAS in monitoring wells		x		Baseline data	Cont	Cont			Injection well at caprock and reservoir level	No large events in caprock or at faults (re-activation)		Large events in the caprock or at faults	Additional measurements like seismic contingency measurements to identify shallow gas accumulations, evaluate whether injection can be continued safely	Very large events in the caprock or at faults	If considered a safety issue then stop injection, additional measurements and seismic contingency measurements to identify shallow gas accumulations, evaluate whether injection can be continued at lower...

Table 19-2 – P18-6 Base case monitoring plan, overview of project phases.

P18-6 CO2 storage base-case monitoring plan

Legend:
- Mandatory monitoring according to Annex II of the EU directive
- Preliminary estimation of required monitoring
- Contingency monitoring
- Period of time t.b.d.
- Decommisioning of the platform

#	Parameter	Method	Pre-injection	Injection	Post-injection	Post-injection (Abandonment)	Post-injection (Transfer of liability)
	Injection Proces						
1	Injection rate	Flow meter		Continuous			
2	Injection stream CO2 concentration	Gas samples & analysis: online system		Continuous or 1-3 hourly			
3	Injection stream composition	Gas samples & analysis: Additional samples for calibration		Quarterly			
4	Water measurement	Gas measurement		Continuous			
5	Discontinuous emissions through leakage, venting or incidents	Combination of techniques		Yearly reporting according to protocol			
	Well Integrity						
6	Annular pressure	Pressure device	Baseline	Continuous			
7	Well integrity	Wireline Logging (selection of tools like: CBL, PMIT, EMIT, USIT, WAF, optical)	Single baseline before start of the injection	Frequency should be determined and adapted during the course of the project			
8	Well head pressure	Pressure device		Continuous			
9	Well head temperature	Temperature device		Continuous			
10	Plug integrity	Pressure test and inspection			Assessment of the quality of the plug		
	Reservoir Integrity						
11	Reservoir pressure (FBHP) (see also line 8)	pressure device		Continuous or monthly with memory gauges (frequency can be adapted according to findings) - (Calculated from FTHP, AND potentially downhole permanent sensor (large risk of failure) or downhole memory gauges)			
12	Reservoir Temperature (FBHT) (see also line 9)	thermometer or DTS		Continuous or monthly with DTS or memory gauges (frequency can be adapted according to findings) - (Calculated from FTHT AND potentially downhole permanent sensor (large risk of failure) or downhole memory gauges)			
13	Stabilized pressure (CIBHP) (gradient) during shut-in period	pressure device (wireline tool or memory gauge) combined with shut-in		Shut-in pressure measurement every year			
14	Stabilised temperature (CIBHT) (gradient) during shut-in period	thermometer or DTS (wireline tool or memory gauge) combined with shut-in		Shut-in temperature measurement every year (DTS for permanent installation or memory gauges)			
15	Suspected leakage	Surface seismic survey		Survey in case of irregularities			
	Environmental Monitoring						
16	Pockmarks at the seabottom	Multi-beam echosounding	Baseline			survey	survey / survey
17	Presence of shallow gas or gas chimneys in the subsurface	Baseline seismic data	Interpretation can be on existing data				
18	Migration pathways for gas in the shallow subsurface	Time-lapse seismic data acquisition (2D or 3D)		Survey in case of irregularities			
19	CO2 in soil at pockmarks	Gas samples using vibrocore + lab analysis		Survey in case of irregularities			
20	Bubble detection at wellhead	Acoustic bubble detector		Survey in case of irregularities			
21	Microseismic monitoring	Permanent geophones or DAS in (monitoring) wells		Continuous in monitoring or injection well (considered required monitoring but subject to technical feasibility)			